The Dissertation Committee for Carla Allison Patrice Armorgan Certifies that this is the approved version of the following dissertation:

Investigation of Tertiary Structure of Electrosprayed Ribosomal Protein L9 by Fourier Transform Ion Cyclotron Resonance Mass Spectrometry using Low Energy Dissociation Techniques

Committee:

David A. Laude, Supervisor

Jennifer S. Brodbelt

James A. Holcombe

Peter J. Rossky

Christine Schmidt

Investigation of Tertiary Structure of Electrosprayed Ribosomal Protein L9 by Fourier Transform Ion Cyclotron Resonance Mass Spectrometry using Low Energy Dissociation Techniques

by

Carla Allison Patrice Armorgan, B.S.

Dissertation

Presented to the Faculty of the Graduate School of

The University of Texas at Austin

in Partial Fulfillment

of the Requirements

for the Degree of

Doctor of Philosophy

The University of Texas at Austin

December, 2003

DEDICATION

To husband, Todd, who helps make me whole. To my parents and family, who constantly inspire and support me in every endeavor.

ACKNOWLEDGEMENTS

My husband Todd is perfect for me and having met him here only served to confirm that everything happens as a part of a master plan. His acceptance of the person I am, with all my idiosyncrasies, is proof of how special he is. Thank you for everything, for coming into my life and enriching every single day.

Even though geography separates me from my family, I have always been privileged to feel their love and support irrespective of distance. This degree is the culmination of everything they have taught me over the past 27 years, and I am thrilled to have reached this milestone with them all at my side. I could not be the person I am, and enjoy the successes that I do, without your unconditional love.

Christine Flynn was my partner in crime for 5 year and remains my best friend. She is, unequivocally, one of the best human beings that I know. Thanks for the laughs, the tears, the tacos, the margaritas, and for standing up at my wedding. I will not think of Austin without thinking of you. Here's to new times in the northeast! Amy Engbrecht constantly reminded me of the value of girlfriends when it is so easy to forget. There is comfort in knowing that someone out there that will

let you laugh, cry, wail, and judge others without ever judging you in return. I am forever in your debt. Phillicia Waite, Tunisia Barnes, Kathryn McCabe, and Karen Russell have each been a critical member of my support team. Thank you for always believing I could do this, especially when I was overcome with doubts.

To the past and present members of the Laude research group especially, Rich Lochte, Liz Stevenson, Chad Ostrander, Richard Arkin, Matt Lasater, Greg Blakney, and Mike Fiorentino. You each gave of your time and attention when I needed it. Thank you for being patient and generous with your knowledge and your friendship.

At the helm of this group: David Laude. I am unsure how you kept faith in me during the course of my tenure here. That, in itself, is a testimony of the type of person you are. Thank you for being patient, and for believing that I could do this. Your unwavering faith pulled me through some very dark times. As a result of knowing you, I have grown as a person and as a scientist.

Conversations with Dr. David Hoffman and Dr. Jarle Lillemoen were invaluable in creating the understanding needed to work with this molecule. Dan Pantos generously gave his time and his computer system for the molecular modeling simulations to be performed.

Investigation of Tertiary Structure of Electrosprayed Ribosomal Protein L9 by Fourier Transform Ion Cyclotron Resonance Mass Spectrometry using Low Energy Dissociation Techniques

Publication No._____

Carla Allison Patrice Armorgan, Ph.D.

The University of Texas at Austin, 2003

Supervisor: David A. Laude

Tandem mass spectrometry, using infrared multi-photon dissociation (IRMPD), sustained off-resonance irradiation (SORI), and complementary pair analysis has been applied to small proteins in the 3 kDa range. In this dissertation, these techniques are evaluated on a larger protein, Ribosomal Protein L9, which was subjected to tandem mass spectrometry on a 9.4 Tesla Fourier Transform Ion Cyclotron Resonance (FT-ICR) mass spectrometer. This protein was selected for its large size (16.3 kDa), capacity for multiple charging, and distinctive tertiary structure. It consists of two terminal globular domains joined by a rigid α-helix.

The sixteen observable charge states of L9 (+10 through +25) were individually isolated and dissociated. The resulting complementary pairs and fragments were analyzed. Utilizing the rules of gas-phase basicity, Coulombic

repulsions, and the complementary pair data; the order of addition and location of the charged residues were determined. It is shown that for a molecule this size, the protons are added to preferential sites in a sequential manner.

Molecular modeling was used to assist with visualizing how the structure changes when charge is added. The X-ray structure was used as a starting point and the charge was added to locations as determined in Chapter 4. Energy minimizations yielded new structures for each charge state that did not retain their secondary characteristics. Correlating the torsion angles between the original and model structures showed local areas of high correlation that ranged from 5 to 15 residues long.

Threshold energy data separated the charge states into two groups based on their dissociation energies. +10 to +19 dissociated with a laser power of 10 Watts or greater, while +20 to +25 dissociated with a laser power range of 0 to 6 Watts. It was determined that the protonation of Lys109 may be responsible for a structural change that exposed the hidden His106 thereby allowing it to become charged.

Table of Contents

CHAPTER 1: INTRODUCTION AND BACKGROUND

1.1 DISSERTATION OVERVIEW

The purpose of this dissertation is to address where charges add in a large protein and if those locations affect its tertiary structure. Ribosomal Protein L9 (MW 16.3 kDa) was subjected to low energy dissociation to evaluate the applicability of Complementary Pair Analysis (CPA) as a viable technique over a wide range of protein sizes. The locations of the charges were successfully determined using CPA and it is evident that protons are added to a protein in a systematic manner. The rules of gas-phase basicity and Coulombic repulsion are adhered to and both direct the location of protons.

Previous work by Stevenson developed Complementary Pair Analysis as a technique to locate the sites where charges reside. Bee Venom Melittin (MW 2864 Da) was selected as the model protein because of its small size and limited charging. The location of charge was successfully determined using low energy fragmentation. This forms the basis of the work presented in this dissertation and was the initial demonstration of CPA as a viable technique for assigning charge location in an electrosprayed protein.

L9 structures were created based on the X-ray structure and the defined charge locations arrived at via Complementary Pair Analysis. Molecular modeling simulations were performed on each model to correlate the torsion angles between

pairs of amino acids from the simulated models and the X-ray structure. A number of correlations between the models and the known solid-state structure were calculated, and the areas corresponding to the loops and turns in the X-ray structure displayed the highest correlation.

Threshold energies for dissociation for IRMPD were derived from experimental data and a calibration calculation against the SORI dissociation data. The +20 was a point of division in threshold energies; charge states less than +20 had high dissociation energies. Charge states +20 and above had low dissociation energies. This is indicative of a conformational shift in the +20 range. The site of protonation was determined to be directly responsible for the conformational shift.

1.2 INTRODUCTION AND BACKGROUND

Mass spectrometry has developed into the major analytical tool for investigating biological compounds within the past two decades. The advent of ionization methods capable of delivering high mass ions into the gas phase, such as electrospray ionization (ESI) and matrix assisted laser desorption ionization (MALDI), has made mass spectrometry an integral tool in the of analysis of both sequence and structure of proteins. [1,2] The ease of coupling these ionization methods to mass spectrometric techniques has resulted in them becoming the main sources of ionizing large biomolecules into the gas-phase for various forms of

analysis. Fourier transform ion cyclotron resonance (FTICR) mass spectrometry is easily coupled with either of these techniques and has proven to be a reliable analytical technique for biomolecules because of its non-destructive nature, high mass accuracy, and high resolution capabilities.

The following sections contain the background information necessary to understand the data and conclusions presented in this dissertation. The sections include information on some conventional techniques for investigating protein structure, FTICR as a mass spectrometric technique, and the low energy dissociation methods employed for these studies.

1.3 CONVENTIONAL TECHNIQUES FOR STRUCTURAL ANALYSIS OF PROTEINS

1.3.1 Protein Digests and Gel Electrophoresis

Solution phase digests have been at the core of techniques for structural analysis of proteins. In 1953, Fredrick Sanger was the first to succeed in defining the complete amino acid sequence of the polypeptide bovine insulin.[3] Since then, the steps for analysis have been refined and automated. The process begins with the chemical cleavage of disulphide bonds between polypeptides in a multi-subunit protein. The individual chains are then separated, purified, and the amino acid composition is determined. A digest enzyme, such as trypsin or chymotrypsin, is

used to cleave each chain at specific residues. The resulting fragments of the chain are separated, purified and subjected to repeated cycles of Edman degradation to determine the amino acid sequence. This process is repeated to produce several sets of amino acid sequences that are compared in order to determine the actual sequence of residues for the individual chains. The location of disulfide linkages can be determined by repeating the sequencing process on intact disulfide linked fragments. In addition to primary sequence information, protein digests can also be used to ascertain locations of variants that arise from mutations or chemical modifications. These experiments are typically lengthy and result in poor yield, which severely limit the utility of protein digest methods for probing large proteins (>10,000 Da).

The products of digests are typically analyzed by gel electrophoresis[4] in which molecules are inserted into a cross-linked polyacrylamide or agarose gel support and separated by their rates of migration in an electric field. Their migration rates depend on their ionic charge and size. The main disadvantages of this technique are the relatively long time scale and the low mass accuracy that it provides (~5-10%). [5] This poor mass accuracy is attributed to variations in protein conformation which affect protein mobility through the gel.

1.3.2 Circular Dichroism

Circular dichroism (CD) is an indirect method used to probe protein secondary and tertiary structure in solution. CD has the capability to measure the difference in absorption by a protein of right-handed and left-handed circularly polarized ultraviolet (UV) light. Secondary structural characteristics of proteins, like α-helices and β-pleated sheets, are distinguishable. For α-helices there are two characteristic bands of absorption at about 208 and 222 nm.[6] This method has been extensively used because of its sensitivity, ease of equipment operation, fast and consistent data collection, nondestructive measurements, and its ability to look at conformation in the solution phase.[6,7] CD is also a powerful method of comparing the structure of an engineered protein to its parent protein. CD is limited by low resolution and interferences from aromatic amino acids which also absorb UV light in this region. Another drawback is that CD spectra do not provide detailed structural information, as is produced by nuclear magnetic resonance spectroscopy and X-ray crystallography.

1.3.3 Nuclear Magnetic Resonance

Nuclear magnetic resonance (NMR) is another technique used to examine secondary and tertiary structure of proteins in solution.[8,9] By measuring the short and long range spin coupling of neighboring atoms, NMR can produce a description

of protein conformation. Improvements in NMR technology, data processing and analysis procedures have resulted in performing multi-dimensional experiments on 1H, 13C, and 15N labeled proteins. Proteins with larger molecular weights (20-25 kDa) and more residues (150-200 amino acids) can be analyzed. [6] NMR provides the advantages of being able to produce spectra with atomic resolution and can yield dynamic information on samples in physiological conditions. There are drawbacks of this method, however, including slow data acquisition and the need for sample sizes in the mg range. A compounding disadvantage is the complexity of spectral interpretation for proteins greater than 20 kDa in size.

1.3.4 X-Ray Crystallography

X-ray crystallography (XRC) has spectral resolution that is comparable to that of NMR.[10] In this technique a protein crystal (~1 mm in size) is exposed to monochromatic X-rays; the intensity of the X-ray is detected in Cartesian space and correlated to the position of atoms in the crystal. The structure of the protein typically resembles the solution phase conformation because the protein crystal retains some water during the crystallization process.[5] The process of purifying and growing the high resolution crystals is very difficult and this is a major limitation of X-ray crystallography. In many cases, the position of atoms cannot be determined because of poor resolution within the crystal structure. As with NMR,

X-ray crystallography experiments are time consuming, expensive, and involve extensive equipment training.

1.4 MASS SPECTROMETRY

Mass spectrometry (MS) has experienced tremendous growth in its applications to the biochemical field during the past twenty years. Traditional methods of ionization like thermospray (TS), plasma desorption (PD), and fast atom bombardment (FAB) are destructive to the sample. These techniques also have low ionization efficiencies and the upper-limit of the molecular weights that can be successfully ionized is low (only about 10 kDa). The development of MALDI and ESI has resulted in the production of ions from intact biomolecules with much higher upper mass limits of molecular weight (> 100 MDa).[11-14] Electrospray is especially well suited to the study of nonvolatile biological samples because of the multiply charged ions it generates where MALDI typically produces singly charged ions. The significance of this attribute is discussed later.

1.4.1 Electrospray Ionization

Electrospray was investigated by Zelany in the early 20th century.[15] But it was not until the work of Dole et al. in 1968 that the technique gained an analytical application.[16] It was first successfully coupled to a mass spectrometer

in 1984 by Yamashita and Fenn.[2] Electrospray ionization (ESI) has since been exploited for its ability to produce multiply charged ions to the point where it is now the most widely used ionization method for non-volatile biological compounds.[17-19] It is a gentle technique that ionizes very large molecules without depositing sufficient internal energy to result in fragmentation or dissociation.

Several reviews have been written to describe the proposed mechanisms for the formation of ions during ESI.[20-25] The transfer of ions from the solution phase to the gas phase occurs via a two-stage process. The first stage involves the generation of charged solvated droplets. The analyte solution is flowed through a needle, with a 1-5 kV potential, that acts as an electrode to ionize the sample. A Taylor cone forms at the tip of the needle and when the potential gradient generated between the needle and the adjacent capillary (100-400 V) exceeds the surface tension of the Taylor cone, then a small spray of charged droplets is expelled.[26] Low surface tension solvents such as methanol are typically used in ESI to help facilitate this expulsion process.

The second stage of the electrospray mechanism is the desolvation process that produces bare ions. Desolvation of the ions is achieved either by flowing the charged droplets through a counter-current gas flow or through a resistively heated capillary.[27] There are two widely debated theories describing the emergence of a bare ion from a charged droplet. The ion evaporation model states that when the droplet reaches a certain size, that the electric field is intense enough to result in the

direct expulsion of analyte ions.[28,29] The charge residue model postulates that a series of Coulombic fissions occur. The few remaining solvent molecules simply evaporate leaving the charged analyte ion.[16] Previous work conducted by Lasater shows that both electrospray theories are correct, but apply in different size regimes.[30] Ions with a mass of about 1 kDa or less follow the ion evaporation model, while ions larger than 2.5 kDa follow the charge residue model.

Electrospray is a soft ionization technique that produces intact ions and preserves the higher order structure of large biomolecules.[31] There are many benefits of ESI including the low limits of detection, high ionization efficiencies, and ability to generate positive and negative ions.[32-34] Also, the production of multiply charged ions is another benefit of ESI since increasing the number of charges effectively decreases the mass to charge ratio, m/z. This makes analyte ions generated by ESI compatible with the mass range of most instruments. Increased Coulombic forces associated with multiple charging of ions also allows for efficient dissociation within the trapped ion cell. ESI was first coupled to FTICR in 1989.[35]

1.4.2 Fourier Transform Ion Cyclotron Resonance Mass Spectrometry

Fourier transform ion cyclotron resonance mass spectrometry uses the interaction between a magnetic field and electric fields to trap charged particles. There are three types of motion characteristic of ions in FTICR experiments: cyclotron motion, trapping motion, and magnetron motion. In a homogenous magnetic field, a particle with charge q experiences a Lorentz force perpendicular to the magnetic field. This force causes the charged particle of mass m to be constrained to a circular orbit of a particular frequency (ω) and radius defined by the translational energy of the ion. This frequency known as the effective cyclotron frequency, is typically on the order of 10-300 kHz, and allows for the high resolution detection. This motion is described by the fundamental equation for the cyclotron frequency (Hz), where B is the magnetic field strength in Tesla, q is the charge of the particle and m is the mass:[36]

$$\omega = \frac{qB}{m} \qquad \text{Equation 1.1}$$

The direction of the magnetic field is conventionally designated as the z-axis, and the Lorentz force confines the motion in the x- and y-planes. Since an ion has the freedom of motion along the z-axis in a strong magnetic field, the ions must be constrained along this axis to achieve FTICR analysis. This is accomplished by two trapping electrodes to which an electrostatic potential is applied that is

perpendicular to the magnetic field. This creates a potential well and causes the low energy ions to oscillate between the trap plates. The observed oscillatory frequency has three components, as shown in Figure 1.1.

Magnetron motion occurs as a result of the interaction of the magnetic and applied electric fields. The radial field that induces magnetron motion is strongest at the center of the trapped ion-cell and weakens radially towards the cell boundary. Subsequently, the potential energy is greatest at the center of the cell and decreases with increasing radial distance. Unwanted curvature of the electric field lines, from the finite trapping electrodes, causes the formation of a radial electric field in the cell that opposes cyclotron motion. As a result, the effective cyclotron frequency observed is smaller than the true cyclotron frequency. The observed cyclotron frequency (ω_o) is:

$$\omega_o = \omega_c - \omega_m \qquad \text{Equation 1.2}$$

where ω_c is the unperturbed cyclotron frequency and ω_m is the magnetron frequency. Any cooling of the ion magnetron motion, through neutral collisions for example, results is the expansion of the magnetron radius and will ultimately result in the loss of the ion from the confinement of the cell.

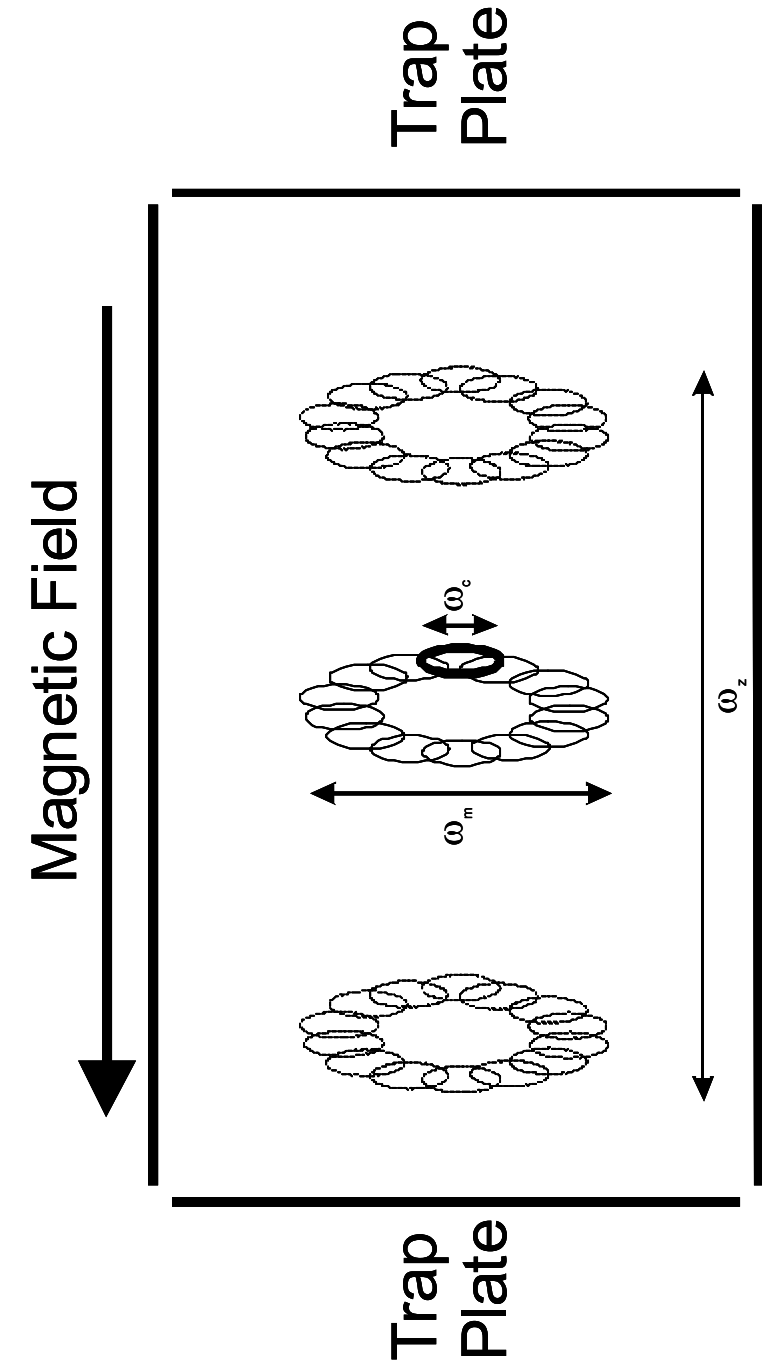

Figure 1.1: Illustration of the three motions of a trapped ion in a FTICR cell: cyclotron (ω_c), magnetron (ω_m) and axial (ω_z).

Once the ions are confined to the cell, their m/z ratios can be detected. FTICR utilizes excitation and detection electrodes that are collinear with the magnetic field for detection. A radio frequency (rf) excitation is applied to one set of parallel plates (the excitation electrodes) on resonance with the cyclotron frequency of an ion packet. As the ions absorb this energy, the radius of motion expands to slightly less than the dimension of the trapped ion cell. Upon termination of the excitation event, the ions maintain a trajectory that brings them in close proximity of the detection electrodes. An image current is induced on the detection plates. The oscillating frequency of this image current is equal to the observed cyclotron frequency (ω_o), and the magnitude of the current is proportional to the number of ions detected. The measured transient signal consists of cyclotron frequencies generated by several ions of different masses if a broadband excitation is used. Processing these data, using Fourier transform, results in deconvolution of the combined frequencies to the individual cyclotron frequencies. Calibration of the resulting frequency domain signal generates the accurate mass to charge values of the ions.

Modifications of the FTICR experiment can improve the performance and facilitate investigations of gas phase chemistry. The application of a quadrupolar rf excitation results in interconversion of the magnetron and cyclotron motions.[37] The conversion of magnetron motion to cyclotron motion, followed by collisional damping of the cyclotron radius is known as quadrupolar axialization (QA).[38]

Axialization improves many aspects of the FTICR experiment such as mass resolving power, mass accuracy, cooling of internal energy, mass selectivity for MS^n, and ion remeasurement efficiencies.[36]

Individual ions can be isolated and subjected to dissociation techniques or gas phase reactants prior to the excitation and detection events. Stored waveform inverse Fourier transform (SWIFT) is the most flexible method for the selective broadband ejection of ions.[39] Performing an inverse Fourier transform of a specific magnitude/phase excitation spectrum produces an excitation waveform. Ions trapped in the cell are subjected to this excitation waveform and unwanted ions are ejected by being excited to cyclotron radii larger than the dimensions of the trap. The remaining, isolated ions are unaffected by the ejections of the unwanted ions.

1.4.3 Instrumentation

Coupling ESI to FTICR presents a challenge because electrospray ions are produced at atmospheric pressure, and high performance FTICR requires pressures on the order of 10^{-8} - 10^{-10} Torr. Thus a pressure differential of ten orders of magnitude must be accomplished to move from the ionization stage to the detection stage. Three to five stages of differential pumping is typically employed to achieve the necessary pressure reduction. In addition to differential pumping across small orifices, shuttering devices are also used to limit the presence of background neutrals in the analyzer region.

Maintaining a focused ion beam as it traverses the pressure gradient is also another concern, because a spatially and kinetically broad beam of ions is typically generated from ESI. The fringing magnetic field can deflect some of this ion beam as it approaches the magnet, which is known as the magnetic mirror effect.[40] Overcoming the magnetic mirror effect has been approached in two ways. Most FTICR instruments generate the ions outside the magnetic field by utilizing an external source. The incorporation of either electrostatic lenses and/or rf guides have been designed and successfully used to inject the ions into the analyzer region of the instrument. Figure 1.2 shows a diagram of the 9.4 Tesla system at the National High Magnetic Field Laboratory (Tallahassee, FL), which uses an external microspray ionization source (flow rates of ~ 0.3 μL/min) and octupole rods for ion focusing.[41]

The other approach that minimizes the magnetic mirror effect is the placement of the ionization source directly inside the strong magnetic field, where it is adjacent to the analyzer region. A more complex pumping system is required in this configuration. Figures 1.3 shows the 3.0 Tesla systems designed at the University of Texas at Austin. The instrument employs a series of concentric tubes of decreasing diameter in the vacuum chamber that reduces the pressure from the ion source to the trapped ion cell.[42-45] A mechanical shutter is placed before the trapped ion cell and acts as an additional conductance limit between the ion source and the analyzer region. The shutter is opened to allow injection of ions into the

cell and then closed to permit efficient pumping in the detection region. Each of these instruments allows for flexibility and variety in the types of experiments that can be performed, and produce high resolution FTICR spectra.

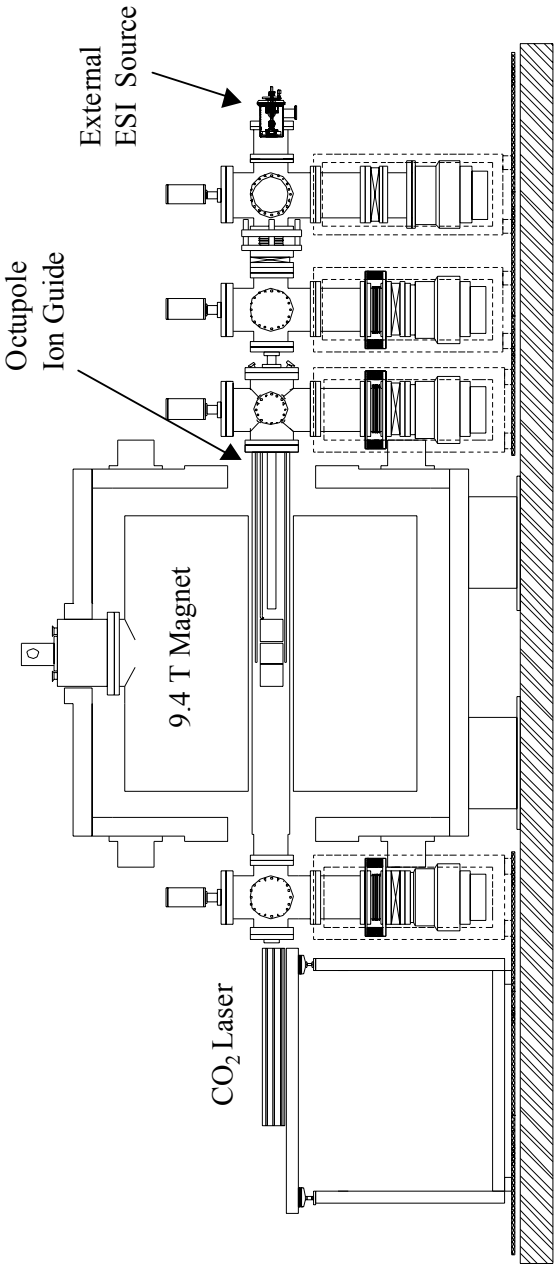

Figure 1.2: Schematic for an external 9.4 Tesla ESI/FTICR mass spectrometer.

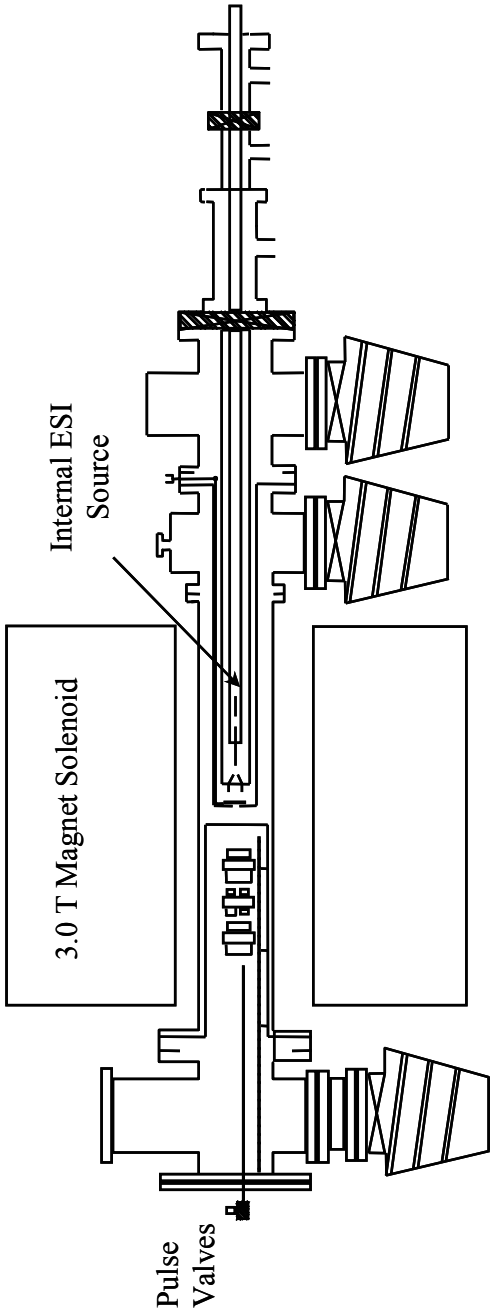

Figure 1.3: Schematic for internal source 3.0 Tesla FTICR mass spectrometer, with three differential pumping stages.

1.5 UNIQUE FEATURES OF THE FTICR EXPERIMENT

1.5.1 Non-destructive Detection

FTICR offers a non-destructive method of detection, unlike other mass spectrometric techniques where ions are typically detected via collision of the ions with a surface. Since detection is accomplished using an image current, the ions only need to be in the vicinity of the detection plates for the detection event to be successful. If the ion packet can be returned to the center of the cell, the single packet of ions can be re-excited and detected repeatedly for it to be studied.[46,47] Hendrickson, et al. have demonstrated that the technique of remeasurement produced a ten-fold increase in signal to noise (S/N) of the peptide melittin.[48] Additionally, the same ion population can be used to investigate consecutive ion-molecule reactions by applying ion remeasurement capabilities. [49]

1.5.2 High Mass Resolution and Mass Accuracy

One of the most distinguishing characteristics of FTICR is its unmatched high resolution capabilities. The ability to attain ultra-high resolution results from long observation times; the time scale for detection is on the order of milliseconds. These long transient lifetimes allow for better definition of the cyclotron motion, and thus higher mass resolution is achieved. Low background pressures enable detection of long transients by minimizing ion loss and expansion of the ion packet

through collisions. Recently, unit resolution on a protein with mass of 112 kDa, at 9.4T, and 2 million resolving power on bovine ubiquitin (MW 8645 Da) were reported.[50,51]

For large biomolecule analysis, high resolution offers several benefits. Differentiation of adducted species (e.g. metals) and degradation products (e.g. water or ammonia) from the protonated molecular ions can be identified and distinguished. Also, isotopic resolution allows for accurate assignments of charge states because the spacing between adjacent peaks is equal to z-1.

Mass accuracy is related to the correct assignment of charge states; accurate mass assignments are therefore enhanced by high resolution. When this is coupled with the ability of modern electronics to precisely measure frequency, better than parts per million (ppm) mass accuracy is common in FTICR measurements. Senko and co-workers have demonstrated mass accuracy of 0.35 Da for carbonic anhydrase (29,023.73 Da).[52]

1.5.3 Sensitivity and Detection Limits

FTICR has proven to be an extremely sensitive method of ion detection. One example of this sensitivity is seen in the work of Limbach and co-workers where it was theoretically argued that in a 3.0 T system as few as 177 singly charged ions can be detected in a trapped cell.[53] Experimentally, McLafferty et al. used a “pico-spray” ionization source and reported detection limits as low as 0.9

attomoles for bovine ubiquitin.[54] Electrospray ionization greatly enhances the sensitivity because the sensitivity is dependent on the amplitude of the image current produced by the charges. Consequently, biomolecules with multiple charges produce an amplified signal. Recent studies by Chen et al. provide evidence of the improved sensitivity when a single DNA ion of mass 110 MDa with $z \approx 28{,}000$ was detected.[55]

1.6 STRUCTURAL ANALYSIS OF PROTEINS

1.6.1 Primary Structure Analysis

The application of dissociation studies for the determination of amino acid sequences and identification of point mutations, the amino terminus of N-terminally blocked proteins, sites of enzyme modifications or post-translational modifications has been well documented.[56-63] Successive stages of dissociation are called multi-stage or tandem mass spectrometry, or also MS/MS/MS or MS3. Protein sequencing by tandem ESI/MS has been accomplished by many research groups.[64-71] A straightforward procedure is the chemical or enzymatic digestion on solution followed by MS/MS.[72,73]

1.6.2 Secondary and Tertiary Structure Analysis

Initial mass spectrometric studies of protein conformation involve the manipulation of solution conditions and observation of the effect of those manipulations on the charge state distribution of the electrosprayed protein. It was thought that proteins had fewer accessible ionization sites when they are in their tightly folded native conformations. When unfolding occurs, more ionization sites become available for protonation and the result is increased abundance of higher charge states. Denaturation of proteins in solution is achieved by the altering pH, adding organic solvents, increasing temperature, and reducing disulfide bonds. [74-84] Even though differences in charge state distribution are observed when solution conditions are perturbated, the relationship between charge state distribution and solution phase conformation is not fully understood. This correlation needs to be studied in greater detail before it can serve as a reliable method for probing structure.

1.6.2.1 Ion Mobility

Collisional cross-section is a characteristic that is used to study tertiary structure of proteins and is referred to as ion-mobility experiments. Different conformers are separated on the basis of kinetic energy differences resulting from collisions with background neutrals. Ions traverse a high pressure tube and undergo

numerous collisions. Those with a more open conformation undergo more collisions and achieve a slower velocity than ions with a more closed conformation. Early research in this field by Bowers identified carbon clusters based on ion mobility differences.[85] Clusters up to C^{10+} had a linear structure and more complicated ring structures existed for clusters larger than C^{84+}. Numerous other studies have been performed and show the utility of separating protein conformers on the basis on ion-mobility differences.[86-92]

1.6.2.2 Hydrogen/Deuterium Exchange

The exchange of labile protons for deuterium is a valuable method for probing higher order structure. In this process, a deuterated solvent is reacted with the protein of interest. Monitoring the number of incorporated deuteriums can provide information on the extent protein folding. There are two factors that affect the number of deuteriums incorporated. The first is the protein conformation and the second is the proton affinity of the exchange sites. A low proton affinity difference (~100 kJ/mol) between the deuterated solvent and a proton on the protein would result in exchange at that site.[93-95] Steric factors can also affect the extent of exchange by blocking access to the exchange sites. It is generally accepted that if a protein could exist in folded and unfolded states, that the folded state would experience fewer deuteriums incorporated while the unfolded conformation would

have more incorporation. The use of this method for evaluating conformation of gas phase proteins is very common place.[96]

1.6.2.3 Ion Dissociation

Determination of protein sequence and structure by ion dissociation is very commonly used in conjunction with FTICR because the high mass accuracy and the ultra high resolution provided makes it amenable to the identification of fragments formed from the dissociation.[97] A number of dissociation techniques exist that vary in selectivity and rate of energy deposition. The earliest of these was nozzle-skimmer dissociation.[98-100] This method produced fragments by varying the potential difference between the capillary and skimmer cone in the high pressure ESI region. The resulting dissociation was very efficient, but there was no precursor ion selection and this lead to complicated spectral interpretations. This front end dissociation generally produced fragment ions that would normally be seen in later stages of multi-stage dissociation by more controlled techniques.

The more conventional and commonly utilized dissociation techniques are performed on isolated ions in the trapped ion cell. These techniques include collisional activated dissociation (CAD), surface induced dissociation (SID), blackbody infrared radiative dissociation (BIRD), sustained off-resonance irradiation (SORI), infrared multi-photon dissociation (IRMPD), and electron capture dissociation (ECD).[22,52,65,67,69,99-119] These methods are employed

after ions are injected into the trapped ion cell and a charge state of interest is isolated. By fragmenting only the ions of interest, the analysis of the resulting daughter ions is simplified. SORI and IRMPD are of particular importance to the work presented in this dissertation since they were the dissociation methods employed.

SORI is a dissociation method that fragments ions by depositing small amounts of energy and is a highly selective technique. Radio frequency excitations approximately 1-2 kHz off-resonance are applied to the ions of interest. Ions experiencing the out-of-phase excitation are activated and deactivated in the cell. Collisions with background neutral gas present in the cell slowly deposits internal energy on the 100 ms time scale until fragmentation occurs along a low energy pathway. Threshold dissociation pathways can be investigated because the amount of energy deposited is so low. Fragment ions formed (typically y and b) with cyclotron frequencies corresponding to the applied excitation frequency are ejected from the cell and cannot be detected. This is a disadvantage of using SORI since blind spots are created in the spectra where these fragments should have been detected. This shortcoming can be circumvented by performing two separate experiments in which the off-resonance excitation frequency is applied above and below the frequency of the precursor ion. In SORI, dissociation occurs near the center of the cell, so the efficiency of fragment retention is high. High fragmentation efficiency (~90%) and high resolving power (~106) are typically

achieved in the product ion spectra.[109] Analysis of the fragment ions provides extensive information about the primary sequence and secondary structure.

IRMPD is a dissociation technique whose coupling to FTICR offers a number of advantages. Infrared photons of wavelength of ~1 μm are used to fragment large multiply charged ions. Activation times range from 0.1 s up to 100 s. Since the laser that produces the infrared photons is on axis, the dissociation products are also generated on axis. This improves the retention efficiency and increases the performance of multi-stage ion dissociation. Additionally, it is not necessary to subject the system to high gas loads that may decrease the sensitivity and resolution of the instrument. IRMPD produces fragmentation spectra that are very similar to SORI with the addition of internal fragments. Typical dissociation efficiencies are in the 30-80% range.[67]

Electron capture dissociation uses low energy electrons (<0.2 eV) to routinely produce abundant fragmentation of multiply charged electrospray proteins with masses up to 10 kDa (though fragmentation of proteins as heavy as 42 kDa has been demonstrated).[120] The fragmentation observed from ECD varies from other dissociation techniques because it results in extensive backbone cleavages. This results from the amine bond cleavage and produces predominantly c and z· fragments, while other dissociation methods produce b and y fragments from the amide bond cleavage.[121] Precursor ions are fragmented with an efficiency of 80 ± 15%, and this method is an excellent source of both sequence and structural

information because of the high extent of fragmentation and the ease of spectral interpretation. Sequence positions of post-translational modifications, like carboxylation, glycosylation and sulfation, are more easily assigned by ECD since these functionalities are intact post-dissociation.[122]

1.7 CONTEXT FOR DISSERTATION

Previous work, conducted by Liz Stevenson, established Complementary Pair Analysis (CPA) as a viable method to identify the location of charge in a small peptide.[123] The inconclusive nature of traditional methods to investigate gas-phase structure resulted in the use of low energy dissociation to generate b/y fragments, which, if arising from the cleavage of the same peptide bond with a mass and charge summing to that of the parent ion, form a complementary pair. When complementary pairs arise from a series of different peptide bond cleavages over the backbone, the location of the charge can be bracketed and assigned to a specific basic residue.

The peptide subjected to this analysis was Bee Venom Melittin, which was chosen because of its relatively small size (2846.5 Da), well-defined α-helical conformation, and limited charging. Analysis of the complementary pairs yielded definitive charge locations for charge states +2 through +5. Synthetic analogs of melittin, in which basic residues were substituted with neutral alanine, were

employed to corroborate the preferential addition of the charge to the peptide. The analogs supported that both gas-phase basicity of the basic residue and Coulombic repulsions contributed to the next site of proton addition.

Using the locations of charge identified by CPA, the charged peptides were subjected to molecular modeling simulations in an effort to visualize the gas-phase structure of each charge state. Simulations showed that the addition of the 5th charge resulted in the movement of the residue's side chain, and thereby changing the shape of the molecule.

These findings form the basis of this dissertation. Understanding the specific location of charge in a protein and how those locations affect the dissociation patterns is a notable contribution to the field. Knowledge of how the charge influences structure and how structure influences fragmentation will increase the value of the information contained in low energy dissociation mass spectra.

1.8 CHAPTER OVERVIEWS

1.8.1 Chapter 2: Literature Review of Ribosomal Protein L9.

This chapter presents the justification for selecting Ribosomal Protein L9 as the subject of these studies. It was selected for its distinctive three-dimensional structure which has been characterized by X-ray crystallography. The protein has a dumb-bell like appearance with two terminal globular regions that are joined by a

rigid α-helix. The globular regions are a combination of α-helices, β-sheets, loops, and turns. The literature shows that the α-helix is one of the strongest helices known to man, that the terminal globular regions fold with different rates and independently of each other. These characteristics enable independent consideration of the three regions which aids in data interpretation. The 30 basic residues and N-terminus promote multiple charging during the electrospray process, thereby enabling the 16 observable charge states, from +10 to +25 to be dissociated using low energy dissociation techniques.

1.8.2 Chapter 3: Dissociation Data for Ribosomal Protein L9.

Chapter 3 catalogs all of the b/y fragments detected and identified from the dissociation of the 16 observable charge states using infra-red multi-photon dissociation (IRMPD) and sustained off-resonance irradiation (SORI). Variable laser power was used to fragment the isolated charge states by IRMPD. The resulting fragmentation occurred in localized areas of the protein, with hardly any fragmentation of the α-helix being detected. Locations adjacent to acidic residues and lysines showed increased fragmentation. Loss of neutral molecules (water and ammonia) was observed at high laser powers for the low charge states and at low laser powers for the high charge states. SORI data was collected for charge states +20 through + 22 because of the inconsistent behavior of fragmenting at 0 Watts of laser power.

1.8.3 Chapter 4: Complementary Pair Analysis to Assign Charge Location in L9.

Complementary pair analysis was successfully applied to the fragmentation data and the location of charge in electrosprayed L9 was assigned. A complementary pair is produced when a b/y fragment pair results from the cleavage of the same peptide bond and the summation of mass and charge of both fragments results in the parent ion. Other fragments generated from the dissociation process were used to confirm the information derived from the complementary pairs. The rules of both residue gas-phase basicity and Coulombic repulsions were applied when regions of ambiguity arose. The use of sequential charge states allowed the determination of not only location of charge, but also the order of charge addition. L9 has 31 potential charge sites and +25 is the maximum charge state observed.

1.8.4 Chapter 5: Molecular Modeling Simulations of the Charge States of L9.

Model structures of each charge state generated from the X-ray structure and the charge location assignments were subjected to an AMBER force field energy minimization using HyperChem. The simulations were unable to preserve the secondary structure of the ions, but it outputted a structure of loose loops on both

termini separated by an extended chain of residues. Torsion angles were used to correlate the structures. Correlation over the enter sequence of the protein was poor between the models and the X-ray structure. When analyzed locally, the regions of high correlation between the models and X-ray were identified as loops and turns from the X-ray structure. When the model of $(M+nH)^{+n}$ was compared to the model from n+1, the lower charge states were better correlated that the upper charge states.

1.8.5 Chapter 6: How Threshold Dissociation and Fragmentation Pathways Relate to Structure.

A structural change is proposed to be occurring at charge state +20. Threshold dissociation of +10 to +19 required at least 10 Watts for threshold fragmentation, while +20 to +25 required laser powers of less than 6 Watts. Calibration against the SORI data showed internal energies of the +20 and +21 ions to be 0.7 eV, compared to ~4 eV (+10 to +19) and ~2 eV (+22 to +25). The appearance of neutral fragments in the low power dissociation spectra of charge states over +20 (inclusive) also indicates a change. From the assignment of charge, no histidines have been protonated before +20. At +20, His 106 is protonated and the remaining two residues at +23 and +24. The protonation of histidines in the higher charge states could explain the dramatic shift in the behavior from the lower charge states to the upper charge states.

1.9 REFERENCES

1. Tanaka, K., H. Waki, Y. Ido, S. Akita, Y. Yoshida, and T. Yoshida, *Protein and Polymer Analyses up to m/z 100000 by Laser Ionization Time-of-Flight Mass Spectrometry.* Rapid Commun. Mass Spectrom., 1988. **2**: p. 151-3.
2. Yamashita, M. and J.B. Fenn, *Electrospray Ion Source. Another Variation on the Free-Jet Theme.* J. Phys. Chem., 1984. **88**: p. 4451-4459.
3. Sanger, F. and E.O.P. Thompson, *Amino acid sequence in the glycycl chain of insulin. II. Peptides from enzymic hydrolyzates.* Biochem. J., 1953. **53**: p. 366-74.
4. Wu, D. and F.E. Regnier, *Native protein separations and enzyme microassays by capillary zone and gel electrophoresis.* Anal. Chem., 1993. **65**(1): p. 2029-35.
5. Voet, D. and J.G. Voet, *Biochemistry*. 1 ed. 1990, New York: John Wiley & Sons, Inc. 1223.
6. Havel, H.A., *Spectroscopic Methods for Determining Protein Structure in Solution*. 1994, New York: VCH Publishers, Inc. 250.
7. Nakanishi, K., N. Berova and R.W. Woddy, *Circular Dichroism: Principles and Applications*. 1994, New York: VCH Publishers, Inc.
8. Bax, A., *Multidimensional nuclear magnetic resonance methods for protein studies.* Curr. Opin. Struct. Biol., 1994. **4**: p. 738-44.
9. Yi, Q. and D. Baker, *Direct evidence for a two-state protein unfolding transition from hydrogen-deuterium exchange, mass spectrometry, and NMR.* Protein Science, 1996. **6**(5): p. 1060-1066.
10. Rost, B. and r.C. Sande, *Jury returns on structure prediction.* Nature, 1992. **360**(6404): p. 540.
11. Fenn, J.B., M. Mann, C.K. Meng, S.F. Wong and C.M. Whitehouse, *Electrospray Ionization- Principles and Practice.* Mass Spectrom. Rev., 1990. **9**: p. 37-70.
12. Karas, M., U. Bahr, A. Ingendoh and F. Hillenkamp, Angew. Chem. Int. Ed. Engl., 1989. **28**: p. 760-1.

13. Hillenkamp, F., M. Karas, R.C. Beavis and B.T. Chait, *Matrix-Assisted Laser Desorption/Ionization Mass Spectrometry of Biopolymers.* Anal. Chem., 1991. **63**(24): p. 1193A-1203A.

14. Nelson, R.W., D. Dogruel and P. Williams, *Detection of human IgM at m/z approximately 1 MDa.* Rapid Commun. Mass Spectrom., 1995. **9**(7): p. 625.

15. Zeleny, J., J. Phys. Rev., 1917. **10**: p. 1.

16. Dole, M., L.L. Mack, R.L. Hines, R.C. Mobley, L.P. Ferguson, and M.B. Alice, *Molecular beams of macroions.* J. Phys. Chem., 1968. **49**: p. 2240.

17. Agnes, G.R. and G. Horlick, *Determination of solution ions by electrospray mass spectrometry.* Appl. Spectrosc., 1994. **48**(6): p. 655-61.

18. Fenn, J.B., M. Mann, C.K. Meng, S.F. Wong and C.M. Whitehouse, *Electrospray Ionization for Mass Spectrometry of Large Biomolecules.* Science, 1989. **246**: p. 64-71.

19. Laude, D.A., E. Stevenson and J.M. Robinson, *Electrospray ionization/Fourier transform ion cyclotron resonance mass spectrometry*, in *Electrospray Ionization Mass Spectrometry*, R.B. Cole, Editor. 1997, John Wiley & Sons, Inc.: New York. p. 291-319.

20. *Electrospray Ionization Mass Spectrometry*. 1 ed, ed. R.B. Cole. 1997, New York: John Wiley & Sons, Inc.

21. Smith, R.D., J.A. Loo, R.R. Ogorzalek Loo, M. Busman and H.R. Udseth, *Electrospray MS Review.* Mass Spectrom. Rev., 1991. **10**: p. 359-451.

22. Smith, R.D., J.A. Loo, C.G. Edmonds, C.J. Barinaga and H.R. Udseth, *New Developments in Biochemical Mass Spectrometry: Electrospray Ionization.* Anal. Chem., 1990. **62**: p. 882-99.

23. Fenn, J.B., M. Mann, C.K. Meng, S.F. Wong and C.M. Whitehouse, *Electrospray.* Mass Spectrom. Rev., 1990. **9**: p. 37-70.

24. Loo, J.A. and R.R. Ogorzalek Loo, *Electrospray Ionization Mass Spectrometry of Peptides and Proteins*, in *Electrospray Ionization Mass Spectrometry*, R.B. Cole, Editor. 1997, John Wiley & Sons, Inc.: New York. p. 385.

25. Kebarle, P. and L. Tang, *From Ions in Solution to Ions in the Gas Phase: The Mechanism of Electrospray Mass Spectrometry.* Anal. Chem., 1993. **65**: p. 972A-986A.

26. Siuzdak, G., *Mass Spectrometry for Biotechnology*. 1st. ed. 1996, San Diego: Academic Press, Inc. 161.

27. Tanaka, K., H. Waki, Y. Ido, S. Akita and S. Yoshida, Rapid Commum. Mass Spectrom., 1991. **5**: p. 117.

28. Thomson, B.A. and J.V. Iribarne, *Field-induced ion evaporation from liquid surfaces at atmospheric pressure.* J. Chem. Phys., 1979. **71**: p. 4451.

29. Iribarne, J.V. and B.A. Thomson, *On the evaporation of small ions from charged droplets.* J. Chem. Phys., 1976. **64**(6): p. 2287-94.

30. Lasater, M.A., *Studies of Sub-Micron Sized Electrospray Droplets in Mass Spectrometry*, Dissertation Thesis, Department of Chemistry and Biochemistry, 2001, The University of Texas at Austin.

31. Smith, R.D., K.J. Light-Wahl, B.E. Winger and J.A. Loo, *Preservation of non-covalent associations in electrospray ionization mass spectrometry: multiply charged polypeptide and protein dimers.* Org. Mass. Spectrom., 1992. **27**(7): p. 811-21.

32. Emmett, M.R. and R.M. Caprioli, *Micro-Electrospray Mass Spectrometry: Ultra-High-Sensitivity Analysis of Peptides and Proteins.* J. Am. Soc. Mass Spectrom., 1994. **5**: p. 605-13.

33. Smith, R.D., J.A. Loo, C.G. Edmonds, C.J. Barinaga and H.R. Udseth, *New developments in biochemical mass spectrometry: electrospray ionization.* Anal. Chem., 1990. **62**: p. 882-899.

34. Wu, Q., X. Cheng, S.A. Hofstadler and R.D. Smith, *Specific metal-oligonucleotide binding studied by high resolution tandem mass spectrometry.* J. Mass Spectrom., 1996. **31**(6): p. 669-75.

35. Henry, K.D., E.R. Williams, B.-H. Wang, F.W. McLafferty, J. Shabanowitz, and D.F. Hunt, *Fourier-Transform Mass Spectrometry of Large Molecules by Electrospray Ionization.* Proc. Natl. Acad. Sci. U.S.A., 1989. **86**: p. 9075-8.

36. Marshall, A.G., C.L. Hendrickson and G.S. Jackson, *Fourier Transform Ion Cyclotron Resonance Mass Spectrometry: A Primer.* Mass Spectrom. Rev., 1998. **17**(1): p. 1-35.

37. Guan, S., *Generation of Optimal Excitation Pulses for Two Energy Level Systems Using an Inverse FT Method.* J. Chem. Phys., 1992. **96**: p. 7959-64.

38. Guan, S., H.S. Kim, A.G. Marshall, M.C. Wahl, T.D. Wood, and X. Xiang, *Shrink-Wrapping an Ion Cloud for High-Performance Fourier Transform Ion Cyclotron Resonance Mass Spectrometry.* Chem. Rev., 1994. **94**(8): p. 2161-82.

39. Guan, S. and A.G. Marshall, *Stored waveform inverse Fourier transform (SWIFT) ion excitation in trapped-ion mass spectrometry: Theory and applications.* Int. J. Mass Spectrom. Ion Processes, 1996. **157/158**: p. 5-37.

40. McIver, R.T., Jr., *Trajectory Calculations for Axial Injection of Ions Into a Magnetic Field: Overcoming the Magnetic Mirror Effect With an R. F. Quadrupole Lens.* Int. J. Mass Spectrom. Ion Processes, 1990. **98**(1): p. 35-50.

41. Senko, M.W., et al., *Electrospray Ionization FT-ICR Mass Spectrometry at 9.4 Tesla.* Rapid Commun. Mass Spectrom., 1996. **10**: p. 1824-8.

42. Hofstadler, S.A. and D.A. Laude, *Ion ejection from Fourier transform mass spectrometry trapped ion cells due to non-adiabatic changes in trapping potentials.* Int. J. Mass Spectrom. Ion Processes, 1990. **101**(1): p. 65-78.

43. Guan, Z., V.L. Campbell, J.J. Drader, C.L. Hendrickson and D.A. Laude, *High performance detection of biomolecules using a high magnetic field electrospray ionization source/Fourier transform ion cyclotron resonance mass spectrometer.* Rev. Sci. Instrum., 1995. **66**(9): p. 4507-15.

44. Harper, C.J., T.A. Torres, E.G. Schmidt, C.R. Arkin and D.A. Laude, *On-Line HPLC Interface for a Magnetic Field Focusing ESI/FTICR.* Proc. 44th Amer. Soc. Mass Spectrom. Conf. on Mass Spectrom. & Allied Topics, 1996: p. 486.

45. Hofstadler, S.A., E. Schmidt, Z. Guan and D.A. Laude, Jr., *Concentric tube vacuum chamber for high magnetic field, high-pressure ionization in a Fourier transform ICR mass spectrometer.* J. Am. Soc. Mass Spectrom., 1993. **4**: p. 168-76.

46. Guan, Z., S.A. Hoftstadler and D.A. Laude, Jr., *Remeasurement of Electrosprayed Proteins in the Trapped Ion Cell of a Fourier Transform ICR Mass Spectrometer.* Anal. Chem., 1993. **65**: p. 1588-93.

47. Speir, J.P., G.S. Gorman, C.C. Pitsenberger, C.A. Turner, P.P. Wang, and I.J. Amster, *Remeasurement of Ions Using Quadrupolar Excitation Fourier Transform Ion Cyclotron Resonance Spectrometry.* Anal. Chem., 1993. **65**(13): p. 1746-52.

48. Hendrickson, C.L. and D.A. Laude, Jr., *Quadrupolar axialization for improved control of electrosprayed proteins in FTICR mass spectrometry.* Anal. Chem., 1995. **67**: p. 1717-1721.

49. Guan, Z., J.J. Drader, V.L. Campbell and D.A. Laude, *Real-Time Monitoring of the Gas Phase Reactions of Single Ion Population Using the*

Remeasurement Experiment in Fourier Transform Ion Cyclotron Resonance Mass Spectrometry. Anal. Chem., 1995. **67**: p. 1453-8.

50. Kelleher, N.L., M.W. Senko, M.M. Siegel and F.W. McLafferty, *Unit Resolution Mass Spectra of 112 kDa Molecules with 3 Da Accuracy.* J. Am. Soc. Mass Spectrom., 1997. **8**: p. 380-3.

51. Senko, M.W., S.C. Beu and F.W. McLafferty, *Determination of monoisotopic masses and ion populations for large biomolecules from resolved isotopic distributions.* J. Am. Soc. Mass Spectrom., 1995. **6**: p. 229-33.

52. Senko, M.W., S.C. Beu and F.W. McLafferty, *High-Resolution Tandem Mass Spectrometry of Carbonic Anhydrase.* Anal. Chem., 1994. **66**: p. 415-7.

53. Limbach, P.A., P.B. Grosshans and A.G. Marshall, *Experimental Determination of the Number of Trapped Ions, Detection Limite, and Dynamic Range in Fourier Transform Ion Cyclotron Resonance Mass Spectrometry.* Anal. Chem., 1993. **65**: p. 135-140.

54. Valaskovic, G.A., N.L. Kelleher, D.P. Little, D.J. Aaserud and F.W. MdLafferty, *Attomole-Sensitivity Electrospray Source for Large-Molecule Mass Spectrometry.* Anal. Chem., 1995. **67**: p. 3802-5.

55. Chen, R., et al., *Trapping, Detection, and Mass Determination of Coliphage T4 DNA Ions of 10^8 Da by Electrospray Ionization Fourier Transform Ion Cyclotron Resonance Mass Spectrometry.* Anal. Chem., 1995. **67**: p. 1159-63.

56. Miao, S., L. Ziser, R. Aebersold and S.G. Withers, *Identification of Glutamic Acid 78 as the Active Site Nucleophile in Bacillus subtilis Xylanase Using Electrospray Tandem Mass Spectrometry.* Biochem., 1994. **33**(23): p. 7027-32.

57. Rossomando, A.J., et al., *Identification of Tyr-185 as the site of tyrosine autophosphorylation of recombinant mitogen-activated protein kinase p42mapk.* Proc. Natl. Acad. Sci. U.S.A., 1992. **89**(13): p. 5779-83.

58. Carr, S.A., M.J. Huddleston and M.F. Bean, *Selective identification and differentiation of N- and O-linked oligosaccharides in glycoproteins by liquid chromatography-mass spectrometry.* Protein Sci., 1993. **2**(2): p. 183-96.

59. Papac, D.I., J.E.J. Oatis, R.K. Crouch and D.R. Knapp, *Mass spectrometric identification of phosphorylation sites in bleached bovine rhodopsin.* Biochem., 1993. **32**(23): p. 5930-4.

60. Thulin, C.D. and K.A. Walsh, *Identification of the Amino Terminus of Human Filaggrin Using Differential LC/MS Techniques: Implications for Profilaggrin Processing.* Biochem., 1995. **34**(27): p. 8687-92.

61. Bischoff, R., et al., *Sequence-specific deamidation: isolation and biochemical characterization of succinimide intermediates of recombinant hirudin.* Biochem., 1993. **32**(2): p. 725-34.

62. Papayannapoulos, I.A., *The interpretation of collision-induced dissociation tandem mass spectra of peptides.* Mass Spectrom. Rev., 1995. **14**(1): p. 49-73.

63. de Hoffman, E., *Tandem mass spectrometry: a primer.* J. Mass Spectrom., 1996. **31**(2): p. 129-37.

64. Baker, T.R., T. Keough, R.L. Dobson, T.A. Riley, J.A. Hasselfield, and P.E. Hesselberth, *Antisense DNA oligonucleotides. I: The use of ionspray tandem mass spectrometry for the sequence verification of methylphosphonate oligodeoxyribonucleotides.* Rapid Commun. Mass Spectrom., 1993. **7**(3): p. 190-4.

65. Barinaga, C.J., C.G. Edmonds, H.R. Udseth and R.D. Smith, *Sequence determination of multiply charged peptide molecular ions by electrospray-ionization tandem mass spectrometry.* Rapid Commun. Mass Spectrom., 1989. **3**(5): p. 160-4.

66. Poulter, L. and L.C.E. Taylor, *A Comparison of Low and High Energy Collisionally Activated Decomposition MS-MS for Peptide Sequencing.* Int. J. Mass Spectrom. Ion Processes, 1989. **91**: p. 183-97.

67. Little, D.P., J.P. Speir, M.W. Senko, P.B. O'Connor and F.W. McLafferty, *Infrared Multiphoton dissociation of large multiply-charged ions for biomolecule sequencing.* Anal. Chem., 1994. **66**(18): p. 2809-15.

68. Dikler, S., J.W. Kelly and D.H. Russell, *Improving mass spectrometric sequencing of arginine-containing peptides by derivatization with acetylacetone.* J. Mass Spectrom., 1997. **32**(12): p. 1337-49.

69. Loo, J.A., C.G. Edmonds and R.D. Smith, *Tandem mass spectrometry of very large molecules: serum albumin sequence information from multiply charged ions formed by electrospray ionization.* Anal. Chem., 1991. **63**(21): p. 2488-99.

70. Tang, X.J. and P.B. Thibault, R. K., *Fragmentation reactions of multiply-protonated peptides and implications for sequencing by tandem mass spectrometry with low-energy collision-induced dissociation.* Anal. Chem., 1993. **65**(20): p. 2824-34.

71. Roepstorff, P., *Proposal for a common nomenclature for sequence ions in mass spectra of peptides.* Biomed. Mass Spectrom., 1984. **11**(11): p. 601.

72. Smith, R.D., J.A. Loo, C.J. Barinaga, C.G. Edmonds and H.R. Udseth, *Capillary zone electrophoresis and isotachophoresis-mass spectrometry of polypeptides and proteins based upon an electrospray ionization interface.* J. Chromatogr., 1989. **480**: p. 211-32.

73. Stacey, C.C., et al., *Reverse-phase Liquid Chromatography/Electrospray-Ionization Fourier-Transform Mass Spectrometry in the Analysis of Peptides.* Rapid Commun. Mass Spectrom., 1994. **8**(7): p. 513-6.

74. Chowdhury, S.K., V. Katta and B.T. Chait, *Differences in Charge States of Electrosprayed Native and Denatured Proteins.* J. Am. Chem. Soc., 1990. **112**: p. 9012.

75. Konermann, L. and D.J. Douglas, *Acid-induced unfolding of cytochrome c at different methanol concentrations: Electrospray ionization mass spectrometry specifically monitors changes in the tertiary structure.* Biochem., 1997. **36**(40): p. 12296-302.

76. Le Blanc, J.C.Y., D. Beuchemin, K.W.M. Siu, R. Guevremont and S.S. Berman, *Thermal denaturation of some proteins and its effect on their electrospray mass spectra.* Org. Mass Spectrom., 1991. **26**(10): p. 831-9.

77. Loo, J.A., C.G. Edmonds, H.R. Udseth and R.D. Smith, *Effect of reducing disulfide-containing proteins on electrospray ionization mass spectra.* Anal. Chem., 1990. **62**(7): p. 693-8.

78. Loo, J.A., R.R. Ogorzalek Loo, H.R. Udseth, C.G. Edmonds and R.D. Smith, *Solvent-Induced Conformational Changes of Polypeptides Probed by Electrospray-Ionization Mass Spectrometry.* Rapid Commun. Mass Spectrom., 1991. **5**(3): p. 101-5.

79. Ogorzalek Loo, R.R., N. Dales and P.C. Andrews, *Surfactant effects on protein structure examined by electrospray ionization mass spectrometry.* Protein Sci., 1994. **3**(11): p. 1975-83.

80. Loo, J.A., R.R. Ogorzalek Loo and P.C. Andrews, *Primary to quaternary protein structure determination with electrospray ionization and magnetic sector mass spectrometry.* Org. Mass Spectrom., 1993. **28**(12): p. 1640-9.

81. Mirza, U.A., S.L. Cohen and B.T. Chait, *Heat-induced conformational changes in proteins studied by electrospray ionization mass spectrometry.* Anal. Chem., 1993. **65**(1): p. 1-6.

82. Katta, V. and B.T. Chait, *Conformational changes in proteins probed by hydrogen-exchange electrospray-ionization mass spectrometry.* Rapid Commun. Mass Spectrom., 1991. **5**(4): p. 214-7.

83. Allen, M.H. and M.L. Vestal, *Design and performance of a novel electrospray interface.* J. Am. Soc. Mass Spectrom., 1992. **3**: p. 18-26.

84. Feng, R. and Y. Konishi, *Stepwise Refolding of Acid-Denatured Myoglobin: Evidence from Electrospray Mass Spectrometry.* J. Am. Soc. Mass Spectrom., 1993. **4**: p. 638-45.

85. von Helden, G., M.T. Hsu, P.R. Kemper and M.T. Bowers, *Structures of carbon cluster ions from 3 to 60 atoms: Linears to rings to fullerenes.* J. Chem. Phys., 1991. **95**: p. 3835-37.

86. Covey, T. and D.J. Douglas, *Collision Cross Sections for Protein Ions.* J. Am. Soc. Mass Spectrom., 1993. **4**: p. 616-23.

87. Cox, K.A., R.K.J. Julian, R.G. Cooks and R.E.J. Kaiser, *Conformer selection of protein ions by ion mobility in a triple quadrupole mass spectrometer.* J. Am. Soc. Mass Spectrom., 1994. **5**(3): p. 127-363.

88. Clemmer, D.E., R.R. Hudgins and M.F. Jarrold, *Naked Protein Conformations: Cytochrome c in the Gas Phase.* J. Am. Chem. Soc., 1995. **117**: p. 10141-2.

89. Valentine, S.J., *Probing gas-phase biomolecular ion conformation with ion mobility/mass spectrometry techniques*, Dissertation Thesis, 2000, Indiana University.

90. Purves, R.W., D.A. Barnett and R. Guevremont, *Separation of protein conformers using electrospray-high field asymmetric waveform ion mobility spectrometry-mass spectrometry.* Int. J. Mass Spectrom., 2000. **197**: p. 163-77.

91. Badman, E.R., C.S. Hoaglund-Hyzer and D.E. Clemmer, *Monitoring structural changes of proteins in an ion trap over apprx.10-200 ms: Unfolding transitions in cytochrome c ions.* Anal. Chem., 2001. **73**(24): p. 6000-7.

92. Purves, R.W., D.A. Barnett, B. Ells and R. Guevremont, *Gas-phase conformers of the [M + 2H]2+ ion of bradykinin investigated by combining high-field asymmetric waveform ion mobility spectrometry, hydrogen/deuterium exchange, and energy-loss measurements.* Rapid Commun. Mass Spectrom., 2001. **15**(16): p. 1453-6.

93. Gur, E.H., L.J. De Koning and N.M.M. Nibbering, *Gas-phase hydrogen-deuterium exchange of protonated alkyldipeptides with (S)- and (R)-butan-2-ol.* J. Mass Spectrom., 1996. **31**(3): p. 325-7.

94. Gard, E., M.K. Green, J. Bregar and C. Lebrilla, *Gas Phase Hydrogen/Deuterium Exchange as a Molecular Probe for the Interaction of Methanol and Protonated Peptides.* J. Am. Soc. Mass Spectrom., 1994. **5**: p. 623-31.

95. Green, M.K., E. Gard, J. Bregar and C.B. Lebrilla, *H-D exchange kinetics of alcohols and protonated peptides: effects of structure on proton affinity.* J. Mass Spectrom., 1995. **30**: p. 1103-10.

96. Suckau, D., et al., *Co-Existing Stable Conformations of Gaseous Protein Ions.* Proc. Natl. Acad. Sci. U.S.A., 1993. **90**: p. 790-3.

97. Wu, Q., S. Van Orden, X. Cheng, R. Bakhtiar and R.D. Smith, *Characterization of Cytochrome c Variants with High-resolution FTICR Mass Spectrometry: Correlation of Fragmentation and Structure.* Anal. Chem., 1995. **67**: p. 2498-509.

98. Loo, J.A., H.R. Udseth and R.D. Smith, *Collisional Effects on the Charge Distribution of Ions from Large Molecules, Formed by Electrospray-ionization Mass Spectrometry.* Rapid Commun. Mass Spectrom., 1988. **2**(10): p. 207-10.

99. Beu, S.C., M.W. Senko, J.P. Quinn, F.M. Wampler, III and F.W. McLafferty, *FT Electrospray Instrumentation for Tandem High-Resolution MS of Large Molecules.* J. Am. Soc. Mass Spectrom., 1993. **4**: p. 557-65.

100. Loo, J.A., J.P. Quinn, S.I. Ryu, K.D. Henry, M.W. Senko, and F.W. McLafferty, *High-resolution Tandem Mass Spectrometry of Large Biomolecules.* Proc. Natl. Acad. Sci. U.S.A., 1992. **89**: p. 286-9.

101. Williams, E.R., *Tandem FTMS of Large Biomolecules.* Anal. Chem., 1998. **70**(5): p. 179A-185A.

102. Smith, R.D., J.A. Loo, C.J. Barinaga, C.G. Edmonds and H.R. Udseth, *Collisonal activation and collison-activated dissociation of large multiply charged polypeptides and proteins produced by electrospray ionization.* J. Am. Soc. Mass Spectrom., 1990. **1**(1): p. 53-65.

103. Speir, J.P., M.W. Senko, D.P. Little, J.A. Loo and F.W. McLafferty, *High-resolution Tandem Mass Spectra of 37-67 kDa Proteins.* J. Mass Spectrom., 1995. **30**(1): p. 39-42.

104. Price, W.D., P.D. Schnier, R.A. Jockusch, E.F. Strittmatter and E.R. Williams, *Unimolecular Reaction Kinetics in the High-Pressure Limit without Collisions.* J. Am. Chem. Soc., 1996. **118**: p. 10640-4.

105. Edmonds, C.G., J.A. Loo, C.J. Barinaga, H.R. Udseth and R.D. Smith, *Capillary Electrophoresis-Electrospray Ionization Mass Spectrometry.* J. Chromatogr., 1989. **474**: p. 21-37.

106. Rockwood, A.L., M. Busman, H.R. Udseth and R.D. Smith, *Thermally induced dissociation of ions from electrospray mass spectrometry.* Rapid Commun. Mass Spectrom., 1991. **5**(12): p. 582-5.

107. Busman, M., A.L. Rockwood and R.D. Smith, *Activation energies for gas-phase dissociations of multiply charged ions from electrospray ionization mass spectrometry.* J. Phys. Chem., 1992. **96**(6): p. 2397-400.

108. Rockwood, A.L., M. Busman and R.D. Smith, *Coulombic effects in the dissociation of highly charged ions.* Int. J. Mass Spectrom. Ion Processes, 1991. **111**: p. 103-29.

109. Senko, M.W., J.P. Speir and F.W. McLafferty, *Collisional activition of large multiply-charged ions using Fourier transform mass spectrometry.* Anal. Chem., 1994. **66**: p. 2801-8.

110. McLafferty, F.W., *High-Resolution Tandem FT Mass Spectrometry above 10 kDa.* Acc. Chem. Res., 1994. **27**: p. 379-86.

111. Smith, R.D., C.J. Barinaga and H.R. Udseth, *Tandem Mass Spectrometry of Highly Charged Cytochrome c Molecular Ions Produced by Electrospray Ionization.* J. Phys. Chem., 1989. **93**: p. 5019-22.

112. O'Connor, P.B., J.P. Speir, M.W. Senko, D.P. Little and F.W. McLafferty, *Tandem mass spectrometry of carbonic anyhdrase (29 kDa).* J. Mass Spectrom., 1995. **30**: p. 88-93.

113. Chorush, R.A., D.P. Little, S.C. Beu, T.D. Wood and F.W. McLafferty, *Surface-induced dissociation of multiply-protonated proteins.* Anal. Chem., 1995. **67**: p. 1042-6.

114. Pasa Tolic, L., J.E. Bruce, Q.P. Lei, G.A. Anderson and R.D. Smith, *In-Trap Cleanup of Proteins from Electrospray Ionization Using Soft Sustained Off-Resonance Irradiation with Fourier Transform Ion Cyclotron Resonance Mass Spectrometry.* Anal. Chem., 1998. **70**: p. 405-8.

115. Schnier, P.D., W.D. Price, R.A. Jockusch and E.R. Williams, *Blackbody infrared radiative dissociation of bradykinin and its analogues: energetics, dynamics and evidence for salt-bridge structures in the gas phase.* J. Am. Chem. Soc., 1996. **118**: p. 7178-89.

116. Price, W.D., P.D. Schnier and E.R. Williams, J. Phys. Chem. B, 1997. **101**: p. 664-73.

117. Price, W.D., P.D. Schnier and E.R. Williams, *Tandem Mass Spectrometry of Large Biomolecule Ions by Blackbody Infrared Radiative Dissociation.* Anal. Chem., 1996. **68**: p. 859-66.

118. Hofstadler, S.A., J.H. Wahl, R. Bakhtiar, G.A. Anderson, J.E. Bruce, and R.D. Smith, *Capillary Electrophoresis Fourier Transform Ion Cyclotron Resonance Mass Spectrometry with Sustained Off-Resonance Irradiation for the Characterization of Protein and Peptide Mixtures.* J. Am. Soc. Mass Spectrom., 1994. **5**: p. 894-9.

119. Gauthier, J.W., T.R. Trautman and D.B. Jacobson, *Sustained Off-resonance Irradiation for CAD Involving FTMS. CAD Technique that Emulates Infrared Multiphoton Dissociation.* Anal. Chim. Acta, 1991. **246**: p. 199-210.

120. Horn, D.M., Y. Ge and F.W. McLafferty, *Activated Ion Electron Capture Dissociation for Mass Spectral Sequencing of Larger (42 kDa) Proteins.* Anal. Chem., 2000. **70**(20): p. 4778-84.

121. Zubarev, R.A., N.L. Kelleher and F.W. McLafferty, *Electron Capture Dissociation of Multiply Charged Protein Cations. A Nonergodic Process.* J. Am. Chem. Soc., 1998. **120**(13): p. 3265-6.

122. Zubarev, R.A., et al., *Electron capture dissociation for structural characterization of multiply charged protein cations.* Anal. Chem., 2000. **72**(3): p. 563-73.

123. Stevenson, E., *Dissociation Studies of Charge and Structure Effects on Electrosprayed Proteins*, Dissertation Thesis, Department of Chemistry and Biochemistry, 1998, The University of Texas at Austin.

CHAPTER 2: LITERATURE REVIEW OF RIBOSOMAL PROTEIN L9

2.1 INTRODUCTION

Ribosomal protein L9 from *Bacillus stearothermophilus* contains 149 amino acids. It is located in the large subunit of the ribosome and appears to be well-exposed on the ribosome surface.[1] L9 is a molecular strut within the ribosome consisting of two globular, RNA-binding domains separated by a nine-turn connecting helix as seen in Figure 2.1. Details of L9's secondary structure, as elucidated by X-Ray diffraction, are illustrated in Figure 2.2.[2] Based on these data, Hoffman et al. concluded that the N-terminal domain consists of a three-stranded anti-parallel β-sheet sandwiched between a small helix and the N-terminal end of the central helix. Two residues from the central helix (Leu44 and Leu47) abut against the β -sheet and form part of the hydrophobic core of the N-terminal domain. The C-terminal domain contains two long loops, an α-helix, and a three-stranded β -sheet which packs against the C-terminal end of the helix. There are three residues from the central helix (Ala65, Leu68, and Leu72) form part of the hydrophobic core of the C-terminal domain, while Leu62 caps the hydrophobic core and is partially protected from the solvent. The central α-helix, extending from residue 41 through 74, is one of the strongest known α-helical configurations.[3] It

is suggested that it acts as a rigid spacer that helps to orient the positions of the N and C-terminal domains in order to facilitate binding to other RNA proteins.[4-6]

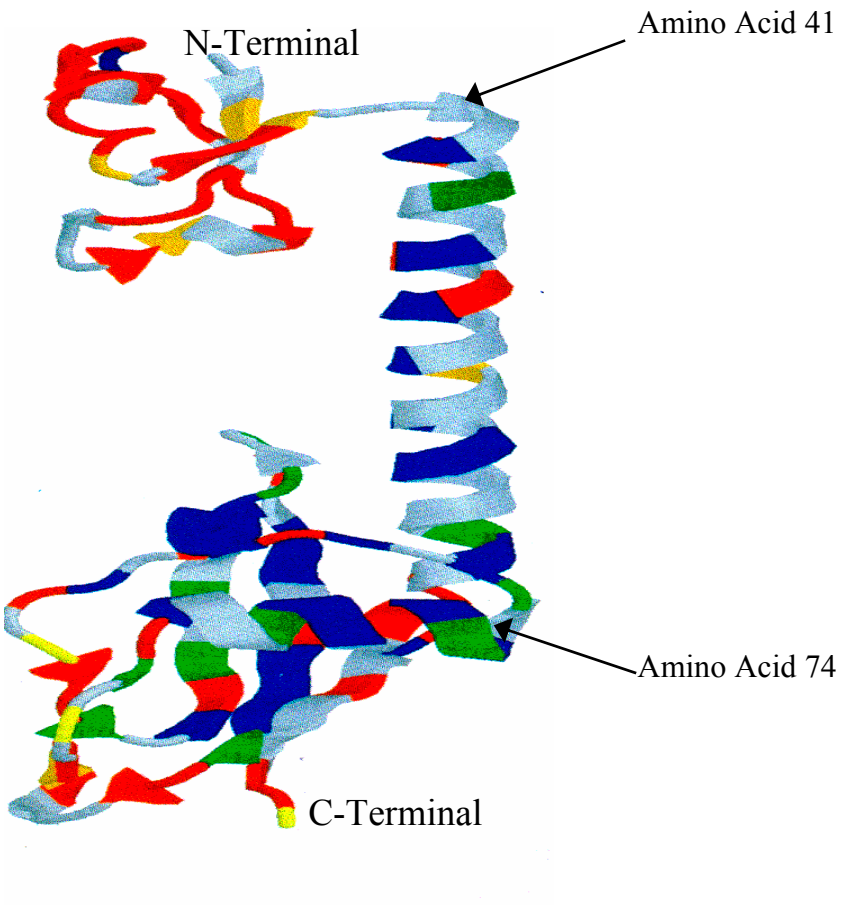

1 5 10 15 20 25 30 35

MKVIF LKDVK GKGKK GEIKN VADGY ANNFL FKQGL AIEAT

PANLK ALEAQ KQKEQ RQAAE ELANA KKLKE 70 QLEKL

TVTIP AKAGE GGRLF GSITS KQIAE SLQAQ 105 HGLKL

DKRKI ELADA IRALG YTNVP VKLHP EVTAT 140 LKVHV

TEQK

Figure 2.1: Ribbon diagram of ribosomal protein L9. MOLSCRIPT was used to generate this diagram.[7] The primary structure for L9 with basic residues bolded and acidic residues underlined is shown.

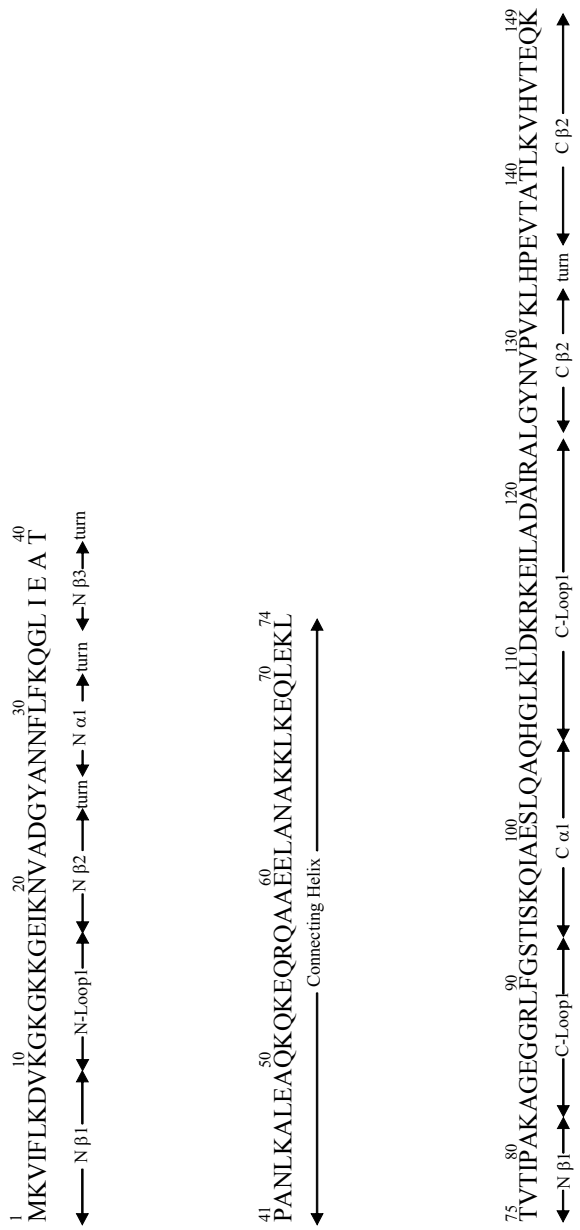

Figure 2.2: Diagram showing secondary structural characteristics of Ribosomal Protein L9.[2]

The length of the long α-helix is invariant across different species and its central residues are predominantly hydrophilic, but the exact sequence of the helix varies considerably. The exceptions are the residues that pack against the two terminal domains, which are conserved among the different species.[2,8] This unusual structure is maintained in aqueous solution.[3,9] It has been proposed that L9 acts as a mechanical sensor in within the ribosome. The average mass of L9 is 16311.17 Da. It contains 30 basic residues in addition to the N-terminal methionine, and 17 acidic residues. Its primary sequence, from the N-terminus, is also shown in Figure 2.1. The basic residues are highlighted in bold typeface and acidic residues are underlined.

2.2 ALPHA-HELIX STABILITY IN RIBOSOMAL PROTEIN L9

The two globular domains of L9 are connected by a nine turn, 34 residue α-helix. In solution phase, the middle 17 residues are exposed to the solvent. The first seven pack against and form part of the N-terminal domain, and the last ten form part of the C-terminal domain. The helix appears to act as a rigid spacer responsible for orienting the N and C-terminal domains so that they are properly positioned to bind to RNA. Kuhlman, et al. shows that a peptide equivalent of the complete central helix in aqueous solution is >85% helical at 1oC, and 68±7% helical at 25^{o}C.[3] When comparable experiments were conducted on the middle 17

residues of the helix in the same group, the protein was found to have only 41±4% helical nature at 1oC. It was shown that the helix has a high intrinsic stability even in the absence of the rest of the protein. Circular dichroism (CD) was used for these determinations. For the 27 residue peptide corresponding to the H-helix of myoglobin, experiments showed it to be only 30% helical at 0^{o}C.[10] There are other proteins that contain long, solvent exposed α-helices in their crystal structure (calmodulin and troponin C) that do not maintain the helical regions in solution. NMR studies show that the helical regions of these molecules are flexible and disordered in solution.[11,12] It has been hypothesized that the critical difference is that the central helix of L9 plays an essential role in while the helices of troponin C and calmodulin do not. To observe typical helical structure, the helix inducing solvent, trifluoroethanol (TFE), is often required. The high propensity of L9 to form and retain its helical structure in aqueous conditions, and in the absence of TFE, highlights a potential role for the helix in early stages of the folding process, and the important relation of its solution structure to function.

2.3 FOLDING OF THE GLOBULAR DOMAINS

NMR and stopped-flow fluorescence studies performed in the Raleigh group, determined folding and unfolding rate constants for the globular domains in L9.[13] It was found that the two domains fold independently and at different rates.

The rate constants for the N-terminal domain were greater than those of the C-terminal domain by two or three orders of magnitude. These constants suggest that the folding of the domains occur independently. The N-terminal domain, both in isolation and in the intact protein, folds very rapidly. Since the biological activity of L9 is dependent on the bilobal structure of the protein, the observed difference in folding rates have not been implicated in its binding to RNA. It has been suggested, however, that the rapid folding of the N-terminal domain may offer some protection from proteolysis.[14]

2.4 ANALYSIS OF INDIVIDUAL L9 DOMAINS

Luisi, et al. synthesized and studied peptides representative of the N-terminal domain.[15] For each region of specific secondary structure, a single peptide was made and their conformational preferences investigated using NMR and circular dichroism. They found that the helices and the turns of the smaller peptides mimicked the secondary structure of the intact domain. They suggested that since the helices and turns can be stabilized by local interactions, they would have a greater tendency to adopt native-like structure in isolation than the peptides derived from the β -sheet regions. Even with the use of another peptide with residues 1-51, the same folds were adopted, and the rates, as measured with stopped-flow fluorescence, were identical to the N-terminal of the intact protein.[16]

The Raleigh group performed pH jump experiments to investigate if the folding of the C-terminal was affected by whether the N-terminal was folded or not.[17] They found that the rate of folding and unfolding of the C-terminal domain was characteristically slower than the rates associated with the N-terminal domain. They found this to be the case regardless of if the N-terminal globule was folded or unfolded. This result suggested that the slow folding of the C-terminal domain was not a consequence of the unfavorable interactions with the rest of the protein.

2.5 CONSIDERATIONS FOR MASS SPECTROMETRIC DISSOCIATION OF L9

The ability to integrate information about protein fragmentation into the processes of protein identification and peptide sequencing requires understanding how these biomolecules fragment in the gas-phase. The effect of sequence on fragmentation and the relationship between fragmentation and the presence of charge has been previously investigated.[18-22] It has been shown that the presence and location of chargeable amino acids in the primary sequence of the protein important effects on fragmentation. Table 2.1 shows how these acidic and basic amino acids are distributed within the three structural domains of L9. Cleavage of the amide bond is typically dominant during various fragmentation processes and a series of b and y fragments are produced. The fragment nomenclature was first proposed by Roepstorff et al. and subsequently modified by Johnson et al.[23,24]

The nomenclature details are shown in Figure 2.4 and are used throughout this dissertation.

Table 2.1: Distribution and numbers of chargeable amino acids in L9.

	N-Terminal Domain	**α-Helix**	**C-Terminal Domain**
Basic Residues	8 Lys	8 Lys	8 Lys
		1 Arg	3 Arg
			3 His
Acidic Residues	2 Asp	6 Glu	2 Asp
	2 Glu		5 Glu

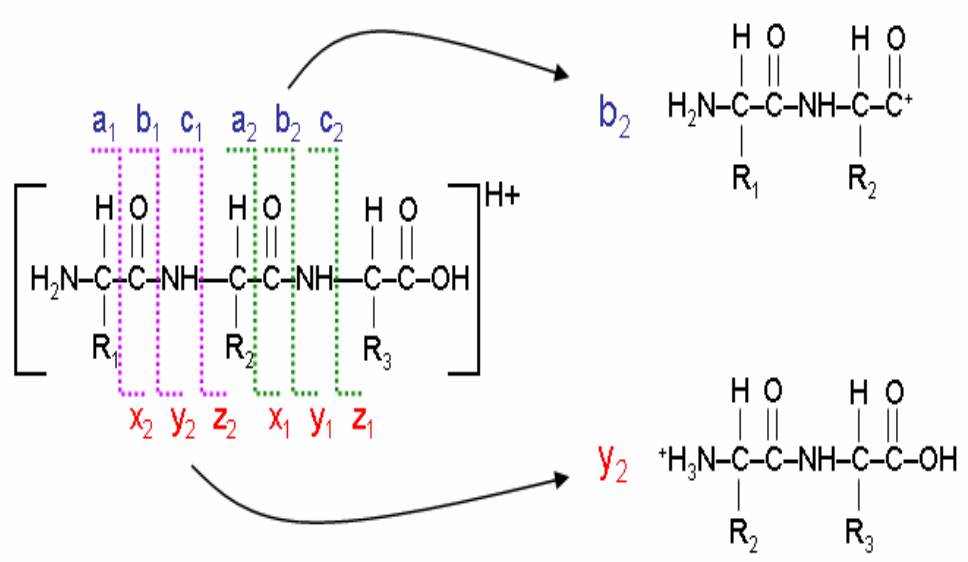

Figure 2.3: Illustration of location of cleavages and the nomenclature of resulting fragment ions generated from backbone amide bond cleavage.

One of the most prominent effects of sequence on fragmentation is the selective cleavage on the C-terminus of acidic residues. This is an enhanced cleavage site because the acidic proton of the side-chain serves to initiate cleavage at the amide bond immediately C-terminal to aspartic acid or glutamic acid, thereby producing an anhydride.[25] A similar enhanced cleavage site occurs when the side-chain of histidine is protonated. The histidine side-chain turns into a weak acid when protonated and it can also initiate backbone cleavage by transferring its proton to the backbone. This histidine enhanced cleavage is different because instead of producing an anhydride, a cyclic structure is made.[26] Studies of short peptides using derivatization to fix charges in specified locations show that when arginine and aspartic acid are both present, and the number of protons exceeds the number of arginines, nonselective cleavages occur.[27] L9 only contains four arginine residues, and change states starting at +10 are observed. So in every case presented in the following chapters, the number of protons added during the ionization process exceeds the number of aspartic acid residues. Fragmentation N-terminal to proline is another cleavage frequently occurring in dissociation studies of proteins and peptides. It was found that when certain residues are found N-terminal to proline (His, Asp, Val, Ile and Leu), there is evidence of enhanced cleavage.[28] There are three such sites in L9 that correspond to the regions of more enhanced cleavage N-terminal to proline.

2.6 CONCLUSIONS

The unique tertiary arrangement of L9 makes it amenable to probing its gas-phase structure using mass spectral techniques. The protein consists of two terminal globular units connected by a nine turn α-helix. Its characteristic structure provides a variety of unique regions with the potential for very different fragmentation patterns in the gas-phase. Previous work by other groups involved investigating the rates of folding of the two domains, the stability of the α-helix, and the interaction of the domains make it possible to consider the three regions of this protein as distinctly different. This ability to define the protein as these three regions proves to be very useful for data analysis and presentation.

The presence of histidines, prolines, and acidic residues provide potential locations of enhanced cleavages. These pathways are further investigated using threshold energy dissociation, and the resulting fragments form the basis of assignments of the sequential charge addition in the observed charge states. The accessibility of alternate low energy pathways for fragmentation is also investigated and presented.

2.7 REFERENCES

1. Lillemoen, J. and D.W. Hoffman, *An investigation of the dynamics of ribosomal protein L9 using heteronuclear NMR relaxation measurements.* J. Mol. Biol., 1998. **281**(3): p. 539-51.
2. Hoffman, D.W., et al., *Crystal Structure of Prokaryotic Ribosomal Protein L9: a bi-lobed RNA-binding Protein.* EMBO J., 1994. **13**: p. 205-12.
3. Kuhlman, B., H.Y. Yang, J.A. Boice, R. Fairman and D.P. Raleigh, *An exceptionally stable helix from the ribosomal protein L9: implications for protein folding and stability.* J. Mol. Biol., 1997. **270**(5): p. 640-7.
4. Branlant, C., A. Krol, J. Sriwidada and R. Brimacombe, *RNA sequences associated with proteins L1, L9, and L5, L18, L25, in ribonucleoprotein fragments isolated from the 50-S subunit of Escherichia coli ribosomes.* Eur. J. Biochem., 1976. **70**(2): p. 483-92.
5. Adamski, F.M., J.F. Atkins and R.F. Gesteland, *Ribosomal protein L9 interactions with 23 S rRNA: the use of a translational bypass assay to study the effect of amino acid substitutions.* J. Mol. Biol., 1996. **261**(3): p. 357-71.
6. Tumminia, S.J., W. Hellmann, J.S. Wall and M. Boublik, *Visualization of protein-nucleic acid interactions involved in the in vitro assembly of the Escherichia coli 50 S ribosomal subunit.* J. Mol. Biol., 1994. **235**(4): p. 1239-50.
7. Kraulis, P.J., *MOLSCRIPT: A Program to Produce Both Detailed and Schematic Plots of Protein Structures.* J. Appl. Crystallogr., 1991. **24**: p. 946-50.
8. Hoffman, D.W., C.S. Cameron, C. Davies, S.W. White and V. Ramakrishnan, *Ribosomal Protein L9: A Structure Determination by the Use of X-ray Crystallography and NMR Spectroscopy.* J. Mol. Biol., 1996. **264**: p. 1058-71.
9. Lillemoen, J., C.S. Cameron and D.W. Hoffman, *The stability and dynamics of ribosomal protein L9: investigations of a molecular strut by amide proton exchange and circular dichroism.* J. Mol. Biol., 1997. **268**(2): p. 482-93.
10. Waltho, J.P., V.A. Feher, G. Merutka, H.J. Dyson and P.E. Wright, *Peptide Models of Protein Folding Sites. 1. Secondary Structure Formation by Peptides Corresponding to the G- and H-helicies of myoglobin.* Biochem., 1993. **32**: p. 6337-47.
11. Barbato, G., M. Ikura, L.E. Kay, R.W. Pastor and A. Bax, *Backbone Dynamics of Calmodulin Studied by N15 Relaxation Using Inverse Detected*

Two-Dimensional NMR Spectroscopy: the Central Helix is Flexible. Biochem., 1992. **31**: p. 5269-78.
12. Slupsky, C.M. and B.D. Sykes, *NMR Solution Structure of Calcium-Saturated Skeletal Muscle Troponin C.* Biochem., 1995. **34**: p. 563-7.
13. Sato, S., B. Kuhlman, W.-J. Wu and D.P. Raleigh, *Folding of the multidomain ribosomal protein L9: The two domains fold independently with remarkably different rates.* Biochem., 1999. **38**(17): p. 5643-50.
14. Sato, S. and D.P. Raleigh, *pH Dependent Stability and Folding Kinetics of a Protein with an Unusual alpha-beta Topology: The C-Terminal Domain of Ribosomal Protein L9.* J. Mol. Biol., 2002. **318**: p. 571-82.
15. Luisi, D.L., W.-J. Wu and D.P. Raleigh, *Conformational Analysis of a Set of Peptides Corresponding to the Entire N-terminal Domain of the Ribosomal Protein L9: Evidence for a Stable Native-like Secondary Structure in the Unfolded State.* J. Mol. Biol., 1999. **287**: p. 395-407.
16. Luisi, D.L., B. Kuhlman, K. Sideras, P.A. Evans and D.P. Raleigh, *Effects of Varying the Local Propensity to form Secondary Structure on the Stability and Folding Kinetics of a Rapid Folding alpha/beta Protein: Characterization of a Truncation Mutant of the N-Terminal Domain of the Ribosomal Protein L9.* J. Mol. Biol., 1999. **289**: p. 167-74.
17. Sato, S., D.L. Luisi and D.P. Raleigh, *pH Jump Studies of the Folding of the Multidomain Ribosomal Protein L9: The Structural Organization of the N-Terminal Domain Does Not Affect teh Anomolously Slow Folding of the C-Terminal Domain.* Biochem., 2000. **39**(16): p. 4995-62.
18. Downard, K.M. and K. Beimann, *The effect of charge state and the localization of charge on the collision-induced dissociation of peptide ions.* J. Am. Soc. Mass Spectrom., 1994. **5**(11): p. 966-75.
19. Summerfield, S.G. and S.J. Gaskell, *Fragmentation efficiencies of peptide ions following low energy collisional activation.* Int. J. Mass Spectrom. Ion Processes, 1997. **165/166**: p. 509-21.
20. Wattenberg, A., A.J. Organ, K. Schneider, R. Tyldesley, R. Bordoli, and R.H. Bateman, *Sequence Dependent Fragmentation of Peptides Generated by MALDI Quadrupole Time-of_Flight (MALDI Q-TOF) Mass Spectrometry and its Implications for Protein Identification.* J. Am. Soc. Mass Spectrom., 2002. **13**: p. 772-83.
21. Wells, J.M., J.L. Stephenson and S.A. McLuckey, *Charge dependance of protonated insulin decompositions.* Int. J. Mass Spectrom., 2000. **203**(1-3): p. A1-A9.
22. Butcher, D.J., K.G. Asano, D.E. Goeringer and S.A. McLuckey, *Thermal dissociation of gaseous bradykinin ions.* J. Phys. Chem. A, 1999. **103**(43): p. 8664-71.
23. Roepstorff, P., *Proposal for a common nomenclature for sequence ions in mass spectra of peptides.* Biomed. Mass Spectrom., 1984. **11**(11): p. 601.

24. Johnson, R.S., S.A. Martin, K. Biemann, J.T. Stults and J.T. Watson, *Novel Fragmentation Process of Peptides by Collision-Induced Decomposition in a Tandem Mass Spectrometer: Differentiation between Leucine and Isoleucine.* Anal. Chem., 1987. **59**: p. 2621-5.
25. Wysocki, V.H., G. Tsaprailis, L.L. Smith and L.A. Breci, *Mobile and localized protons: a framework for understanding peptide dissociation.* J. Mass Spectrom., 2000. **35**: p. 1399-406.
26. Tsaprailis, G., A. Somogyi, E.N. Nikolaev and V.H. Wysocki, *Refining the model for selective cleavage at acidic residues in arginine-containing protonated peptides.* Int. J. Mass Spectrom., 2000. **195/196**: p. 467-79.
27. Gu, C., G. Tsaprailis, L. Breci and V.H. Wysocki, *Selective Gas-Phase Cleavage at the Peptide Bond C-Terminal to Aspartic Acid in Fixed-Charge Derivative of Asp-Containing Peptides.* Anal. Chem., 2000. **72**: p. 5804-13.
28. Breci, L.A., D.L. Tabb, J.R.I. Yates and V.H. Wysocki, *Cleavage N-Terminal to Proline: Analysis of a Database of Peptide Tandem Mass Spectra.* Anal. Chem., 2003. **75**(9): p. 1963-71.

CHAPTER 3: DISSOCIATION DATA FOR ELECTROSPRAYED RIBOSOMAL PROTEIN L9 USING FTICR-MS

3.1 INTRODUCTION

This chapter presents the dissociation data that were acquired when L9 was subject to infrared multi-photon dissociation (IRMPD) and sustained off-resonance irradiation (SORI) using FT-ICR-MS. The isolation of each of L9's observable charge states enabled low energy dissociation to be performed. The general fragmentation presented here is used in subsequent chapters to define the location of charge using complementary pair analysis. The location of charge was used to create model structures that were subjected to molecular modeling simulations. Threshold energy for dissociation was determined to establish the lowest energy fragmentation pathways.

When L9 is electrosprayed in the positive mode, sixteen charge states are observed. Each charge state is subjected to dissociation experiments while varying the dissociation energy thus yielding a large body of data. In order to extract useful information from these results, it is necessary to catalog the spectra and the data contained in each spectrum. These data are the foundation of the analyses presented in Chapters 4, 5, and 6. Tabulated lists of b and y fragments are presented, with the complete collection of spectra cataloged in the Appendix A. Regions that are highly

susceptible to cleavage are highlighted, along with situations that promote losses of small neutral molecules, like water and ammonia.

Only b and y fragments are presented since they are the fragment types typically observed when sustained off-resonance irradiation (SORI) and infrared multi-photon dissociation (IRMPD) are used to effect dissociation.[1,2] Internal fragments, generated from the b/y cleavage of two peptide bonds and containing neither terminus, were likely formed because of the nature of IRMPD. The fragment ions are produced on axis at the center of the cell, and remain in the laser beam's cross-section thereby increasing the likelihood of internal fragment formation.[2] These internal fragments have not been identified because of to the very high number of possible internal fragments (~40,000) that could be generated. The presence of multiple fragments of the same average mass and the same charge state makes their assignment impractical. Even with FTICR's excellent resolution, and mass accuracy, the internal fragments could not be definitively identified.

3.2 EXPERIMENTAL

3.2.1 Sample Preparation

The original ribosomal protein L9 sample was provided by Dr. David Hoffman (Austin, TX) as a stock solution with a concentration of 2 mg/mL in water, and was used without further purification. L9 solutions with final analyte

concentrations of 10 □M in a 50:49:1 (v:v:v) methanol:water:acetic acid or 50:50 (v:v) methanol:water were prepared. Samples were introduced into the electrospray chamber at a flow rate of 0.5 μL/min, using a syringe pump (Harvard Apparatus, South Natick, MA).

3.2.2 Instrumentation

Experiments were performed on a 9.4 Tesla external source ESI/FTICR/MS (National High Magnetic Field Laboratory, Tallahassee, FL). The details of the spectrometer have been described elsewhere.[3] A Chait-style electrospray source, with a 25 μm i.d. fused silica spray needle, was interfaced to this system. Ion desolvation was accomplished using a resistively heated, 500 μm i.d. stainless steel desolvating capillary. Upon exiting the desolvating capillary, ions were focused into a 0.8 mm i.d. octopole rod set with the use of an electrostatic tube lens. The ions passed through a 0.8 mm diameter skimmer to a 60 cm RF-only long octopole, where they were accumulated by biasing its entrance and exit conductance limits to a positive potential for 2-5 s.[4] They were then transferred by a second octopole (2 m in length) to a 4-inch diameter open cylindrical Penning ion trap.[3]

The charge state of interest was isolated using a stored waveform inverse Fourier transform (SWIFT) waveform.[5] Upon isolation, infrared multi-photon dissociation (IRMPD) and or sustained off-resonance irradiation (SORI) was applied to the ions to induce fragmentation. IRMPD was achieved using 0.5 s shots from a continuous wave CO2 laser. The laser power was varied from 1 W to 20 W,

with an additional blank spectrum collected for each charge state where the laser power was set to 0 W. SORI was performed on the +20, +21, and +22 charge states in order to provide additional information on these charge states. The excite frequency was applied at 1000 Hz above and below the observed cyclotron frequency of the precursor ion. The ions were subjected to the off-resonance excite frequency for 0.25 s at cell pressures of 1 x 10^{-6} Torr of nitrogen.

After a cooling delay of up to 5 s, fragment ions were excited with a frequency excitation sweep from 36 kHz to 655 kHz at 215 Hz/μs. Spectra were acquired in direct mode over a 640 kHz bandwidth with 1 M data points. Spectra shown are the sum of a minimum of 25 scans. Typical cell pressures were in the mid- 10^{-9} Torr range during the detection events. The MIDAS data station controlled the instrument and data acquisition.[6]

3.2.3 Data Analysis

Primary data analysis was performed in MIDAS Analysis. Peak lists were generated using THRASH, the built-in automatic functions for peak picking, applying centroid fitting for each peak.[7] The automatic peak selection was inspected visually and adjusted when necessary. Peaks with signal-to-noise less than 3:1 were not included in the peak list. Each peak list was then reduced to a list of isotopic clusters and the monoisotopic mass to charge was used to determine the fragment identity. A total list of fragments as generated by MS-Product was also used to verify the identity of the peaks.[8] Spectra are presented as figures

generated from ICR 2LS.[9] This experimental outline applies to the data in Chapters 4, 5, and 6.

3.3 RESULTS AND CONCLUSIONS

Figure 3.1 shows the full charge state envelope of L9. Charge states +10 through +25 were routinely detected. Isotopic resolution is demonstrated by the insets for charge states +10, +17, and +25. The ability to observe isotopic resolution is essential to assigning charge states to the fragments that result from dissociation.

The charge state envelope displayed a bimodal distribution with the +17 was the most abundant charge state. A high abundance distribution involving the +17, +19, and +20 charge states was observed, and a lower abundance distribution comprised of the remaining charge states. Konermann presented evidence that changes in tertiary structure are reflected in the abundance and distribution of the charge states in the charge envelope.[10] The shift from low to high charge states occurred as a result of the breakdown in tertiary structure. Recent studies have been focused on how charge-state distribution and abundance can indicate changes in secondary and tertiary structure.[11-14] It has suggested that Coulombic repulsion considerations override intermolecular stabilizations resulting in more compact conformations of the higher charge states. Babu *et al.* related bimodal distributions to partially unfolded proteins with induced α-helices when methanol is the

solvent.[15] Other experiments showed that the two distributions may be inter-converting conformers.

Figure 3.2 shows the general regions of L9 where elevated amounts of fragmentation were observed. On the N-terminus, Lys7 through Lys15 showed high fragmentation. Also on the N-terminus, Asp23/Gly24 was a very facile cleavage point. Leu35 through Thr40 was the final region on the N-terminus that showed high fragmentation across most of the charge states. On the α-helix, fragmentation was prominently lacking except for pair, Glu70/Gln71, in only 4 charge states. On the C-terminal, fragmentation was predominantly localized between Val132 and Lys149. There were two pairs of amino acids showed fragmentation across most of the charge states, Asp111/Lys112 and Asp119/Ala120. Other b/y fragments are present, but these highlight the area that repeated show up in different charge states.

Also evident is the appearance of loss of neutral molecules in some of the spectra. The data showed that the loss of water and ammonia molecules was most widespread in the lower charge states and at high dissociation energies. But at the +20, this was the first instance in which neutral molecule losses appeared in the low energy spectra.

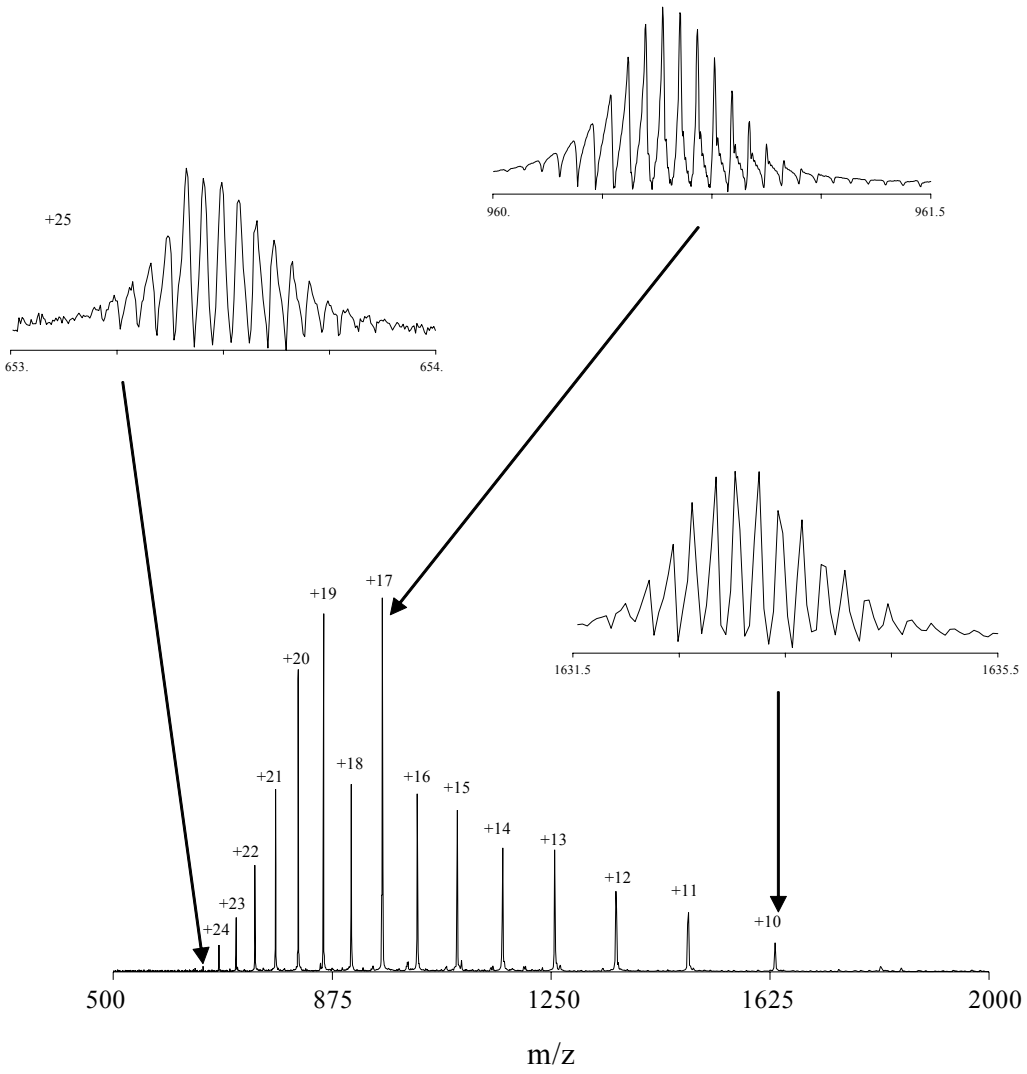

Figure 3.1: Charge state envelope of electrosprayed Ribosomal Protein L9. Charge states +10, +17, and +25 are shown in insets to illustrate the isotopic resolution capabilities of the 9.4 Tesla mass spectrometer.

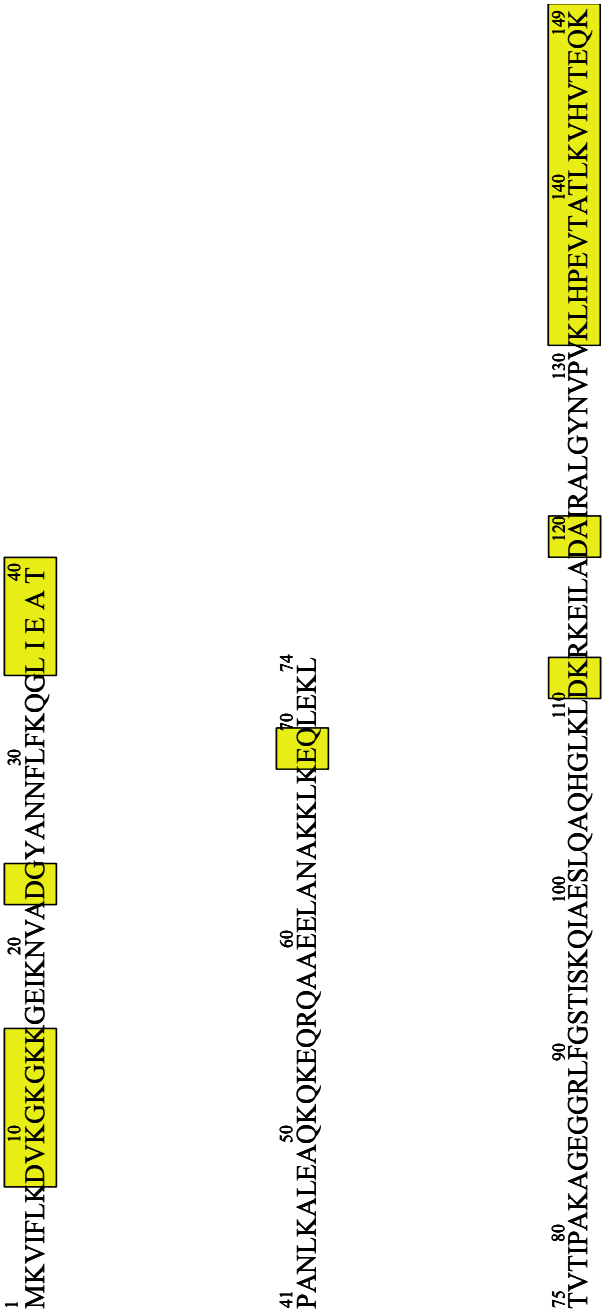

Figure 3.2: Amino acid map of L9 showing the general areas of fragmentation across the charge states.

Table 3.1 shows a matrix identifying the IRMPD data that were obtained. This data set consists of 115 spectra acquired at varying laser powers. A blank spectrum was always obtained, with the laser power set to 0 Watts, as a control. The fragments that were detected in these blank spectra were usually of very low relative abundances.

Tables 3.2 through 3.17 show all of the identified b and y fragments, and their charge, for each of the spectra obtained.[16] Tables 3.18 through 3.20 provide the analagous results from the sustained off-resonance irradiation of the +20 through +22 charge states. The nature of the off-resonance excitation in SORI results in a blind spot in the spectrum, so two spectra were collected for each SORI data point. The tables display the merging of the resulting fragments from the both spectra so as to eliminate the blind spot. Complementary pair analysis is used to determine where charge is located on the protein. A complementary pair is a pair of b/y fragments that result from cleavage of one peptide bond and the addition of their masses and charges result in the parent ion's mass and charge. Chapter 4 makes extensive use of these data and the presence of complementary pairs therein to deduce the location of the charge for each observable charge state. The fragment tables are also used to determine the threshold dissociation laser power for the IRMPD data. The implications of the threshold dissociation data are discussed in Chapter 6.

Table 3.1: Matrix of the dissociation spectra obtained by IRMPD for each charge state of L9. The laser power for dissociation is in Watts.

	Charge State															
Laser Power	+10	+11	+12	+13	+14	+15	+16	+17	+18	+19	+20	+21	+22	+23	+24	+25
0W	+	+	+	+	+	+	+	+	+	+	+	+	+	+	+	+
1W											+					
2W								+		+	+	+	+		+	
3W									+		+	+	+	+	+	+
4W						+	+	+	+	+	+	+	+	+	+	+
5W								+				+	+	+	+	+
6W						+		+	+	+		+	+	+	+	+
7W	+	+				+						+	+	+		+
8W	+	+	+	+		+	+	+	+	+		+	+	+	+	
9W	+	+	+						+							+
10W	+	+	+			+	+			+						
11W		+	+													+
12W	+	+	+	+	+	+	+		+	+		+				+
14W			+	+	+				+							
16W		+	+		+	+			+	+						
18W					+											
20W					+		+		+	+						

Table 3.2: Fragments for the +10 charge state at varying laser power (Watts).

0W	7W	8W	9W	10W	12W
b-4 +1	b-23 +2	b-23 +2	b-23 +2	b-10 +1	b-10 +1
b-8 +2	b-8 +2	y-148 +10	b-4 +1	b-23 +2	b-14 +2
y-138 +9	y-138 +9		b-7 +3	y-126 +8	b-23 +2
y-4 +1	y-5 +2		b-8 +4	y-133 +9	b-37 +3
	y-8 +2		y-133 +9	y-138 +9	b-4 +1
			y-138 +9	y-148 +10	b-40 +3
			y-8 +4	y-4 +1	b-6 +1
				y138-NH3 +9	b-7 +1
					b-9 +2
					y-126 +8
					y-138 +9
					y-148 +10
					y-5 +2
					y138-H2O +9

Table 3.3: Fragments for the +11 charge state at varying laser power (Watts).

0W	7W	8W	9W	10W	11W	12W	16W
b-11 +3	b-10 +1	b-10 +1	b-10 +1	b-10 +1	b-10 +1	b-10 +1	b-10 +1
b-4 +1	b-147 +11	b-23 +2	b-139 +10	b-116 +8	b-15 +2	b-139 +10	b-112 +8
b-8 +2	b-23 +2	b-24 +4	b-23 +2	b-13 +2	b-19 +2	b-15 +2	b-12 +2
y-139 +10	b-8 +2	y-139 +10	b-4 +1	b-139 +10	b-23 +2	b-19 +2	b-12 +1
y-4 +1	y-139 +10	y-4 +1	y-147 +10	b-15 +2	b-36 +3	b-23 +2	b-14 +2
y-6 +1	y-15 +4	y-5 +2	y-7 +3	b-19 +2	b-4 +1	b-35 +3	b-15 +2
y-8 +2	y-4 +1	y-6 +1	y-8 +2	b-23 +2	b-7 +1	b-36 +3	b-18 +2
	y-6 +1	y-7 +3		b-4 +1	b-8 +2	b-7 +1	b-19 +2
	y-8 +2			b-7 +1	y-125 +9	b-70 +5	b-23 +2
				b-70 +5	y-134 +10	b-8 +1	b-36 +3
				b-8 +2	y-148 +11	b-9 +1	b-37 +3
				y-134 +10	y-33 +3	y-125 +9	b-39 +4
				y-139 +10	y-38 +4	y-139 +10	b-39 +3
				y-148 +11	y-8 +2	y-148 +11	b-6 +1
				y-33 +3	b23-H2O +2	y-2 +1	b-7 +1
				y-4 +1		y-30 +3	b-8 +2
				y-8 +4		y-33 +3	b-8 +1
				y-8 +3		y-38 +4	b-9 +1
				y-8 +2		y-6 +1	y7-H2O +1
				y8-NH3 +1		y-7 +3	b15-H2O +2
				y148-H2O +11		y33-H2O +3	b8-H2O +1
						b36-H2O +3	b19-H2O +2
						y139-H2O +10	y30-H2O +3
						b70-H2O +5	y20-H2O +2
							y33-H2O + 3
							b36-H2O +3
							b37-H2O +3

Table 3.4: Fragments for the +12 charge state at varying laser powers (Watts), continued on next page.

0W	8W	9W	10W	11W	12W	14W	16W
b-8 +2	b-147 +11	b-147 +11	b-10 +1	b-10 +1	b-10 +1	b-111 +8	b-10 +1
y-6 +2	b-23 +2	b-23 +2	b-14 +2	b-119 +8	b-116 +9	b-119 +8	b-110 +8
	y-126 +10	y-126 +10	b-147 +11	b-14 +2	b-116 +8	b-12 +2	b-116 +8
	y-130 +10	y-126 +8	b-23 +2	b-147 +11	b-139 +11	b-14 +2	b-12 +2
	y-139 +11	y-130 +10	b-4 +1	b-23 +2	b-14 +2	b-148 +12	b-12 +1
	y-142 +11	y-139 +11	b-70 +6	b-36 +4	b-147 +11	b-23 +3	b-129 +10
		y-142 +11	y-126 +10	b-37 +4	b-23 +2	b-23 +2	b-139 +11
		y-8 +2	y-126 +9	b-70 +6	b-38 +4	b-36 +4	b-14 +2
			y-130 +10	b-70 +5	b-39 +4	b-36 +3	b-14 +1
			y-139 +11	b-8 +2	b-39 +3	b-37 +4	b-145 +11
			y-142 +11	y-109 +9	b-70 +6	b-38 +4	b-147 +11
			y-30 +4	y-126 +10	b-70 +5	b-38 +3	b-148 +12
			y-130 +10	y-126 +9	y-109 +9	b-39 +4	b-15 +2
			y126-H2O +10	y-126 +8	b-40 +4	b-39 +3	b-17 +2
				y-109 +8	y-110 +9	b-19 +2	b-23 +3
				y-134 +10	y-111 +8	b-7 +1	b-23 +2
				y-139 +11	y-126 +10	b-70 +6	b-36 +4
				y-139 +9	y-126 +8	b-70 +5	b-36 +3
				y-139 +8	y-130 +10	b-8 +2	b-37 +4
				y-141 +11	y-134 +10	b-9 +1	b-38 +4
				y-142 +11	y-135 +10	y-109 +9	b-38 +3
				y-30 +4	y-139 +11	y-110 +9	b-39 +4
				y-38 +5	y-139 +9	y-111 +9	b-4 +1
				y-64 +7	y-142 +11	y-111 +8	b-40 +4
				y-8 +2	y-30 +4	y-126 +10	b-7 +1
				y139-NH3 +11	y-33 +4	y-126 +9	b-70 +6
				b147-H2O +11	y-38 +5	y-126 +10	b-8 +2
					y-38 +4	y-130 +10	b-9 +1
					y-64 +7	y-134 +10	y-106 +7
					y-79 +7	y-135 +10	y-109 +9
					y139-NH3 +11	y-139 +11	y-110 +10
					y126-H2O +10	y-139 +10	y-110 +8
					b147-NH3 +11	y-139 +9	y-111 +9
						y-141 +11	y-111 +8
						y-142 +11	y-123 +9
						y-147 +11	y-126 +10
						y-30 +4	y-126 +9
						y-30 +2	y-126 +8
						y-33 +4	y-130 +10
						y-38 +5	y-134 +10
						y-4 +1	y-135 +10
						y-64 +7	y-139 +11
						y30-H2O +4	y-141 +11
						b23-H2O +2	y-148 +12
						y139-H2O +11	y-17 +2
						y142-NH3 +11	y-20 +2
						y139-NH3 +10	y-30 +4
						y126-H2O +9	y-30 +3
						y139-H2O +9	y-30 +2
							y-33 +4
							y-33 +3
							y-36 +4
							y-37 +4
							y-38 +5
							y-38 +4
							y-64 +7
							y-64 +6
							y-8 +2
							y-83 +7

0W	8W	9W	10W	11W	12W	14W	16W
							b147-H2O +11
							b15-NH3 +2
							b19-H2O +2
							b23-H2O +2
							b36-H2O +3
							b37-NH3 +4
							b38-H2O +3
							b70-H2O +6
							y110-H2O +8
							y110-NH3 +9
							y111-H2O +9
							y126-H2O +10
							y126-H2O +9
							y135-H2O +10
							y139-NH3 +11
							y30-H2O +4
							y31-H2O +2
							y33-NH3 +3
							y38-H2O +4
							y38-NH3 +5
							y64-H2O +7

Table 3.5: Fragments for the +13 charge state at varying laser powers (Watts).

0W	8W	12W	14W
b-23 +2	b-10 +1	b-10 +1	b-10 +1
b-4 +1	b-23 +2	b-111 +9	b-111 +9
b-8 +2	b-8 +2	b-12 +2	b-12 +2
y-4 +1	y-4 +1	b-15 +2	b-23 +2
y-8 +2	y-6 +1	b-19 +2	b-37 +4
	y-7 +2	b-23 +2	b-38 +4
	y-8 +2	b-35 +4	b-40 +4
		b-37 +4	b-8 +2
		b-38 +4	y-30 +4
		b-39 +4	y-38 +5
		b-40 +4	y-8 +2
		b-7 +1	
		b-70 +6	
		y-30 +4	
		y-33 +4	
		y-38 +5	
		y-5 +2	
		y-6 +1	
		b37-NH3 +4	

Table 3.6: Fragments for the +14 charge state at varying laser powers (Watts).

0W	12W	14W	16W	18W	20W
b-27 +5	b-111 +10	b-111 +10	b-12 +2	b-10 +1	b-10 +1
y-24 +7	b-12 +2	b-12 +2	b-14 +2	b-111 +9	b-111 +10
	b-23 +2	b-23 +2	b-23 +2	b-12 +2	b-12 +2
	b-38 +4	b-35 +4	b-35 +4	b-14 +2	b-14 +2
	b-8 +2	b-37 +4	b-36 +4	b-23 +2	b-23 +2
	y-30 +4	b-38 +4	b-37 +4	b-35 +4	b-35 +4
	y-38 +5	b-39 +5	b-38 +4	b-36 +4	b-36 +4
		b-39 +4	b-39 +4	b-37 +4	b-38 +4
		b-40 +4	b-40 +4	b-38 +4	b-39 +5
		b-6 +3	y-110 +10	b-39 +4	b-39 +4
		y-111 +10	y-30 +4	b-40 +4	b-4 +1
		y-30 +4	y-38 +5	b-6 +2	b-40 +4
		y-38 +5	y-4 +1	b-7 +1	b-7 +1
		y-6 +3	y-64 +7	b-8 +1	b-8 +1
			y38-H2O +5	b-85 +7	b-85 +7
			b38-H2O +4	y-109 +10	y-30 +4
				y-110 +10	y-33 +4
				y-111 +10	y-38 +5
				y-142 +13	y30-H2O +4
				y-25 +6	y38-H2O +5
				y-27 +7	b38-H2O +4
				y-30 +4	
				y-33 +4	
				y-38 +5	
				y-6 +3	
				y30-H2O +4	
				y38-H2O +5	
				b36-NH3 +4	

Table 3.7: Fragments for the +15 charge state at varying laser powers (Watts).

0W	4W	6W	7W	8W	10W	12W	16W
b-8 +4	b-126 +13	b-126 +13	b-111 +10	b-10 +2	b-12 +2	b-10 +2	b-10 +2
	y-4 +1	b-30 +11	b-12 +2	b-12 +2	b-23 +3	b-111 +10	b-10 +1
	y-6 +3	b-31 +6	b-25 +4	b-27 +5	b-23 +2	b-12 +2	b-111 +10
		y-107 +11	b-39 +5	b-4 +1	b-35 +4	b-14 +2	b-12 +2
		y-6 +3	y-107 +11	b-6 +3	b-36 +4	b-15 +2	b-12 +1
		b126-NH3 +13	y-30 +4	y-132 +13	b-38 +4	b-17 +2	b-14 +2
				y-27 +8	b-8 +1	b-19 +3	b-15 +2
				y-30 +4	y-107 +11	b-23 +3	b-19 +3
				y-38 +5	y-141 +14	b-23 +2	b-19 +2
				y-79 +8	y-30 +4	b-31 +4	b-22 +3
				y-8 +2	y-38 +5	b-35 +4	b-23 +3
					y-64 +7	b-36 +3	b-23 +2
					y-7 +3	b-37 +4	b-27 +5
					y-79 +8	b-38 +4	b-28 +7
						b-39 +4	b-31 +3
						b-7 +1	b-35 +4
						b-8 +2	b-36 +4
						b-8 +1	b-36 +3
						b-85 +8	b-37 +4
						y-11 +2	b-38 +4
						y-111 +10	b-39 +4
						y-114 +11	b-40 +4
						y-117 +11	b-6 +1
						y-141 +14	b-7 +1
						y-2 +1	b-8 +4
						y-20 +3	b-8 +1
						y-30 +4	b - 9
						y-33 +4	y-111 +10
						y-38 +5	y-13 +2
						y-5 +2	y-2 +1
						y-64 +7	y-20 +3
						y-67 +7	y-20 +2
						y-70 +7	y-30 +4
						y-79 +8	y-33 +4
						y30-H2O +4	y-36 +4
						b15-H2O +2	y-38 +5
						y117-H2O +11	y-4 +1
							y-6 +1
							y-64 +7
							y-7 +1
							y-70 +7
							y-72 +6
							y-8 +3
							y-8 +2
							y33-H2O +4
							b8-NH3 +1
							b36-H2O +4
							y64-H2O +7
							y70-H2O +7
							b111-H2O +10
							y111-NH3 +10
							b23-H2O +2
							b36-NH3 +3

Table 3.8: Fragments from the +16 charge state at varying laser power (Watts).

0W	4W	8W	10W	12W	20W
b-23 +2	b-23 +2	b-23 +2	b-134 +13	b-10 +2	b-10 +2
y-5 +2	b-4 +1	b-6 +2	b-14 +2	b-10 +1	b-10 +1
	y-7 +3	y-137 +14	b-19 +3	b-12 +2	b-12 +2
	b-8 +2	y-38 +5	b-23 +2	b-14 +2	b-14 +2
	y-4 +1	y-4 +1	b-38 +4	b-17 +2	b-17 +2
		y-8 +2	b-4 +1	b-19 +3	b-19 +3
			b-85 +9	b-23 +3	b-23 +3
			b-85 +8	b-23 +2	b-23 +2
			y-130 +13	b-36 +4	b-36 +4
			y-15 +3	b-38 +4	b-38 +4
			y-30 +4	b-39 +4	b-39 +4
			y-38 +5	b-40 +4	b-40 +4
			y-4 +1	b-43 +4	b-43 +4
			y-5 +2	b-6 +1	b-6 +1
			y-64 +7	b-7 +1	b-7 +1
			y-7 +3	b-8 +1	b-8 +1
			y-8 +4	b-9 +1	b-9 +1
				y-125 +8	y-125 +8
				y-16 +2	y-16 +2
				y-2 +1	y-2 +1
				y-30 +4	y-30 +4
				y-33 +4	y-33 +4
				y-38 +5	y-38 +5
				y-4 +1	y-4 +1
				y-64 +7	y-64 +7
				y-7 +3	y-7 +3
				y-7 +1	y-7 +1
				y-8 +4	y-8 +4
				b23-H2O +3	b6-H2O +1
				y38-H2O +5	b23-H2O +3
				b36-H2O +4	y38-H2O +5
				b43-NH3 +4	b8-H2O +1
					b36-H2O +4
					b38-H2O +4
					b43-NH3 +4

Table 3.9: Fragments of the +17 charge state at varying laser powers (Watts).

0W	2W	4W	5W	6W	8W	12W
b-4 +1		y-5 +2	b-15 +6	b-4 +1	b-11 +3	b-23 +2
				y-4 +1	y-4 +1	b-39 +6
						y-30 +4
						y-38 +5

Table 3.10: Fragments of the +18 charge state at varying laser powers (Watts).

0W	3W	4W	6W	8W	9W	12W	14W	16W	20W
y-38 +5	b-39 +6	b-39 +5	b-111 +12	b-30 +5	b-147 +17	b-111 +13	b-10 +2	b-10 +2	b-10 +2
	b-39 +5	b-4 +1	b-35 +5	b-39 +5	b-36 +5	b-12 +2	b-111 +13	b-12 +2	b-12 +2
	b-7 +3	y-15 +3	b-36 +5	b-8 +2	b-36 +4	b-35 +5	b-119 +13	b-19 +3	b-14 +2
	b-8 +2	y-2 +1	b-36 +4	y-15 +3	y-2 +1	b-36 +4	b-12 +2	b-23 +4	b-19 +3
	y-2 +1	y-38 +6	y-113 +13	y-2 +1	y-30 +5	b-38 +5	b-19 +3	b-28 +4	b-23 +4
	y-38 +6		y-15 +3	y-38 +6	y-38 +6	y-15 +3	b-28 +4	b-29 +4	b-23 +3
	y-8 +2		y-2 +1	y-5 +2	y-38 +5	y-2 +1	b-29 +4	b-30 +4	b-23 +2
			y-30 +5		y-8 +2	y-30 +5	b-30 +4	b-35 +5	b-28 +4
			y-38 +6			y-30 +4	b-35 +5	b-35 +4	b-29 +5
			y-38 +5			y-38 +6	b-36 +5	b-36 +5	b-29 +4
						y-38 +5	b-36 +4	b-36 +4	b-30 +5
							b-38 +5	b-37 +4	b-30 +4
							b-7 +1	b-38 +5	b-31 +4
							y-11 +2	b-38 +4	b-31 +3
							y-113 +13	b-40 +5	b-35 +5
							y-15 +3	b-7 +1	b-36 +5
							y-2 +1	b-8 +1	b-36 +4
							y-20 +3	b-85 +9	b-37 +4
							y-30 +5	y-15 +3	b-38 +5
							y-30 +4	y-2 +1	b-38 +4
							y-37 +5	y-20 +3	b-39 +4
							y-38 +6	y-30 +5	b-40 +4
							y-38 +5	y-30 +4	b-6 +1
							y-4 +1	y-37 +5	b-7 +1
							y-95 +12	y-38 +6	b-8 +1
							y38-H2O +6	y-38 +5	b-9 +1
							y38-H2O +5	y-64 +8	y-11 +2
							b111-H2O +13	y-8 +2	y-15 +3
							y113-H2O +13	y38-H2O +6	y-2 +1
								y38-H2O +5	y-20 +3
								y64-H2O +8	y-30 +5
									y-30 +4
									y-37 +5
									y-38 +6
									y-38 +5
									y-4 +1
									y-72 +7
									y-8 +2
									b12-H2O +2
									y38-H2O +6
									b29-H2O +4
									y30-H2O +4
									b23-H2O +3
									y38-H2O +5
									b31-H2O +4
									b8-H2O +1

Table 3.11: Fragments of the +19 charge state at varying laser powers (Watts).

0W	2W	4W	6W	8W	10W	12W	16W	20W
b-11 +3	y-15 +3	b-11 +3	b-7 +1	b-39 +6	b-111 +13	b-111 +13	b-15 +3	b-12 +2
b-39 +6	y-38 +6	b-6 +2	y-4 +1	b-6 +2	b-8 +2	b-29 +4	b-19 +3	b-19 +3
y-11 +3	y-38 +5	y-15 +3	y-41 +8	y-15 +3	y-38 +6	b-36 +4	b-23 +4	b-23 +3
	y-4 +1	y-7 +3	y-5 +2	y-38 +6	y-4 +1	y-15 +3	b-23 +3	b-23 +2
	y-5 +1			y-4 +1	y-5 +2	y-30 +5	b-28 +4	b-29 +4
	y-8 +2					y-38 +6	b-29 +4	b-30 +4
						y-38 +5	b-30 +4	b-36 +4
						y-5 +1	b-34 +4	b-7 +1
						y-95 +12	b-36 +4	y-15 +3
						b111-H2O +13	b-37 +4	y-2 +1
							b-38 +5	y-20 +3
							y-15 +3	y-30 +5
							y-2 +1	y-30 +4
							y-20 +3	y-38 +6
							y-30 +5	y-38 +5
							y-30 +4	y-4 +1
							y-37 +6	y-8 +2
							y-38 +6	y38-H2O +6
							y-38 +5	b36-H2O +4
							y-4 +1	
							y-71 +7	
							y38-H2O +6	
							y38-H2O +5	

Table 3.12: Fragments of +20 charge state at varying laser powers (Watts).

0W	1W	2W	3W	4W	5W
b-10 +1	b-10 +1	b-15 +1	b-10 +1	b-10 +1	b-10 +1
b-15 +1	b-111 +8	b-23 +2	b-111 +8	b-15 +1	b-147 +19
b-23 +2	b-37 +5	b-37 +5	b-15 +1	b-37 +5	b-15 +1
b-39 +6	b-39 +5	b-6 +2	b-20 +2	b-39 +5	b-19 +2
b-39 +5	b-4 +1	b-7 +1	b-23 +2	b-7 +1	b-23 +2
y-30 +4	b-7 +1	b-8 +1	b-37 +5	b-8 +1	b-37 +5
y-38 +6	b-8 +1	y-11 +2	b-7 +1	b-9 +4	b-39 +6
y-6 +2	b-9 +1	y-110 +8	b-8 +1	y-125 +8	b-39 +5
b23-H2O +2	y-125 +8	y-30 +4	y-125 +8	y-126 +8	b-4 +1
	y-30 +4	y-38 +5	y-30 +4	y-30 +4	b-7 +1
	y-38 +5	y-4 +1	y-38 +6	y-38 +6	b-8 +1
	y-6 +2	y-71 +5	y-38 +5	y-6 +2	y-109 +7
	y-8 +2	y-8 +2	y-4 +1	y-8 +2	y-126 +8
	b8-H2O +1	y8-NH3 +1	y-6 +2	b8-H2O +1	y-30 +4
		b8-H2O +1	y-71 +5	b15-H2O +1	y-38 +6
		b23-NH3 +2	y-8 +2		y-38 +5
		b23-H2O +2	b8-H2O +1		y-45 +12
			b15-H2O +1		b23-NH3 +2
					b15-H2O +1

Table 3.13: Fragment of +21 charge state at varying laser power (Watts).

0W	2W	3W	4W	5W	6W	7W	8W	12W
b-12 +2	b-10 +1	b-10 +1	b-23 +2	b-10 +1	b-10 +1	b-10 +1	b-10 +1	b-10 +2
b-23 +2	b-111 +15	b-111 +14	b-28 +4	b-23 +2	b-23 +2	b-111 +14	b-111 +14	b-10 +1
b-29 +5	b-111 +10	b-23 +2	b-29 +5	b-28 +4	b-29 +5	b-111 +11	b-119 +15	b-111 +15
b-29 +4	b-23 +2	b-28 +4	b-29 +4	b-29 +5	b-29 +4	b-147 +20	b-23 +2	b-111 +14
b-30 +5	b-29 +6	b-29 +6	b-30 +5	b-30 +5	b-30 +5	b-23 +3	b-28 +5	b-111 +11
b-36 +5	b-29 +5	b-29 +5	b-36 +5	b-35 +4	b-36 +9	b-23 +2	b-28 +4	b-15 +3
b-37 +6	b-29 +4	b-29 +4	b-37 +4	b-36 +4	b-36 +5	b-28 +5	b-29 +5	b-23 +4
b-37 +7	b-30 +5	b-30 +5	b-38 +4	b-38 +4	b-36 +4	b-28 +4	b-29 +4	b-23 +3
b-38 +4	b-36 +5	b-36 +5	b-39 +5	b-39 +5	b-37 +6	b-29 +5	b-30 +5	b-23 +2
b-39 +7	b-36 +4	b-36 +4	b-39 +4	y-120 +16	b-37 +4	b-29 +4	b-34 +5	b-27 +4
b-39 +5	b-37 +6	b-37 +6	b-8 +2	y-15 +3	b-38 +4	b-30 +5	b-34 +4	b-28 +5
b-39 +4	b-38 +4	b-38 +4	y-15 +3	y-2 +1	b-39 +7	b-34 +4	b-36 +5	b-28 +4
b-8 +2	b-39 +4	b-39 +7	y-2 +1	y-30 +5	b-39 +5	b-35 +4	b-36 +4	b-29 +5
b-8 +1	b-7 +1	b-39 +5	y-30 +4	y-30 +4	b-39 +4	b-36 +5	b-37 +6	b-29 +4
y-110 +15	b-70 +6	b-39 +4	y-38 +6	y-38 +6	b-4 +1	b-36 +4	b-39 +7	b-30 +5
y-15 +3	y-112 +15	b-8 +2		b36-H2O +4	b-8 +2	b-37 +6	b-39 +5	b-30 +4
y-2 +1	y-15 +3	y-109 +15			y-110 +15	b-38 +4	b-4 +1	b-34 +4
y-30 +5	y-2 +1	y-112 +15			y-113 +15	b-39 +7	b-40 +4	b-35 +4
y-30 +4	y-30 +4	y-15 +3			y-119 +16	b-39 +5	b-8 +2	b-36 +5
y-38 +6	y-38 +6	y-2 +1			y-120 +16	b-39 +4	y-109 +15	b-36 +4
y-64 +7	y-38 +5	y-30 +5			y-15 +3	y-110 +15	y-110 +15	b-36 +3
y-72 +7		y-38 +6			y-2 +1	y-111 +15	y-113 +16	b-37 +4
y-72 +6		y-4 +1			y-30 +5	y-113 +16	y-113 +15	b-38 +5
y-8 +2		y-64 +7			y-38 +6	y-113 +15	y-119 +16	b-38 +4
b39-NH3 +5		y-8 +2			y-8 +2	y-119 +16	y-120 +16	b-39 +7
					y111-H2O +20	y-139 +11	y-121 +16	b-39 +4
						y-15 +3	y-15 +3	b-40 +4
						y-2 +1	y-2 +1	b-8 +2
						y-30 +5	y-30 +5	b-8 +1
						y-38 +7	y-38 +6	b-80 +10
						y-38 +6	y-4 +1	y-15 +3
						y-64 +7	y110-NH3 +19	y-2 +1
						y-8 +2	y120-H2O +16	y-20 +4
						y111-H2O +15	y113-H2O +15	y-20 +3
						b36-H2O +4		y-30 +6
								y-30 +5
								y-30 +4
								y-38 +7
								y-38 +6
								y-38 +5
								y-6 +3
								y-8 +2
								y30-H2O +6
								b29-H2O +5
								y38-H2O +6
								b36-NH3 +5
								b111-NH3 +14

Table 3.14: Fragments of +22 charge state for varying laser powers (Watts).

0W	2W	3W	4W	5W	6W	7W	8W
b-29 +6	b-23 +2	b-28 +5	b-28 +5	b-28 +5	b-28 +5	b-28 +5	b-11 +3
b-39 +6	b-29 +6	b-29 +6	b-29 +6	b-29 +6	b-29 +6	b-29 +6	b-28 +5
y-6 +2	b-29 +5	b-29 +5	b-29 +5	b-29 +5	b-29 +5	b-29 +5	b-29 +6
y-6 +1	y-2 +1	b-6 +2	b-8 +2	b-6 +1	b-39 +6	b-30 +5	b-29 +5
	y-38 +6	y-6 +1	y-4 +1		b-6 +2	b-36 +6	b-30 +5
	y-38 +5	y-7 +2	y-8 +2		y-120 +16	b-36 +4	b-34 +5
	y-4 +1				y-38 +6	y-110 +16	b-36 +6
	y-5 +2				y-6 +1	y-112 +15	b-36 +5
	y-6 +1				y-7 +1	y-113 +16	b-39 +7
					y-8 +2	y-119 +17	b-39 +5
						y-38 +5	y-110 +16
						y-4 +1	y-113 +16
						y-7 +3	y-120 +16
						y-8 +2	y-38 +6
						y112-H2O +15	y-6 +1
							y-8 +2

Table 3.15: Fragments of +23 charge state at varying laser powers (Watts).

0W	3W	4W	5W	6W	7W	8W
b-10 +1	b-10 +1	b-10 +1	b-10 +1	b-10 +1	b-10 +1	b-10 +1
b-111 +10	b-12 +2	b-23 +3	b-111 +16	b-12 +2	b-111 +16	b-111 +16
b-23 +2	b-23 +2	b-23 +2	b-23 +3	b-15 +3	b-12 +2	b-12 +2
b-29 +6	b-28 +5	b-29 +6	b-23 +2	b-23 +3	b-23 +3	b-23 +2
b-29 +5	b-28 +4	b-29 +5	b-28 +4	b-23 +2	b-23 +2	b-27 +5
b-36 +5	b-29 +6	b-36 +5	b-29 +6	b-28 +5	b-28 +5	b-28 +5
b-36 +4	b-29 +5	b-36 +4	b-29 +5	b-28 +4	b-28 +4	b-28 +4
b-38 +4	b-29 +4	b-37 +7	b-29 +4	b-29 +6	b-29 +6	b-29 +6
b-39 +7	b-30 +5	b-38 +4	b-30 +5	b-29 +5	b-29 +5	b-29 +5
b-39 +4	b-30 +4	b-39 +7	b-30 +4	b-29 +4	b-29 +4	b-29 +4
b-40 +4	b-36 +4	b-39 +6	b-35 +4	b-30 +6	b-30 +6	b-30 +5
b-7 +1	b-36 +3	b-39 +4	b-36 +6	b-30 +5	b-30 +5	b-30 +4
y-11 +2	b-37 +7	b-7 +1	b-36 +5	b-30 +4	b-30 +4	b-31 +5
y-120 +17	b-38 +4	y-120 +17	b-36 +4	b-31 +4	b-31 +5	b-34 +4
y-15 +3	b-39 +7	y-15 +3	b-36 +3	b-36 +6	b-34 +8	b-35 +5
y-18 +2	b-39 +5	y-2 +1	b-37 +7	b-36 +5	b-34 +5	b-36 +5
y-2 +1	b-39 +4	y-30 +4	b-37 +4	b-36 +4	b-34 +4	b-36 +4
y-30 +4	b-40 +4	y-38 +5	b-38 +4	b-37 +7	b-35 +5	b-37 +4
y-38 +5	b-7 +1	y-75 +7	b-39 +7	b-37 +6	b-36 +7	b-38 +4
	b-8 +2		b-39 +4	b-37 +4	b-36 +6	b-39 +6
	y-120 +17		b-40 +4	b-38 +4	b-36 +5	b-39 +5
	y-15 +3		b-6 +1	b-39 +7	b-36 +4	b-39 +4
	y-2 +1		b-7 +1	b-39 +6	b-37 +7	b-7 +1
	y-30 +5		y-109 +16	b-39 +5	b-37 +6	y-109 +16
	y-30 +4		y-120 +18	b-39 +4	b-37 +4	y-113 +18
	y-5 +2		y-120 +17	b-40 +7	b-38 +4	y-113 +16
	y-75 +7		y-15 +3	b-40 +4	b-39 +7	y-119 +18
			y-2 +1	b-6 +2	b-39 +5	y-120 +18
			y-30 +5	b-7 +2	b-39 +4	y-120 +17
			y-30 +4	b-7 +1	b-7 +1	y-15 +3
			y-38 +7	y-109 +16	b-8 +2	y-2 +1
			y-38 +5	y-110 +16	y-111 +17	y-30 +6
			y-5 +1	y-111 +11	y-112 +16	y-30 +5
			y-75 +7	y-112 +16	y-113 +17	y-30 +4
				y-113 +17	y-113 +16	y-31 +6
				y-113 +16	y-119 +18	y-38 +8
				y-120 +18	y-120 +18	y-38 +7
				y-120 +17	y-120 +17	y-5 +1
				y-15 +3	y-142 +17	y-6 +1
				y-15 +2	y-15 +3	b28-NH3 +5
				y-2 +1	y-30 +5	b30-NH3 +5
				y-30 +4	y-30 +4	y119-H2O +18
				y-38 +8	y-38 +8	y120-NH3 +18
				y-38 +5	y-38 +6	y120-NH3 +17
				y-64 +7	y-64 +7	
				y-8 +2	y120-H2O +18	
					b111-H2O +16	
					b36-H2O +4	

Table 3.16: Fragments of +24 charge state at varying laser powers (Watts).

0W	2W	3W	4W	5W	6W	8W
b-29 +6	b-28 +5	b-29 +6	b-111 +17	b-28 +5	b-111 +17	b-111 +17
b-29 +5	b-29 +6	b-29 +5	b-28 +7	b-28 +4	b-111 +16	b-111 +18
b-5 +2	b-29 +5	b-29 +4	b-28 +4	b-29 +6	b-28 +6	b-23 +5
y-27 +7	b-30 +5	b-39 +7	b-29 +6	b-29 +5	b-28 +5	b-23 +4
y-29 +8	b-39 +7	y-10 +2	b-29 +5	b-30 +6	b-28 +4	b-25 +5
y-30 +8	b-4 +1	y-120 +18	b-30 +5	b-30 +5	b-29 +6	b-27 +5
y-6 +1	y-120 +18	y-38 +8	b-36 +6	b-35 +5	b-29 +5	b-28 +6
	y-2 +1	y-8 +2	b-36 +5	b-36 +7	b-29 +4	b-28 +5
	y-8 +2		b-37 +7	b-36 +6	b-30 +6	b-28 +4
			b-39 +7	b-37 +7	b-30 +5	b-29 +6
			y-119 +18	b-39 +7	b-30 +4	b-29 +5
			y-120 +18	b-7 +3	b-31 +6	b-29 +4
			y-29 +8	y-109 +17	b-35 +5	b-30 +5
			y38 +8	y-110 +17	b-36 +6	b-31 +5
				y-114 +17	b-36 +5	b-35 +5
				y-119 +18	b-37 +7	b-36 +5
				y-120 +18	b-39 +7	b-39 +6
				y-2 +1	b-40 +7	b-8 +2
				y-38 +8	b-7 +2	y-113 +17
				y-8 +4	b-8 +2	y-15 +4
				y110-H2O +17	y-112 +17	y-15 +3
				y120-H2O +18	y-114 +17	y-2 +1
					y-120 +18	y-30 +6
					y-15 +3	y-30 +5
					y-2 +1	y-38 +8
					y-31 +6	y-38 +7
					y-38 +8	y-47 +9
					y-38 +7	y-6 +3
					b8-H2O +2	b28-NH3 +5
					b30-H2O +6	y38-H2O +7
					b28-NH3 +5	b29-NH3 +5
					b111-H2O +17	b30-NH3 +5
					y112-H2O +17	b111-NH3 +17
					y120-H2O +18	y113-H2O +17
					y114-H2O +18	b35-NH3 +5
					b111-H2O +16	

Table 3.17: Fragments of +25 charge state at varying laser powers (Watts).

0W	3W	4W	5W	6W	7W	9W	11W
b-29 +6	b-28 +5	b-29 +6	b-29 +6	b-111 +17	b-111 +17	b-111 +18	b-112 +18
b-29 +5	b-29 +6	b-29 +5	b-29 +5	b-28 +5	b-28 +6	b-25 +5	b-23 +4
b-8 +2	b-29 +5	b-30 +6	b-30 +6	b-28 +4	b-28 +5	b-27 +5	b-28 +6
y-5 +2	b-36 +5	b-36 +6	b-36 +6	b-29 +6	b-28 +4	b-28 +6	b-28 +5
y-8 +2	b-39 +7	b-39 +7	b-37 +7	b-29 +5	b-29 +6	b-28 +5	b-28 +4
	b-4 +1	b-4 +1	b-39 +7	b-29 +4	b-29 +5	b-28 +4	b-29 +6
	y-38 +8	y-38 +8	y-38 +8	b-30 +6	b-29 +4	b-29 +6	b-29 +5
	y-4 +1	y-38 +7	y-38 +7	b-30 +5	b-30 +6	b-29 +5	b-29 +4
		y-4 +1	y-47 +9	b-34 +5	b-30 +5	b-29 +4	b-30 +5
		y-6 +2	y-47 +8	b-35 +5	b-34 +6	b-30 +5	b-30 +4
		y-8 +2	y-50 +9	b-36 +7	b-34 +5	b-35 +5	b-31 +5
				b-36 +6	b-35 +5	b-36 +6	b-35 +5
				b-36 +5	b-36 +6	b-36 +5	b-36 +5
				b-37 +7	b-36 +5	b-8 +2	b-8 +2
				b-39 +7	b-37 +7	y-110 +17	y-110 +18
				y-110 +18	b-8 +2	y-15 +4	y-110 +17
				y-112 +18	y-110 +18	y-30 +6	y-15 +4
				y-38 +8	y-38 +8	y-38 +8	y-15 +3
				y-38 +7	y-38 +7	y-38 +7	y-2 +1
				y-4 +1	y-4 +1	y-4 +1	y-30 +6
				y-47 +9	y-5 +2	y-47 +9	y-38 +8
				y-8 +2	b28-NH3 +5	y-47 +8	y-38 +7
				y112-H2O +18	b36-NH3 +6	y-5 +2	y-47 +9
				b111-NH3 +17	y110-NH3 +18	y-50 +9	y-47 +8
					b111-H2O +17	b29-H2O +6	y-5 +2
						y38-H2O +8	y-7 +3
						b28-NH3 +5	b29-H2O +6
						b111-H2O +18	b28-NH3 +5
						y110-H2O +17	y38-H2O +7
						b35-NH3 +5	b29-NH3 +5
							y110-H2O +17
							b35-NH3 +5

Table 3.18: Fragments generated by SORI dissociation of +20 charge state. (Excitation at ± 1000 Hz)

Blank	0.5 V	1.0 V	1.5 V	2.0 V	2.5 V	3.0 V
b36 +4	b111 +14	b111 +14	b147 +19	b111 +14	b111 +14	b110 +14
y38 +6	b147 +19	b147 +19	b36 +4	b36 +4	b12 +2	b111 +14
	b36 +4	b36 +4	b36 +5	b8 +2	b147 +19	b147 +19
	y38 +6	b4 +1	b6 +2	y 111 +7	b23 +4	b36 +4
	y111 +7	b8 +2	y111 +7	y126 +8	b36 +5	b39 +6
	y126 +7	y112 +7	y126 +8	y38 +6	b36 +4	b40 +6
		y126 +8	y38 +6	y7 +3	b6 +2	y126 +8
		y139 +8	y4 +1		y126 +8	y126 +7
		y38 +6	y5 +2		y13 +2	y13 +2
		y6 +2	y6 +2		y15 +3	y139 +8
		y5 +2			y30 +5	y38 +6
		y7+3			y31 +6	y7 +3
					y38 +6	
					y4 +1	

Table 3.19: Fragments generated by SORI dissociation of +21 charge state. (Excitation at ± 1000 Hz)

Blank	0.5 V	1.0 V
	b28 +4	b29 +5
	b29 +4	b30 +5
	b7 +1	b36 +4
	b8 +2	b37 +6
	y107 +16	b4 +1
	y120 +16	b7 +1
	y2 +1	b8 +1
	y38 +6	y30 +5
	y4 +1	y38 +5
	y6 +2	y4 +1
	y7 +3	

Table 3.20: Fragments generated by SORI dissociation of +22 charge state. (Excitation at ± 1000 Hz)

Blank	0.5 V	1.0 V	1.5 V
	b29 +5	b28 +4	b28 +4
	y14 +2	b29 +5	b29 +5
	y4 +1	b39 +7	b34 +4
		b39 +6	b39 +6
		b8 +2	b4 +1
		y111 +15	y110 +15
		y111-H2O +15	y111 +15
		y113 +14	y111-H2O +15
		y120 +17	y113 +16
		y120-H2O +17	y120 +16
		y38 +6	y120-NH3 +16
			y38 +6
			y8 +2

3.4 REFERENCES

1. Gauthier, J.W., T.R. Trautman and D.B. Jacobson, Sustained Off-resonance Irradiation for CAD Involving FTMS. CAD Technique that Emulates Infrared Multiphoton Dissociation. Anal. Chim. Acta, 1991. **246**: p. 199-210.
2. Little, D.P., J.P. Speir, M.W. Senko, P.B. O'Connor and F.W. McLafferty, Infrared Multiphoton dissociation of large multiply-charged ions for biomolecule sequencing. Anal. Chem., 1994. **66**(18): p. 2809-15.
3. Senko, M.W., et al., Electrospray Ionization FT-ICR Mass Spectrometry at 9.4 Tesla. Rapid Commun. Mass Spectrom., 1996. **10**: p. 1824-8.
4. Senko, M.W., C.L. Hendrickson, M.R. Emmett, S.D.-H. Shi and A.G. Marshall, External Accumulation of Ions for Enhanced Electrospray Ionization Fourier Transform Ion Cyclotron Resonance Mass Spectrometry. J. Am. Soc. Mass Spectrom., 1997. **8**: p. 970-6.
5. Marshall, A.G., T.-C.L. Wang and T.L. Ricca, Tailored Excitation for Fourier Transform Ion Cyclotron Resonance Mass Spectrometry. J. Am. Chem. Soc., 1985. **107**: p. 7893-7.
6. Senko, M.W., J.D. Canterbury, S. Guan and A.G. Marshall, A High-Performance Modular Data System for FT-ICR Mass Spectrometry. Rapid Commun. Mass Spectrom., 1996. **10**: p. 1839-44.
7. Horn, D.M., R.A. Zubarev and F.W. McLafferty, Automated reduction and interpretation of high resolution electrospray mass spectra of large molecules. J. Am. Soc. Mass Spectrom., 2000. **11**: p. 320-32.
8. Baker, P.R. and K.R. Clauser, Protein Prospector. 1995-2003, The University of California: San Fransisco.
9. Anderson, G.A., J.E. Bruce and R.D. Smith, ICR-2LS. 1996, Pacific Northwest National Laboratories: Richland, WA.
10. Konermann, L. and D.J. Douglas, Acid-induced unfolding of cytochrome c at different methanol concentrations: Electrospray ionization mass spectrometry specifically monitors changes in the tertiary structure. Biochem., 1997. **36**(40): p. 12296-302.

11. Grandori, R., Origin of the conformational dependence of protein charge-state distributions in electrospray ionization mass specrometry. J. Mass Spectrom., 2003. **38**: p. 11-15.

12. Badman, E.R., C.S. Hoaglund-Hyzer and D.E. Clemmer, Monitoring structural changes of proteins in an ion trap over apprx.10-200 ms: Unfolding transitions in cytochrome c ions. Anal. Chem., 2001. **73**(24): p. 6000-7.

13. Lin, H. and C. Dass, Conformational changes in b-endorphin as studied by electrospray ionization mass spectrometry. Rapid Commun. Mass Spectrom., 2001. **15**(23): p. 2341-6.

14. Wang, G. and R. Cole, Solution, Gas-Phase and Instrumental Parameter Influences on Charge-State Distributions in Electrospray Ionization Mass Spectrometery, in Electrospray Ionization Mass Spectrometry, R.B. Cole, Editor. 1997, John Wiley & Sons, Inc.: New York. p. 137-74.

15. Babu, K.R. and A.D. Moradian, D. J., The methanol-induced conformational transitions of b-lactoglobulin, cytochrome c, and ubiquitin at low pH: a study by electrospray ionization mass spectrometry. J. Am. Soc. Mass Spectrom., 2001. **12**(3): p. 317-28.

16. Roepstorff, P., Proposal for a common nomenclature for sequence ions in mass spectra of peptides. Biomed. Mass Spectrom., 1984. **11**(11): p. 601.

CHAPTER 4: COMPLEMENTARY PAIR ANALYSIS TO ASSIGN CHARGE LOCATION IN L9

4.1 INTRODUCTION AND BACKGROUND

This chapter will show the successful application of complementary pair and fragmentation analysis of fragments to assign the location of charge in electrosprayed Ribosomal Protein L9. Low energy dissociation techniques were used to dissociate each of the isolated charge states of L9 and the resulting fragments used for charge location assignments. In addition to the identified fragments, gas-phase basicities of the basic residues and Coulombic interactions were also considered when assigning the location of the charge.

Considerable efforts have been devoted to elucidating the mechanisms for ion formation and the factors that affect it.[1-6] The charge distribution is determined by the state of the ions after desolvation, therefore many experiments are performed on the ions in this stage, including ion/molecule reactions and dissociation experiments. It is important to understand where the charge resides in a gas-phase protein because it is a fundamental determinant of the behavior of the protein in the gas-phase; charge location can affect the tertiary structure, the chemical behavior, and fragmentation mechanism of the analyte. Understanding

these trends may enable the predictions about fragmentation and the development of new applications for the analysis of more complex protein systems and reactions.

Thus far, gas-phase basicity measurements and calculations have been the primary methods for determining the sites of protonation in multiply charged biomolecules. It has been shown that the protonation or cationization of the basic residues (Arg, Lys, His, and NH2-terminus) result in the formation of positive ions, while deprotonation of acidic residues (Asp, Glu, Tyr, COOH-terminus) cause negative ions to be formed.[2,3,7] Kinetic methods and equilibrium bracketing have established values for gas-phase basicities for each of the α-amino acids and are reviewed elsewhere.[8-10] These studies show arginine as the most favorable site for protonation since its gas-phase basicity values are approximately 13 kcal mol-1 higher than the next most basic residues (Lys, His).[9]

The published gas-phase basicity values of the amino acids are mainly derived from experiments involving isolated amino acids or singly charged model peptides. When considering a specific site in a multiply charged ion, the effects of electrostatic repulsions, intramolecular interactions, steric distances and angles, chirality of the protonation sites, and the overall conformation of the ion must all be accounted for. The existence of multiple conformations of an individual charge state can further complicate these measurements. Multiple conformations of single charge states have been demonstrated for both cytochrome c and ubiquitin by H/D exchange, electron capture dissociation, and ion mobility studies.[11-16] The

contributions of these factors make it very complicated to perform calculations and can significantly obscure measurements with reference bases. Improvements in the methodology of gas-phase basicity measurements have generated better approximations to the true values.[17-23]

It is generally accepted that both the number and location of basic sites play an important role in the dissociation of proteins. Both high and low energy dissociation studies have been conducted to investigate fragmentation pathways in multiply charged peptides.[22,24-32] There is presently no single, accepted mechanism that can be generally applied to bond cleavage by low energy dissociation of intact biomolecules. One theory suggests that the ionization process results in a population of peptide ions with different protonation sites which are then fixed after the ionization, and there is no interaction between the charge and the reaction site.[33] The other theory, the mobile proton model, suggests that rapid intramolecular shuffling occurs prior to the dissociation event so charge can be transferred to the cleavage site.[25]

This work is a systematic investigation of the location of charge in individual charge states of an electrosprayed protein using low energy dissociation. Dissociation spectra were obtained for the +10 through +25 charge states of ribosomal protein L9 using a Fourier transform ion cyclotron resonance (FTICR) mass spectrometer. When coupled with ESI, FTICR offers considerable advantages over other types of mass spectrometers. The non-destructive nature of the ion cell is

directly related to these benefits. Energy to fragment intact ions can be imparted because the ion population can be held in the cell for extended periods of time. In a typical FTICR experiment, dissociation is initiated after the isolation and cooling of a particular charge state, and the ejection of possible interferences like other charge states, adducted species, or sample contaminants. Moreover, the ultra-high resolution capability available with FTICR enables the indisputable assignment of charge and mass, which is essential to the accurate identification of the products of fragmentation.

4.2 EXPERIMENTAL

The experimental procedure outlined in Chapter 3 was used to collect the data shown in this chapter.

4.3 RESULTS AND DISCUSSION

4.3.1 Dissociation of L9 by IRMPD

Assigning the location of charge in this protein was possible because of the assumption that the proton does not undergo scrambling between the time it is ionized and dissociated. Downard suggests that despite the potential for charge migration during the dissociation event, the data showed that charge-bearing protons

were reasonably localized when dissociation occurred.[31] Work by Stevenson and others supports this concept and make this a reasonable postulation to be carried forth in this work.[25,34,35]

In order to assign the location of the added protons in each of the charge states, complementary fragment pairs were used. Similar to how tandem mass spectrometry is used to determine the primary sequence of proteins, product fragments are used to determine the sites of protonation and sequence of charge addition to each charge state. Complementary pairs are defined as the y and b fragments that result from the cleavage of the same peptide bond and whose individual charges sum to give the charge of the parent ion. These pairs are useful because an individual fragment identifies the number of charges on it, and suggests the localization of charge with the presence of its complement. Most of the observable charge states produced at least one pair of complementary fragments. The other fragment ions that resulted from dissociation were used to provide additional information about the location of the charges. It is assumed throughout the assignment of charge process that since arginine is the most basic amino acid, the four arginine residues present in the protein will always be protonated before the remaining lysines and histidines acquire additional protons.

4.3.2 Charge Location Assignments

4.3.2.1 +10 Charge State

For the +10 charge state, the complementary pair of $b23^{+2}$ and $y126^{+8}$ is observed. The $b23^{+2}$ fragment shows that there are two protons located in the first twenty-three residues of the N-terminus. It is unlikely that the N-terminal methionine is protonated since its has the lowest gas-phase basicity of the potential chargeable sites, with a value of 213.0 kcal/mol.[36] None of the four arginines are located in the N-terminal domain; they are at positions 56, 88, 113, and 122. Therefore, neither of the two charges indicated by the $b23^{+2}$ fragment can be attributed to arginines. The $y126^{+8}$ fragment shows that other 8 additional protons reside on the remaining C-terminal section of the protein. Since the 4 arginines are located therein, there are only 4 remaining protons to be assigned within that fragment. The $y148^{+10}$ confirms that the N-terminal methionine is not protonated. The $b4^{+1}$ ion reinforces that Lys2 must be protonated, while the $b6^{+1}$, $b7^{+1}$, and $b9^{+1}$ confirm that the Lys7 is not. The protonation of Lys10 is confirmed by the presence of the $y138^{+9}$ ion. The fact that $y138^{+9}$ is also present in the spectrum confirms that the lysines located at positions twelve, fourteen, and fifteen. The cleavages at positions Ile37 and Thr40 both with +3 charges, confirm that only three charges reside on the N-terminus in the +10 charge state. Since b23 has a charge of +2 and b37 has a charge of +3, this indicated that a proton must be located at Lys32, the

only basic residue in present between the two points of cleavage. Looking at the C-terminal side of the protein, the $y4^{+1}$ confirms that Lys149 is protonated. The $y9^{+2}$ fragment shows that Lys142 is protonated, not His134, because of the differences between their gas-phase basicities. This methodology was applied to assigning the location of charge for all charge states and is outlined for individually in the subsequent sections.

4.3.2.2 +11 Charge State

Complementary pairs were seen in this spectrum for the $b10^{+1}/y139^{+10}$ and $b116^{+8}/y33^{+3}$. Since the first pair of fragments was seen in the +10 charge state, it can be inferred that the 11th proton has been added to a basic amino acid that resides on the y139 fragment since it appears in this spectrum with an additional charge. Fragment $b70^{+5}$ shows that the proton must have been added to the region N-terminal to this cleavage. A second complementary pair was seen in this dissociation spectrum, $b116^{+8}/y33^{+3}$. This pair is consistent with the location of protons in this charge state. The presence of both the y139 and y134 fragments with +10 charge means that none of the lysines located between residues 10 and 15 have been protonated. Since two charges are present N-terminal to $b23^{+2}$, the remaining three charges must be in region between residues 23 and 70, with Lys32 and Arg56 already known to be protonated. No other fragments indicate which of the remaining basic residues could be protonated, so the Coulombic repulsion idea of

the charges adding to locations for maximum separation was invoked and the final charge was assigned to Lys67.

4.3.2.3 +12 Charge State

Three complementary pairs were detected for the +12 dissociation, $b10^{+1}/y139^{+11}$, $b23^{+2}/y126^{+10}$, and $b119^{+8}/y30^{+4}$. The presence of the b10+1/y139+11 indicates that the 12th proton added C-terminal to the point of cleavage. The $b119^{+8}/y30^{+4}$ fragment narrows down the location by showing that the proton must have been added to C-terminal to that point of cleavage. The existence of the $y8^{+2}$ fragment suggests that only two protons are located on that fragment, so the charge must be located between residues Ala120 and Leu141. Arg122 is already protonated and the most basic amino acid in that region is Lys132, so the location of the 12th proton was assigned there.

4.3.2.4 +13 Charge State

The +13 charge state does not have any complementary pairs of fragments present. The $b111^{+9}$ fragment does show that the 13th proton added N-terminal to that point of cleavage. The series of fragments from b35 through b40, each with a

charge of +4, and $b70^{+6}$ eliminates the region between Thr40 and Glu70 as the location of the next proton. There are already two protons located in this region at Arg56 and Lys67. The $y33^{+4}$ fragment maintains that four charged residues are located C-terminal to that cleavage. This leaves the region between Gln71 and Asp111. The location that gives maximum separation of charge is Lys96, so the 14th proton is assigned to this location.

4.3.2.5 +14 Charge State

One complementary pair of fragments was observed for this charge state, $b38^{+4}/y111^{+10}$. The $b38^{+4}$ was also present in the +13 spectrum, so the next proton to add to the protein must be located C-terminal to that cleavage. The $y111^{+10}$, in conjunction with the $y38^{+5}$, narrows the location of the added proton to between Ala39 and Asp110. For maximum separation of charge, the 14th proton was assigned to Lys45.

4.3.2.6 +15 Charge State

One complementary pair was detected for this charge state, $b8^{+1}/y141^{+14}$. But there are three important fragment ions that confirm the previous charge assignments and point to the location of the 15th charge. The combination of the $y79^{+8}$ and the $y107^{+11}$ narrow confirms the location of three charges between Asn43 and Glu70. Three charges have already been assigned in this region, Lys45, Lys56,

and Lys66. The $y64^{+7}$ fragment along with $y79^{+8}$ locates the charge as residing between Gln71 and Glu85. The charge is assigned to Lys74 to accommodate maximum charge separation.

4.3.2.7 +16 Charge State

There were three complementary pairs present in the +16 threshold dissociation spectrum, $b19^{+3}/y130^{+13}$, $b85^{+9}/y64^{+7}$, and $b134^{+13}/y15^{+3}$. Six charges must be located between Lys19 and Glu85 according to these complementary pairs. Five charges have already been assigned in that region. This 16th charge was assigned to Lys82, because it allowed for the charges to experience maximum separation.

4.3.2.8 +17 Charge State

This charge state had an unusually low number of fragments when dissociated using IRMPD. The threshold spectrum did not contain any complementary pairs. Even though the number of fragments was very low, the $b11^{+3}$ fragment indicated three charges in the first 11 residues. The charge was therefore assigned to Lys7 since it is more basic that the N-terminal methionine.

4.3.2.9 +18 Charge State

Three pairs of complementary fragments were observed for this charge state, $b36^{+5}/y113^{+13}$, $b111^{+12}/y38^{+6}$, and $b119^{+14}/y30^{+4}$. The $b111^{+12}/y38^{+6}$ and the $b119^{+14}/y30^{+4}$ pair dictate that the charge must be added between Lys112 and Asp119. There are two possible locations here and both are adjacent to and already charged Arg113. The charge was assigned to Lys112.

4.3.2.10 +19 Charge State

Only one complementary pair was observed for the +19 charge state, $b111^{+13}/y38^{+6}$. When this is compared with the complementary pair produced from breaking the same bond in the +18, the proton is location of the proton is determined to be N-terminal to the point of cleavage. The $b8^{+2}$ fragment shows that the N-terminal methionine is protonated since the only other chargeable amino acid in this region is already protonated.

4.3.2.11 +20 Charge State

The +20 charge state showed a significant amount of dissociation at 0 Watts of laser power, though no complementary fragments were seen in this spectrum.

The $b39^{+6}$ and $y38^{+6}$ fragments indicate that eight charges must reside between residues Ala39 and Lys112. This region already has seven charges assigned. To maintain charge separation, the charge should add to either His106 or Lys109. The location of the 20th charge can be narrowed down to these two residues, but it cannot be definitively determined from the fragments obtained. Subsequent modeling was performed on both using both possible charge locations and those results are shown in Chapter 4.

4.3.2.12 +21 Charge State

This charge state also exhibited a significant amount of fragmentation when the laser power was completely turned off. The resulting fragments did not yield any complementary fragments. The presence of two fragments, $b111^{+15}$ and $y110^{+15}$, together show that the 21st charge adds between Thr40 and Glu111. Two possible sites were flagged as potential locations for charge from the +20 charge state, and the fragments show that a charge was added in that same region. So the location of the 21st charge was assigned to the second possible location that remained from the +20 charge state. So in this charge state, both the His106 and Lys109 are protonated.

4.3.2.13 +22 Charge State

No complementary pairs were observed in this charge state. The only fragment that indicates where the charge can be assigned is $b29^{+6}$, since six charges must be on this fragment and the threshold dissociation spectrum of the +21 contained the $b29^{+5}$ fragment. The charge was assigned to Lys15.

4.3.2.14 +23 Charge State

One pair of complementary fragments was observed in the +23 charge state, $b29^{+6}/y120^{+17}$. Since $b29^{+6}$ was also present in the +22, the charge must have added C-terminal to the point of cleavage. There are three fragments that point to the location of the 23rd charge. The presence of the $y38^{+7}$ fragment indicates that the additional charge must be between Lys112 and the C-terminal lysine because the $y38^{+6}$ ion was seen in the threshold spectrum of +22. The region from Lys112 to Glu119 is eliminated as a possibility since two charges have been assigned here and the $y30^{+5}$ confirms that. Ala120 to Val131 is also eliminated because the $y15^{+3}$ fragment confirms the two charges which have already been assigned here. The only remaining amino acid that could possibly retain the charge is His144, so the charge was assigned to this residue.

4.3.2.15 +24 Charge State

One complementary fragment pair was detected for the +24 charge state, $b23^{+6}/y120^{+18}$. This pair was also seen in the +23 charge state but the charge of the y fragment was reduced by one. This indicates that the charge must have added C-terminal to the point of fragmentation. The fragment at $y38^{+8}$ shows that one additional fragment was added between Lys112 and the C-terminal lysine. There are two potential charge locations, one at His134 and the other at Lys114. There are already two charges located on adjacent residues Lys112 and Arg113 which makes it very unfavorable for the charge to add to L114. As a result, the charge location was assigned to His134.

4.3.2.16 +25 Charge State

Two complementary pairs were seen in the threshold dissociation spectrum of +25, $b37^{+9}/y110^{+18}$ and $b111^{+17}/y38^{+8}$. The two pairs isolate the addition of the final charge to the amino acids between Thr40 and Glu111. No other fragments provided information in this region, do the final charge was assigned to allow maximum charge separation and was placed on Lys51. A complete fragment map showing the order and location for the sequential addition of charge is shown in Figure 4.7.

19 17 22

MKVIFL**K**DV**K**GKGK**K**GEI**K**NVADGYANNFLF**K**QGLAIEAT

10 20 30 40

14 25 11 15

PANL**K**ALEAQ**K**QKEQ**R**QAAEELANAK**K**LKEQLE**K**L

50 60 70

16 13 * * 18 12 24 23

TVTIPA**K**AGEGG**R**LFGSITS**K**QIAESLQAQ**H**GL**K**LD**KR**K**R**IELADAI**R**ALGYTNVPV**K**L**H**PEVTATL**K**V**H**VTEQ**K**

80 90 100 110 120 130 140

* Denotes that the assignment of the 20th and 21st charges could not be distinguished.

Figure 4.1: Protein map showing the location and order of charge addition for Ribosomal Protein L9 as determined from threshold dissociation spectra and fragment lists.

4.4 CONCLUSIONS

Complementary pair analysis and fragment analysis was successfully applied to Ribosomal Protein L9. This analysis yielded both the location of and the sequential order in which the charges added on to the protein. This represents the first time that charge locations have been definitively demonstrated for a protein of this size. Charge location involves two factors, the intrinsic gas-phase basicity of the amino acids, and the electrostatic interactions between charges. For example, the most basic amino acid, arginine strongly favors protonation, but as the charge increases, protonation is able to occur in regions of high charge density. The determination of charge location in L9 was accomplished by using the influence of both of these factors.

The sequential addition and localization of charge is strongly supported by the observation of similar fragments that become more highly charged for the higher charge states. Even though the number of fragments generated was large, and the number of potential sites for charge addition was high, it was still possible to determine that the addition of charge was sequential and preferential. Complementary pair analysis had been previously applied to melittin, a small peptide with limited charge sites and no acidic residues. This is the first application of this method to a large, high charging, multiple domain protein.

4.5 REFERENCES

1. Cole, R.B., ed. *Electrospray Ionization Mass Spectrometry*. 1997, John Wiley & Sons,Inc.: New York. 1-577.
2. Smith, R.D., J.A. Loo, R.R. Ogorzalek Loo, M. Busman and H.R. Udseth, *Principles and Practice of Electrospray Ionization- Mass Spectrometry for Large Polypeptides and Proteins.* Mass Spectrom. Rev., 1991. **10**: p. 359-451.
3. Smith, R.D., J.A. Loo, C.G. Edmonds, C.J. Barinaga and H.R. Udseth, *New Developments in Biochemical Mass Spectrometry: Electrospray Ionization.* Anal. Chem., 1990. **62**: p. 882-99.
4. Fenn, J.B., *Ion formation from charged droplets: roles of geometry, energy, and time.* J. Am. Soc. Mass Spectrom., 1993. **4**(7): p. 524-35.
5. Loo, J.A. and R.R. Ogorzalek Loo, *Electrospray Ionization Mass Spectrometry of Peptides and Proteins*, in *Electrospray Ionization Mass Spectrometry*, R.B. Cole, Editor. 1997, John Wiley & Sons, Inc.: New York. p. 385-419.
6. Kebarle, P. and L. Tang, *From Ions in Solution to Ions in the Gas Phase: The Mechanism of Electrospray Mass Spectrometry.* Anal. Chem., 1993. **65**: p. 972A-986A.
7. Covey, T.R., R.F. Bonner, B.I. Shushan and J.D. Henion, *The determination of protein, oligonucleotide and peptide molecular weights by ion-spray mass spectrometry.* Rapid Commun. Mass Spectrom., 1988. **2**(11): p. 249-56.
8. Green, M.K.L.C.B., *Ion-molecule reactions as probes of gas-phase structures of peptides and proteins.* Mass Spectrom. Rev., 1997. **16**(2): p. 53.
9. Harrison, A.G., *The Gas-Phase Basicities and Proton Affinities of Amino Acids and Peptides.* Mass Spectrom. Rev., 1997. **16**: p. 201-17.
10. Williams, E., *Proton Transfer Reactivity of Large Multiply Charged Ions.* J. Mass Spectrom., 1996. **31**: p. 831-42.
11. Wagner, D.S. and R.J. Anderegg, *Conformation of cytochrome c studied by deuterium exchange-electrospray ionization mass spectrometry.* Anal. Chem., 1994. **66**(5): p. 706-11.

12. McLafferty, F.W., Z. Guan, U. Haupts, T.D. Wood and N.L. Kelleher, *Gaseous Conformational Structures of Cytochrome c.* J. Am. Chem. Soc., 1998. **120**(19): p. 4732-40.

13. Freitas, M.A., C.L. Hendrickson, M.R. Emmett and A.G. Marshall, *Gas-Phase Bovine Ubiquitin Cation Conformations Resolved by Gas-Phase Hydrogen/Deuterium Exchange Rate and Extent.* Int. J. Mass Spectrom., 1999. **185/186/187**: p. 565-75.

14. Breuker, K., H. Oh, D.M. Horn, B.A. Cerda and F.W. McLafferty, *Detailed unfolding and folding of gaseous ubiquitin ions characterized by electron capture dissociation.* J. Am. Soc. Mass Spectrom., 2002. **124**(22): p. 6407-20.

15. Clemmer, D.E., R.R. Hudgins and M.F. Jarrold, *Naked Protein Conformations: Cytochrome c in the Gas Phase.* J. Am. Chem. Soc., 1995. **117**: p. 10141-2.

16. Wyttenbach, T. and B.M. T., *Gas phase conformations of biological molecules: The hydrogen/deuterium exchange mechanism.* J. Am. Soc. Mass Spectrom., 1999. **10**(1): p. 9.

17. Wu, Z. and C. Fenselau, *Gas-phase basicities and proton affinities of lysine and histidine measured from the dissociation of proton-bound dimers.* Rapid Commum. Mass Spectrom., 1994. **8**(9): p. 777-80.

18. Wu, Z. and C. Fenselau, *Structural determinants of gas phase basicities of peptides.* Tetrahedron, 1993. **49**(41): p. 9197-206.

19. Wu, Z. and C. Fenselau, *Proton affinity of arginine measured by the kinetic approach.* Rapid Commum. Mass Spectrom., 1992. **6**(6): p. 403-5.

20. Schnier, P.D., D.S. Gross and E.R. Williams, *On the Maximum Charge State and Proton Transfer Reactivity of Peptide and Protein Ions Formed by Electrospray Ionization.* J. Am. Soc. Mass Spectrom., 1995. **6**: p. 1086-97.

21. Wu, D. and F.E. Regnier, *Native protein separations and enzyme microassays by capillary zone and gel electrophoresis.* Anal. Chem., 1993. **65**(15): p. 2029-35.

22. Kaltashov, I.A. and C. Fenselau, *Proton Locations in Doubly Charged Peptides and Association with Fragmentation Pathways.* Int. J. Mass Spectrom. Ion Processes, 1997. **160**(1-3): p. 331-8.

23. Kaltashov, I.A. and C. Fenselau, *Thermochemistry of Multiply Charged Melittin in the Gas Phase Determined by the Modified Kinetic Method.* Rapid Commun. Mass Spectrom., 1996. **10**(7): p. 857.

24. Marzluff, E.M. and J.L. Beauchamp. in *Proc. 42nd Amer. Soc. Mass Spectrom. Conf. on Mass Spectrom. & Allied Topics*. 1994. Chicago, IL: Amer. Soc. Mass Spectrom.

25. Dongre, A.R., J.L. Jones, A. Somogyi and V.H. Wysocki, *Influence of peptide composition, gas-phase basicity, and chemical modification on fragmentation efficiency: Evidence for the mobile proton model.* J. Am. Chem. Soc., 1996. **118**(35): p. 8365-74.

26. Nair, H. and V.H. Wysocki, *Are peptides without basic residues protonated primarily at the amino terminus?* Int. J. Mass Spectrom. Ion Processes, 1998. **174**: p. 95-100.

27. Cox, K.A., S.J. Gaskell, M. Morris and A. Whiting, *Role of Site Protonation in the Low Energy Decompositions of Gas-Phase Peptide Ions.* J. Am. Soc. Mass Spectrom., 1996. **7**(6): p. 522-31.

28. Downard, K.M. and K. Beimann, *The effect of charge state and the localization of charge on the collision-induced dissociation of peptide ions.* J. Am. Soc. Mass Spectrom., 1994. **5**(11): p. 966-75.

29. Jockusch, R.A., P.D. Schnier, W.D. Price, E.R. Strittmatter, P.A. Demirev, and E.R. Williams, *Effects of Charge State on Fragmentation Pathways, Dynamics, and Activation Energies of Ubiquitin Ions Measured by Blackbody Infrared Radiative Dissociation.* Anal. Chem., 1997. **69**: p. 1119-26.

30. Ishikawa, K., T. Nishimura, Y. Koga and Y. Niwa, *Role of Coulomb energy in promoting collisionally activated dissociation of multiply charged peptides formed by electrospray ionization.* Rapid Commun. Mass Spectrom., 1994. **8**(12): p. 933-8.

31. Downard, K.M. and K. Beimann, *Charging behavior of highly basic peptides during electrospray ionization. A predilection for protons.* Int. J. Mass Spectrom. Ion Processes, 1995. **148**: p. 191-202.

32. Tang, X.J. and P.B. Thibault, R. K., *Fragmentation reactions of multiply-protonated peptides and implications for sequencing by tandem mass spectrometry with low-energy collision-induced dissociation.* Anal. Chem., 1993. **65**(20): p. 2824-34.

33. Stimson, E., O. Truong, W.J. Richter, M.D. Waterfield and A.L. Burlingame, *Enhancement of charge remote fragmentation in protonated peptides by high energy CID MALDI-TOF-MS using "cold" matrixes.* Int. J. Mass Spectrom. Ion Processes, 1997. **169/170**: p. 231-40.

34. Stevenson, E., *Dissociation Studies of Charge and Structure Effects on Electrosprayed Proteins*, Dissertation Thesis, Department of Chemistry and Biochemistry, 1998, The University of Texas at Austin.

35. Bolaños, B.J., *Study of Higher Order Gas-Phase Protein Structure by Fourier Transform Ion Cyclotron Resonance Mass Spectrometry*, Dissertation Thesis, Department of Chemistry and Biochemistry, 1997, The University of Texas at Austin.

36. Gorman, G.S., J.P. Speir, C.A. Turner and I.J. Amster, *The proton affinities of the twenty commom alpha-amino acids.* J. Am. Chem. Soc., 1992. **114**: p. 3986-8.

CHAPTER 5: MOLECULAR MODELING SIMULATIONS OF THE CHARGE STATES OF L9

5.1 INTRODUCTION

Molecular modeling was used to assist with visualizing how the structure changes when charge is added. The X-ray structure was used as a starting point and the charge was added to locations as determined in Chapter 4. Energy minimizations yielded new structures for each charge state that did not retain their secondary characteristics. Correlating the torsion angles between the original and model structures showed local areas of high correlation that ranged from 5 to 15 residues long.

A chain of amino acids joined by a series of peptide bonds forms a protein which, in an aqueous solution, folds so as to minimize the contact of hydrophobic side-chains with the aqueous environment.[1] These folds occur in response to the protein surroundings, and are governed by the primary sequence, disulphide bonds, and intramolecular interactions. The secondary structure is determined by these interactions and so α-helices, β-pleated sheets, and β-turns are formed as these interactions impart stability to the molecule. Most helices are amphipathic, they have hydrophobic side-chains along one side, and hydrophilic side-chains along the other, which enables one side of the helix to associate with an aqueous environment,

while the other side seeks to "hide" from water or other polar molecules. The tertiary structure is the three-dimensional arrangement of these secondary motifs, and this arrangement of the tertiary structure affords stability to the protein. In its cellular environment, the protein spontaneously folds into its characteristic structure which is directly related to its function in the cell.[2]

The X-ray diffraction structure of ribosomal protein L9, as defined by Hoffman, et al., shows the protein is comprised of two terminal globular units, with well defined secondary structural characteristics, that are joined by a rigid α-helix.[3] There is excellent evidence that this unusual architecture is preserved in solution.[4,5] But when proteins are electrosprayed and enters the gas-phase, it becomes unclear how much of this structure is preserved because of the absence of the influence of solvent molecules.

Kaltashov, et al. investigated the persistence of secondary structural characteristics in the gas-phase using melittin, with its stable α-helix, and dynorphin, a weak β former.[6] They found the secondary structure in melittin to be preserved, but dynorphin did not exhibit any preferred conformation in the gas phase. Investigations of tertiary structure in the gas-phase have utilized the non-Gaussian charge state distributions of the electrosprayed protein charge envelope, hydrogen/deuterium exchange, and ion mobility to probe the presence of and any changes in tertiary structure.[7-15]

Both secondary and tertiary structural characteristics result from the interaction of hydrogen bonds, electrostatic interactions, hydrophobic interactions, and Van der Waals interactions. It is thought that the creation of multiple charge states during the electrospray process should have some effect on the three dimensional structure since it introduces charges to the protein that would influence the interactions that define the structure. Molecular modeling was used as a visualization tool to observe how the protein responded to the protons added by the electrospray process.

Performing modeling simulations on L9 with HyperChem presented a challenge because of the size of the molecule. With a mass of 16.3 kDa, and a composition of 2346 atoms (without addition of protons), software capabilities of the HyperChem package were tested. Due to these limitations in the performance of the program, the simplest calculations were utilized to characterize the structural changes. The most stable conformation was taken to be that within an energy minimum. The structural outputs are an approximation of the system's global minimum since the potential energy surface contains several local minima that are more easily accessed than the true energy minimum. Energy minimizations and geometry optimizations were performed using Bio+(CHARMM) and AMBER force fields.

The Bio+ force field in HyperChem represents a version of the Chemistry at HARvard using Molecular Mechanics (CHARMM) force field.[16] It was designed

primarily to explore macromolecules. This force field option, in its original form and in HyperChem, does not have a hydrogen bonding term, so effects of those interactions are not accounted for with this method. AMBER was developed for use with proteins and nucleic acids and includes the hydrogen bond term in its force field equation.[17] Even though these programs are well developed and frequently used as parts of various modeling platforms, work continues to improve large system simulations, with views toward more precise energy calculations and more accurate conformational renderings.[18,19]

The most reliable way to discuss the structures that are produced by the simulations is in terms of the torsional (dihedral) angles of the backbone atoms. These are the angles of rotation about a specific bond along the backbone of the protein. There are three defined angles of interest, φ (phi), ψ (psi) and ω (omega). The atoms that form these angles are illustrated in Figure 5.1 (a). Values of phi are limited primarily to the range between -60 degrees and -150 degrees. For psi, the range is limited to regions centered about -60 degrees and +120 degrees. The typical value of omega is $+180^{o}$ because the bonds are most often found in the trans configuration. When cis prolines occur (in about 10% of cases), the value of omega is 0^{o}.[2,20] For a fully extended (denatured) chain, these three angles are each $+180^{o}$. Each torsional angle has an allowed range of values associated with the different forms of secondary structure, as shown in Figure 5.1 (b). Peptides and proteins adopt structures typically having φ and ψ angle pairs in the allowed regions

of the Ramachandran plot because these are the most energetically favorable conformations. The white areas in Figure 5.1 (b) correspond to conformations where atoms in the polypeptide come closer than the sum of their van der Waals radii, these regions are sterically disallowed for all amino acids except glycine, which is unique in that it lacks a side chain, which enables freer rotation around the α-carbon.[1] The red regions correspond to conformations where there are no steric clashes, and are the allowed regions for the α-helical and β-sheet conformations. The yellow areas are show the allowed only regions if slightly shorter van der Waals radii are used in the calculation, and the atoms are allowed to approach more closely forming a left-handed α-helix, which is less stable than its right-handed counterpart..

(a)

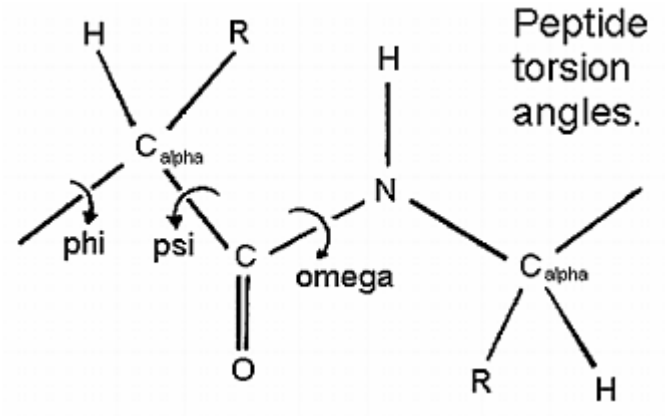

(b)

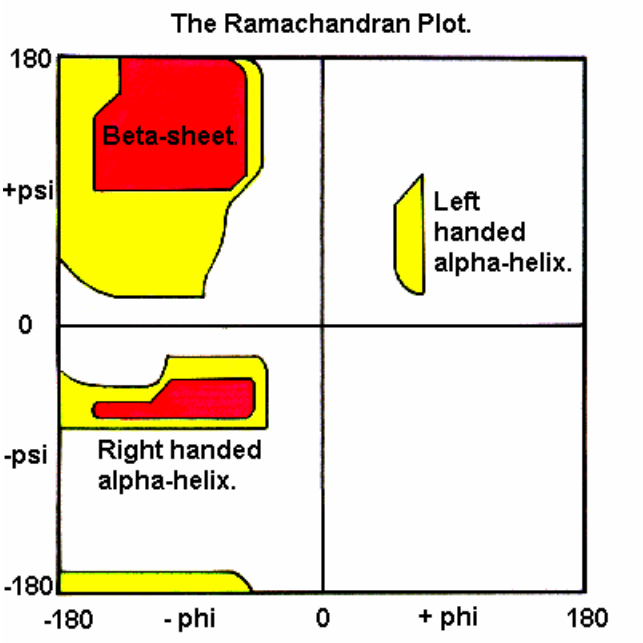

Figure 5.1: (a) Illustration of a protein backbone showing the torsional angles φ (phi), ψ (psi) and ω (omega).

(b) Diagram of Ramachandran plot showing allowed ϕ and ψ angle values and corresponding secondary structure.[21,22]

5.2 EXPERIMENTAL

Molecular mechanics calculations were performed using HyperChem version 7.5 (Hypercube, Inc., Gainesville, FL). The X-ray crystal structure of L9 was obtained as a PDB file from the Protein Data Bank.[23] Each charge state was generated in HyperChem by adding a proton to the basic side chain of the appropriate residue as determined in Chapter 4. AMBER and Bio+ (CHARMM) force fields were used to perform the calculations. When the energies of each charge state was minimized with a convergence of 0.1 kcal/mol, the resulting structure was converted from a HyperChem file to the PDB format using gOpenMol.[24,25] The torsion angles between adjacent amino acids were extracted from the PDB file using MOLMOL.[26]

5.3 RESULTS AND DISCUSSION

5.3.1 Energy Values and Structures derived from Simulations

HyperChem performed the energy minimizations using Bio+(CHARMM) and AMBER. The energy for each of the structures calculated by the program, the average energy and standard deviation are shown in Table 5.1. The AMBER calculations generated structures with an overall lower energy than the Bio+

calculations. Since the AMBER force field includes hydrogen bonding in the parameters used to perform the modeling, it was able to generate lower energy L9 ions, only the analysis of the AMBER data is reported in this chapter.

Table 5.1: Minimized energy (kcal/mol) as calculated by HyperChem for each charge state using Bio+(CHARMM) and AMBER.

	Minimum Energy (kcal/mol)	
Charge State	Bio+ (CHARMM)	AMBER
+10	9233.3	6395.79
+11	9248.27	6327.44
+12	9236.29	6448.81
+13	9231.96	6312.77
+14	9225.6	6348.73
+15	9248.35	6562.02
+16	9264.33	6307.95
+17	9249.46	6320.39
+18	9251.67	6507.29
+19	9286.68	6352.25
+20H106	9356.79	6580.07
+20K109	9354.93	6535.9
+21	9271.64	6304.78
+22	9287.53	6495.66
+23	9259.85	6543.96
+24	9317.04	6616.98
+25	9346.3	6373.59
Mean	9274.71	6431.43
Std. Deviation	42.51	106.71

The structure generated by HyperChem (AMBER) for the +10 charge state is shown in Figure 5.2 in stereoview (To view the image in 3D, hold picture about six inches from your face , cross your eyes and slowly move the picture away from your face. Your focus should be above the page). The results generated from the other charge states are shown in the Appendix B. When a comparison is made between the simulated structures and the X-ray structure, differences are evident, but some subtle similarities remain. For instance residues 41 through 75 (α-helix) are still extended and do not show any folding or bending, which is very similar to original structure, where the α-helix is different from the globular domains. The two terminal domains do exhibit bends and loops in the simulation, and can be identified as different from the original extended area of helical character.

The characteristic secondary motifs visible in the X-ray structure were not preserved by the molecular modeling data. It has been shown experimentally that removal of water molecules from a native protein negates hydrophobic interactions, and preferentially stabilizes the α-helical secondary structure with direct solvation of additional protons, and increases tertiary inter-helix dipole-dipole and hydrogen bonding.[27] Even without confirming this stabilizing effect of water loss, the model structure produced still has remnants of the X-ray structure present in its overall shape. Figure 5.3 sho-ws the side by side Ramachandran plots for the X-ray structure of L9 and the structure generated by AMBER minimization. The plot of the X-ray molecule shows evidence of the three main secondary structural

characteristics present: α-helix, β-sheet, and loops and turns. The torsion angles present for amino acids fall into the regions of the graph that are allowed, and are thus associated with these motifs.

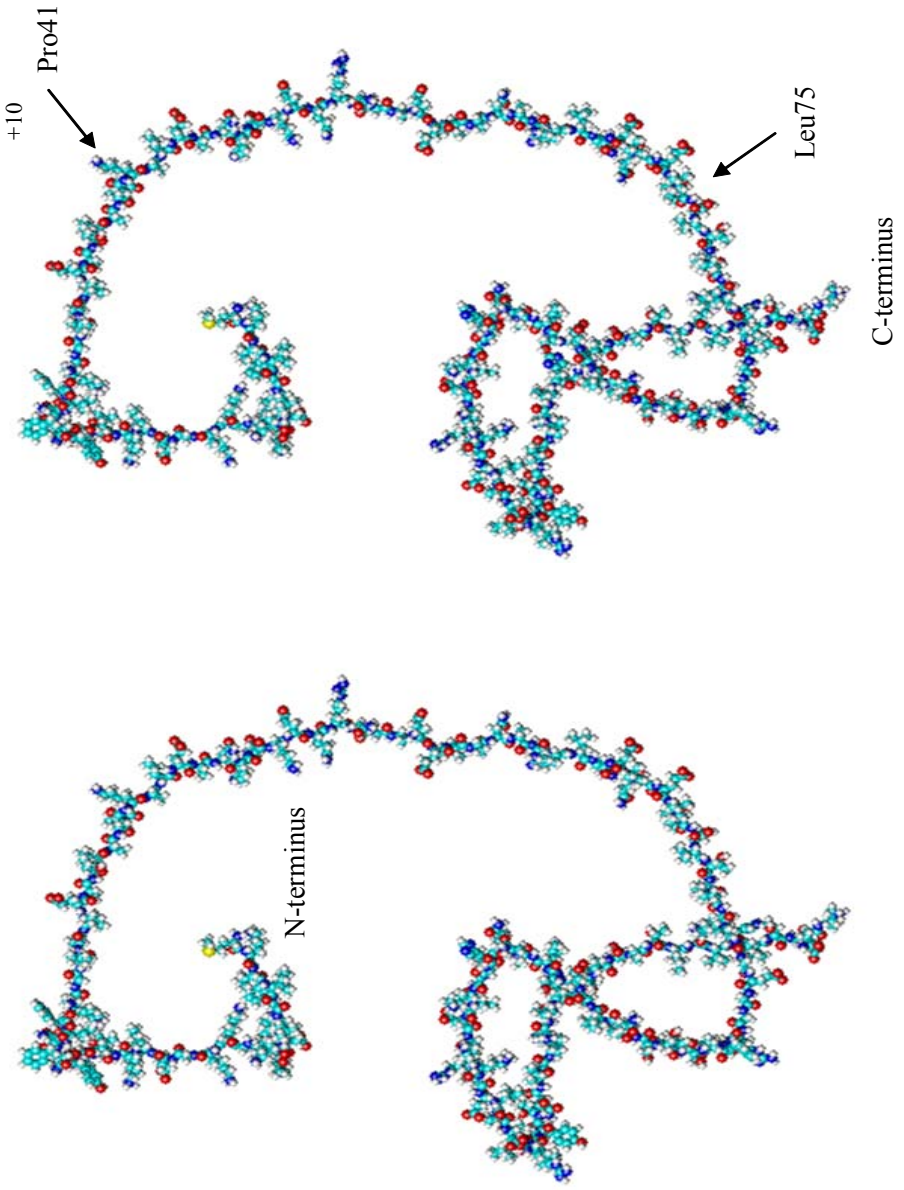

Figure 5.2: Model of the +10 charge state of L9 as produced from AMBER energy minimization by HyperChem. Model is presented in cross-eyed stereoview.

The plot of data for the +10 charge state shows that most of the torsion angles place the amino acids in the region of the plot where turns and loops are allowed. No angles were found in the regions allowed for α-helix or β-sheet. Clearly, the model cannot describe the secondary structure, but the folds and turns were further investigated and discussed in Section 5.3.3. When Ramachandran plots were created for all of the charge states, certain residues repeatedly appeared in the disallowed regions of the graph. With the exception of charge state +10, each charge state had at least one glycine in the disallowed region of the Ramachandran Plot. Table 5.2 shows the disallowed amino acid and the charge states in which their torsion angles are outside the allowed areas. It is not surprising that glycines are predominantly featured in these disallowed regions since the absence of a side chain on the α-carbon allows the formation of configurations that would be sterically hindered if side chains were present.

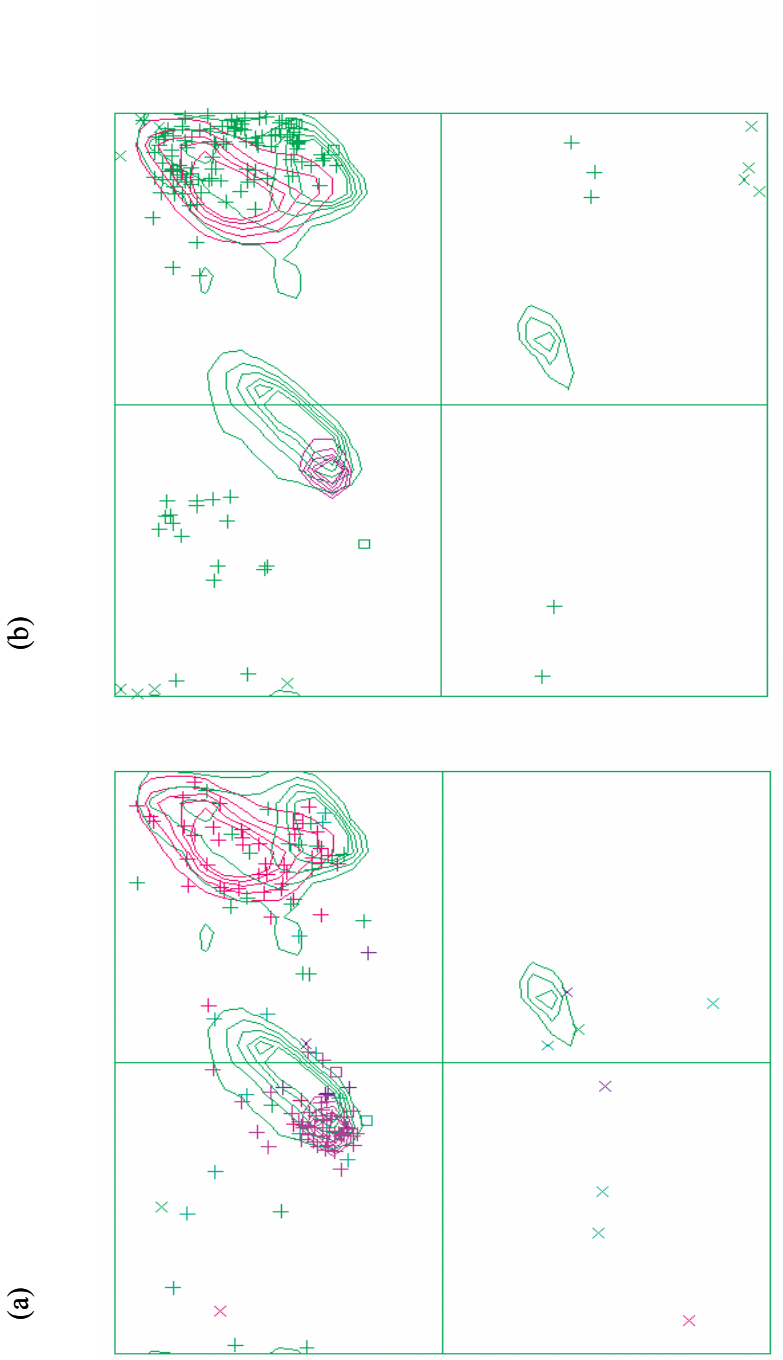

Figure 5.3: Ramachandran plots of L9 from (a) X-ray coordinates, and (b) simulated +10 charge state (AMBER).

Table 5.2: List of amino acids with disallowed torsion angles as designated by their Ramachandran plots.

	Charge States																
Disallowed Torsion	+10	+11	+12	+13	+14	+15	+16	+17	+18	+19	+20 H106	+20 K109	+21	+22	+23 H144	+24	+25
Lys7																+	
Lys10																+	
Gly16							+						+				
Gly24		+	+	+	+	+	+	+	+	+	+	+	+	+	+	+	+
Tyr25	+																
Phe31		+	+			+	+	+				+	+		+	+	
Gln33							+										
Leu62																	+
Gly86				+		+				+	+				+		
Gly87				+	+	+				+	+				+		
Ile98							+						+				
Ala104															+		
Leu133																+	

5.3.2 Global and Regional Correlation of Charge States vs. X-ray

In order to look more closely at how the angles in the original X-ray structure are related to the angles in the modeling data set, correlation analyses were carried out on the two data sets. A series of global and regional correlations were performed using the different aspects of the data: whole protein, N-terminal domain, α-helix, and C-terminal domain. A further set of local correlations were also performed on areas from three to fifteen amino acids. Table 5.3 shows the global and regional correlation values (R). Experimental evidence by Raleigh et al, sited in Chapter 2, showed that the two terminal domains behave independently of the α-helix, thereby justifying the region separation to analyze those correlation values.[28-30] The global and regional correlation analysis showed that the torsion angles of the structures generated by the simulations were not well correlated to those of the X-ray structure. Perfect correlation would have an R value of 1.0 when large values of one data set are associated with large values of the comparative data sent. When small values of one set are perfectly correlated with large values of the other data set, the correlation constant has a value of -1.0. The case of no correlation exhibits a constant R of 0. The correlation calculations performed regionally on the model structures show that the N-terminal domain exhibits the highest correlation among the three regions, while the α-helix exhibits the least.

Table 5.3: Table showing the correlation values (R) for the torsion angles of the. the Charge States models vs. the X-ray structure.

	Correlation (R) for Charge State Models vs. Xray Structure							
	Entire Protein		N-Terminal Domain		Alpha-Helix		C-Terminal Domain	
Charge State	**Phi**	**Psi**	**Phi**	**Psi**	**Phi**	**Psi**	**Phi**	**Psi**
+10	0.2646	0.3150	0.4177	0.4972	0.1833	0.0243	0.1716	0.3418
+11	0.2203	0.2788	0.3322	0.4759	0.0122	-0.0820	0.1696	0.3047
+12	0.2243	0.3175	0.3807	0.5207	0.0740	-0.1440	0.1975	0.3801
+13	0.3123	0.2216	0.4991	0.4228	0.0454	-0.1530	0.2640	0.2501
+14	0.3466	0.1273	0.2217	0.1126	0.1095	-0.1190	0.4288	0.1686
+15	0.3091	0.3076	0.4018	0.5376	0.0520	-0.1170	0.2864	0.3762
+16	0.3194	0.1696	0.5626	0.4145	-0.0820	-0.1720	0.2089	0.3765
+17	0.2427	0.3001	0.4007	0.5079	-0.0060	-0.1180	0.1710	0.3854
+18	0.2656	0.2265	0.3997	0.5421	0.0559	0.0034	0.2168	0.1651
+19	0.3097	0.2808	0.4099	0.4648	0.1475	0.0099	0.2798	0.2834
+20H106	0.3379	0.2447	0.4860	0.2282	0.0969	-0.0920	0.2937	0.3229
+20K109	0.3496	0.2172	0.6065	0.3165	-0.1840	0.2687	0.2215	0.1970
+21	0.3349	0.1968	0.5941	0.1052	0.0744	0.3982	0.2068	0.3416
+22	0.2636	0.3209	0.3937	0.4731	0.2105	0.7047	0.1912	0.3243
+23	0.3135	0.3264	0.4050	0.4765	0.1398	0.6874	0.2891	0.4066
+24	0.2251	0.2963	0.3988	0.6019	0.1273	0.4548	0.1349	0.3395
+25	0.2710	0.2803	0.4452	0.3826	0.2366	0.5806	0.1799	0.3760

5.3.3 Global and Regional Correlation of Adjacent Charge States

Another set of correlation analyses were performed where the modeled charge states were compared to the other charge states instead of to the X-ray structure. This was done sequentially to determine how the models predicted the conformation to change from one charge state to the next charge state with one more charge with stepwise protonation. This was also done as a global correlation for the entire protein chain, and as region correlations for the N-terminal, α-helix, and C-terminal. These data are shown in Table 5.4.

Overall, the correlation values calculated here with higher than those when comparing the charge states to the X-ray structure. Even though there are instances where the correlation constants produced by the phi and psi values respond differently, the overall correlation values for the global, whole protein analysis is high. When looking at the values regionally, they, too, are higher than those values produced from the X-ray comparison. It is deduced from this data that a high correlation value of two adjacent charge states would indicate few differences between the two structures, while a low correlation constant would allude to greater differences.

Table 5.4: Table showing the global and regional correlation (R) values derived from comparing a model charge state to the charge state with one additional proton.

	Correlation values (R) for Charge State Models vs Preceding Charge State							
	Entire Protein		N-Terminal Domain		Alpha-Helix		C-Terminal Domain	
Charge States	**Phi**	**Psi**	**Phi**	**Psi**	**Phi**	**Psi**	**Phi**	**Psi**
+10 v. +11	0.8686	0.7896	0.8106	0.8715	0.7212	0.6370	0.9650	0.8187
+11 v. +12	0.8998	0.7813	0.9319	0.7693	0.8281	0.6310	0.8764	0.8613
+12 v. +13	0.5943	0.7423	0.6844	0.8238	0.8600	0.7064	0.5460	0.7060
+13 v. +14	0.6616	0.6018	0.5581	0.5289	0.4976	0.5360	0.7161	0.7169
+14 v. +15	0.6081	0.5118	0.2975	0.4163	0.6047	0.6461	0.7554	0.5544
+15 v. +16	0.5516	0.7657	0.5330	0.8341	0.7940	0.7225	0.5381	0.7303
+16 v. +17	0.6769	0.7196	0.5214	0.6720	0.8668	0.5202	0.8016	0.8069
+17 v. +18	0.7686	0.5374	0.9598	0.6612	0.6136	0.2941	0.5851	0.5609
+18 v. +19	0.6085	0.6838	0.9868	0.8939	0.2569	0.5666	0.3549	0.6044
+19 v. +20H106	0.9160	0.6510	0.9812	0.7074	0.4164	0.6296	0.9461	0.6607
+19 v. +20K109	0.5754	0.4208	0.7670	0.4025	0.2687	0.3942	0.4798	0.4582
+20 v. +21	0.7383	0.4484	0.7046	0.4022	0.3982	0.3124	0.8514	0.6920
+21 v. +22	0.7259	0.6487	0.7405	0.4380	0.7047	0.4945	0.7139	0.8978
+22 v. +23	0.6683	0.5976	0.9873	0.8493	0.6874	0.3540	0.4323	0.6183
+23 v. +24	0.6856	0.6479	0.7938	0.8404	0.4548	0.4127	0.5146	0.6333
+24 v. +25	0.8129	0.6028	0.8754	0.6484	0.5806	0.5007	0.7789	0.6863

It is interesting to see that for the +20 charge state where the location of that 20th proton was narrowed down to one of two sites, that the structure produced from the H106 site has R values for phi and psi of 0.9160 and 0.6510, respectively, when compared to the +19 charge state. The structure from the protonation of the K109 residue showed R values of 0.5754 and 0.4208 for phi and psi, respectively. This is interpreted as the +20 H106 having a structure that is more similar to the +19 charge state than the +20 K109, because its R values are higher.

5.3.4 Local Correlation Analysis

In order to look more closely at the correlation of the simulated charge state structures to the X-ray structure, a method of looking at the correlation on a local scale was devised. For both the phi and psi angles, sequences of 5, 7, 9, 11, 13, and 15 residues were correlated for each model structure versus the X-ray structure. When the data are reported, a single amino acid is used to denote the center of the sequence used for correlation. For example, correlating Leu30, for five residues, looks at the sequence Asn28, Phe29, Leu30, Phe31, and Lys32 with the named residue at the center. It should be noted that at the termini of the protein, the full series of correlations could not be performed. The analysis starts with Val3 for three residues, but Val3 for 5 or more residues could not be calculated. The correlation value of 0.85 was arbitrarily selected as the cutoff for high correlation. Typically, data sets are considered to be well correlated when the R value is greater than 0.95. Since these data are generated from molecular modeling algorithms that

were the simplest approximation of the protein interactions experienced, in addition to comparisons being made between the gas and solid phases, the value of R for high correlation was decreased. In spite of the weak correlations on the global and regional scales, these data showed the presence of local areas on the modeled structures of the charge states that were highly correlated to the X-ray structure, and are displayed in Tables 5.5 (Phi) and 5.6 (Psi).

The regions of high correlation on the local level align with the areas of the X-ray structure that correspond to loops and turns. On the N-terminal globule, the region between Lys10 and Gly16 forms a loop and this is one of the places that exhibit high local correlation. Between residues Glu23 and Asp27, a turn is present in the X-ray structure and this, too, is a local area of high correlation. On the C-terminal, a loop is present between residues Lys82 and Thr94, this also proves to be a place of high local correlation between the different charge states and the X-ray structure. The region from Leu124 to Thr127 shows extensive correlation to the X-ray structure where it occurs at the intersection of a loop and a β-sheet.

Table 5.5: Local areas of high correlation of the torsion angle Phi (φ) for modeled charge state and X-ray structure. The residue indicates the central amino acid in correlated sequence. The numbers 5-15 indicate the number of amino acids in the correlated sequence.

	Number of Correlated Residues by Charge State																
Central Residue	+10	+11	+12	+13	+14	+15	+16	+17	+18	+19	+20 H106	+20 K109	+21	+22	+23 H144	+24	+25
Ile4	5					5	5		5		5	5		5	5		
Phe5																5	
Lys14				5													
Lys15				7			7										
Gly16	5	5	5	9		5	9	5	5	5	5	5	5	5	5		5
Glu17	7	7	7	11		7	11	7	7	7	7	7	7	7	7	7	7
Asp23		11	5	9	11	9	11	15	11	9	9	9	15	9	11	5	15
Gly24		9	7	9	9	9	9	11	9	9	11	9	13	9	9	7	13
Tyr25		7	7	7	7	7	7	11	7	11	11	7	11	7	7	7	13
Ala36							5										
Gln55	5	5	5	5	5			5		5	5	5	5	5	5	5	5
Asn64								5								5	5
Ala65																7	
Lys66																5	
Lys82			5				5										5
Ala83	5	5			5		5	5				5	5	5			5
Gly84					7											5	
Glu85					9						5						
Gly86					11						7						
Gly87				5	13	5				5	9				5		
Arg88				7		7				7					7		
Leu89				9		9				9					9		
Thr94	5	5	5		5	5		5		5	5	5	5	5	5		5
Leu102															5		
Ile115	5	5		5	5	5										5	5
Arg122												15					
Leu124		11	11	11	11		11	11	11	11	11	11	11	11	11	11	11
Gly125	9	9	9	9	9	9	9	9	9	9	9	9	9	9	9	9	9
Tyr126	7	7	7	7	7	7	7	7	7	7	7	7	7	7	7	7	7
Thr127		5	5	5	5	5	5	5	5	5	5	5	5	5			5

Table 5.6: Local areas of high correlation of the torsion angle Psi (ψ) for modeled charge state and X-ray structure. The residue indicates the central amino acid in correlated sequence. The numbers 5-11 indicate the number of amino acids in the correlated sequence.

	Number of Correlated Residues by Charge State																
Central Residue	+10	+11	+12	+13	+14	+15	+16	+17	+18	+19	+20 H106	+20 K109	+21	+22	+23 H144	+24	+25
Gly13	5	5	5	5		5			5	5				5	5		5
Lys14					5												
Lys15					7												
Gly16					9												
Glu17					11												
Asp23		5											5				5
Gly24		5											7				7
Tyr25		5											5				5
Asn27	5																
Lys45				5			5	5	5				5			5	
Glu73	5																
Lys74	5																
Lys82				5		5					5				5		
Gly84			5														
Gly86	5							7									7
Gly87	5							5									5
Ser101				5		5		5		5		5	5	5			
Gln103	5	5			5						5			5			
Asp111												5					
Tyr126		5				5						5	5	5			5
Glu136	5	5	5	5				5	5	5	5	5	5	5	5	5	5
Ala139							9	9	7							9	
Thr140	5	5		5		5	7	7	7	5	5	5	7			7	7
Leu141	5	5	5	5		5	5	5	5	5		5	5	5	5	5	5

5.4 CONCLUSIONS

Structures generated by molecular modeling simulations, using HyperChem, were correlated to the X-ray structure generated for Ribosomal Protein L9. Three levels of correlations were performed: global, for the entire protein; regional, for the three distinct domains; and local, for series of residues ranging from five to fifteen amino acids in length.

On the global scale, the correlation of the models with the X-ray structure was poor. The R constant values were on average below 0.3. When looking at the entire length of the protein chain, there appeared to be little correlation of the torsion angles between the amino acids, despite the fact the model structure maintained characteristics that were similar to the original X-ray structure. When an individual charge state was correlated to the structure possessing one additional charge, the correlation constant values were higher.

On the regional scale, the correlation of the three domains ranked in order of the N-terminal domain being most correlated, followed by the C-terminal domain, followed by the α-helix. The average correlation values for the torsion angles were approximately 0.5, 0.3, and 0.2 respectively. These values also indicated poor correlations against the X-ray structure.

On the local scale, correlations were calculated for as many as 15 residues. Despite the apparent absence of correlation for the entire protein and the three

structural domains, there exist areas of the protein that are well correlated with the X-ray structure. These regions corresponded to the turns and loops defined in the X-ray structure.

Even though the modeling performed here was of the simplest level, due to the size of the protein, program, and computer limitations, it was successful in generating structures that correlated regions of an intact gas-phase protein structure to its known solid-state X-ray structure.

5.5 REFERENCES

1. Elliott, W.H. and D.C. Elliott, *Biochemistry and Molecular Biology*. 1997, New York: Oxford University Press, Inc. 437.
2. Zubay, G.L., *Biochemistry*. 4th ed. 1998, New York, NY: Wm. C. Brown Publishers. 990.
3. Hoffman, D.W., C.S. Cameron, C. Davies, S.W. White and V. Ramakrishnan, *Ribosomal Protein L9: A Structure Determination by the Use of X-ray Crystallography and NMR Spectroscopy.* J. Mol. Biol., 1996. **264**: p. 1058-71.
4. Lillemoen, J., C.S. Cameron and D.W. Hoffman, *The stability and dynamics of ribosomal protein L9: investigations of a molecular strut by amide proton exchange and circular dichroism.* J. Mol. Biol., 1997. **268**(2): p. 482-93.
5. Kuhlman, B., J.A. Boice, R. Fairman and D.P. Raleigh, *Structure and Stability of the N-terminal Domain of Ribosomal Protein L9: Evidence for Rapid two-state folding.* Biochem., 1998. **37**: p. 1025-32.
6. Kaltashov, I.A., D. Fabris, A. Lee, Z. Szilagyi and C. Fenselau, *Thermochemistry and conformation of multiply charged peptides in a solvent-free environment.* Adv. Mass Spectrom., 1998. **14**.
7. Chowdury, S.K., V. Katta and B.T. Chait, *Probing Conformational Changes in Proteins by Mass Spectrometry.* J. Am. Chem. Soc., 1990. **112**: p. 9012-3.
8. Clemmer, D.E., R.R. Hudgins and M.F. Jarrold, *Naked Protein Conformations: Cytochrome c in the Gas Phase.* J. Am. Chem. Soc., 1995. **117**: p. 10141-2.
9. Konermann, L. and D.J. Douglas, *Acid-induced unfolding of cytochrome c at different methanol concentrations: Electrospray ionization mass spectrometry specifically monitors changes in the tertiary structure.* Biochem., 1997. **36**(40): p. 12296-302.
10. Babu, K.R. and A.D. Moradian, D. J., *The methanol-induced conformational transitions of b-lactoglobulin, cytochrome c, and ubiquitin at low pH: a study by electrospray ionization mass spectrometry.* J. Am. Soc. Mass Spectrom., 2001. **12**(3): p. 317-28.

11. Belva, H., C. Lange and I. Segalas, *Conformational properties of a-dendrotoxin using electrospray mass spectrometry.* Eur. J. Mass Spectrom., 2001. **7**(4&5): p. 373-83.

12. Gill, A.C., J.K. R., W. T. and B.M. T., *Conformations of biopolymers in the gas phase: a new mass spectrometric method.* Int. J. Mass Spectrom., 2000. **196**: p. 685.

13. Mao, D., K.R. Babu, Y.-L. Chen and D.J. Douglas, *Conformations of Gas-Phase Lysozyme Ions Produced from Two Different Solution Conformations.* Anal. Chem., 2003. **75**(6): p. 1325-30.

14. Valentine, S.J., *Probing gas-phase biomolecular ion conformation with ion mobility/mass spectrometry techniques*, Dissertation Thesis, 2000, Indiana University.

15. Wang, F., M.A. Freitas, A.G. Marshall and B.D. Sykes, *Gas-phase memory of solution-phase protein conformation: H/D exchange and Fourier transform ion cyclotron resonance mass spectrometry of the N-terminal domain of cardiac troponin C.* Int. J. Mass Spectrom., 1999. **192**: p. 319-25.

16. Brooks, B.R., R.E. Bruccoleri, B.D. Olafson, D.J. States, S. Swaminathan, and M. Karplus, *CHARMM: A program for macromolecular energy, minimization, and dynamics calculations.* J. Comput. Chem., 1983. **4**: p. 187-217.

17. Manjunatha, K.R. and H. Evans, J., *Molecular Modeling of Proteins: a Strategy for Energy Minimization by Molecular Mechanics in the AMBER force field.* J. Biomol. Struct. Dynamics, 1991. **9**(3): p. 475-88.

18. Okur, A., B. Strockbine, V. Hornak and C. Simmerling, *Using PC Clusters to Evaluate the Transferability of Molecular Mechanics Force Fields for Proteins.* J. Comput. Chem., 2003. **24**(1): p. 21-31.

19. Shirts, M.R., J.W. Pitera, W.C. Swope and V.S. Pande, *Extremely Precise Free Energy Calculations of Amino Acid Side Chain Analogs: Comparison of Common Molecular Mechanics Force Fields for Proteins.* J. Chem. Phy., 2003. **119**(11): p. 5740-61.

20. Garrett, R., H. and C. Grisham, M., *Biochemistry*. 1st ed. 1995, Orlando, FL: Saunders College Publishing. 1100.

21. Ramachandran, G.N. and V. Sasisekharan, *Conformation of polypeptides and proteins.* Adv. Protein Chemistry, 1968. **23**: p. 283-437.

22. Holtje, H.-D. and G. Folkers, *Molecular Modeling: Basic Priniples and Applications*. Methods and Priniciples in Medicinal Chemistry, ed. R.

Mannhold, H. Kubinyi and H. Timmerman. Vol. 5. 1997, New York: VCH Publishers, Inc. 194.

23. H.M. Berman, et al., *The Protein Data Bank.* Nucleic Acids Research, 2000. **28**: p. 235-242.

24. Laaksonen, L., *A Graphics Program for the Analysis and Display of Molecular Dynamics Trajectories.* J. Mol. Graphics, 1992. **10**: p. 33-4.

25. Bergman, D.L., L. Laaksonen and A. Laaksonen, *Visualization of Solvation Structures in iquid Mixtures.* J. Mol. Graph. Model., 1997. **15**: p. 301-6.

26. Koradi, R., M. Billeter and K. Wuthrich, *MOLMOL: A Program for Display and Analysis of Macromolecular Structures.* J. Mol. Graphics, 1996. **14**: p. 51-55.

27. Oh, H., K. Breuker, S.K. Sze, Y. Ge, B.K. Carpenter, and F.W. McLafferty, *Secondary and tertiary structures of gaseous protein ions characterized by electron capture dissociation mass spectrometry and photofragment spectroscopy.* Proc. Natl. Acad. Sci. USA, 2002. **99**(25): p. 15863-8.

28. Sato, S., B. Kuhlman, W.-J. Wu and D.P. Raleigh, *Folding of the multidomain ribosomal protein L9: The two domains fold independently with remarkably different rates.* Biochem., 1999. **38**(17): p. 5643-50.

29. Luisi, D.L., B. Kuhlman, K. Sideras, P.A. Evans and D.P. Raleigh, *Effects of Varying the Local Propensity to form Secondary Structure on the Stability and Folding Kinetics of a Rapid Folding alpha/beta Protein: Characterization of a Truncation Mutant of the N-Terminal Domain of the Ribosomal Protein L9.* J. Mol. Biol., 1999. **289**: p. 167-74.

30. Luisi, D.L., W.-J. Wu and D.P. Raleigh, *Conformational Analysis of a Set of Peptides Corresponding to the Entire N-terminal Domain of the Ribosomal Protein L9: Evidence for a Stable Native-like Secondary Structure in the Unfolded State.* J. Mol. Biol., 1999. **287**: p. 395-407.

CHAPTER 6: HOW THRESHOLD DISSOCIATION AND FRAGMENTATION PATHWAYS RELATE TO STRUCTURE

6.1 INTRODUCTION

Ribosomal protein L9 is studied using IRMPD and SORI to investigate its gas-phase tertiary structure using threshold dissociation. The differences in dissociation energies are a good indicator of conformational shift.[1] Also the resulting points of cleavage from the charge states are used to evaluate the fragmentation mechanisms governing the fragmentation process. Two distinct energy regimes are identified by the IRMPD data with the transition occurring at +20.

Currently, X-ray crystallography remains a reliable method of obtaining detailed information about the tertiary structure of a protein.[2,3] But since the protein is crystallized to obtain X-ray structures, the low energy structure is difficult to correlate to gas and solution phase structures. Multi-dimensional NMR can be used to determine the solution-phase higher order protein structure.[4] But for large proteins with masses over 20 kDa, interpretation of spectral analysis is very complicated.

A number of methods have been developed in mass spectrometry for probing tertiary structure. Ion mobility and hydrogen/deuterium exchange provide

information on protein cross-sections and conformer variance.[5-10] These methods provide general information on the gas-phase structure of the analyte, but they do not give local structural information. It has been demonstrated that various low energy dissociation studies can yield information describing higher-order structure.[11] The differences in dissociation patterns and in energy thresholds have been attributed in part to the gas-phase conformation. Accommodating all the factors that affect conformation is important and necessary to generate realistic models of the fragmentation.

Low energy dissociation methods, IRMPD and SORI, are well documented techniques for sequencing peptides and proteins.[12-14] Work by Gauthier et al. to compare the two methods found that both generated comparable data because of the slow, stepwise deposition of small amounts of internal energy.[15] IRMPD transfers energy to the target ion via a slow, sequential absorption of multiple photons and allows the lowest energy decomposition pathways to be sampled.[16] SORI is accomplished using the energy transferred from multiple collisions of the low energy ions with a neutral target.[17] Since only a small increment of energy is transferred with each collision, SORI also probes the lowest energy dissociation pathway of ions. Threshold data for the dissociation of L9 using both IRMPD and SORI are presented in this chapter.

There are sites in proteins that fragment more easily and more frequently than others. The facile cleavage of peptide bonds adjacent to aspartic acid and

glutamic acid residues is one such example.[18-21] The presence of the labile carboxylic proton on the acidic side chains makes the hydrogen available to initiate the fragmentation reaction. Mechanisms that are both dependent and independent of the adjacent residues have been deduced. The increased occurrence of fragmentation has also been observed adjacent to proline.[22,23] Proline is the only naturally occurring amino acid whose side chain is involved in a ring formation with the peptide backbone. Because of this, prolines are usually the site of a turn or a bend on the backbone. With L9 containing seventeen acidic residues and four prolines, the effects of these enhanced cleavages are seen in L9's dissociation.

In addition to the enhancement of cleavage at certain residues, Coulombic effects can majorly impact the dissociation of proteins. This may be especially applicable for the higher charge states produced by the electrospray process. In areas of the protein with high charge density caused by the close proximity of two or more charges, the Coulombic effect could make these sites more susceptible to cleavage.[24] The effects of Coulombic repulsions can be observed in positive electrospray ions because the fragments will be dominated by charge-induced cleavages occurring adjacent to the basic residues.

6.2 RESULTS AND DISCUSSION

6.2.1 Threshold Dissociation of Ribosomal Protein L9

Charge states +10 through +25 of electrosprayed L9 were individually isolated and subjected to IRMPD. As the laser power was increased to effect dissociation, each resulting spectrum was inspected to determine the threshold laser power required for dissociation, the sites of fragmentation, and subsequently the location were the charges reside. Threshold laser power was determined to be the laser power at which fragments begin to appear in the spectrum. In each case, an experiment was performed where the laser power was set to 0W to serve as a blank measurement.

Figure 6.1 shows the laser power for threshold dissociation of each of the observable charge states. There is a significant delineation of the charge states into two groups according to the power required for threshold dissociation to be achieved. The lower charge states (+10 through +19) required laser powers greater than 10 Watts for significant dissociation fragments to appear in their mass spectra. At charge state +20 and +21, the amount of laser power required for dissociation drops significantly and fragment ions begin appearing in the blank spectra where no laser power was applied. For charge states greater than +21, the threshold laser dissociation power is lower than 6 Watts. Tables 6.1 and 6.2 show the complete list

of the b ad y fragment ions produced at threshold for the 16 observable charge states by IRMPD.

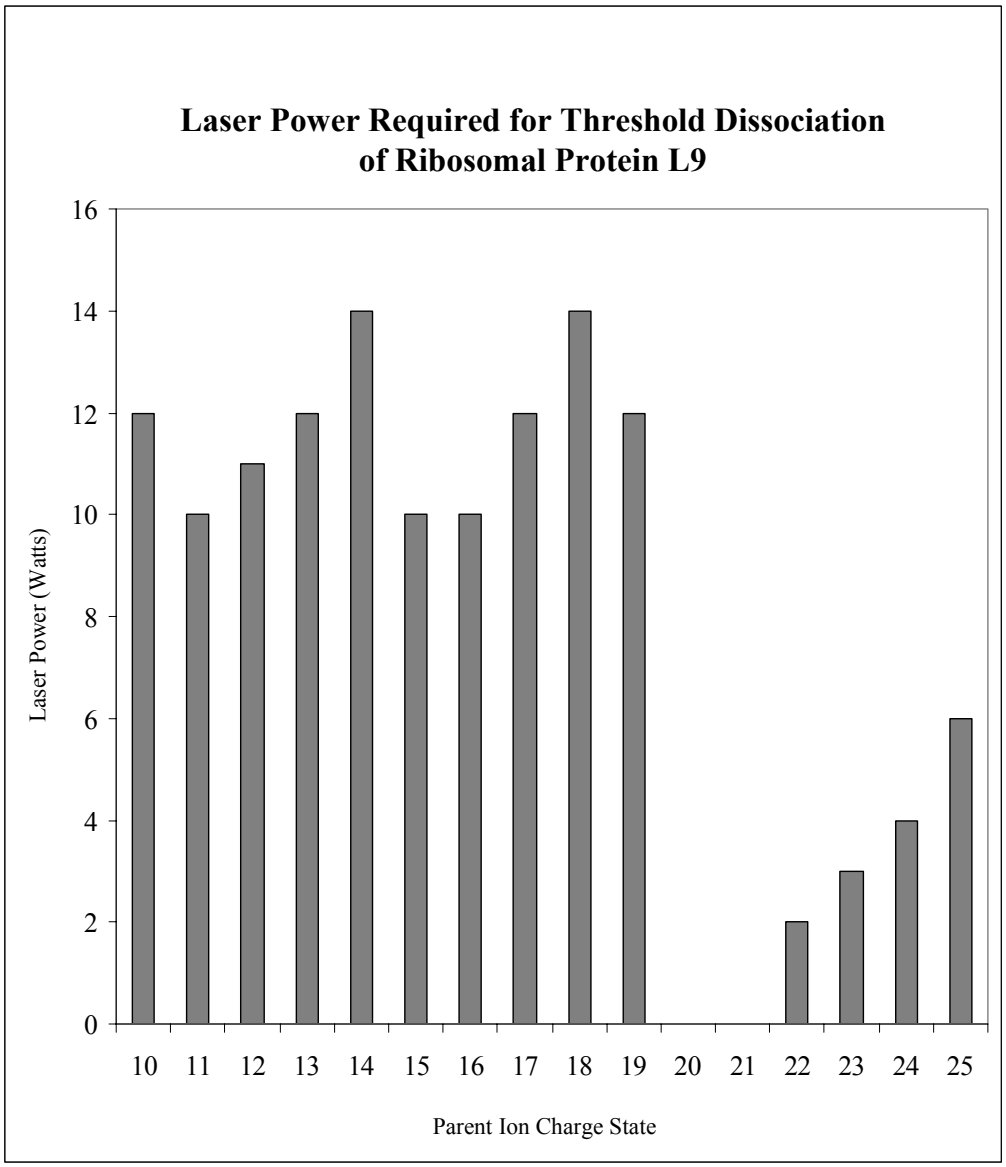

Figure 6.1: Graph of laser power (Watts) used to achieve threshold dissociation for charge state +10 through +25.

Table 6.1: B fragments generated from the IRMPD threshold dissociation of the +10 to +25 charge states of L9 (continued on next page).

		Charge States															
Charge on Fragment	Fragment	+10	+11	+12	+13	+14	+15	+16	+17	+18	+19	+20	+21	+22	+23	+24	+25
1	b10	+	+	+	+							+			+		
2	b10									+							
3	b11								+								
9	b111				+												
10	b111					+											
12	b111									+							
13	b111									+	+						
15	b111												+				
17	b111															+	+
13	b111-H2O									+							
17	b111-NH3																+
8	b116		+														
8	b119			+													
12	b119									+							
13	b119									+							
2	b12				+	+	+			+			+		+		
2	b13		+														
13	b134							+									
10	b139		+														
2	b14	+		+				+									
11	b147			+													
11	b147-H2O			+													
1	b15											+					
2	b15		+		+												
8	b17	+															
2	b19		+		+												
3	b19							+		+							
2	b23	+	+	+	+	+	+	+	+			+	+	+	+		
3	b23						+										
2	b23-H2O											+					
4	b28									+					+	+	+
5	b28														+		+
7	b28															+	
4	b29									+	+		+		+		+
5	b29												+	+	+	+	+
6	b29													+	+	+	+
4	b30									+					+		
5	b30												+		+	+	+
6	b30																+

		Charge States															
Charge on Fragment	Fragment	+10	+11	+12	+13	+14	+15	+16	+17	+18	+19	+20	+21	+22	+23	+24	+25
5	b34																+
4	b35				+	+	+										
5	b35									+							+
3	b36														+		
4	b36			+			+			+	+				+		
5	b36									+			+			+	+
6	b36															+	+
7	b36																+
3	b37	+															
4	b37				+	+							+				
6	b37												+				
7	b37														+	+	+
4	b37-NH3				+												
4	b38				+	+	+	+					+		+		
5	b38									+							
4	b39				+	+							+		+		
5	b39					+						+	+		+		
6	b39								+			+					
7	b39												+		+	+	+
5	b39-NH3												+				
1	b4	+	+					+									
3	b40	+															
4	b40				+	+									+		
1	b6	+															
3	b6					+											
1	b7	+	+		+					+					+		
5	b70		+	+													
6	b70			+	+												
1	b8						+						+				
2	b8		+	+							+		+		+		
8	b85							+									
9	b85							+									
1	b9	+															

Table 6.2: Y fragments generated from the IRMPD threshold dissociation of the +10 to +25 charge states of L9 (continued on pg 26).

		Charge States															
Charge on Fragment	Fragment	+10	+11	+12	+13	+14	+15	+16	+17	+18	+19	+20	+21	+22	+23	+24	+25
11	y107						+										
9	y109			+													
2	y11									+							
15	y110												+				
18	y110																+
10	y111					+											
18	y112																+
18	y112-H2O																+
13	y113									+							
13	y113-H2O									+							
18	y119															+	
17	y120														+		
18	y120															+	
8	y126	+		+													
9	y126			+													
10	y126			+													
10	y130			+													
13	y130							+									
10	y134		+	+													
9	y138	+															
8	y139			+													
9	y139			+													
10	y139		+														
11	y139			+													
11	y139-H2O			+													
11	y141			+													
14	y141						+										
11	y142			+													
10	y148	+															
11	y148		+														
3	y15							+		+	+		+		+		
1	y2									+			+	+	+		
3	y20									+							
8	y29															+	
4	y30			+	+	+	+	+	+	+		+	+		+		
5	y30									+	+		+		+		
3	y33		+														
4	y33				+												
5	y37									+							
5	y38			+	+	+	+	+	+	+	+			+			
6	y38									+	+	+	+	+			
7	y38														+		+

		Charge States															
Charge on Fragment	Fragment	+10	+11	+12	+13	+14	+15	+16	+17	+18	+19	+20	+21	+22	+23	+24	+25
8	y38															+	+
5	y38-H2O									+							
6	y38-H2O									+							
1	y4		+					+		+				+			+
9	y47																+
1	y5										+						
2	y5	+			+			+						+	+		
1	y6				+									+			
2	y6											+					
3	y6					+											
7	y64			+			+	+					+				
3	y7	+					+	+									
6	y72												+				
7	y72												+				
7	y75														+		
8	y79						+										
2	y8		+	+									+				
3	y8		+														
4	y8							+									
1	y8-NH3		+														
12	y95									+	+						

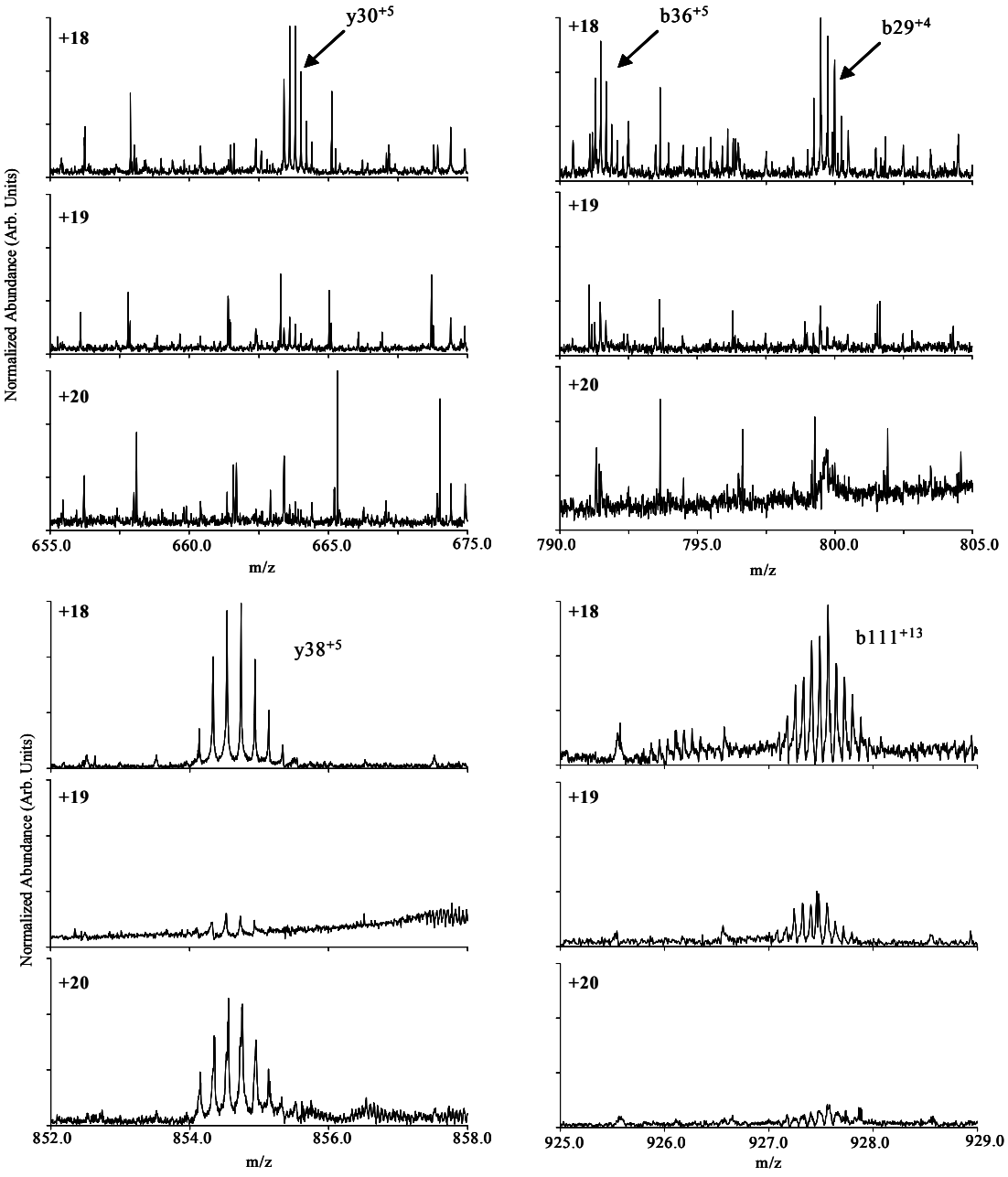

Figure 6.2: Expanded regions of the +18, +19, and +20 IRMPD threshold spectra to illustrate the fragmentation seen, b and y fragments are labeled. Unlabeled peaks are likely unidentified internal fragments.

Protein dissociation is influenced by the location of charge and by the conformation of the electrosprayed ion the gas-phase. Since protein conformation can play an important role in dissociation pathways, looking at the dissociation energy at threshold is important. In the case of an unfolded protein, there may be sections along the backbone which are more susceptible to cleavage because those residues are not experiencing the stabilizing interactions associated with secondary structure. A folded protein could possess a more strained structure that may result in more facile dissociation. Also, the increased charge density of a folded protein containing the same number of charges as its unfolded analog could result in more dissociation. The difference in charge density could explain why lower threshold dissociation energies were needed for the higher charge states.

6.2.2 SORI Threshold Dissociation

SORI was performed on the +20, +21, and +22 charge states in order to confirm the extreme drop in the threshold laser power observed with IRMPD data. The average kinetic energy was calculated for each of these charge states using the Equation 6.1:

$$< E_{tr} > = \frac{E^2 q^2}{4m(\Delta\omega)^2} \qquad \text{Equation 6.1}$$

where q and m are the charge and mass, E is the electric field amplitude, and Δω is the difference, in Hertz, between the excitation frequency and the natural cyclotron

frequency of the ion.[25] The calculated values for the threshold energy for the +20, +21, and +22 were used to calibrate the threshold laser power and the results are shown in Table 6.3. The dramatic drop in average kinetic energy from the +19 to the +20 is highly suggestive of a conformational shift. This difference could be attributed to a more strained conformation occupied by the higher charge states. This tighter conformation puts strain at different sites that become more susceptible to fragmentation.

Table 6.3: Calibration of threshold laser power to eV using the average kinetic energy calculated from the SORI data.

Charge State	Laser Power (Watts)	Avg. Kinetic Energy (eV)
+10	12	4.96
+11	10	4.25
+12	11	4.61
+13	12	4.96
+14	14	5.67
+15	10	4.25
+16	10	4.25
+17	12	4.96
+18	14	5.67
+19	12	4.96
+20	0	0.70
+21	0	0.70
+22	2	1.41
+23	3	1.77
+24	4	2.12
+25	6	2.83

6.3 FRAGMENTATION OF L9

The IRMPD data showed general fragmentation across the N- and C-terminal domains. On the N-terminal, one concentrated region of fragmentation was located from Leu35 to Thr40 which contains only one acidic residue. This region is immediately adjacent to the central α-helix and is defined as a β-sheet from X-ray diffraction. NMR data describe this region as having the characteristics of a hinge, affording movement of the N-terminal domain.[26] This characteristic would explain the increase of fragmentation seen there. Of the 24 peptide bonds locations that were cleaved, 12 of them were adjacent to basic residues, and 4 were adjacent to acidic residues. The relative abundance of the fragments formed from cleavages adjacent to acidic or basic residues was at least an order of magnitude greater than the other abundances. If protons were not sequestered on the side chains, and were freely moving along the backbone, all peptide bonds would cleave with the same probability.[27]

In the charge states +10 through +13, the region from Lys2 to Lys15 showed extensive fragmentation adjacent to basic residues. This series of amino acids forms a loop or random coil and is so defined because there are no characteristic of secondary structure associated with those residues. The absence of secondary structure and the stabilizing interactions it involves could result in more fragmentation being observed.

On the C-terminus, at threshold, the fragment sites were abundant from Lys142 to Gln148, which has a β-sheet secondary structure for X-ray diffraction. Another region with abundant cleavages was from Lys110 to Ile121. Loops do not participate in stabilizing side chain interactions and that could make this area more susceptible to fragmentation.

The α-helix did not exhibit any significant fragmentation. At threshold, three were seven cleavages in the α-helix and six were adjacent to either basic or acidic residues. It appears that the even though the molecular modeling simulations were unable to retain the helical structure of this region, there was some increased stability afforded to it that could be indicative of some retention of the helix in the gas-phase.

6.4 CONCLUSIONS

The discontinuity in the average kinetic energy at threshold between the +19 and +20 charge states is a strong indicator that there is a conformational shift in the protein structure that occurs at this point. The additional in charge could be increasing the charge density on the ion and thus, increasing the Coulombic forces resulting in more facile fragmentation. Alternately, the increase in charge could result in self-solvation and stabilization of a more compact conformation that could introduce additional strain on certain areas of the molecule. It is unclear which of these principles is at work in this system.

A fragmentation pathway is favored that results in cleaves C-terminal to acidic residues. This suggests that the carboxylic hydrogens are inducing the cleavages. The presence of a high number of fragments that occur adjacent to the basic residues also supports this model.

6.5 REFERENCES

1. Bolaños, B.J., *Study of Higher Order Gas-Phase Protein Structure by Fourier Transform Ion Cyclotron Resonance Mass Spectrometry*, Dissertation Thesis, Department of Chemistry and Biochemistry, 1997, The University of Texas at Austin.
2. Bruccoleri, R.E., *Conformational Search and Protein Folding*, in *The Protein Folding Problem and Tertiary Structure Prediction*, K. Merz, Jr. and S. Le Grand, Editors. 1994, Birkhauser: Boston. p. 125-40.
3. Vijay-Kumar, S., C.E. Bugg, K.D. Wilkinson and W.J. Cook, *Structure of ubiquitin refined at 1.8 A resolution.* J. Mol. Biol., 1987. **194**(3): p. 531-44.
4. Bax, A., *Two-Dimensional Nuclear Magnetic Resonance in Liquids*. 1982, Dordrecht, Holland: D. Reidel Publishing Co. 200.
5. Cox, K.A., R.K.J. Julian, R.G. Cooks and R.E.J. Kaiser, *Conformer selection of protein ions by ion mobility in a triple quadrupole mass spectrometer.* J. Am. Soc. Mass Spectrom., 1994. **5**(3): p. 127-363.
6. Clemmer, D.E., R.R. Hudgins and M.F. Jarrold, *Naked Protein Conformations: Cytochrome c in the Gas Phase.* J. Am. Chem. Soc., 1995. **117**: p. 10141-2.
7. Valentine, S.J. and D.E. Clemmer, *H/D Exchange Levels of Shape Resolved Cytochrome c Conformers in the Gas Phase.* J. Am. Chem. Soc., 1997. **119**: p. 3558-66.
8. Suckau, D., et al., *Co-Existing Stable Conformations of Gaseous Protein Ions.* Proc. Natl. Acad. Sci. U.S.A., 1993. **90**: p. 790-3.
9. Wood, T.D., R.A. Chorush, F.M.I. Wampler, D.P. Little, P.B. O'Connor, and F.W. McLafferty, *Gas phase folding and unfolding of cytochrome c cations.* Proc. Natl. Acad. Sci. U.S.A., 1995. **92**: p. 2451-4.
10. Cassady, C.J., J. Wronka, G.H. Kruppa and F.H. Laukien, *Deprotonation reactions of multiply protonated ubiquitin ions.* Rapid Commun. Mass Spectrom., 1994. **8**: p. 394-400.
11. Wu, Q., S. Van Orden, X. Cheng, R. Bakhtiar and R.D. Smith, *Characterization of Cytochrome c Variants with High-resolution FTICR*

Mass Spectrometry: Correlation of Fragmentation and Structure. Anal. Chem., 1995. **67**: p. 2498-509.

12. Biemann, K. and S.A. Martin, *MS/MS of Peptides.* Mass Spectrom. Rev., 1987. **6**: p. 1-76.
13. Fenselau, C., *Beyond Gene Sequencing: Analysis of Protein Structure with Mass Spectrometry.* Ann. Rev. Biophys. Chem., 1991. **20**: p. 205-20.
14. Little, D.P., J.P. Speir, M.W. Senko, P.B. O'Connor and F.W. McLafferty, *Infrared Multiphoton dissociation of large multiply-charged ions for biomolecule sequencing.* Anal. Chem., 1994. **66**(18): p. 2809-15.
15. Gauthier, J.W., T.R. Trautman and D.B. Jacobson, *Sustained Off-resonance Irradiation for CAD Involving FTMS. CAD Technique that Emulates Infrared Multiphoton Dissociation.* Anal. Chim. Acta, 1991. **246**: p. 199-210.
16. Thorne, L.R. and J.L. Beauchamp, *Gas Phase Ion Chemistry*, ed. M.T. Bowers. Vol. 3. 1984, New York: Academic.
17. Gorshkov, M.V., L. Pasa-Tolic and R.D. Smith, *Pressure limited sustained off-resonance irradiation for collision-activated dissociation in Fourier transform mass spectrometry.* J. Am. Soc. Mass Spectrom., 1999. **10**(1): p. 15-8.
18. Yu, W., J.E. Vath, M.C. Huberty and S.A. Martin, *Identification of the Facile Gas-Phase Cleavage of the Asp-Pro and Asp-Xxx Peptide Bonds in Matrix-Assisted Laser Desorption Time-of-Flight Mass Spectrometry.* Anal. Chem., 1993. **65**(21): p. 3015-23.
19. Qin, J. and B.T. Chait, *Preferential Fragmentation of Protonated Gas-Phase Peptide Ions Adjacent to Acidic Amino Acid Residues.* J. Am. Chem. Soc., 1995. **117**: p. 5411-2.
20. Gu, C., G. Tsaprailis, L. Breci and V.H. Wysocki, *Selective Gas-Phase Cleavage at the Peptide Bond C-Terminal to Aspartic Acid in Fixed-Charge Derivative of Asp-Containing Peptides.* Anal. Chem., 2000. **72**: p. 5804-13.
21. Tsaprailis, G., et al., *Influence of Secondary Structure on the Fragmentation of Protonated Peptides.* J. Am. Chem. Soc., 1999. **121**(22): p. 5142-54.
22. Loo, J.A., C.G. Edmonds and R.D. Smith, *Tandem mass spectrometry of very large molecules. 2. Dissociation of multiply charged proline-containing proteins from electrospray ionization.* Anal. Chem., 1993. **65**(4): p. 425-38.
23. Breci, L.A., D.L. Tabb, J.R.I. Yates and V.H. Wysocki, *Cleavage N-Terminal to Proline: Analysis of a Database of Peptide Tandem Mass Spectra.* Anal. Chem., 2003. **75**(9): p. 1963-71.

24. Rockwood, A.L., M. Busman and R.D. Smith, *Coulombic effects in the dissociation of highly charged ions.* Int. J. Mass Spectrom. Ion Processes, 1991. **111**: p. 103-29.

25. Beauchamp, J.L., *ICR Spectroscopy.* Ann. Rev. Phys. Chem., 1971. **22**: p. 527-61.

26. Lillemoen, J., *Internal dynamics of biological macromolecules: investigations of ribosomal protein L9 and bacteriophage T2 gene 32 RNA pseudoknot.*, Dissertation Thesis, Department of Chemistry and Biochemistry, 1998, The University of Texas at Austin.

27. Wattenberg, A., A.J. Organ, K. Schneider, R. Tyldesley, R. Bordoli, and R.H. Bateman, *Sequence Dependent Fragmentation of Peptides Generated by MALDI Quadrupole Time-of_Flight (MALDI Q-TOF) Mass Spectrometry and its Implications for Protein Identification.* J. Am. Soc. Mass Spectrom., 2002. **13**: p. 772-83.

Appendix

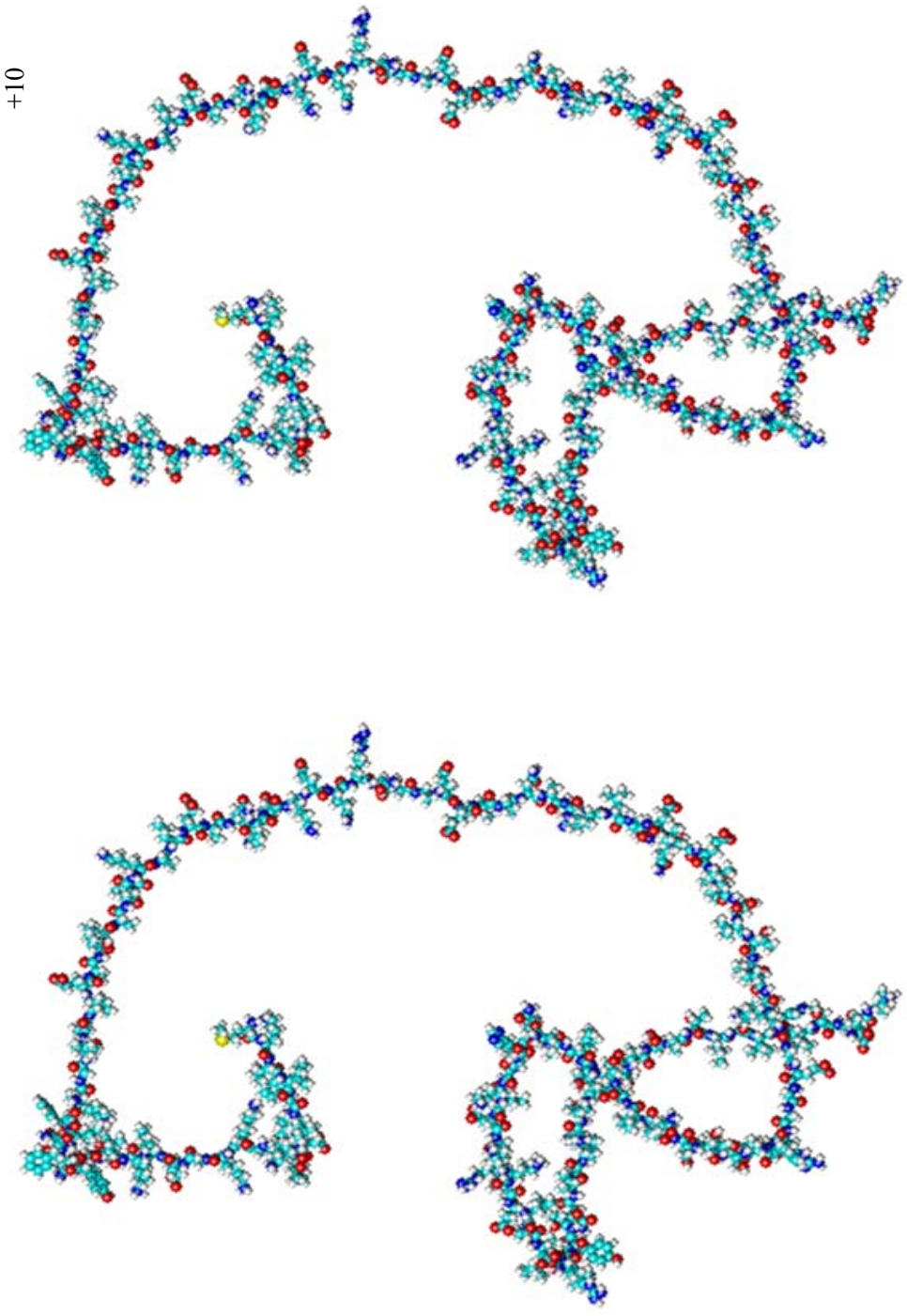
+10

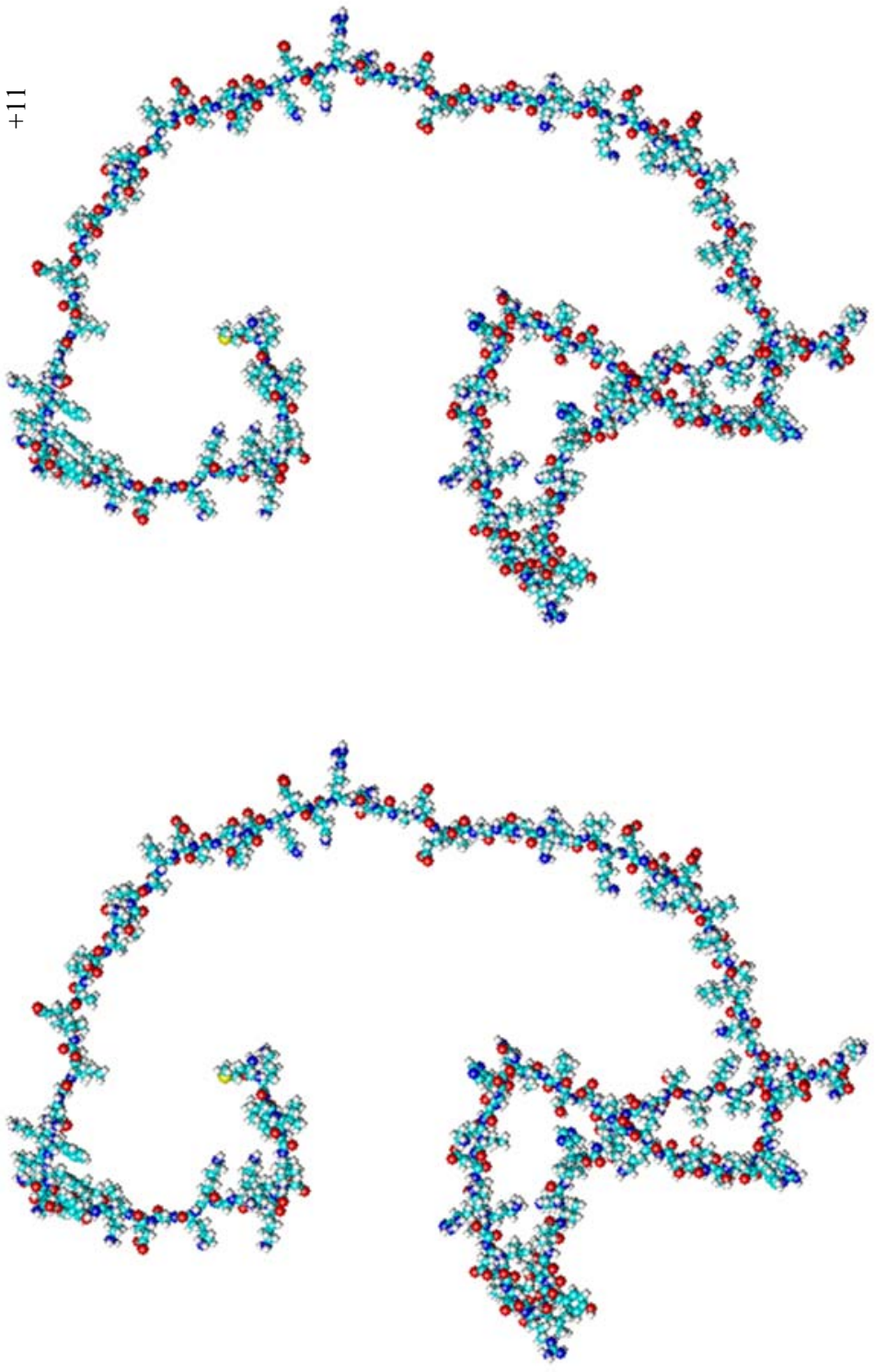
+11

+12

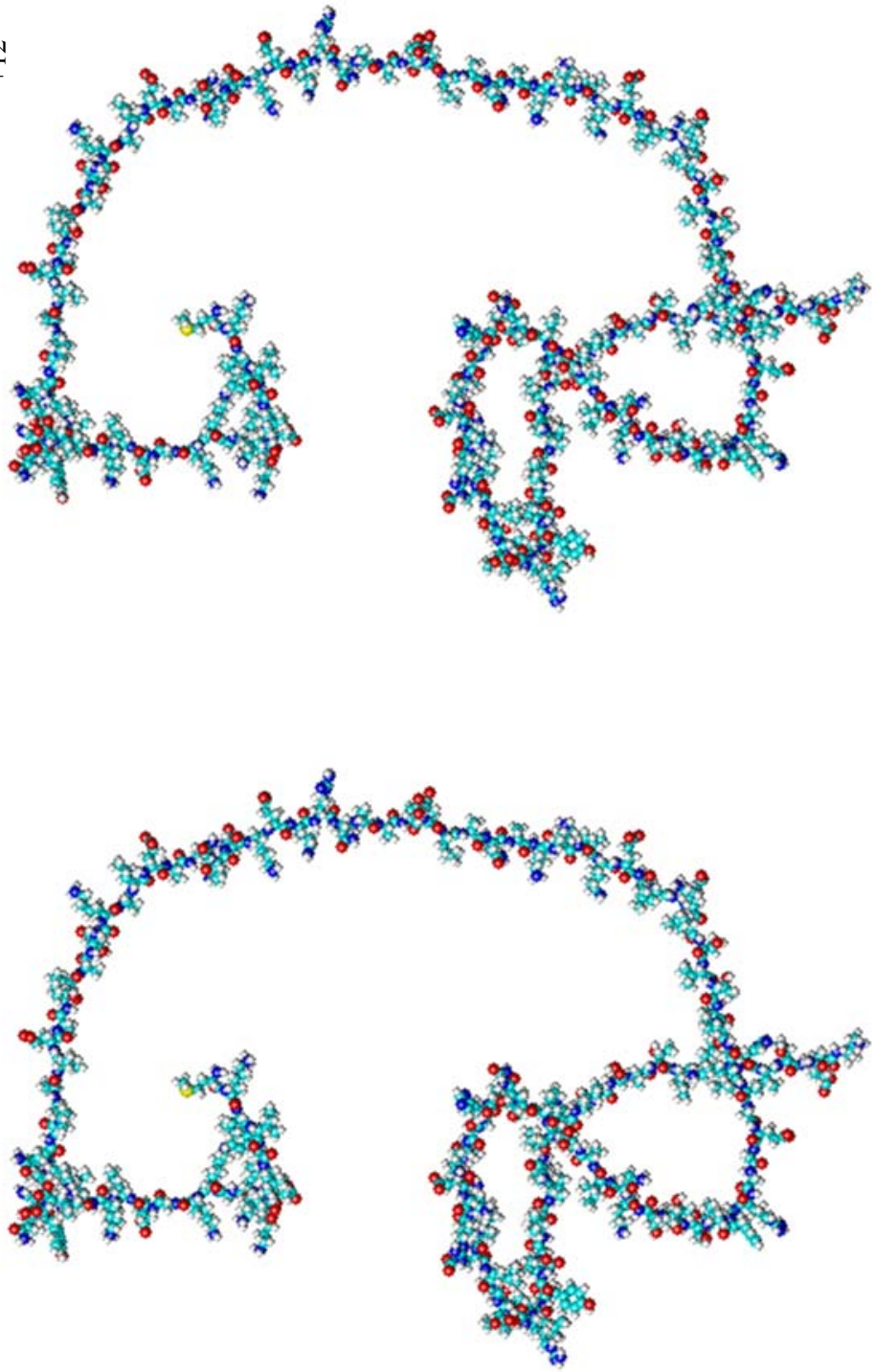

+13

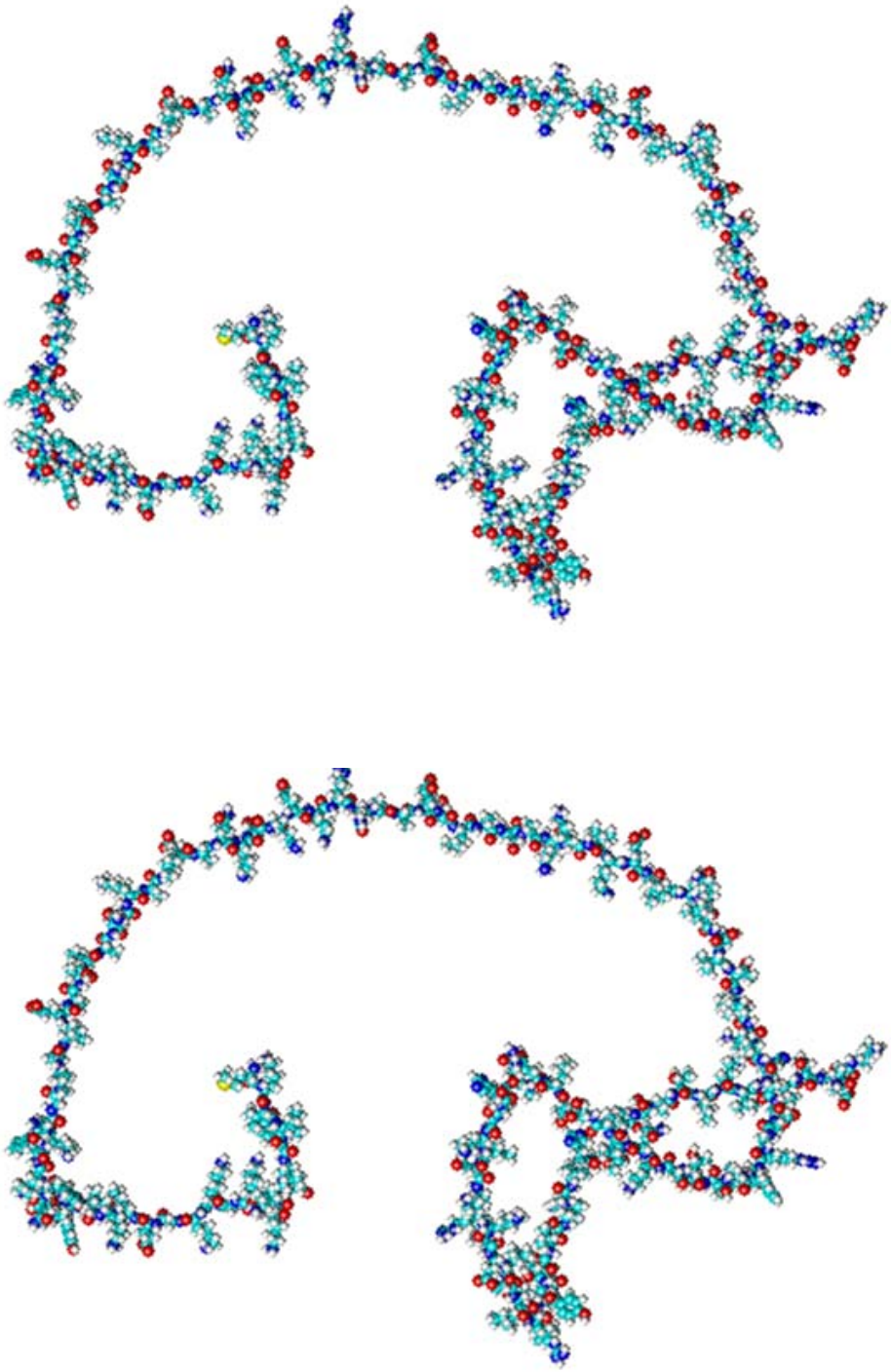

+14

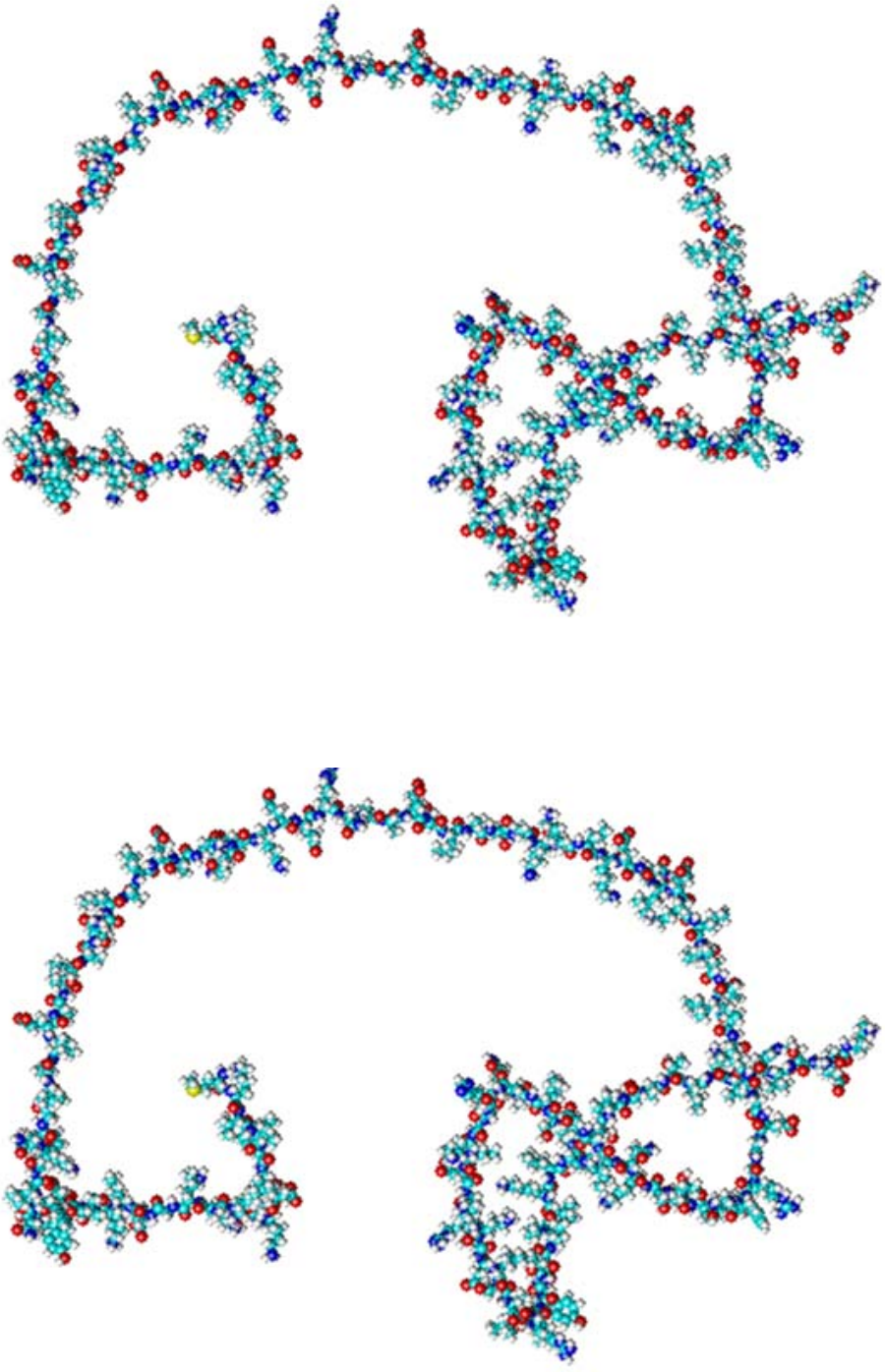

+15

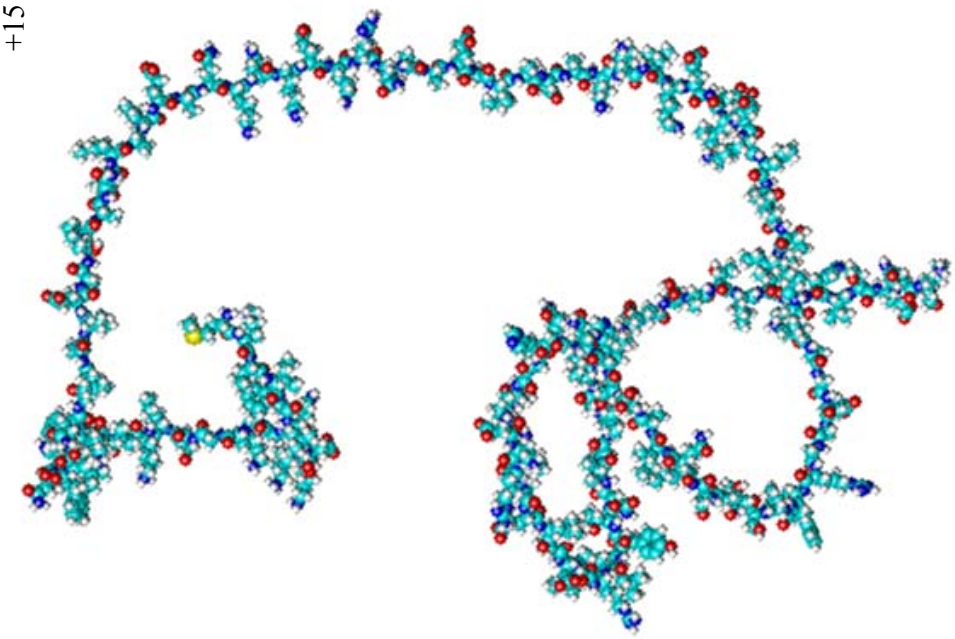

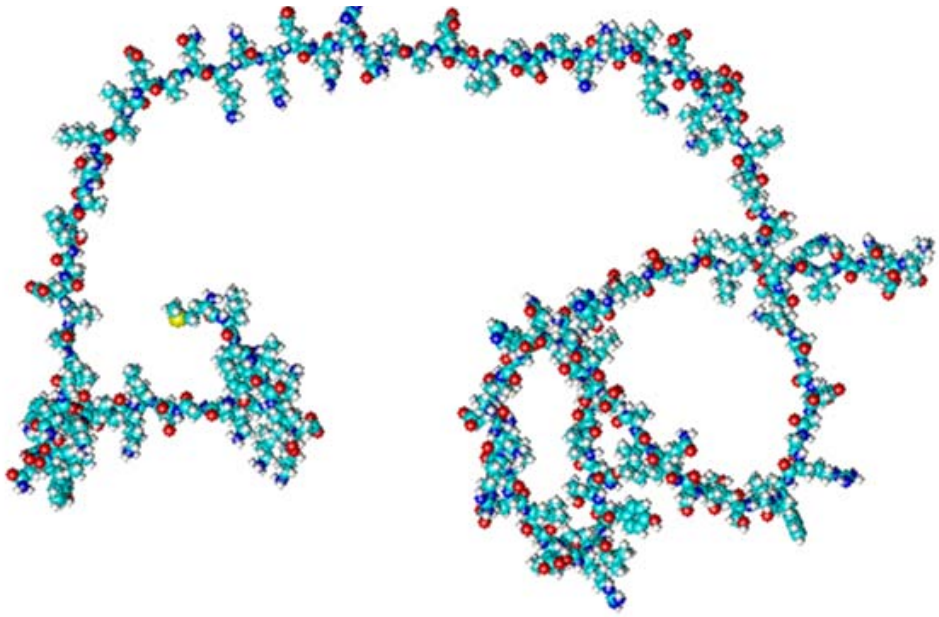

+16

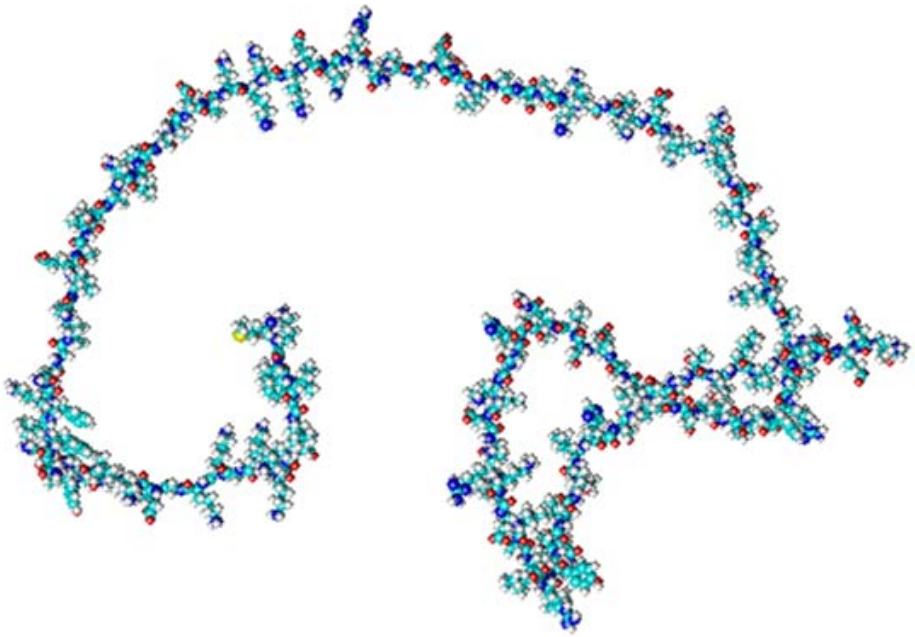

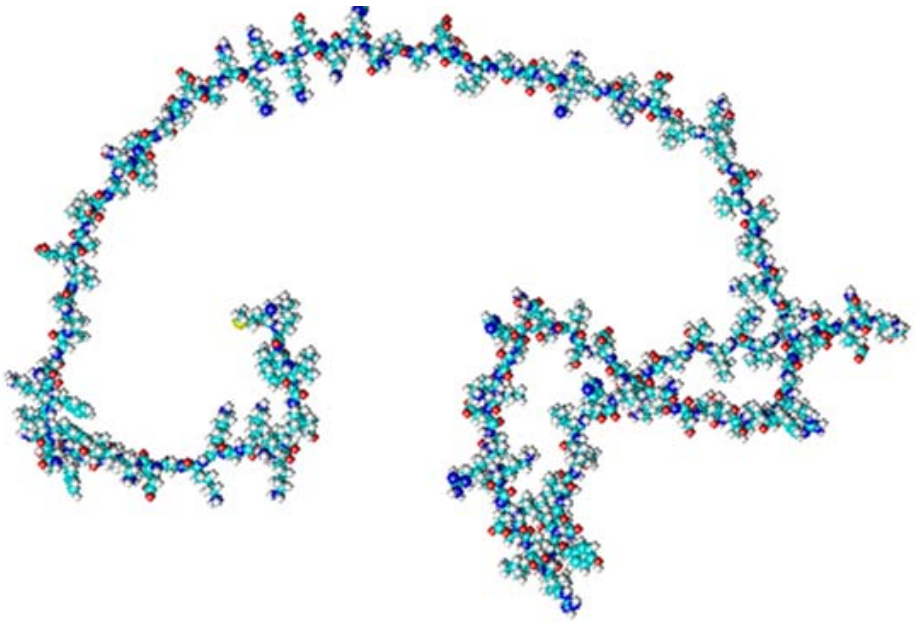

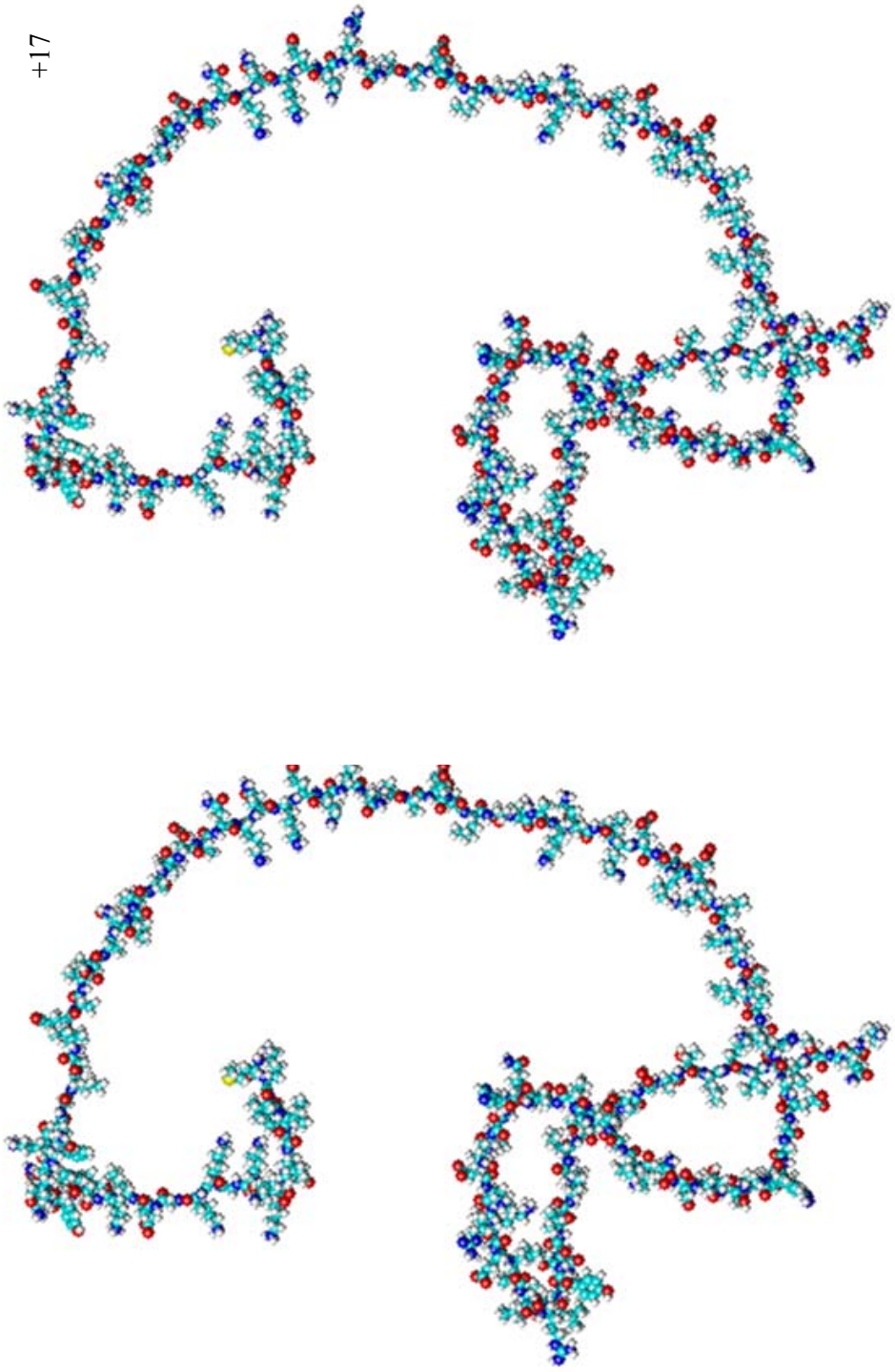
+17

+18

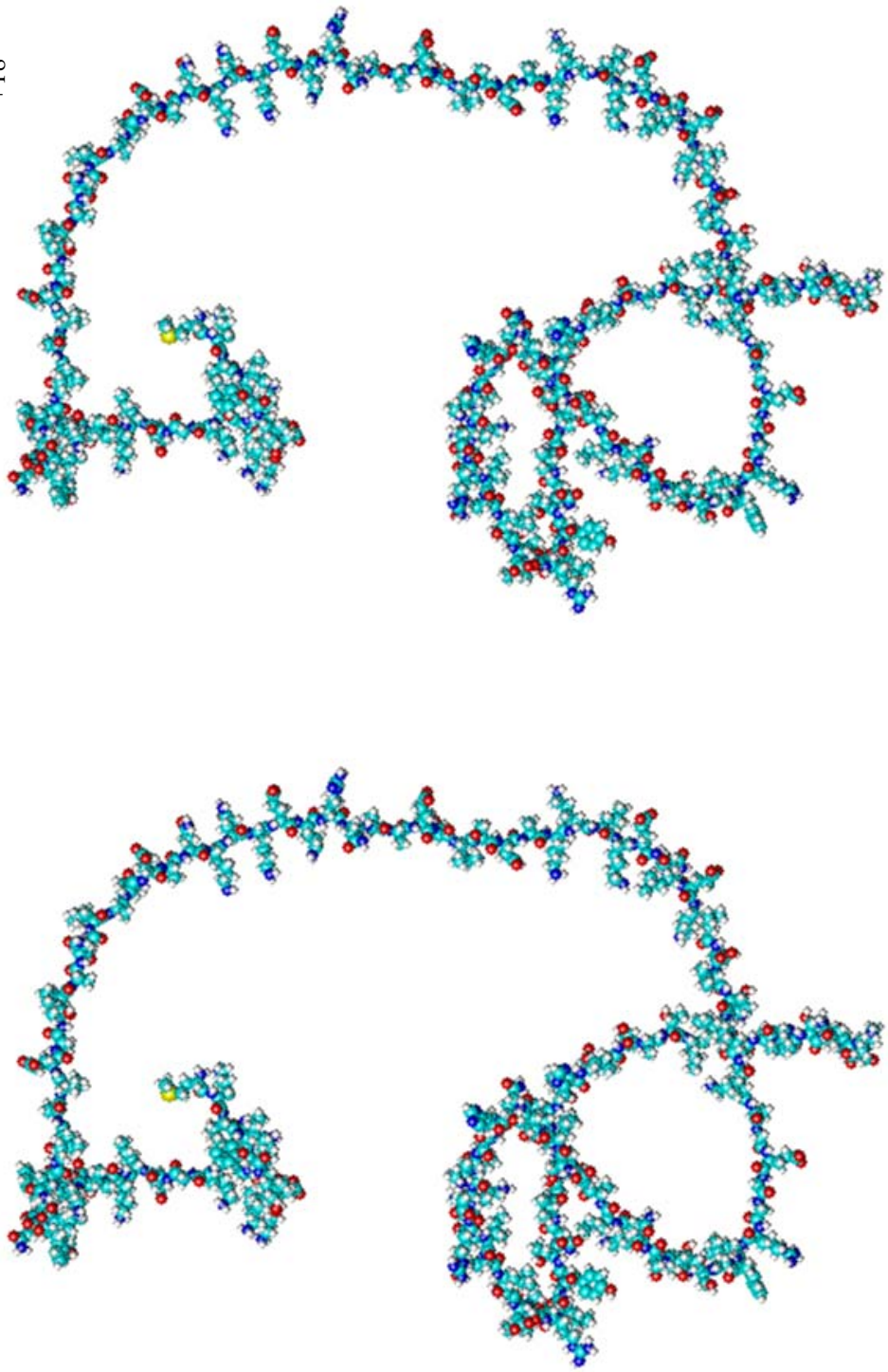

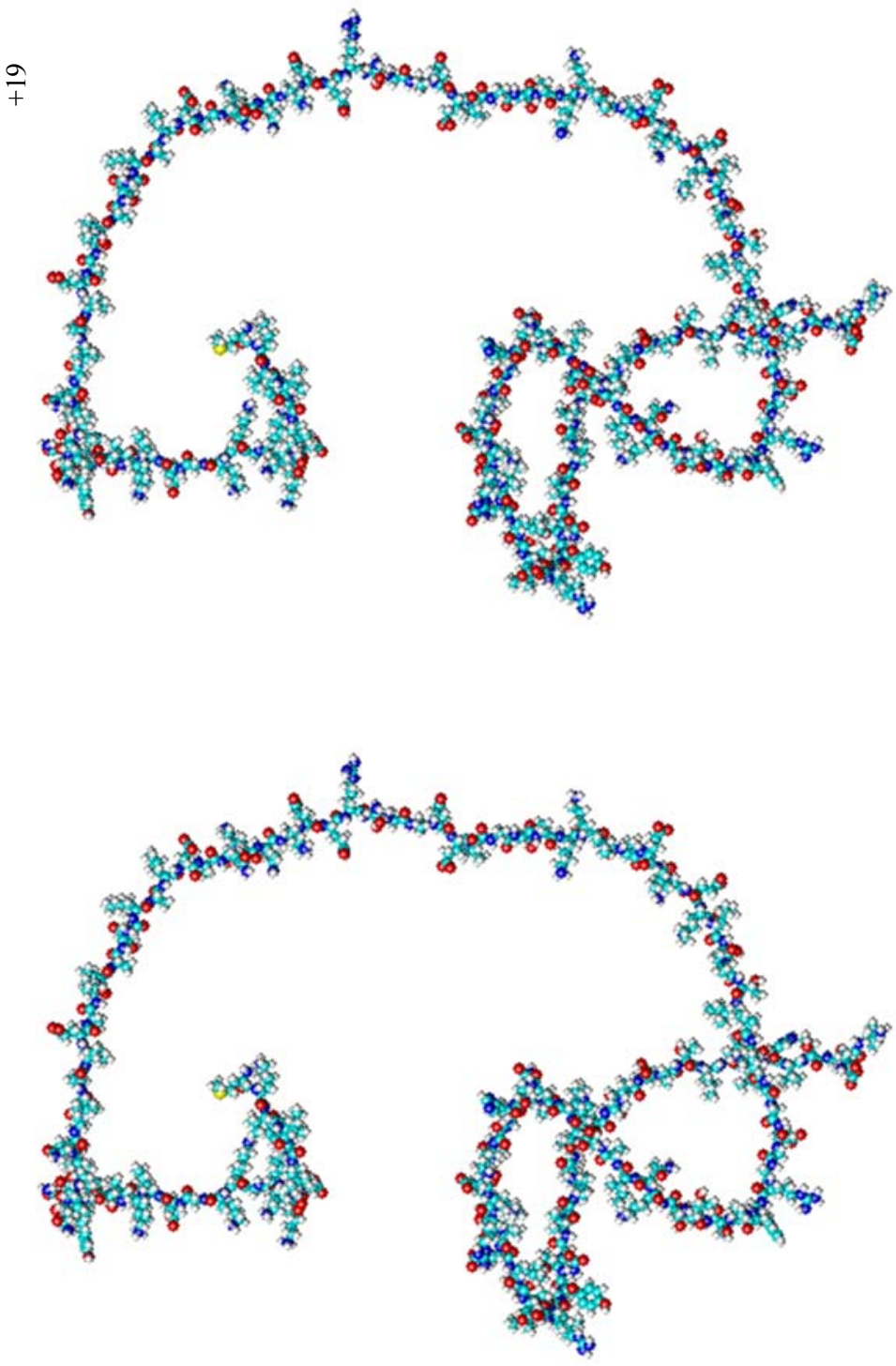
+19

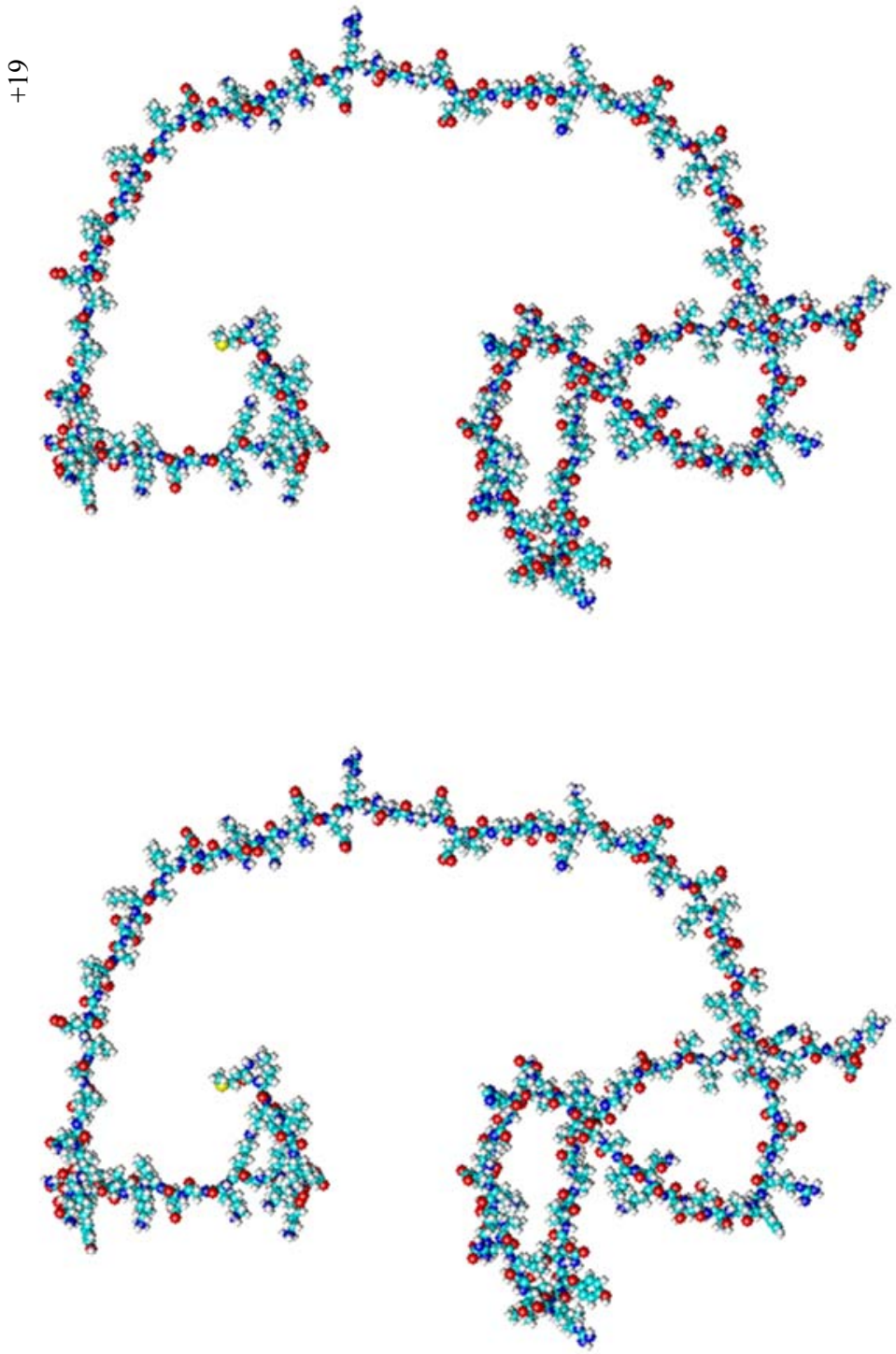
+19

+20K109

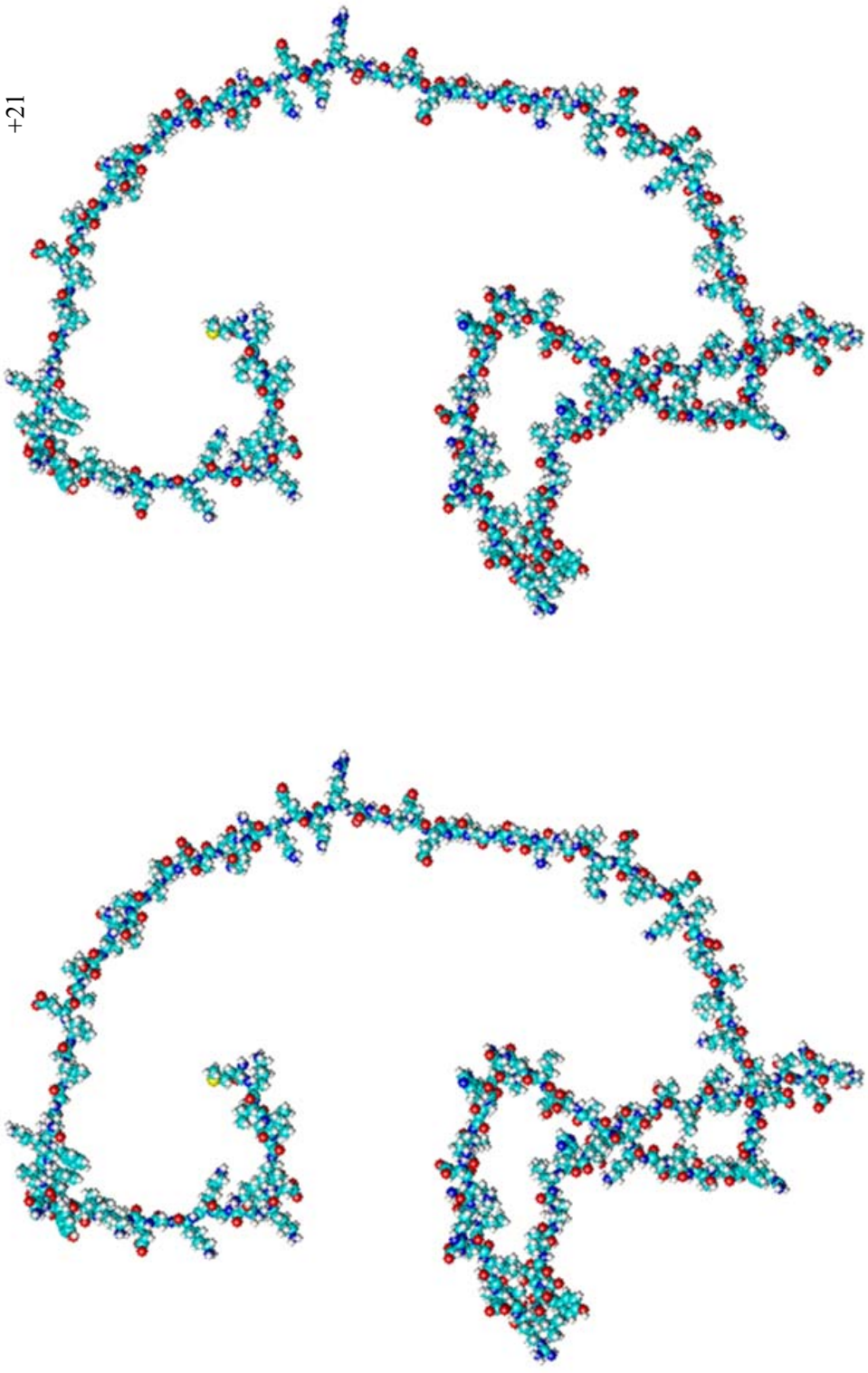
+21

+22

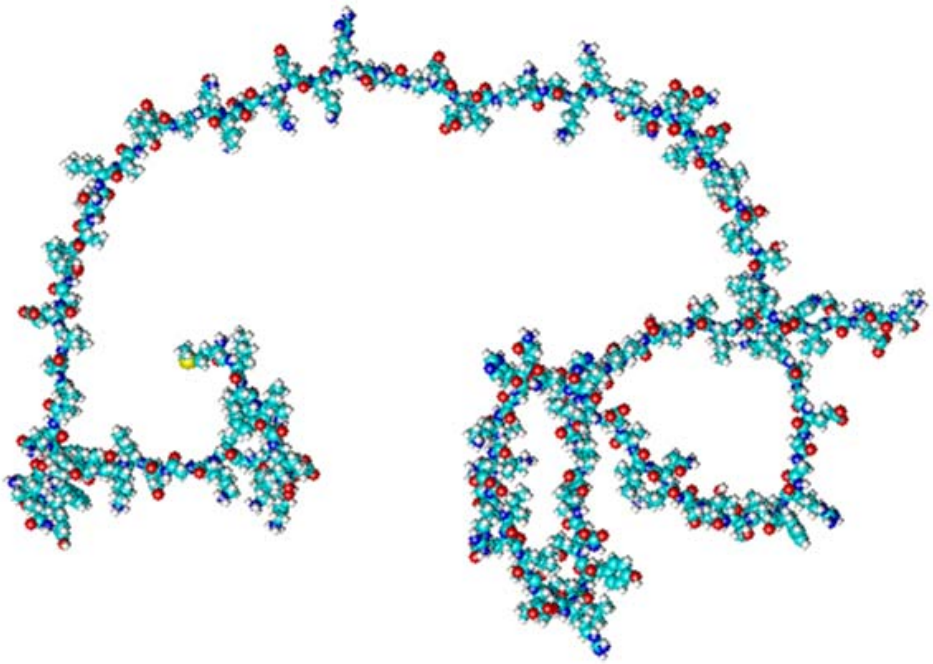

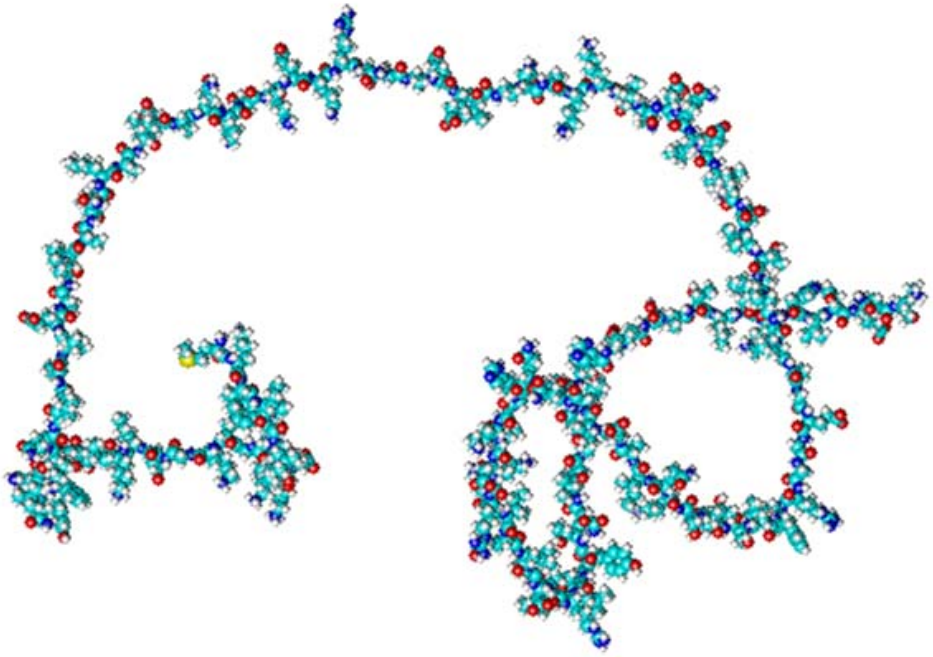

+23

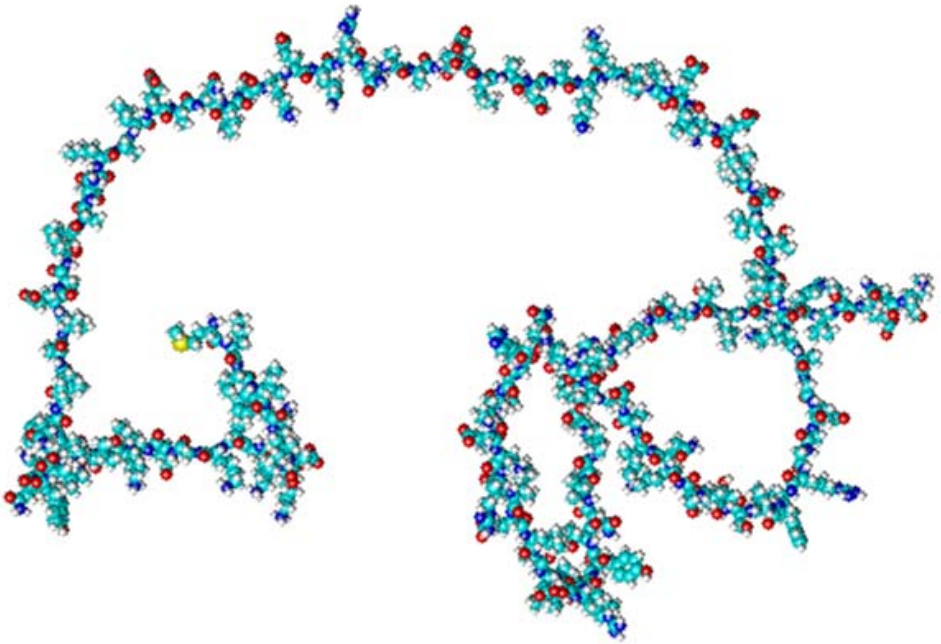

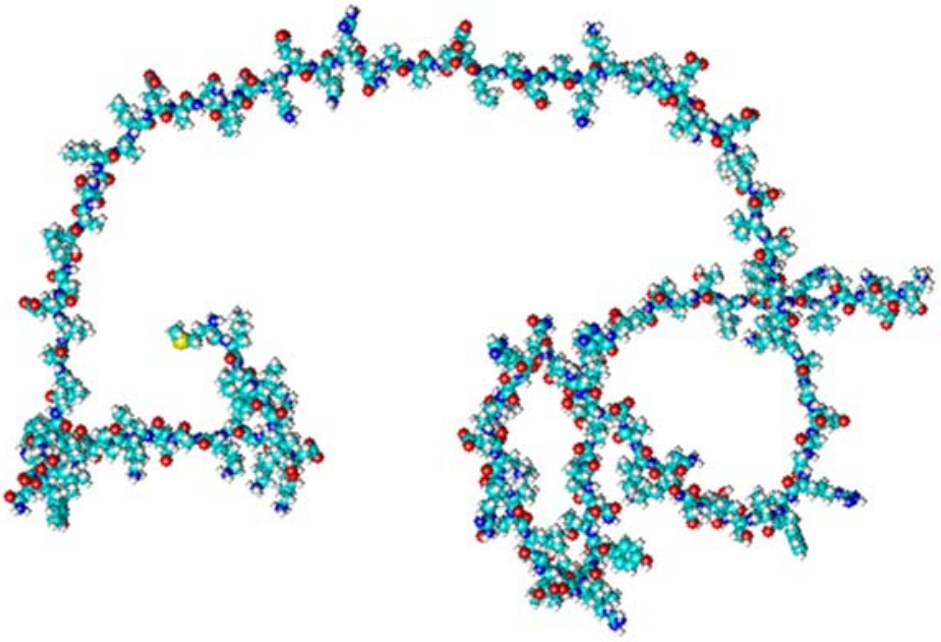

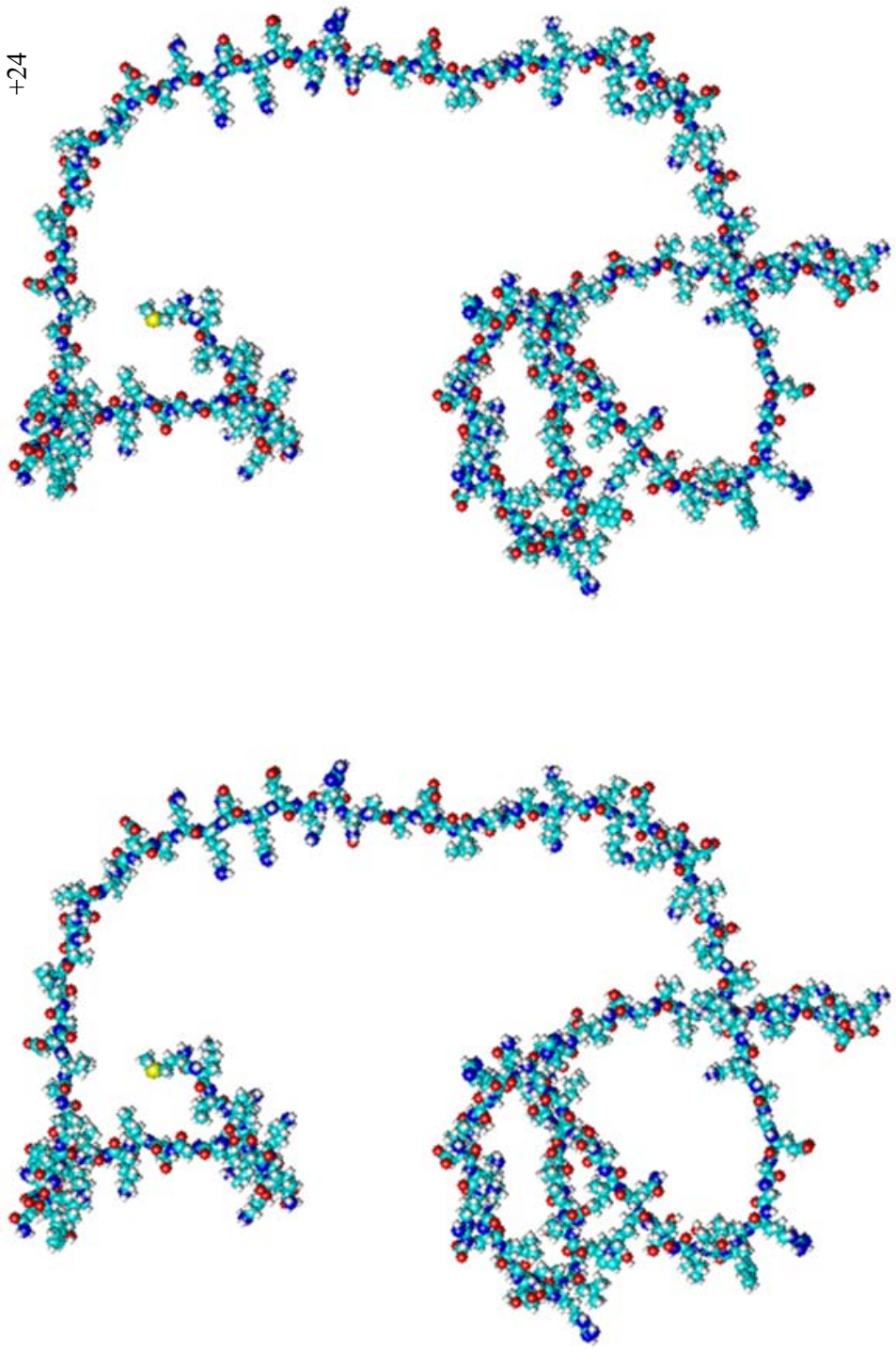
+24

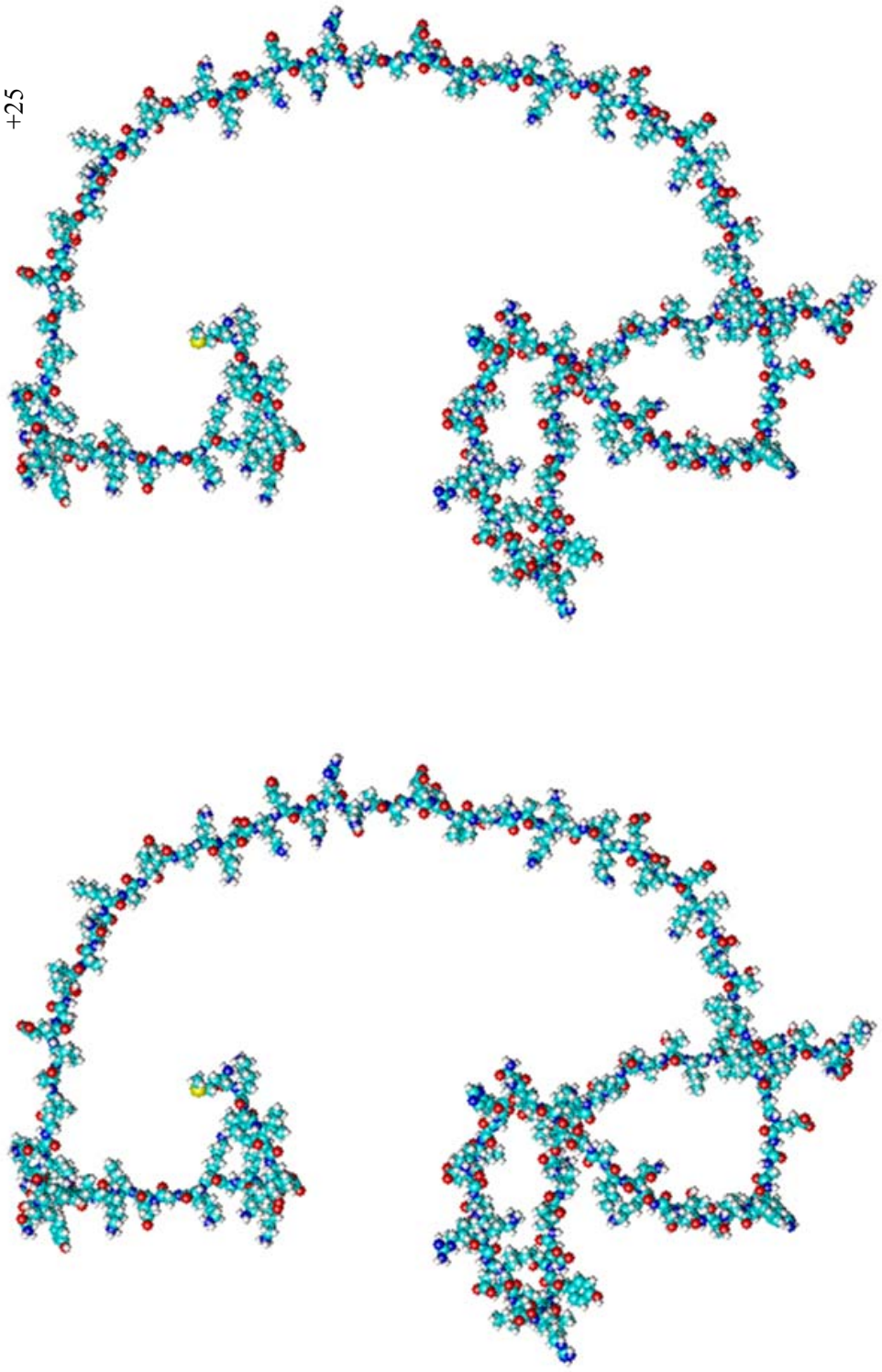
+25

+10

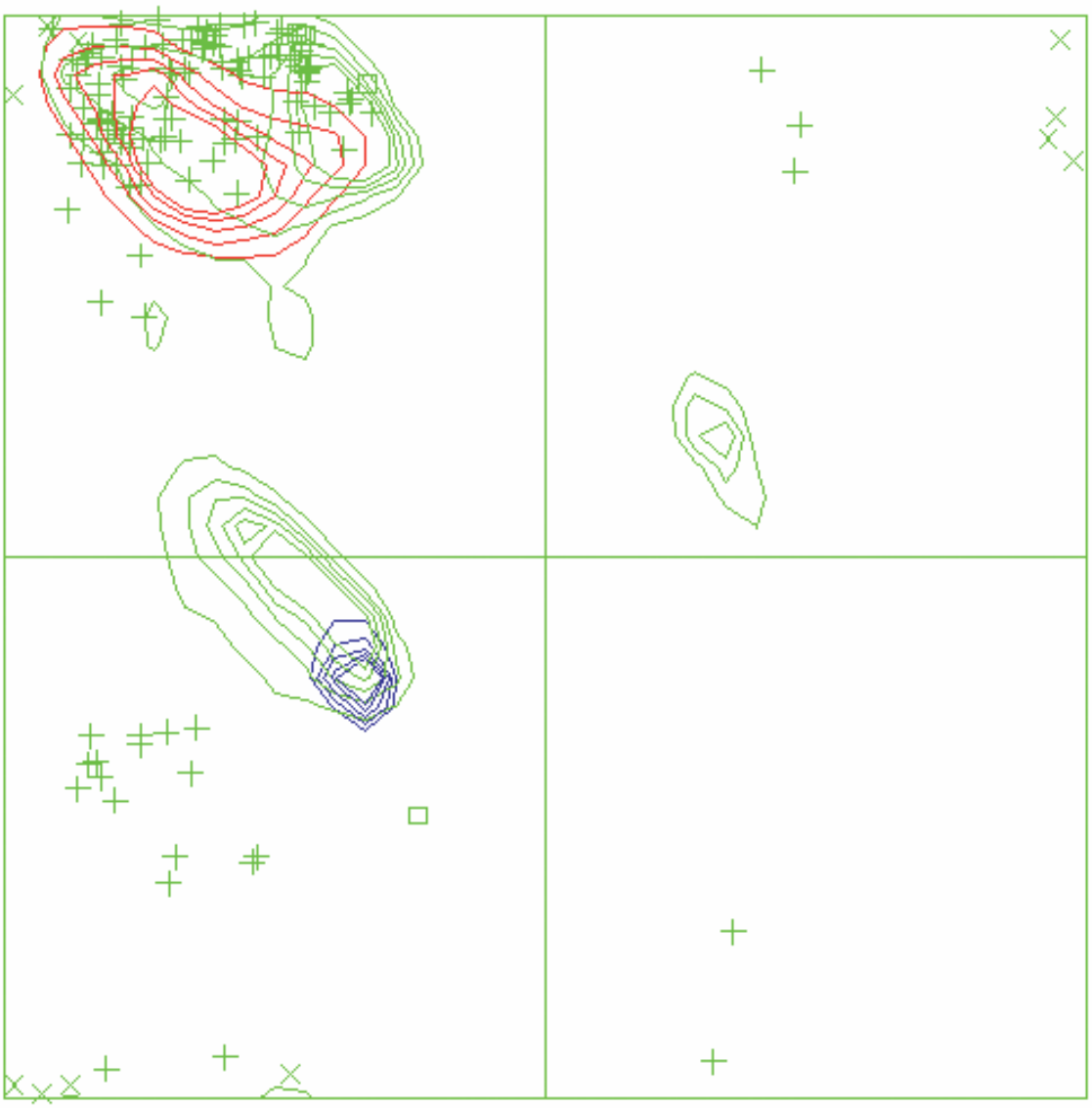

+11

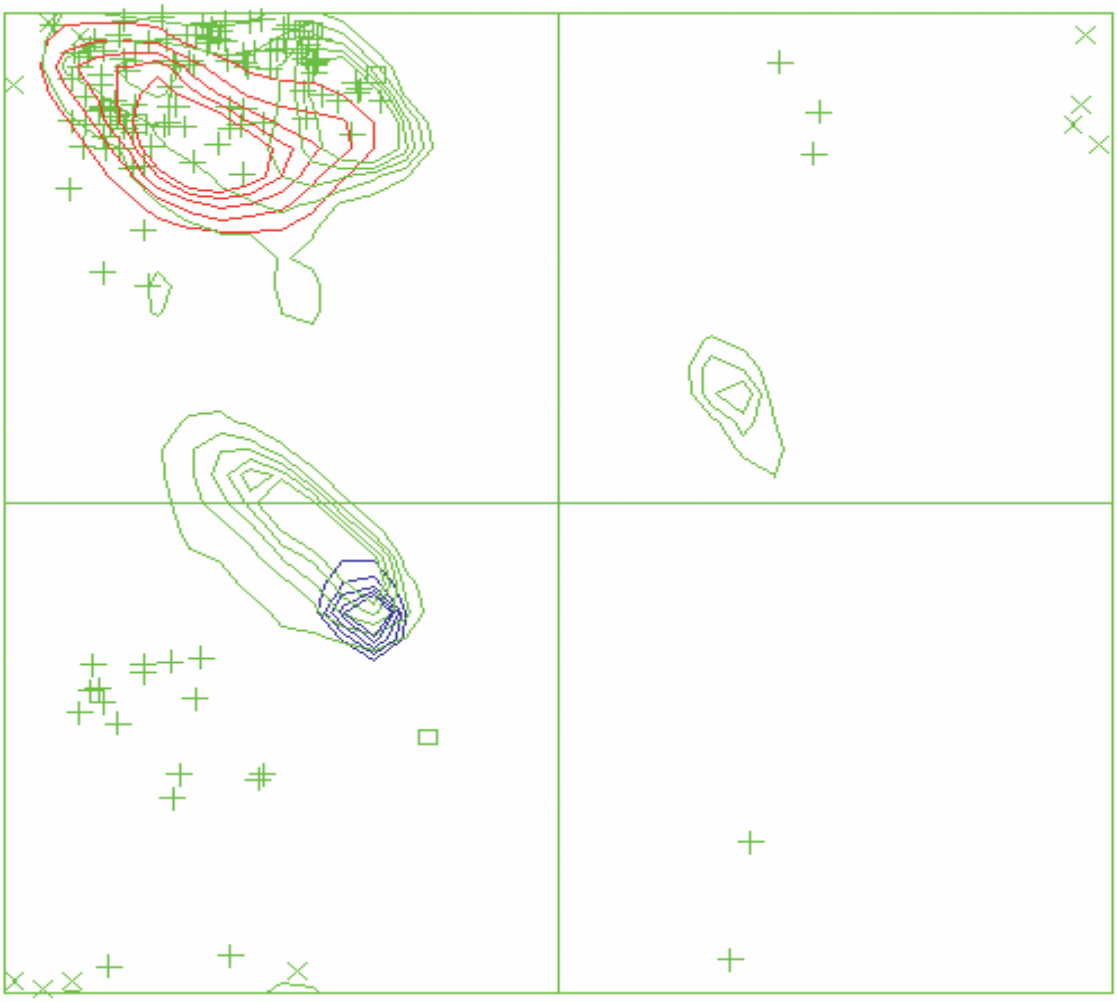

+12

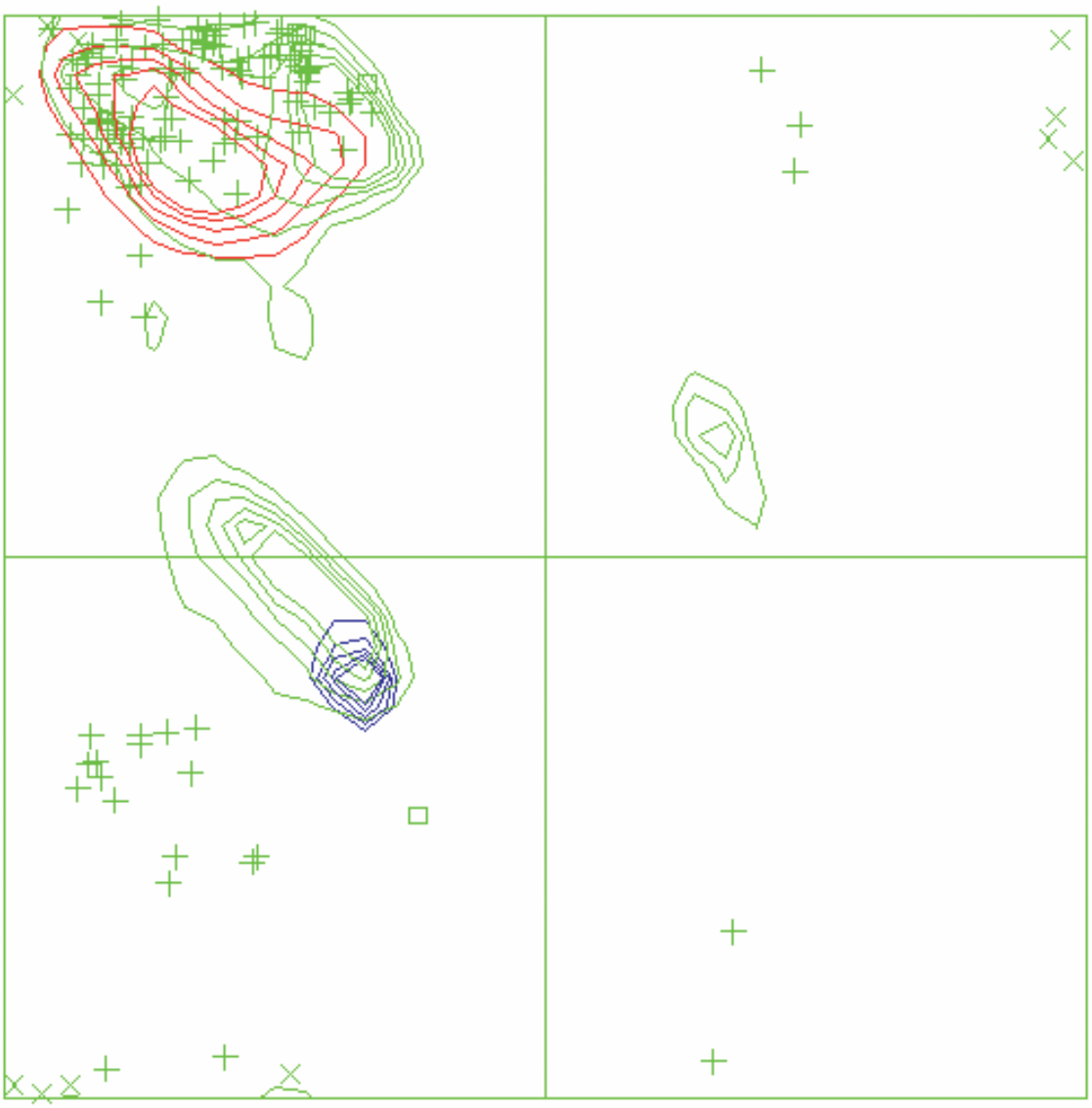

+13

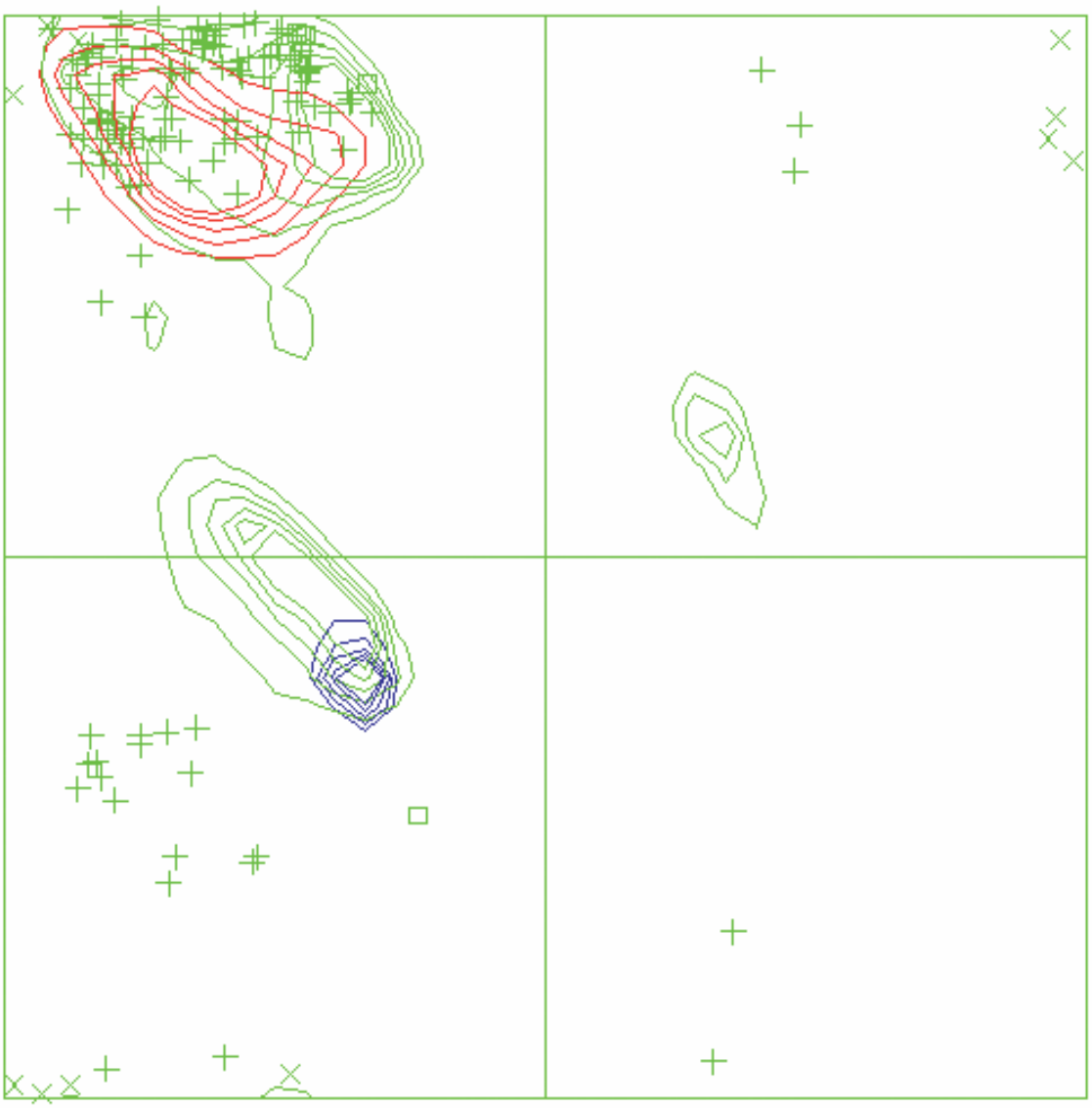

+14

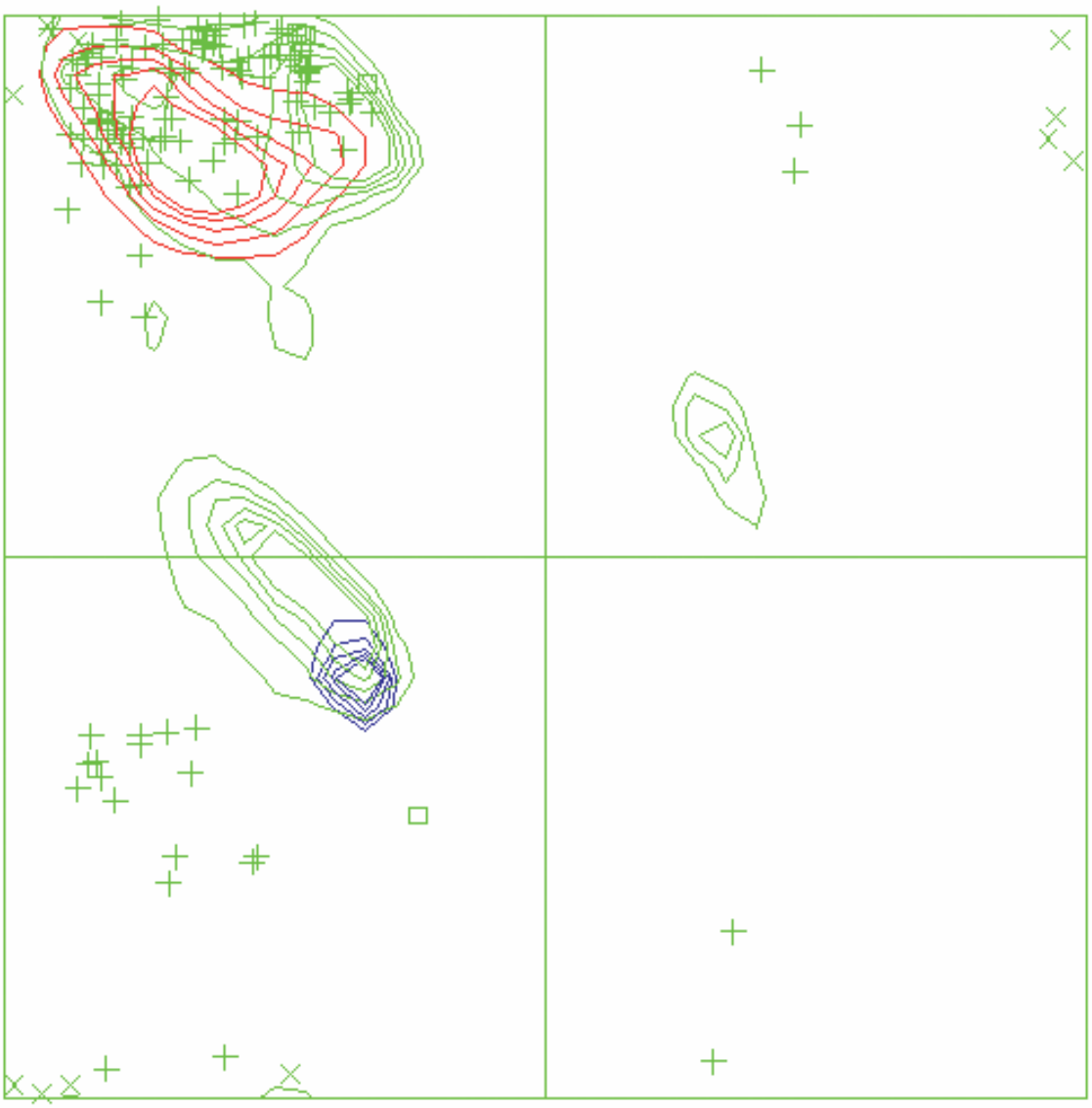

+15

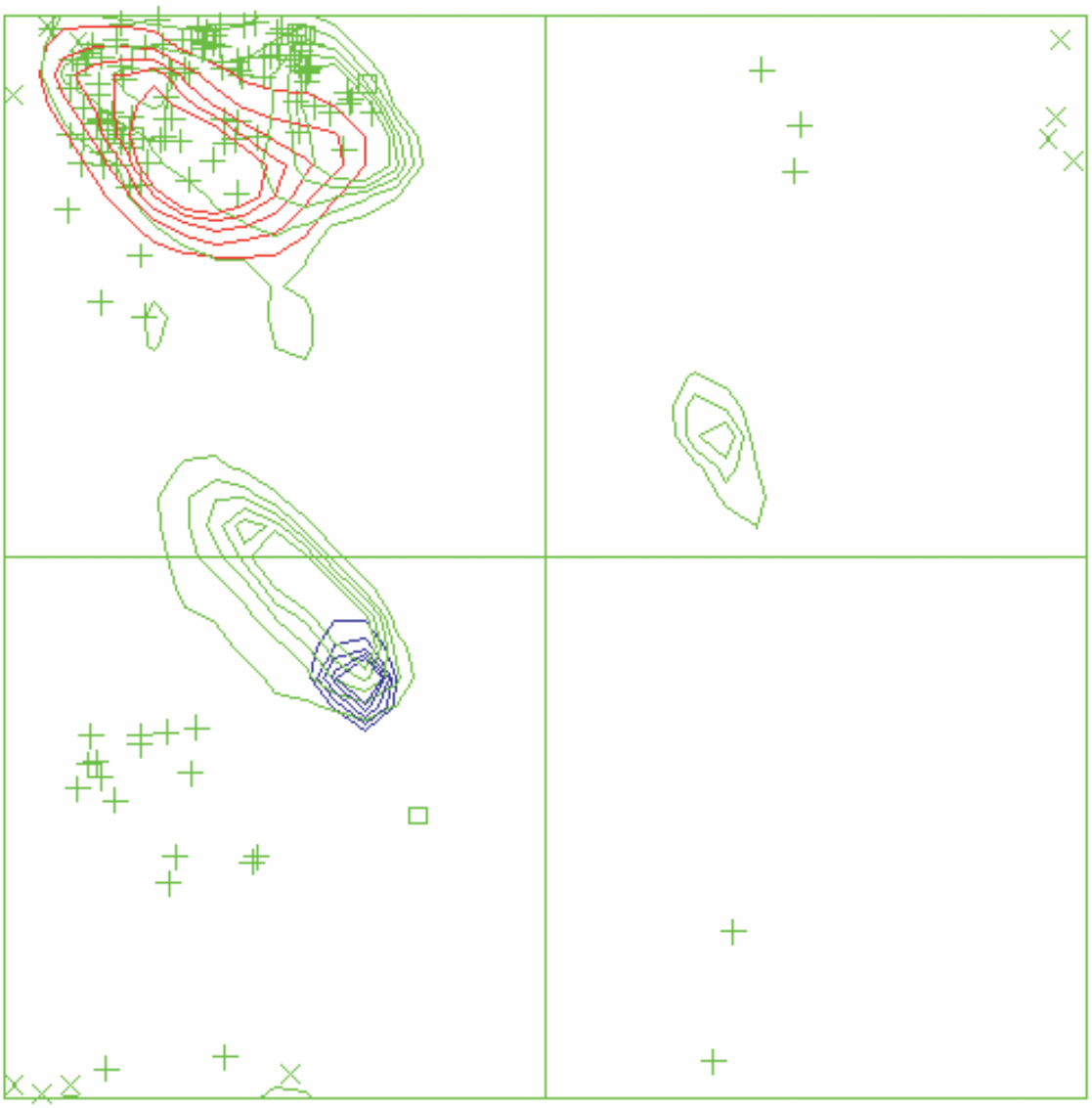

+16

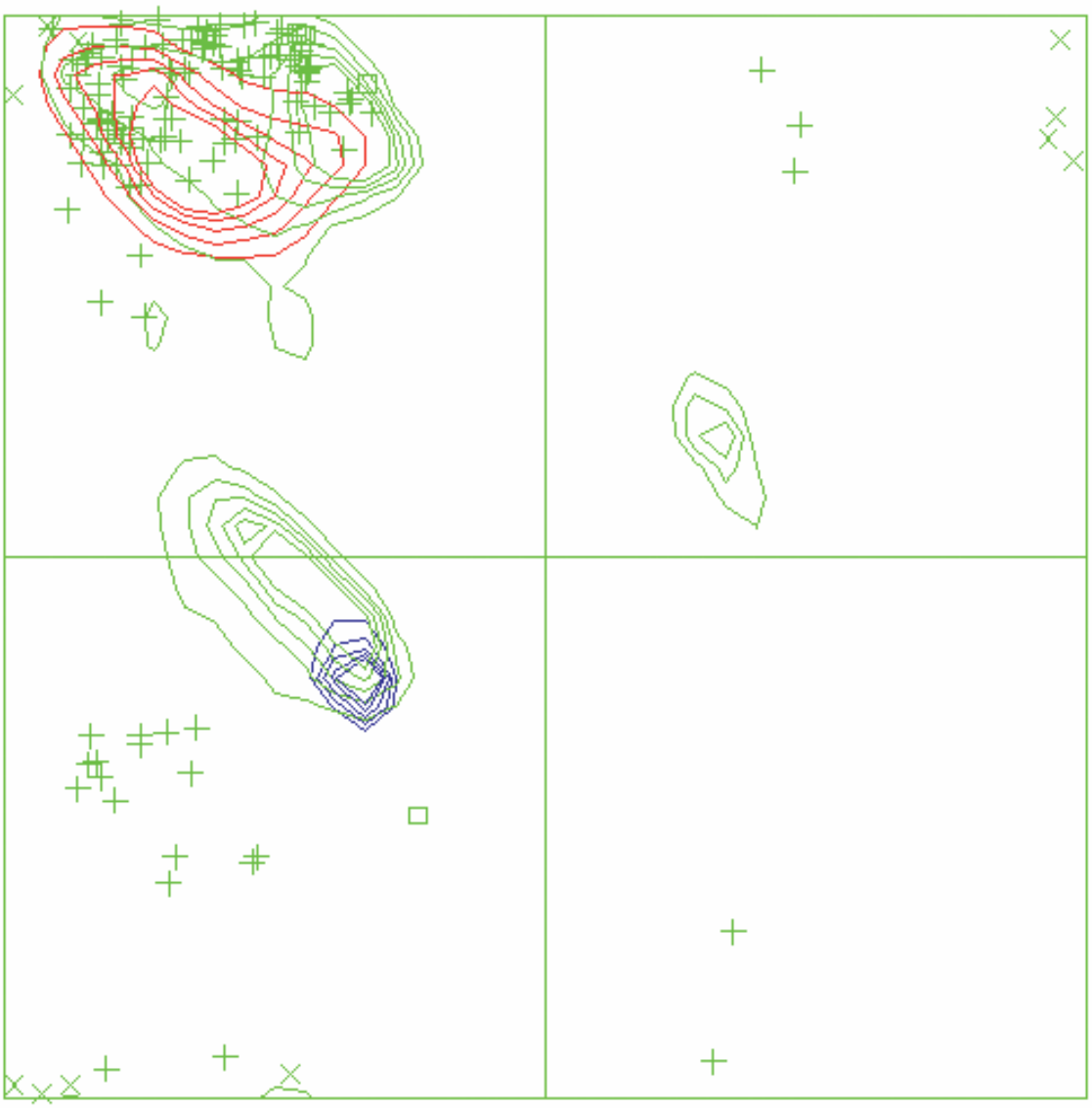

+17

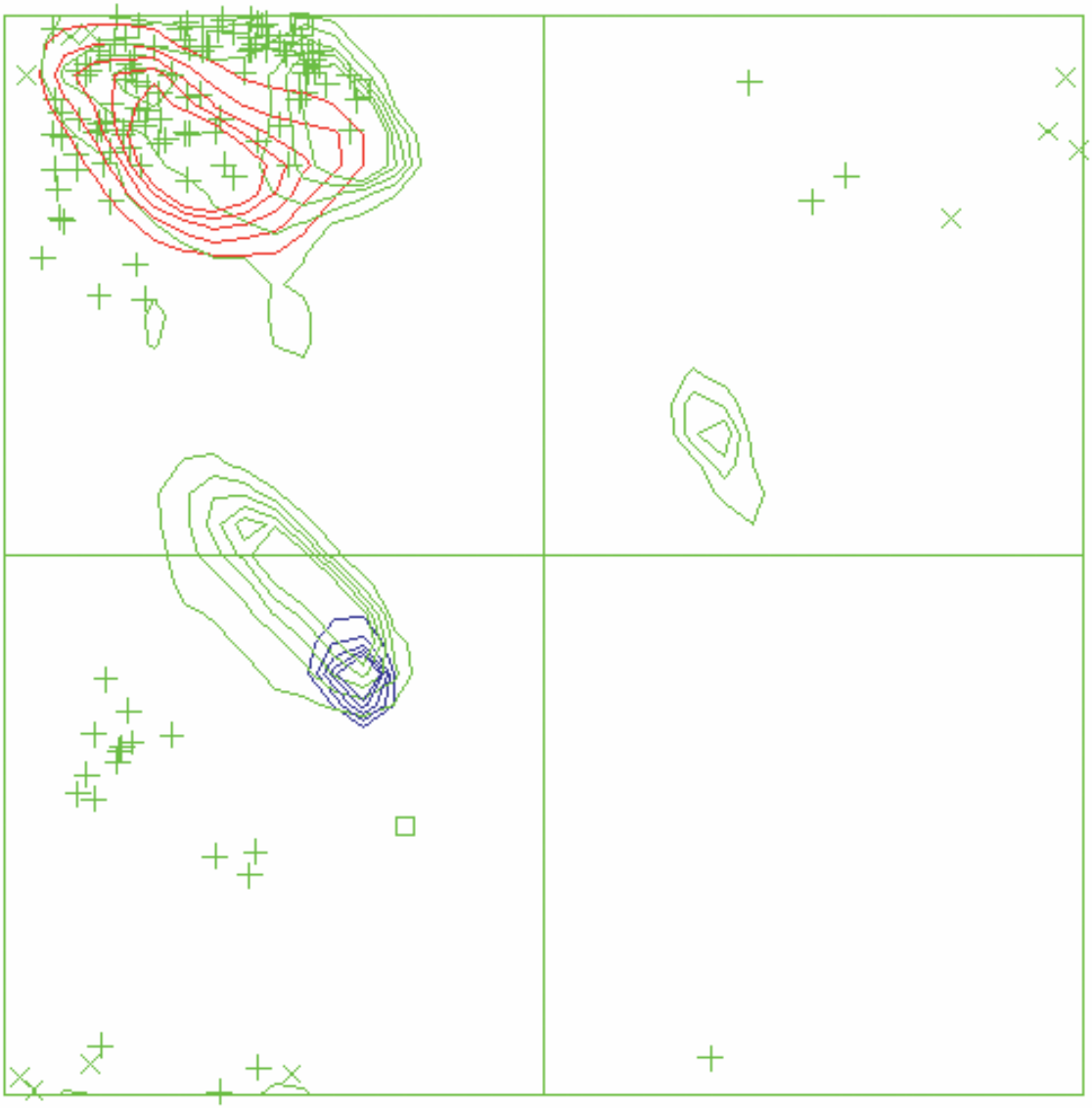

+18

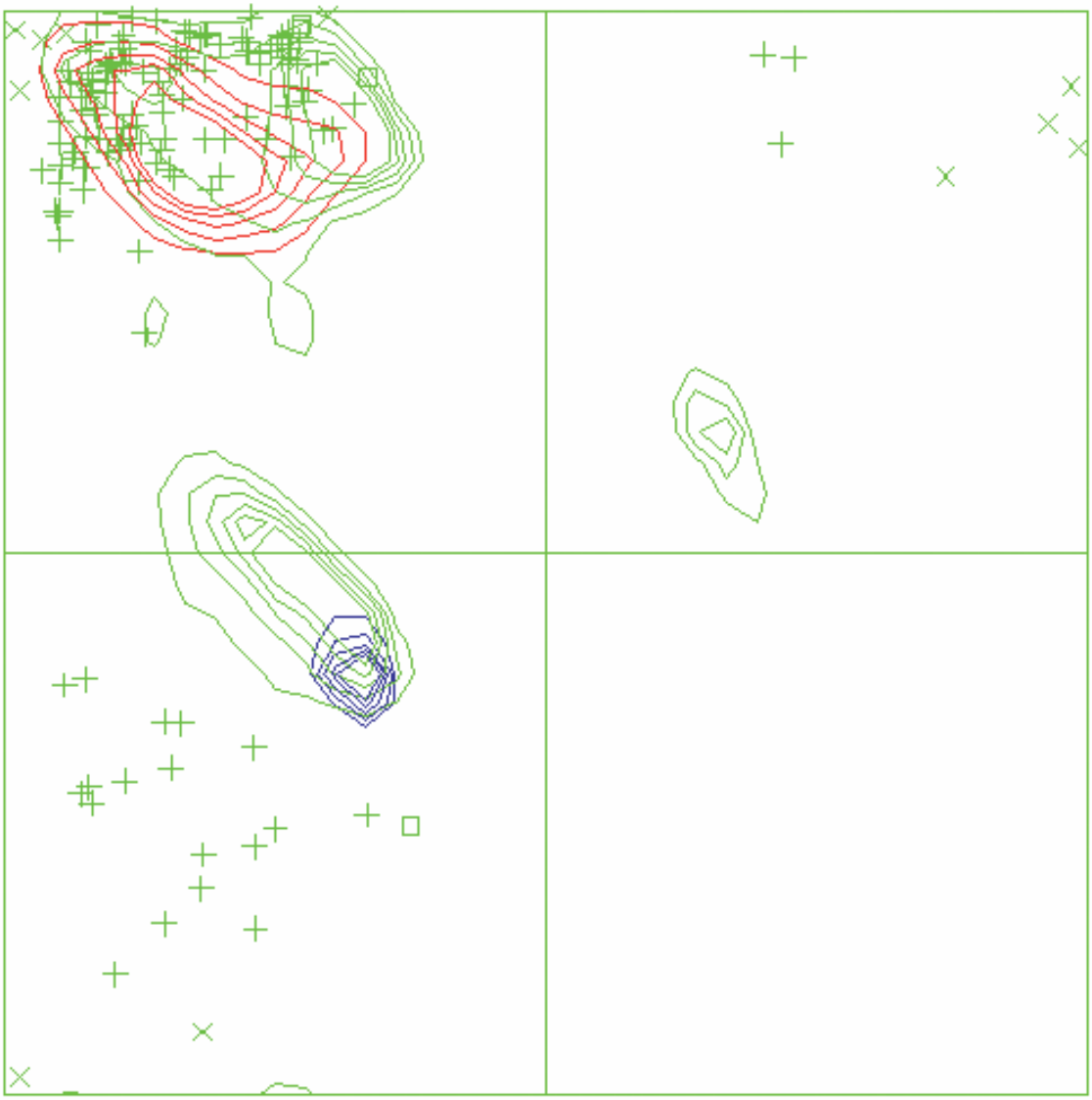

+19

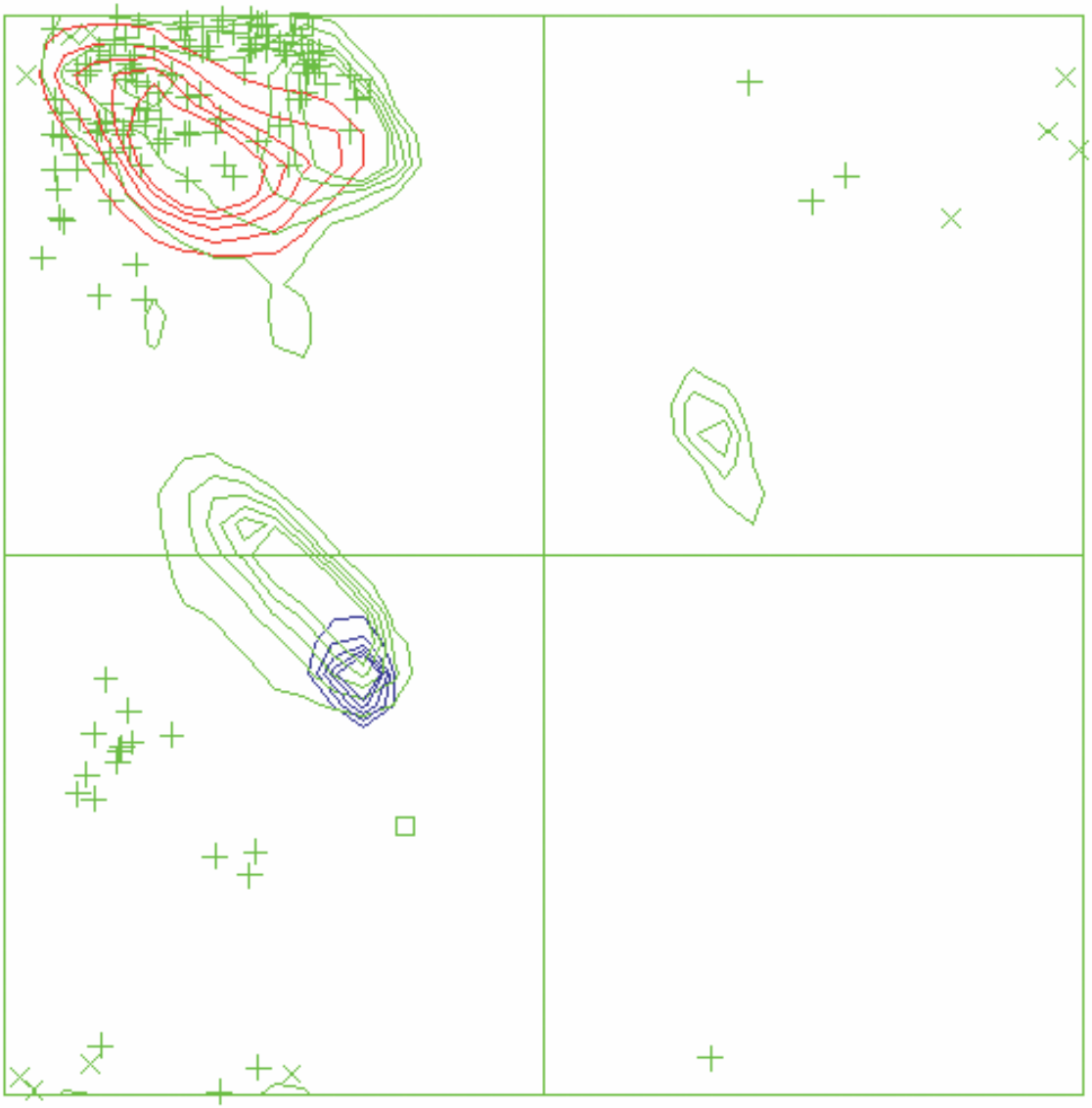

+20 His106

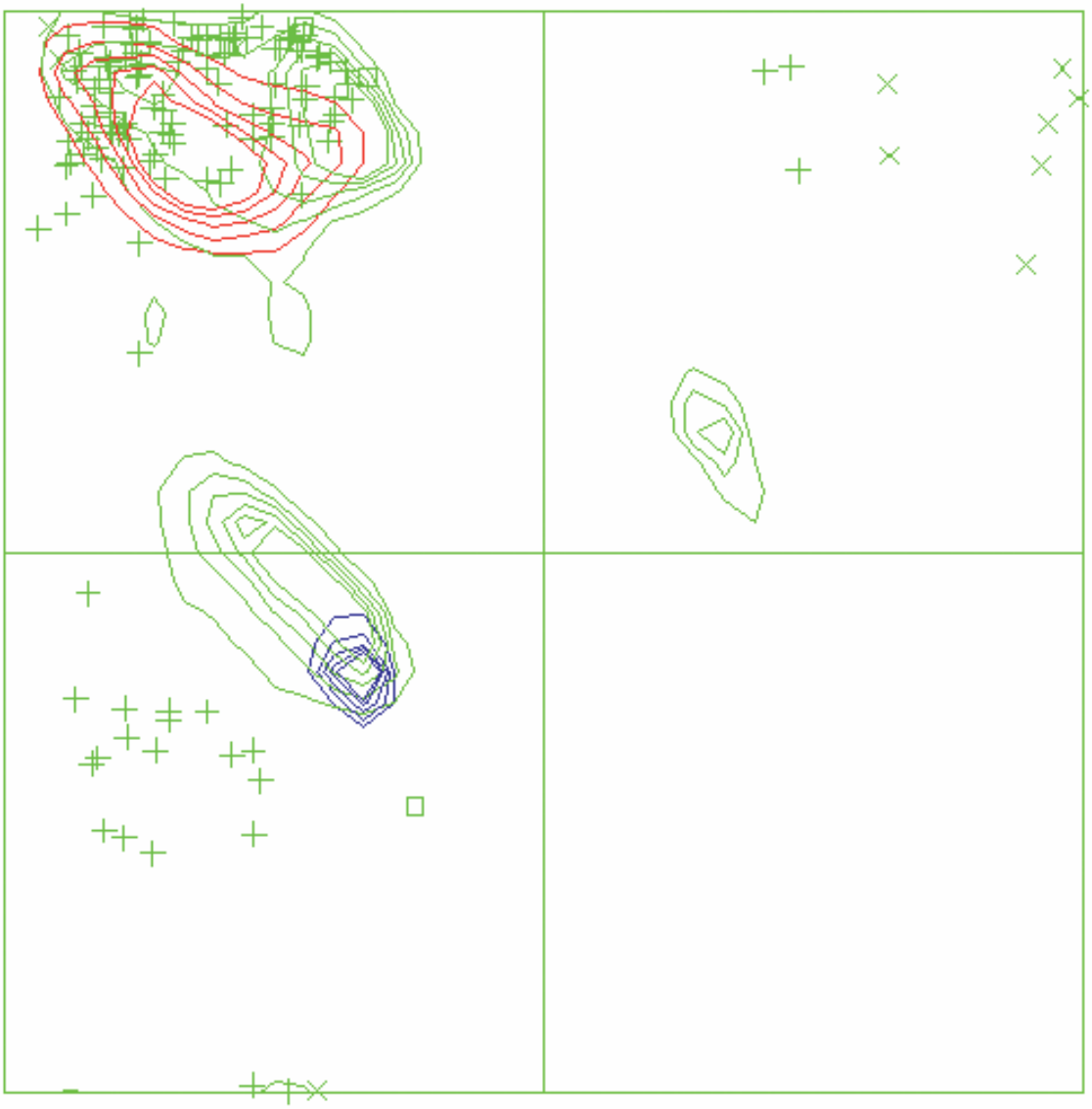

+20 Lys109

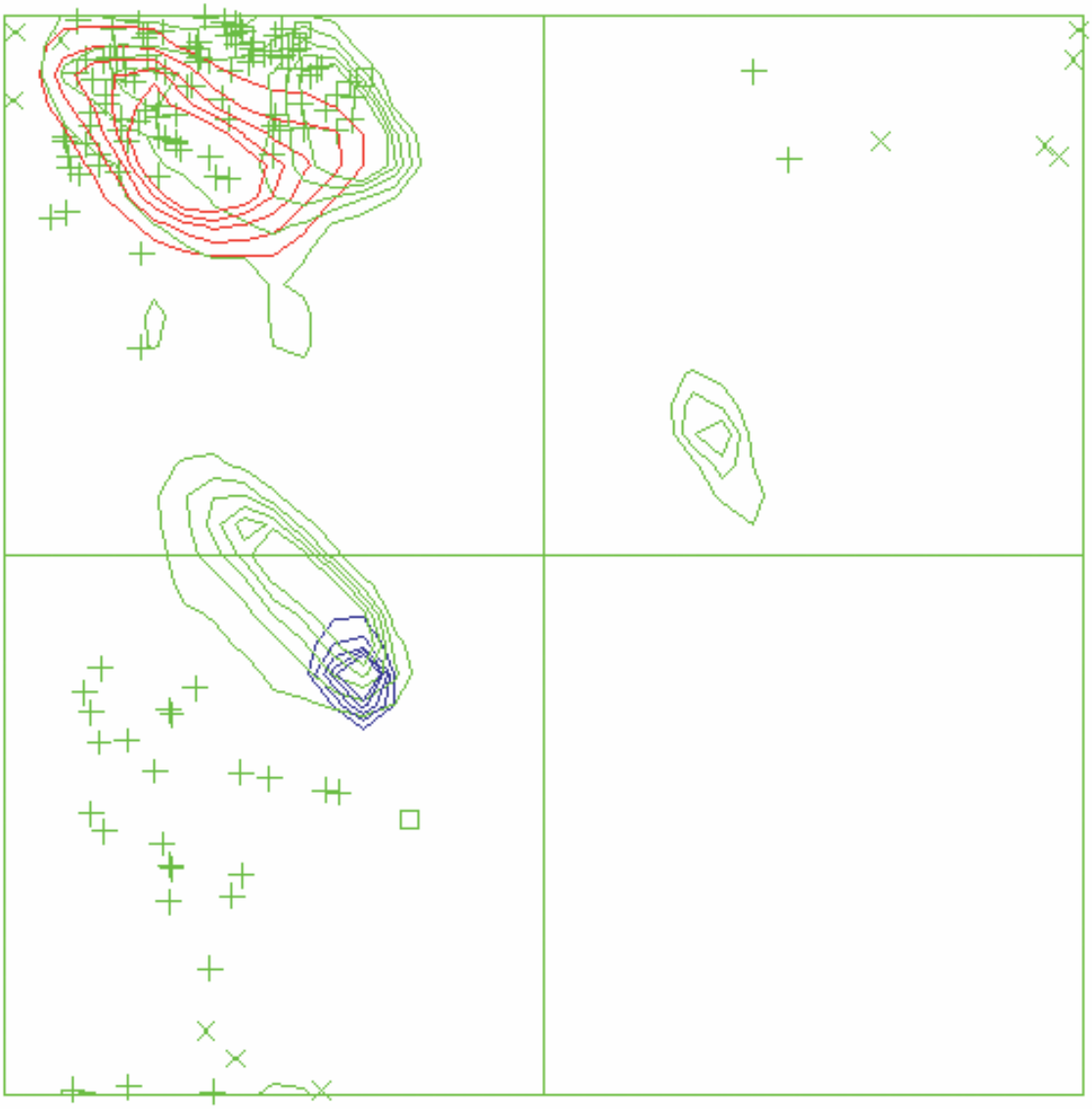

+21

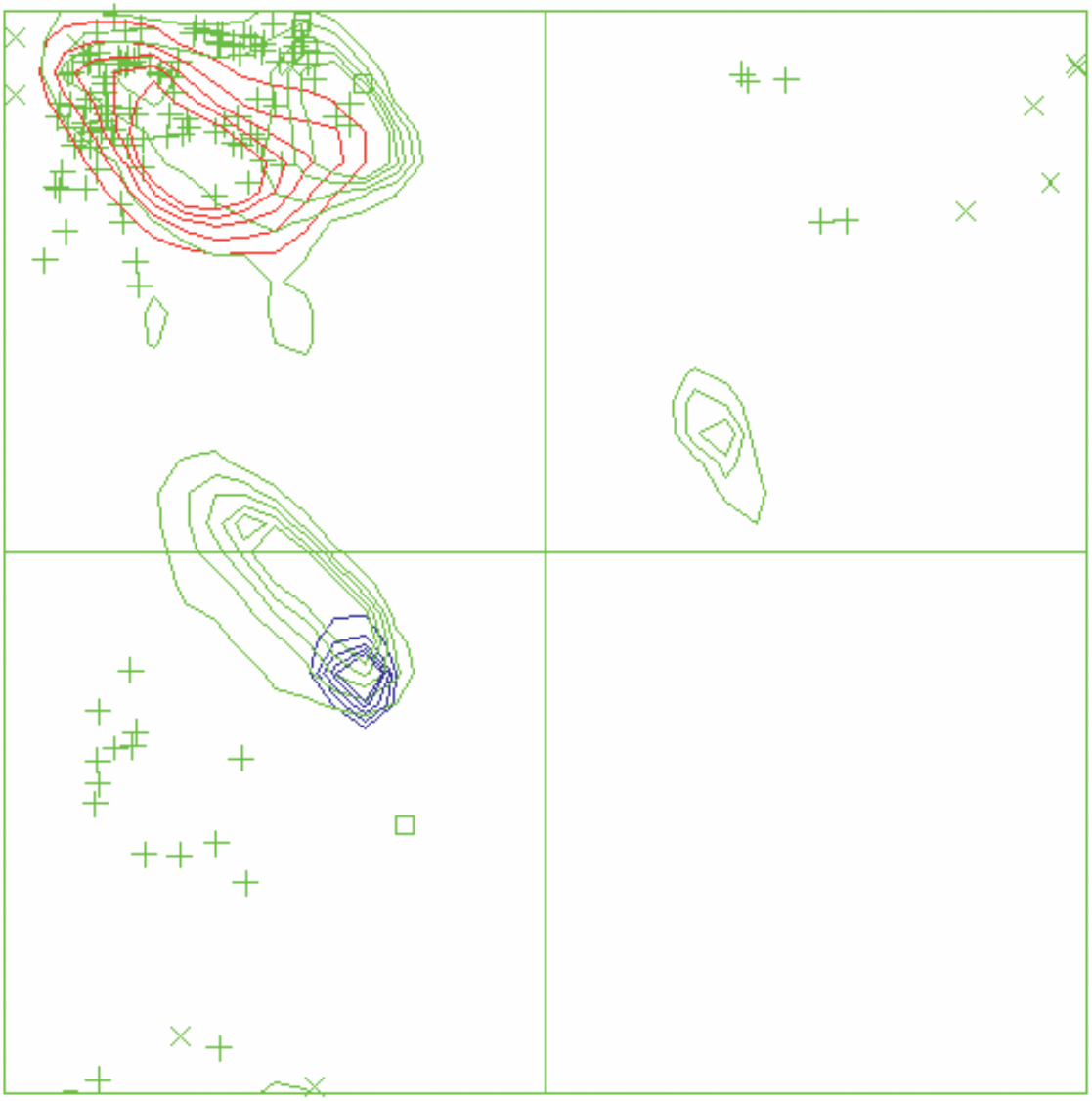

+22

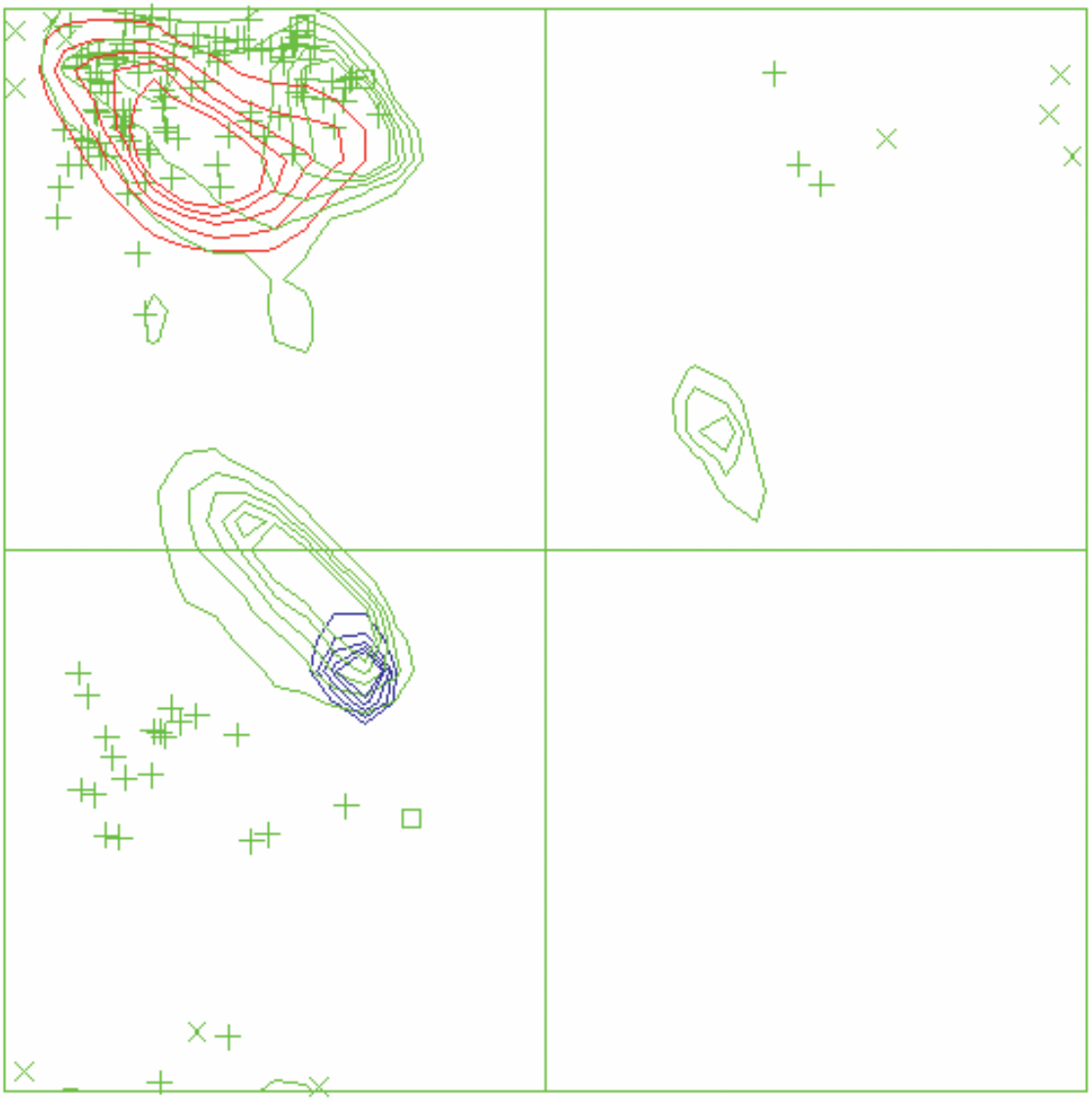

+23

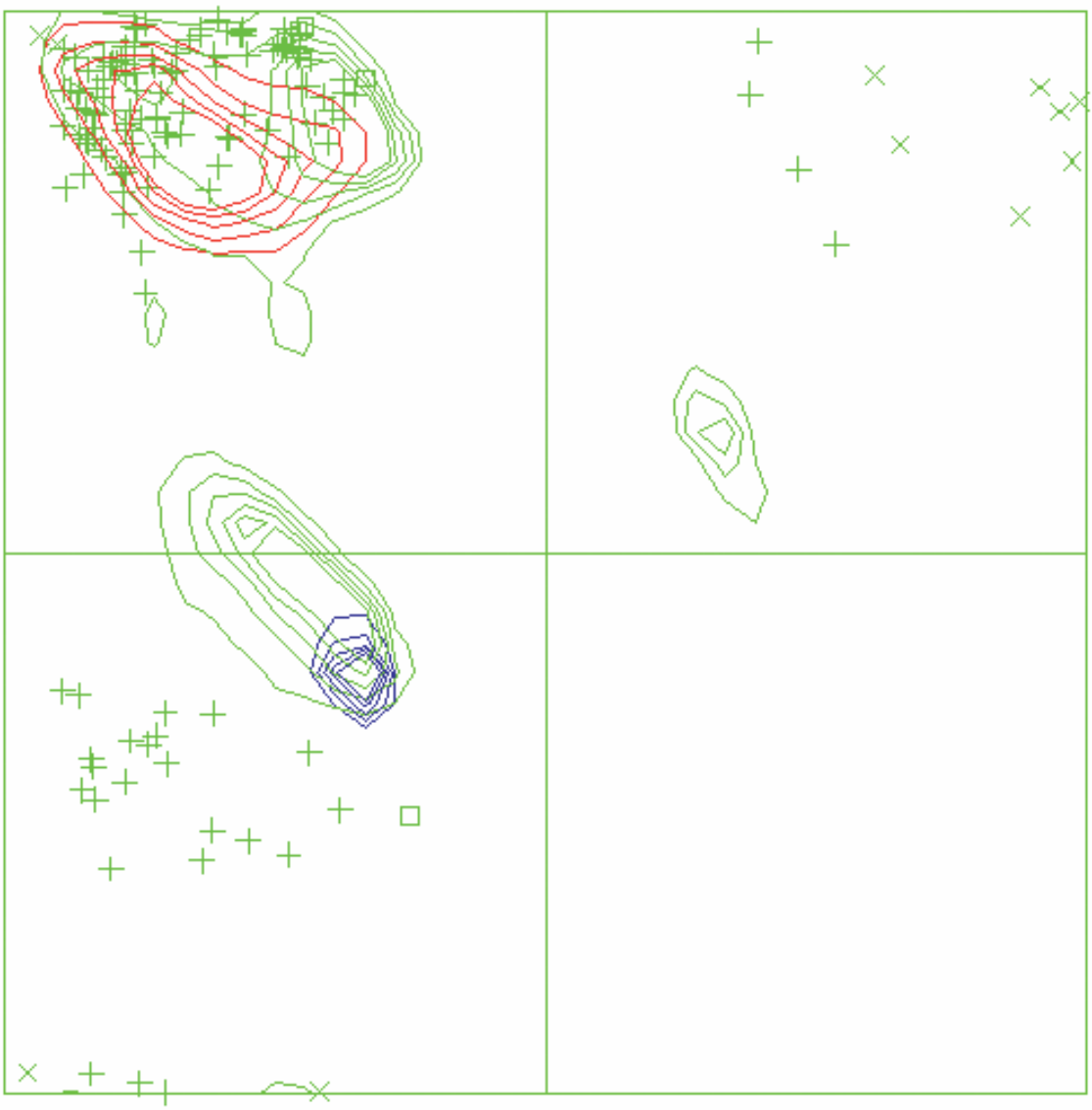

+24

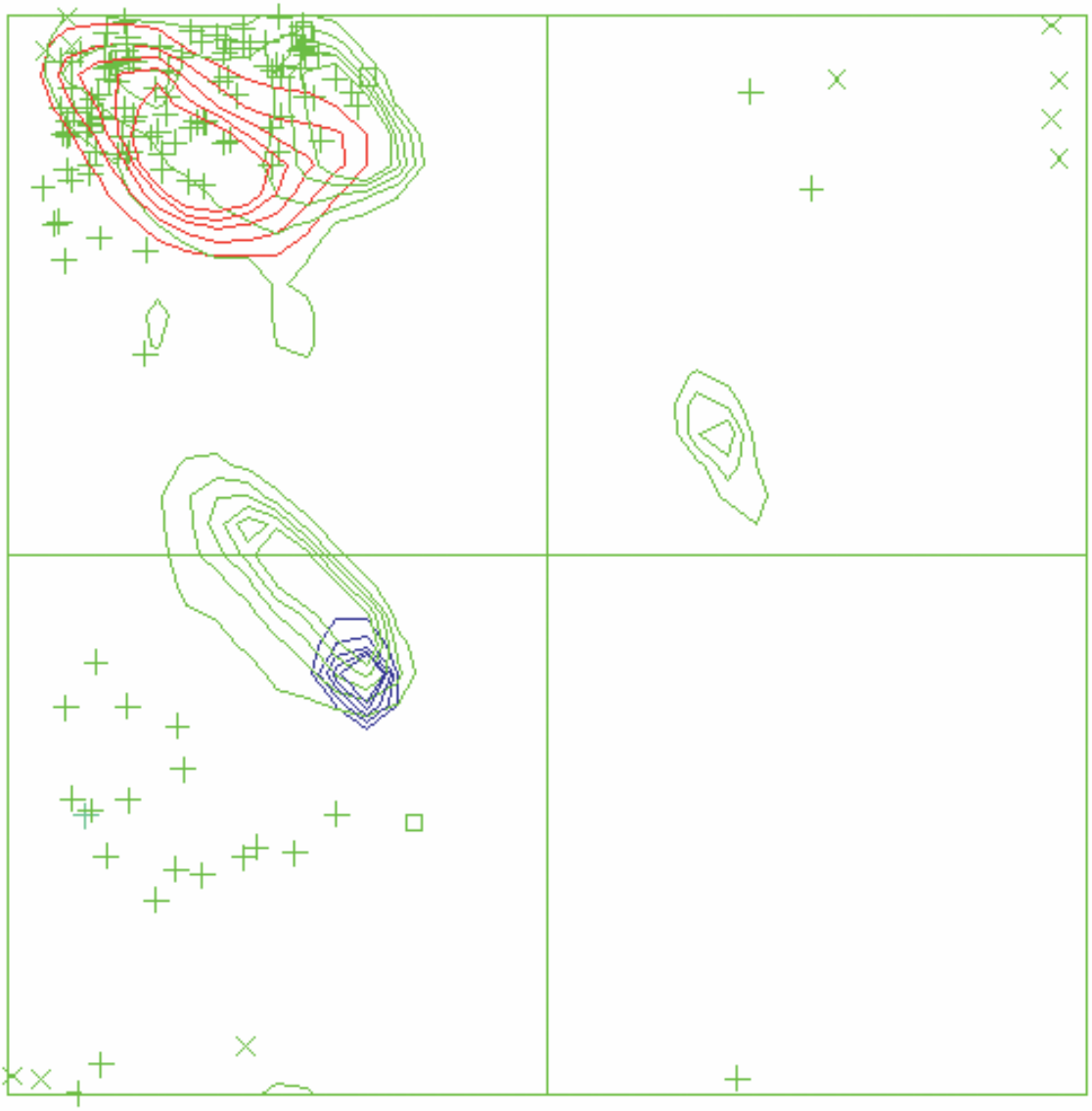

+25

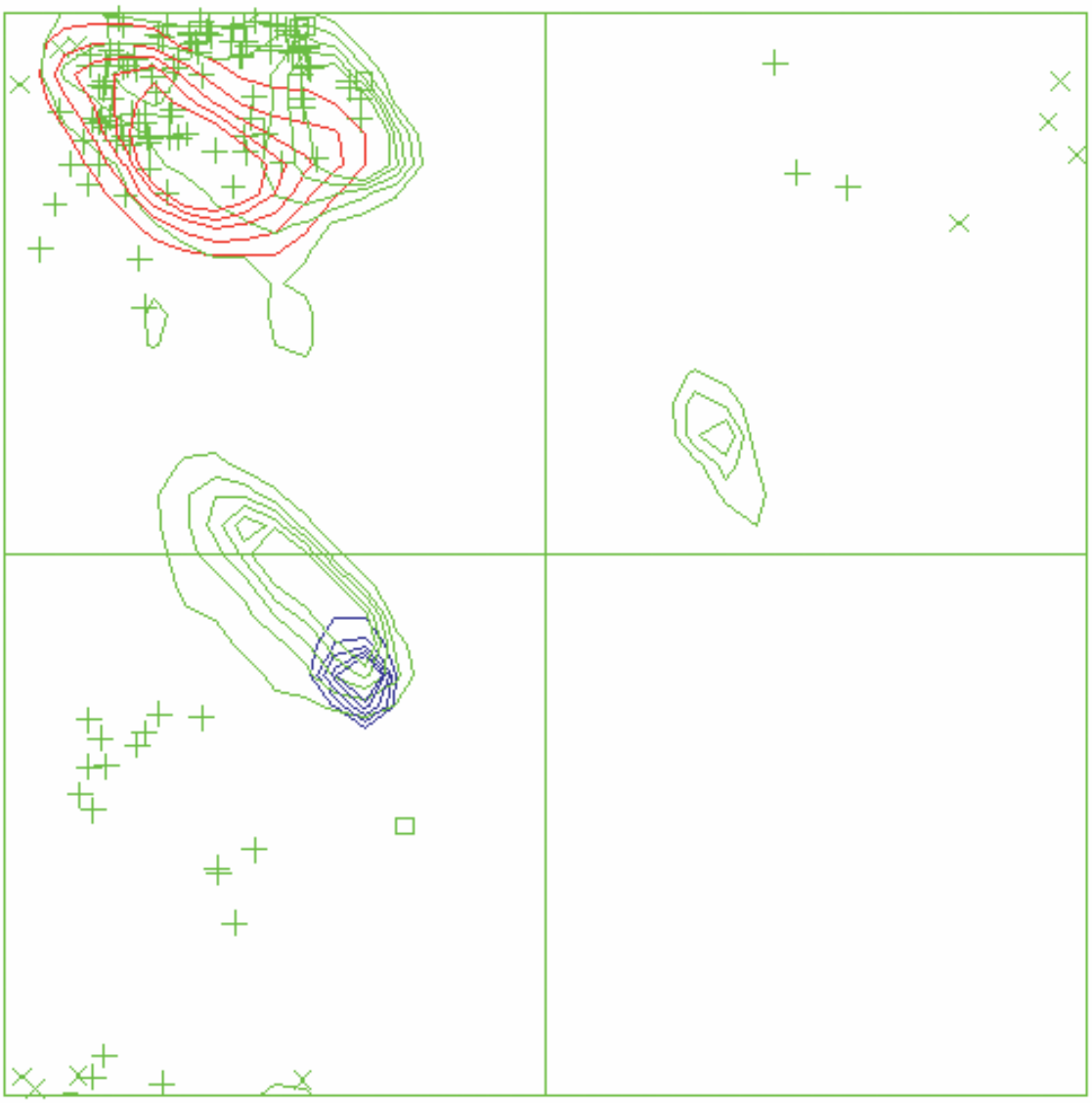

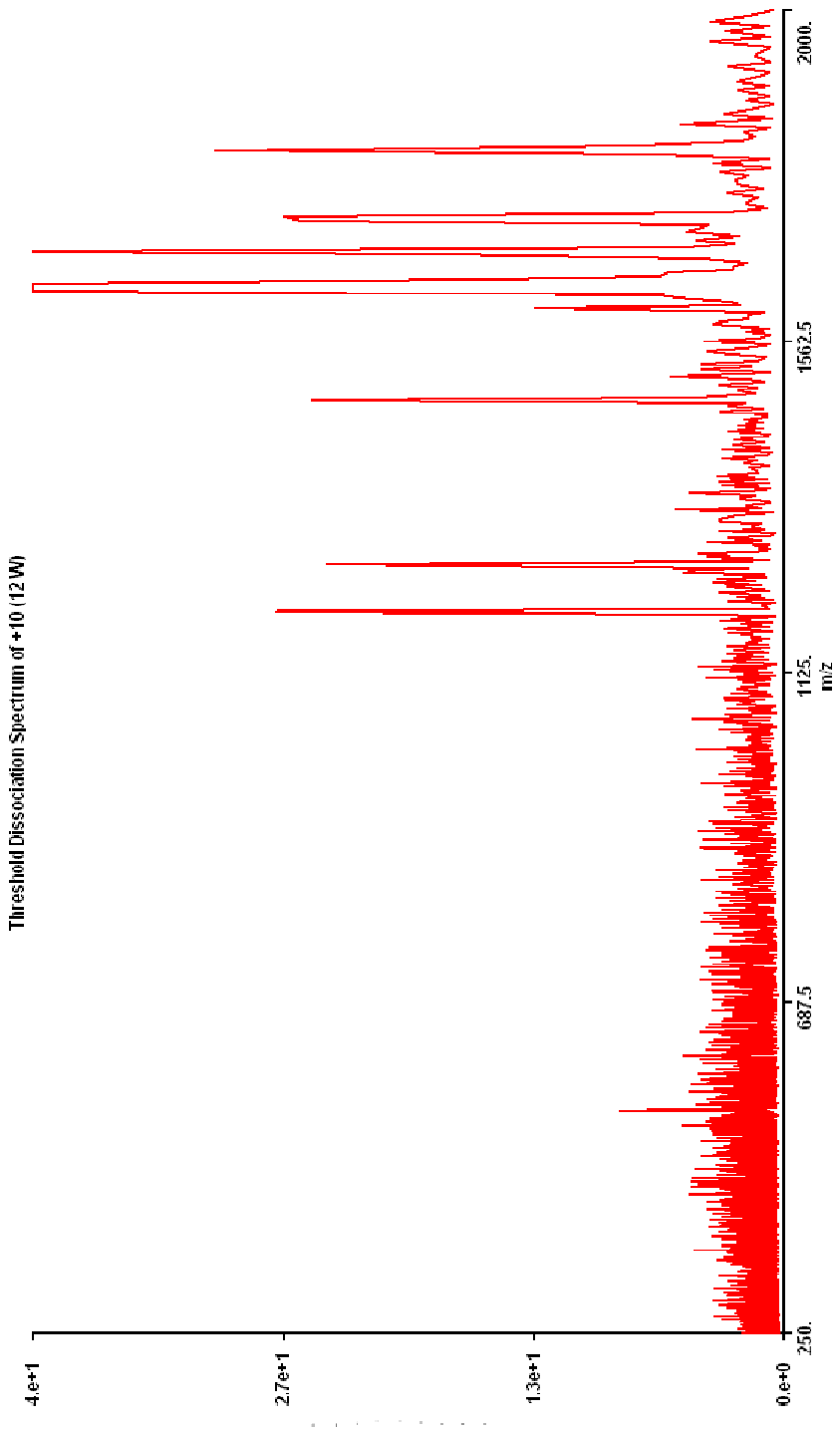
Threshold Dissociation Spectrum of +10 (12 W)
4.e+1
2.7e+1
1.3e+1
0.e+0
250.
687.5
1125.
1562.5
2000.
m/z

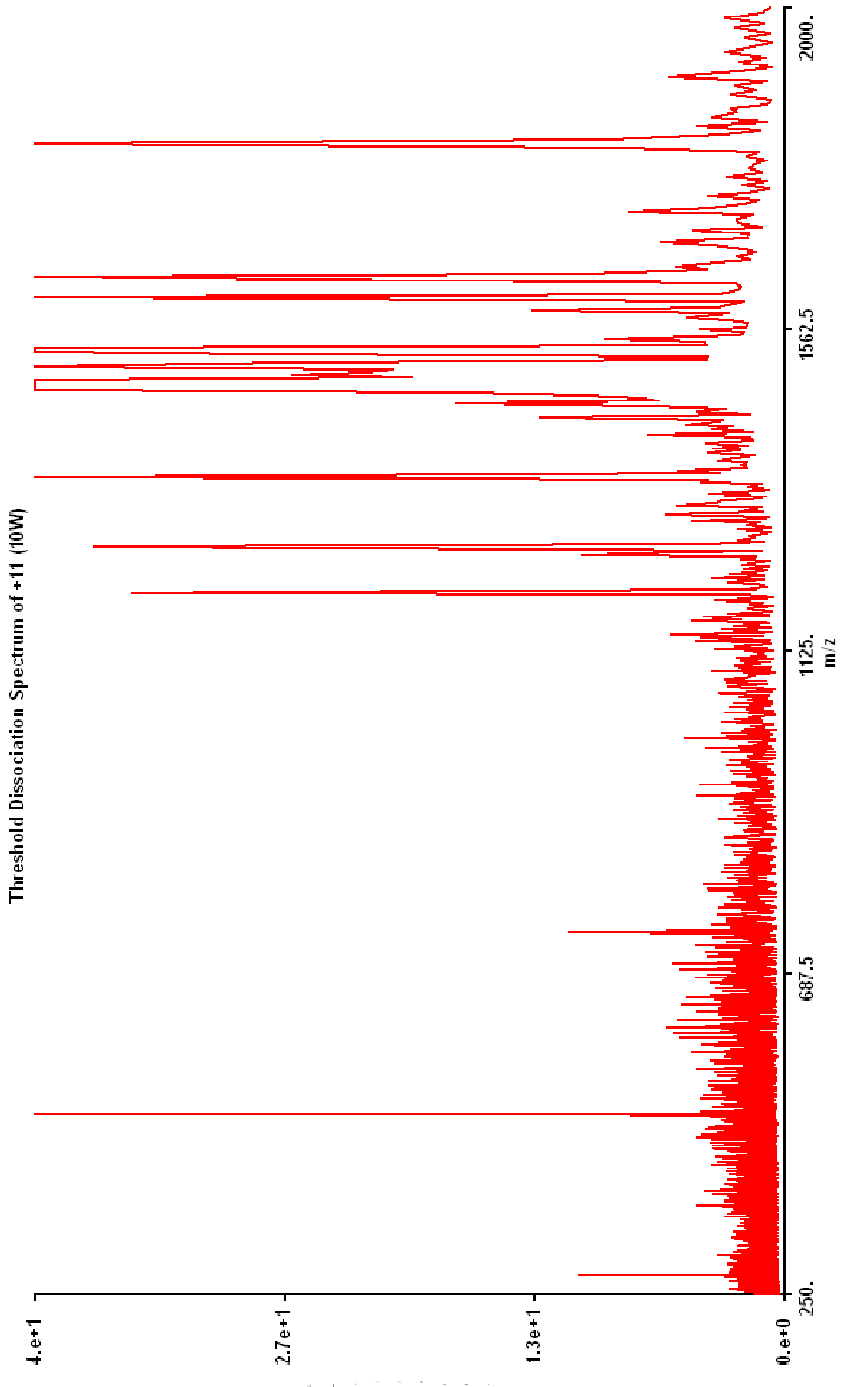
Threshold Dissociation Spectrum of +11 (10W)
4.e+1
2.7e+1
1.3e+1
0.e+0
250.
687.5
1125.
1562.5
2000.
m/z

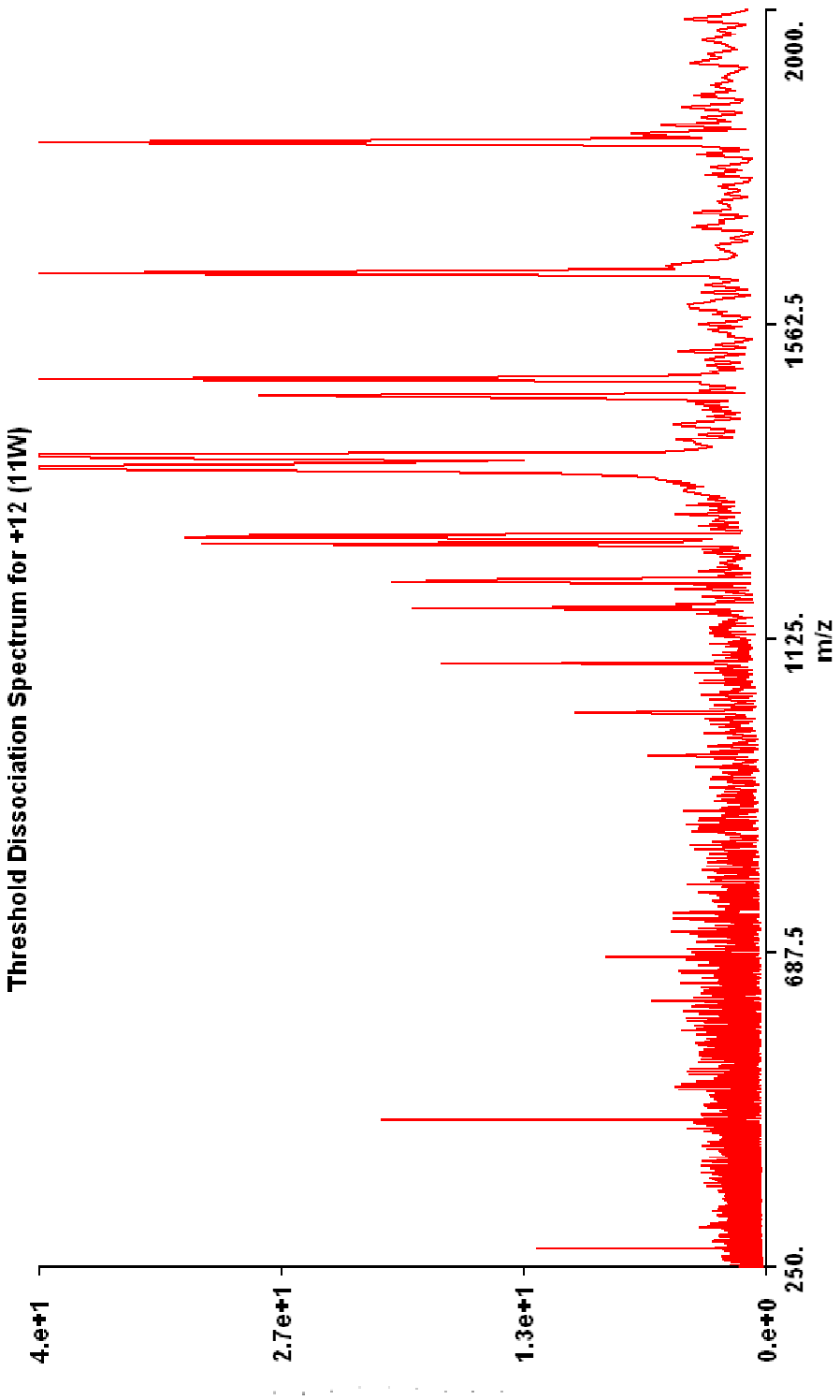
Threshold Dissociation Spectrum for +12 (11W)
4.e+1
2.7e+1
1.3e+1
0.e+0
250.
687.5
1125.
1562.5
2000.
m/z

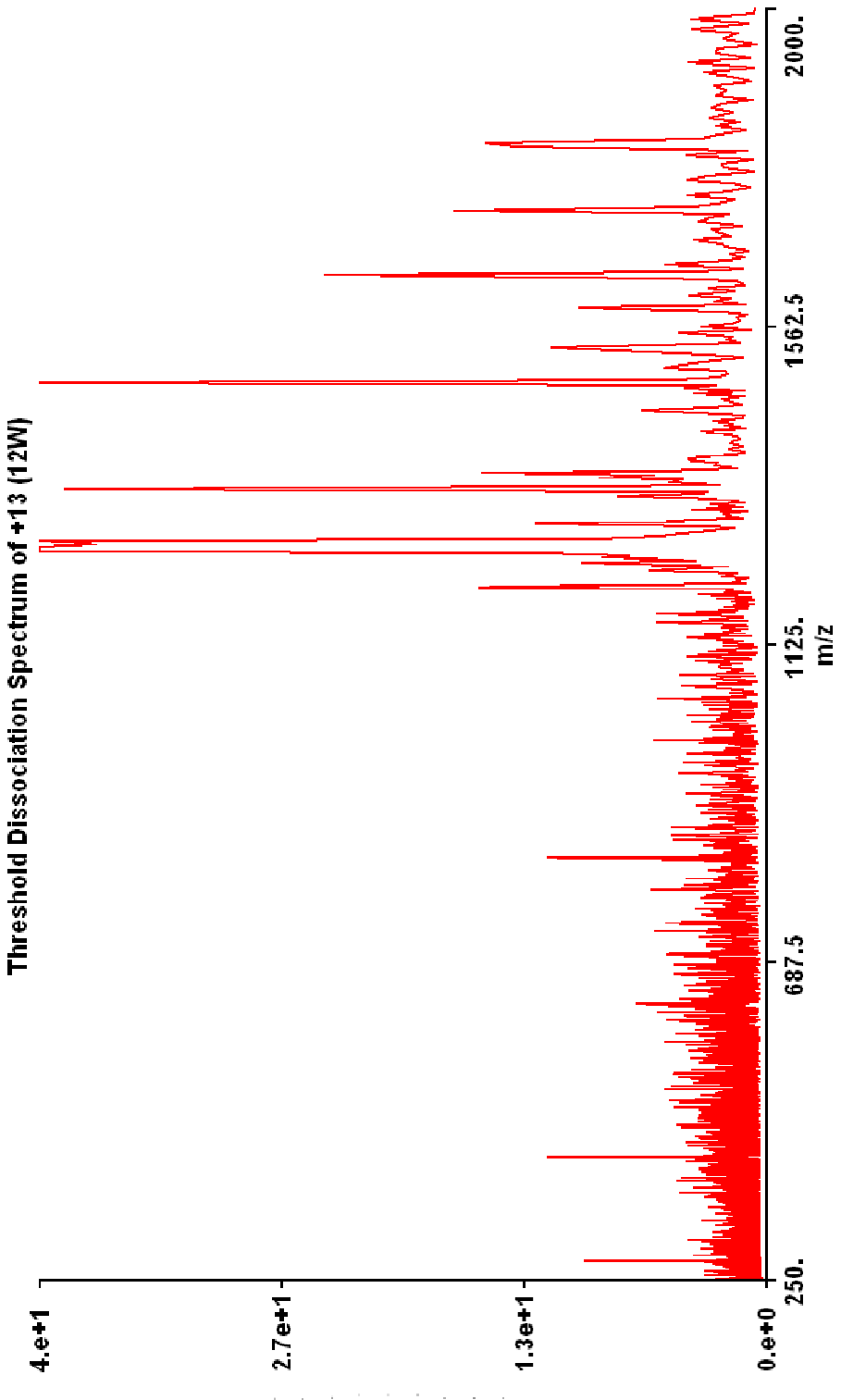
Threshold Dissociation Spectrum of +13 (12W)
4.e+1
2.7e+1
1.3e+1
0.e+0
250.
687.5
1125.
1562.5
2000.
m/z

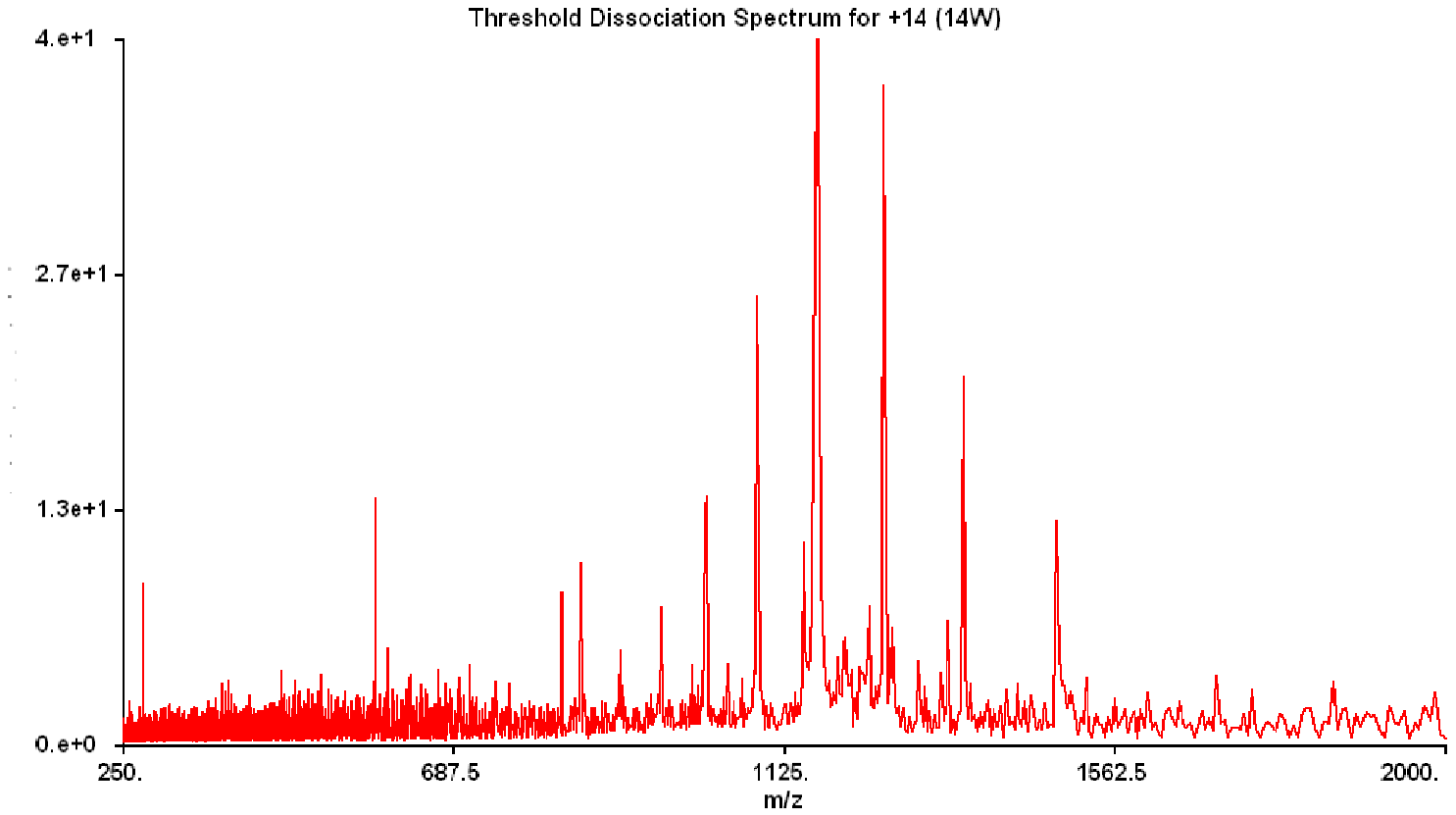
Threshold Dissociation Spectrum for +14 (14W)
4.e+1
2.7e+1
1.3e+1
0.e+0
250.
687.5
1125.
1562.5
2000.
m/z

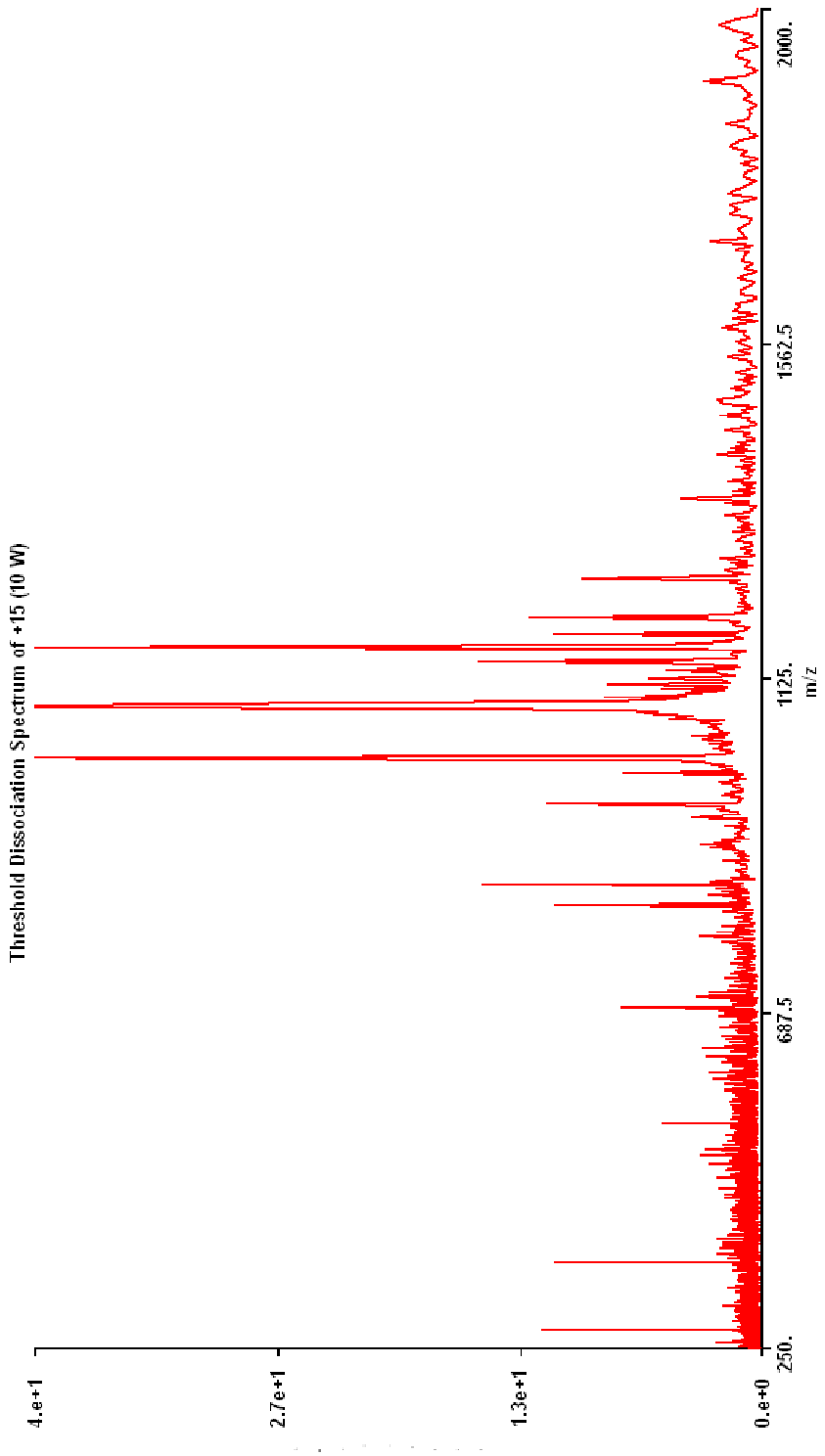
Threshold Dissociation Spectrum of +15 (10 W)
4.e+1
2.7e+1
1.3e+1
0.e+0
250.
687.5
1125.
1562.5
2000.
m/z

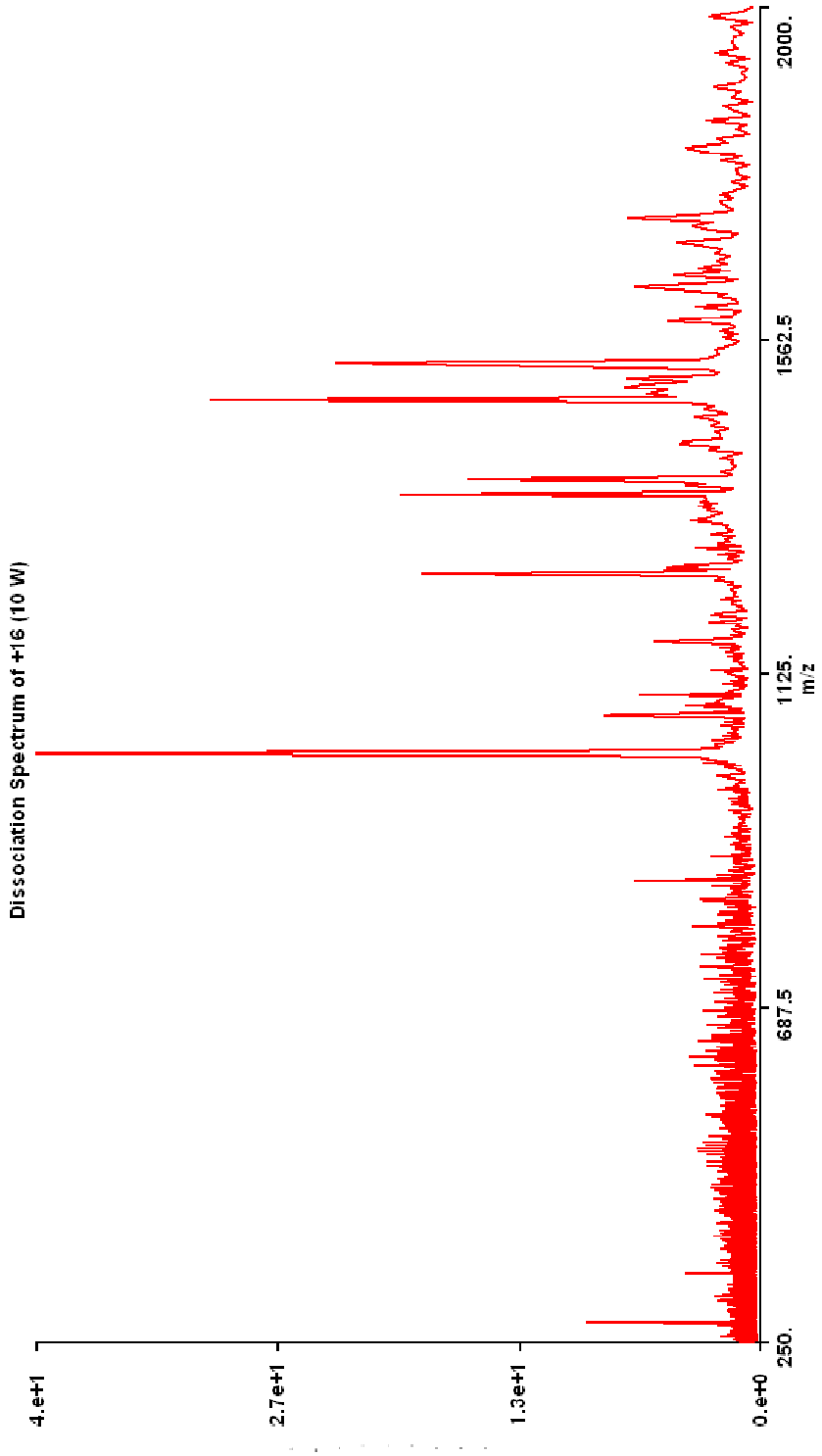
Dissociation Spectrum of +16 (10 W)
4.e+1
2.7e+1
1.3e+1
0.e+0
250.
687.5
1125.
1562.5
2000.
m/z

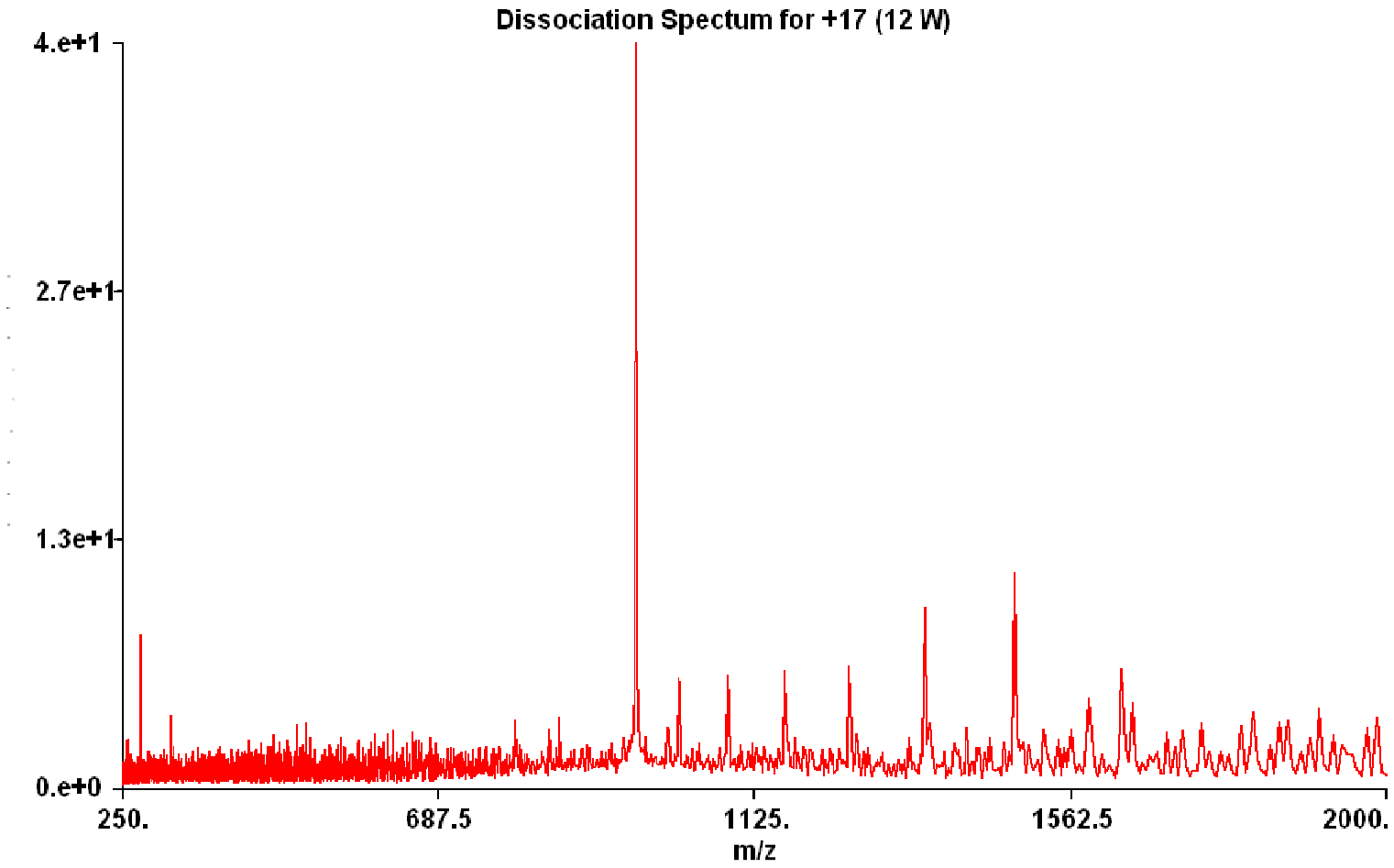
Dissociation Spectum for +17 (12 W)
4.e+1
2.7e+1
1.3e+1
0.e+0
250.
687.5
1125.
1562.5
2000.
m/z

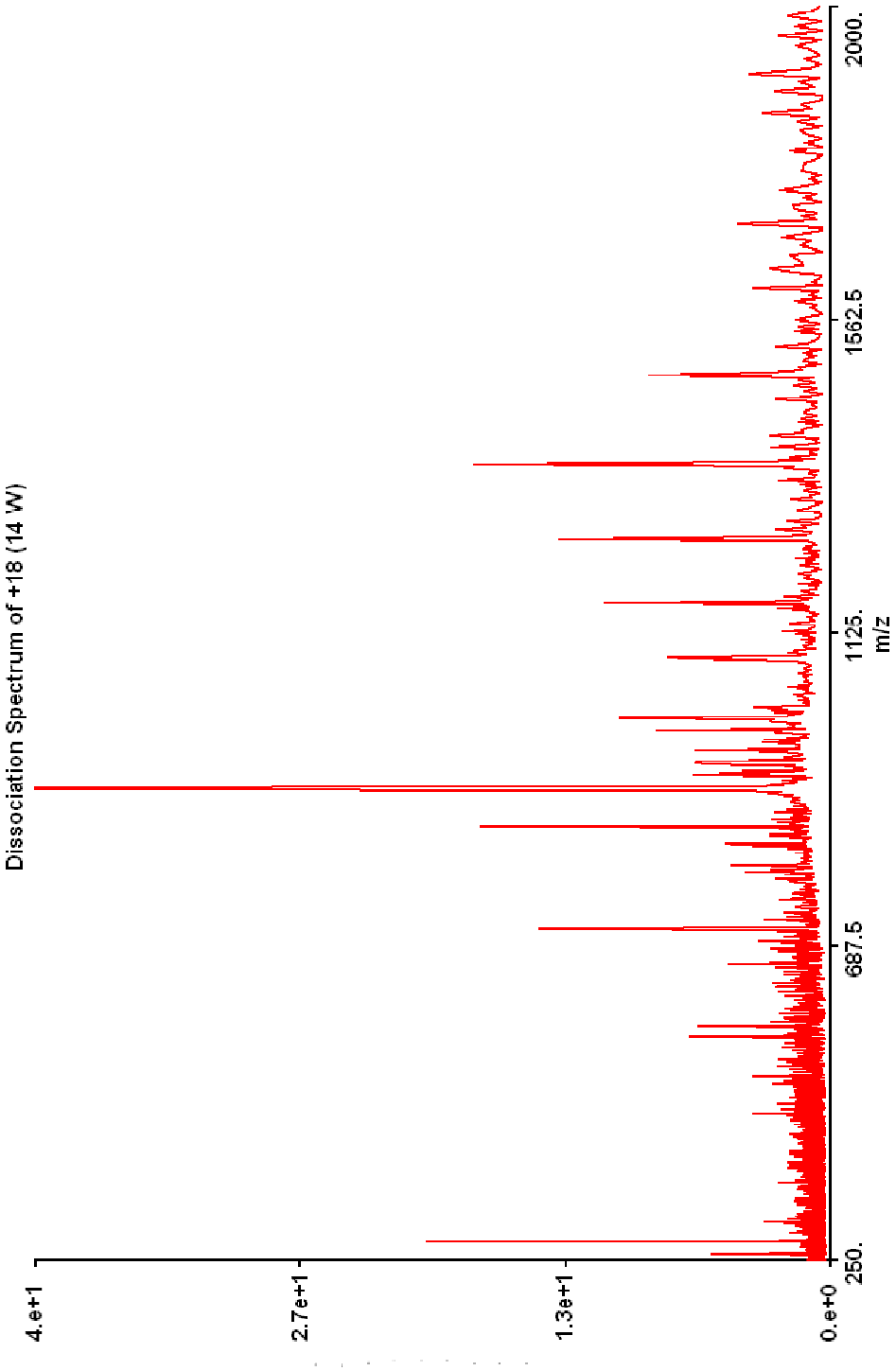
Dissociation Spectrum of +18 (14 W)
4.e+1
2.7e+1
1.3e+1
0.e+0
250.
687.5
1125.
1562.5
2000.
m/z

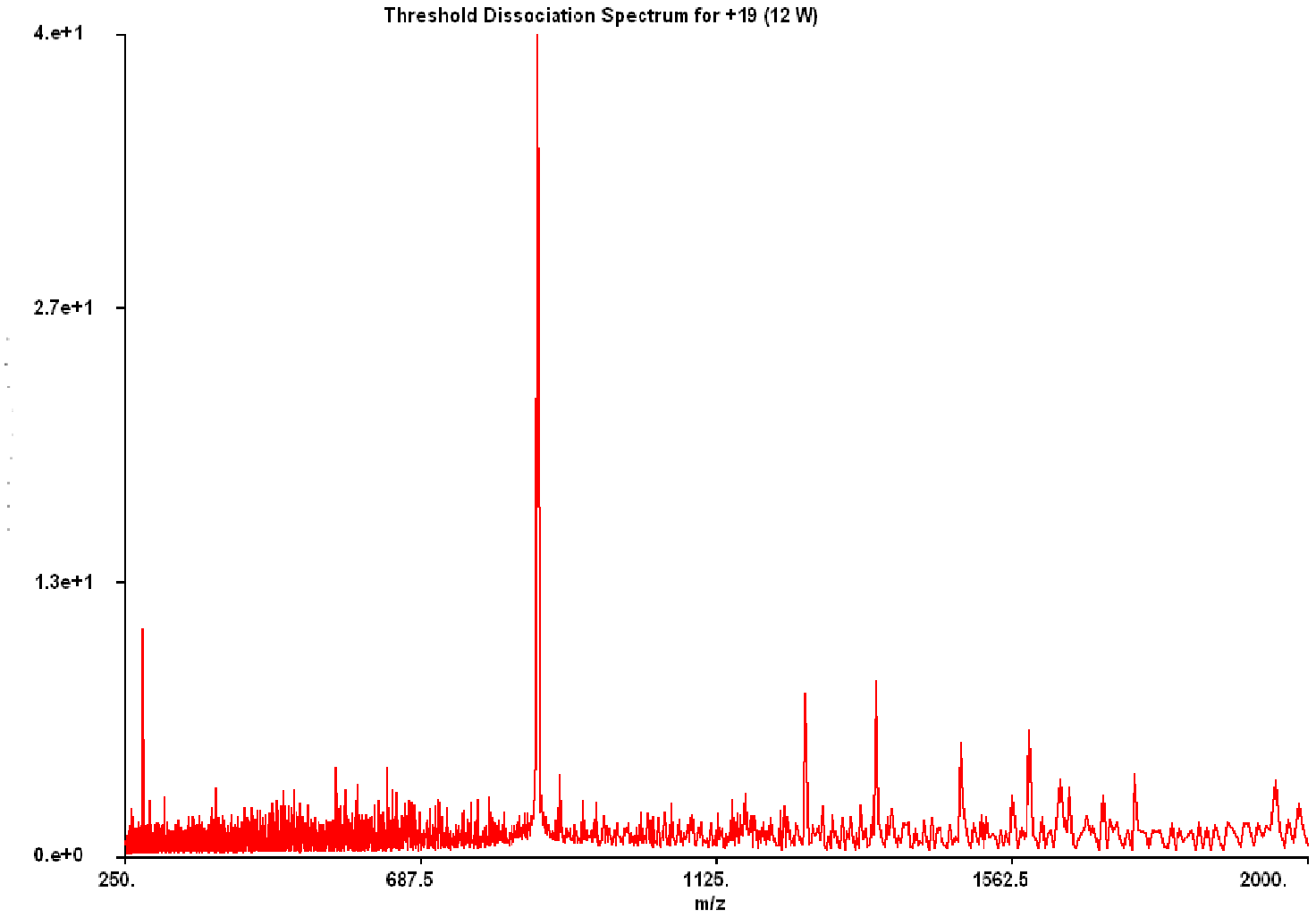
Threshold Dissociation Spectrum for +19 (12 W)
4.e+1
2.7e+1
1.3e+1
0.e+0
250.
687.5
1125.
1562.5
2000.
m/z

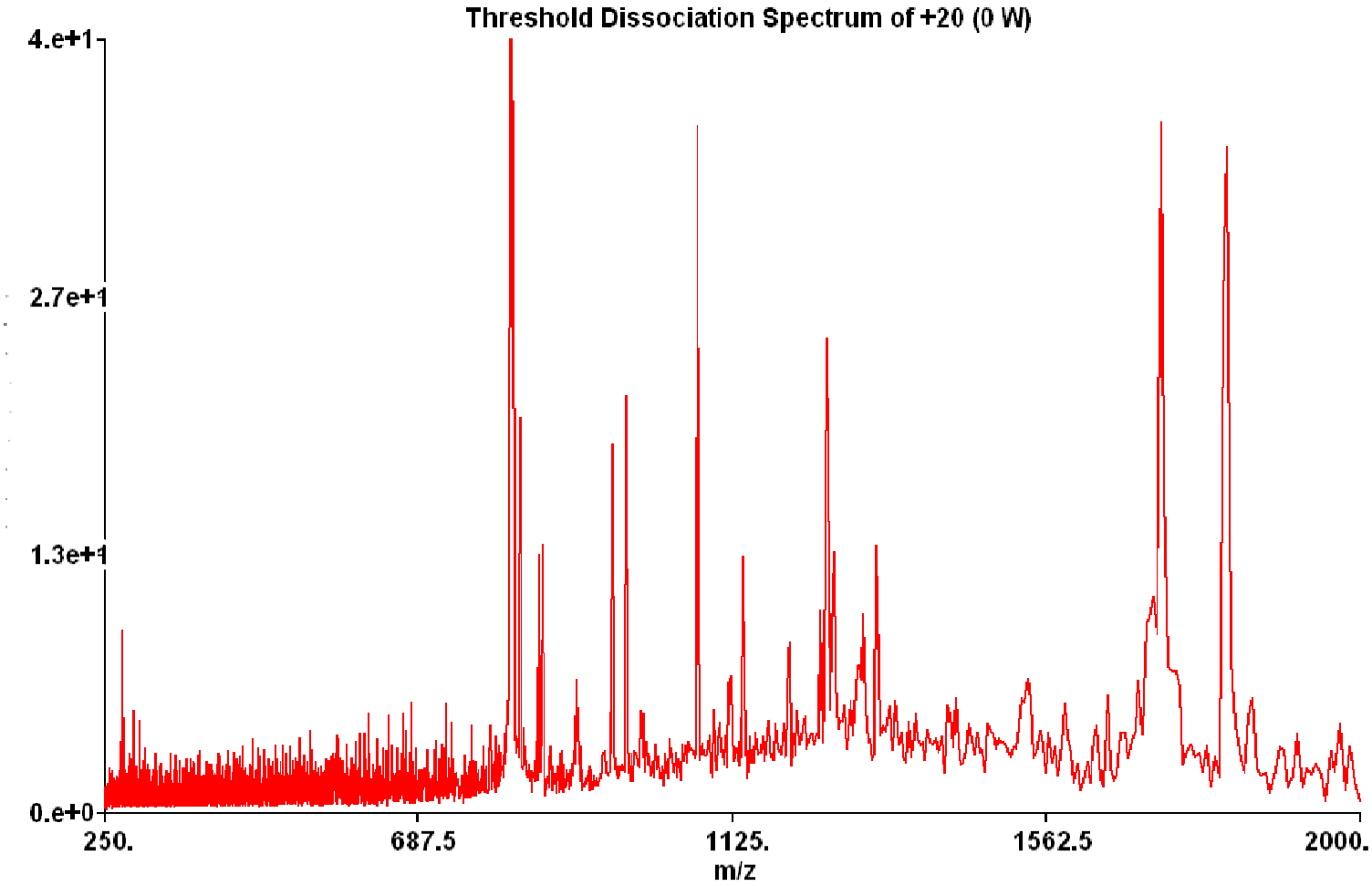
Threshold Dissociation Spectrum of +20 (0 W)
4.e+1
2.7e+1
1.3e+1
0.e+0
250.
687.5
1125.
1562.5
2000.
m/z

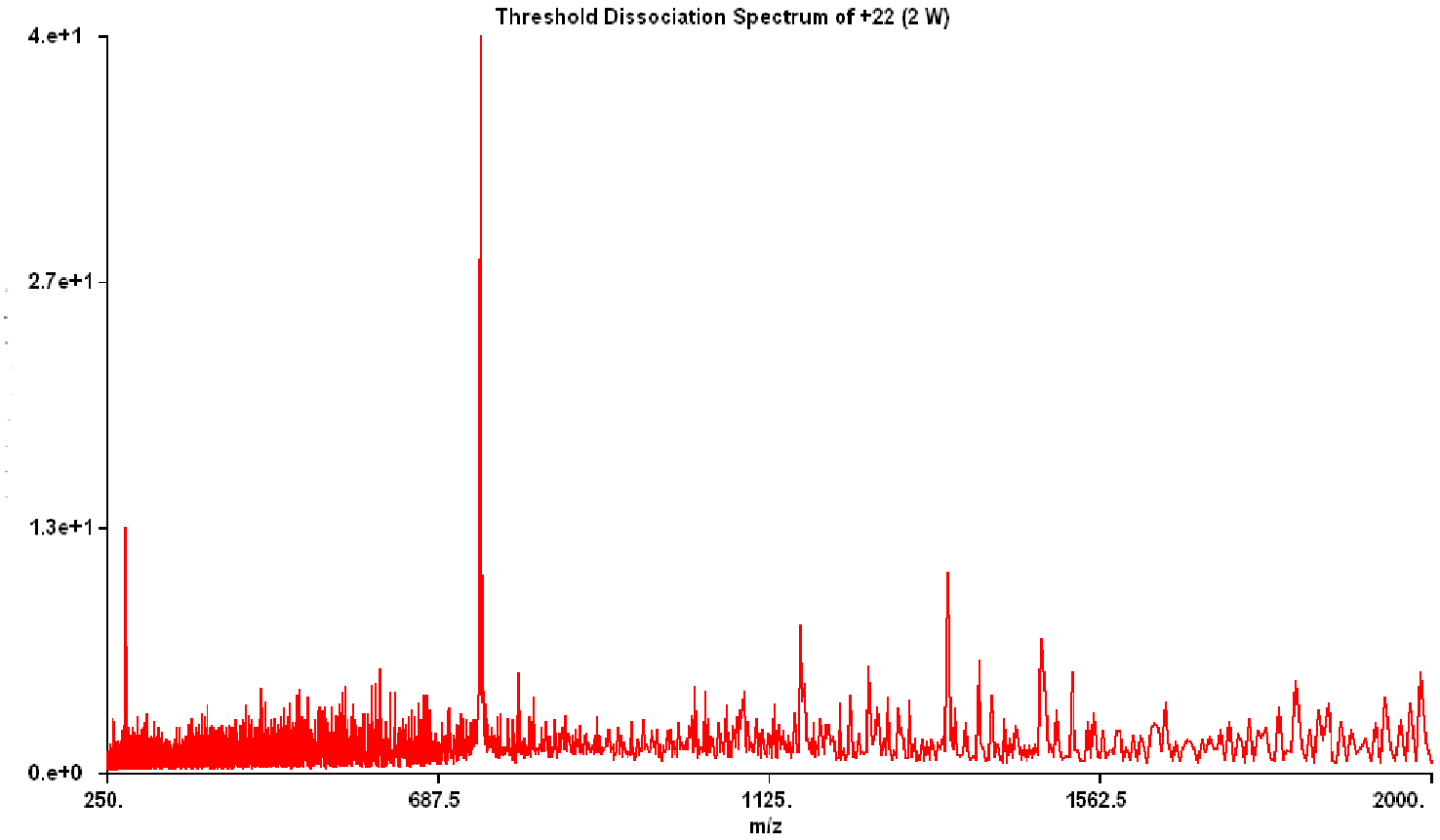
Threshold Dissociation Spectrum of +22 (2 W)
4.e+1
2.7e+1
1.3e+1
0.e+0
250.
687.5
1125.
1562.5
2000.
m/z

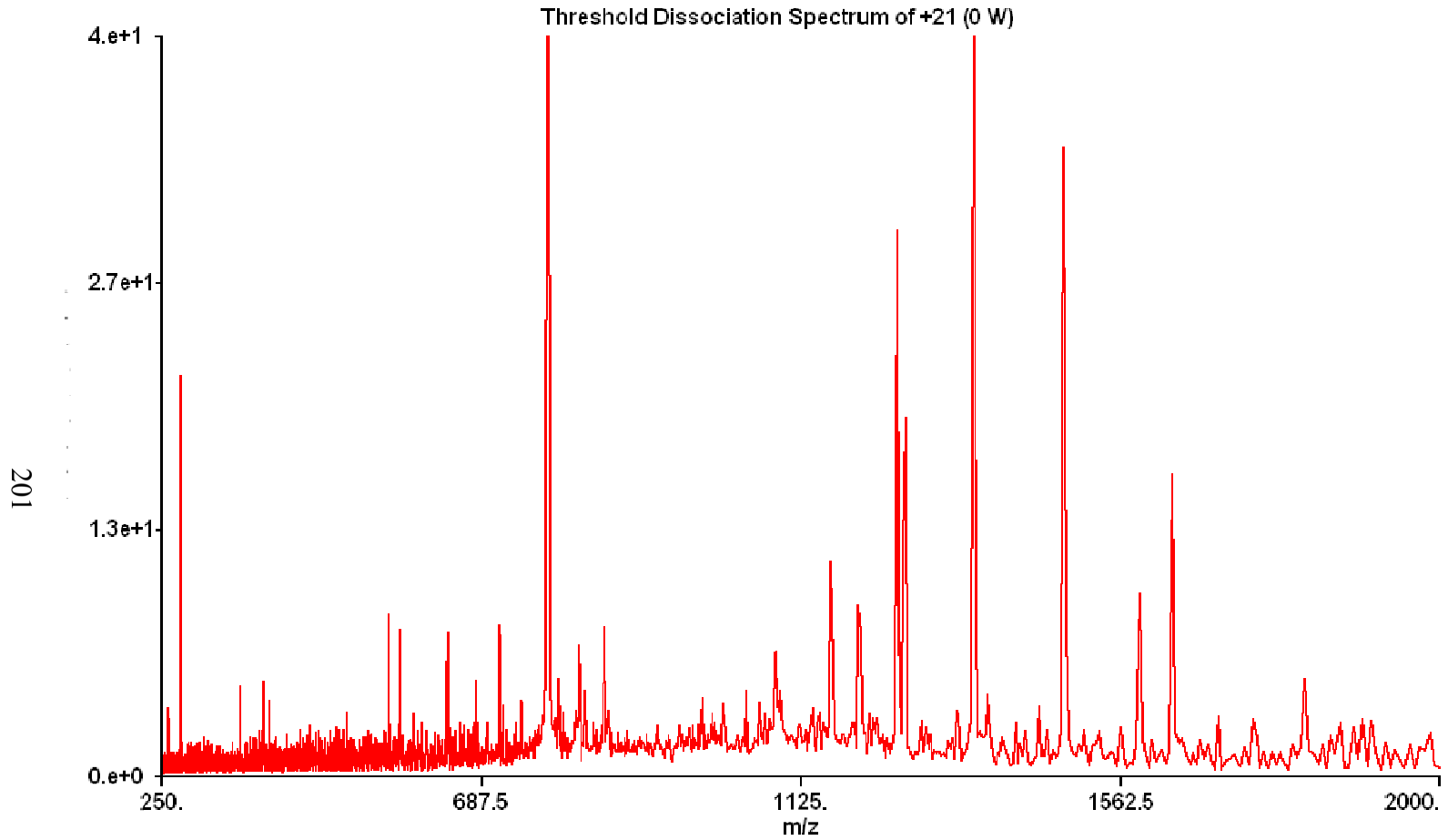
Threshold Dissociation Spectrum of +21 (0 W)
4.e+1
2.7e+1
1.3e+1
0.e+0
250.
687.5
1125.
1562.5
2000.
m/z

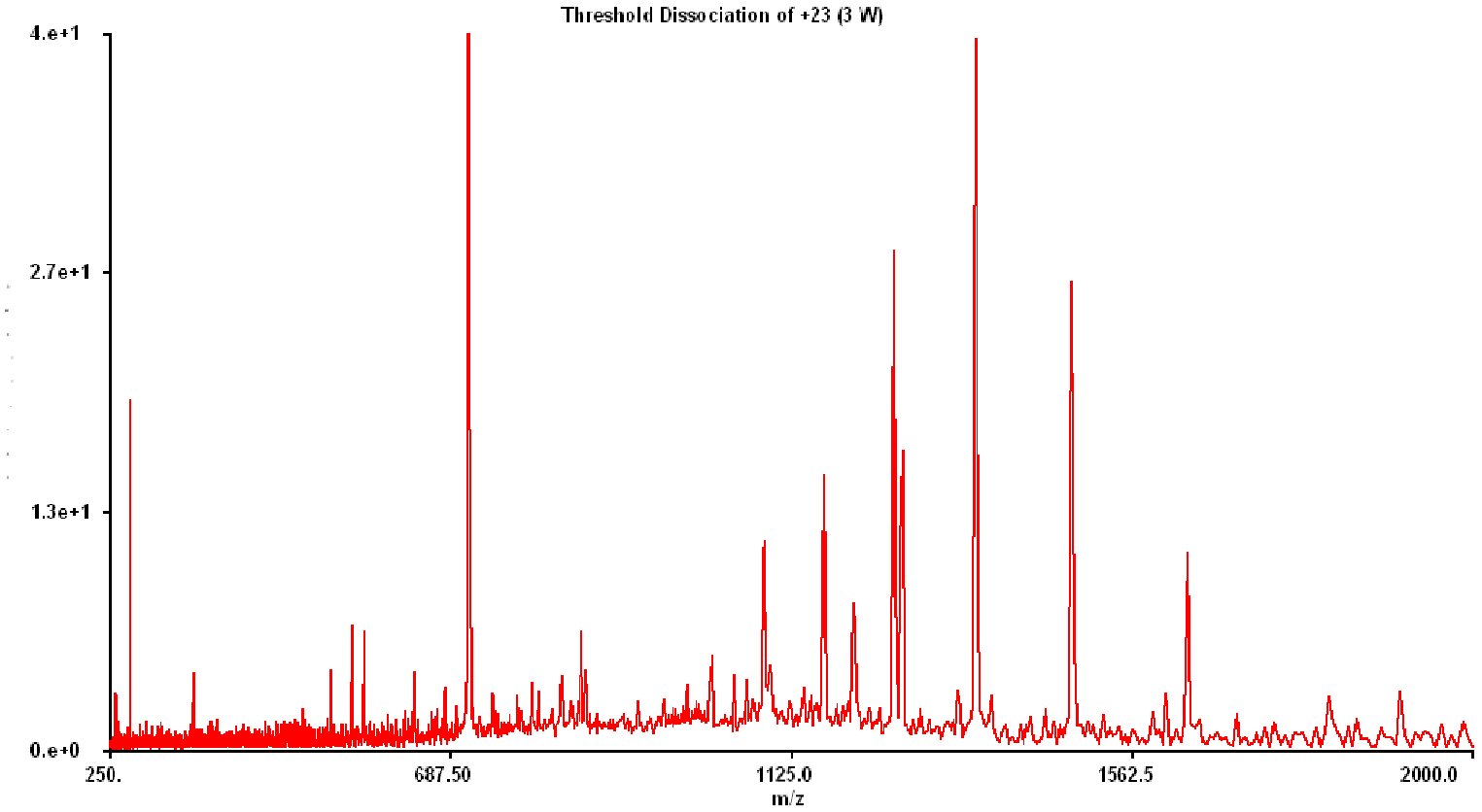
Threshold Dissociation of +23 (3 W)
4.e+1
2.7e+1
1.3e+1
0.e+0
250.
687.50
1125.0
1562.5
2000.0
m/z

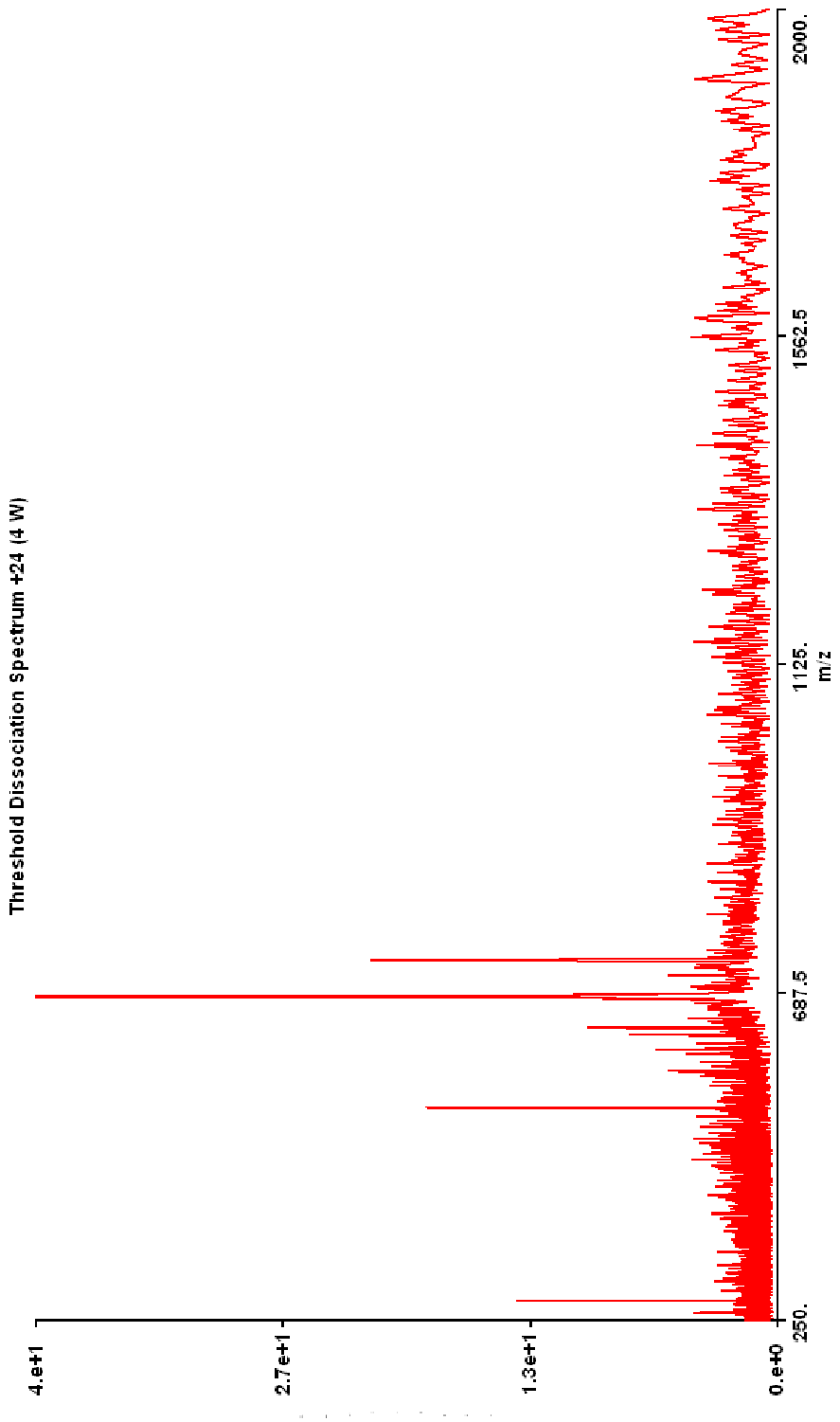
Threshold Dissociation Spectrum +24 (4 W)
4.e+1
2.7e+1
1.3e+1
0.e+0
250.
687.5
1125.
1562.5
2000.
m/z

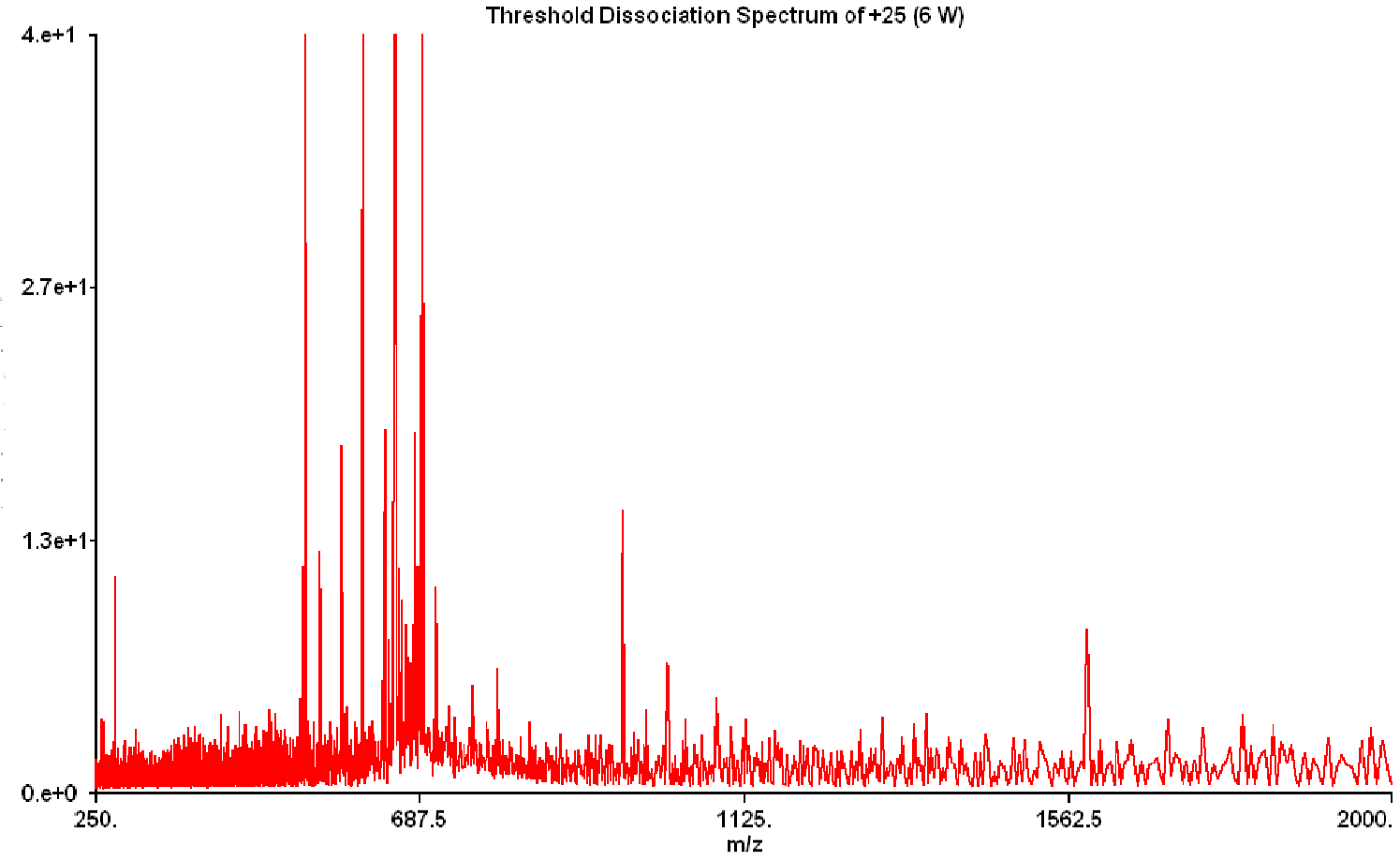
Threshold Dissociation Spectrum of +25 (6 W)
4.e+1
2.7e+1
1.3e+1
0.e+0
250.
687.5
1125.
1562.5
2000.
m/z

Bibliography

Adamski, F.M., J.F. Atkins and R.F. Gesteland, *Ribosomal protein L9 interactions with 23 S rRNA: the use of a translational bypass assay to study the effect of amino acid substitutions.* J. Mol. Biol., 1996. **261**(3): p. 357-71.

Agnes, G.R. and G. Horlick, *Determination of solution ions by electrospray mass spectrometry.* Appl. Spectrosc., 1994. **48**(6): p. 655-61.

Allen, M.H. and M.L. Vestal, *Design and performance of a novel electrospray interface.* J. Am. Soc. Mass Spectrom., 1992. **3**: p. 18-26.

Anderson, G.A., J.E. Bruce and R.D. Smith, *ICR-2LS.* 1996, Pacific Northwest National Laboratories: Richland, WA.

Babu, K.R. and A.D. Moradian, D. J., *The methanol-induced conformational transitions of b-lactoglobulin, cytochrome c, and ubiquitin at low pH: a study by electrospray ionization mass spectrometry.* J. Am. Soc. Mass Spectrom., 2001. **12**(3): p. 317-28.

Badman, E.R., C.S. Hoaglund-Hyzer and D.E. Clemmer, *Monitoring structural changes of proteins in an ion trap over apprx.10-200 ms: Unfolding transitions in cytochrome c ions.* Anal. Chem., 2001. **73**(24): p.

6000-7.

Badman, E.R., C.S. Hoaglund-Hyzer and D.E. Clemmer, *Monitoring structural changes of proteins in an ion trap over apprx.10-200 ms: Unfolding transitions in cytochrome c ions.* Anal. Chem., 2001. **73**(24): p. 6000-7.

Baker, P.R. and K.R. Clauser, *Protein Prospector*. 1995-2003, The University of California: San Fransisco.

Baker, T.R., T. Keough, R.L. Dobson, T.A. Riley, J.A. Hasselfield, and P.E. Hesselberth, *Antisense DNA oligonucleotides. I: The use of ionspray tandem mass spectrometry for the sequence verification of methylphosphonate oligodeoxyribonucleotides.* Rapid Commun. Mass Spectrom., 1993. **7**(3): p. 190-4.

Barbato, G., M. Ikura, L.E. Kay, R.W. Pastor and A. Bax, *Backbone Dynamics of Calmodulin Studied by N15 Relaxation Using Inverse Detected Two-Dimensional NMR Spectroscopy: the Central Helix is Flexible.* Biochem., 1992. **31**: p. 5269-78.

Barinaga, C.J., C.G. Edmonds, H.R. Udseth and R.D. Smith, *Sequence determination of multiply charged peptide molecular ions by electrospray-*

ionization tandem mass spectrometry. Rapid Commun. Mass Spectrom., 1989. **3**(5): p. 160-4.

Bax, A., *Multidimensional nuclear magnetic resonance methods for protein studies.* Curr. Opin. Struct. Biol., 1994. **4**: p. 738-44.

Bax, A., *Two-Dimensional Nuclear Magnetic Resonance in Liquids*. 1982, Dordrecht, Holland: D. Reidel Publishing Co. 200.

Beauchamp, J.L., *ICR Spectroscopy.* Ann. Rev. Phys. Chem., 1971. **22**: p. 527-61.

Belva, H., C. Lange and I. Segalas, *Conformational properties of a-dendrotoxin using electrospray mass spectrometry.* Eur. J. Mass Spectrom., 2001. **7**(4&5): p. 373-83.

Bergman, D.L., L. Laaksonen and A. Laaksonen, *Visualization of Solvation Structures in iquid Mixtures.* J. Mol. Graph. Model., 1997. **15**: p. 301-6.

Beu, S.C., M.W. Senko, J.P. Quinn, F.M. Wampler, III and F.W. McLafferty, *FT Electrospray Instrumentation for Tandem High-Resolution MS of Large Molecules.* J. Am. Soc. Mass Spectrom., 1993. **4**: p. 557-65.

Biemann, K. and S.A. Martin, *MS/MS of Peptides.* Mass Spectrom. Rev.,

1987. **6**: p. 1-76.

Bischoff, R., et al., *Sequence-specific deamidation: isolation and biochemical characterization of succinimide intermediates of recombinant hirudin.* Biochem., 1993. **32**(2): p. 725-34.

Bolaños, B.J., *Study of Higher Order Gas-Phase Protein Structure by Fourier Transform Ion Cyclotron Resonance Mass Spectrometry*, Dissertation Thesis, Department of Chemistry and Biochemistry, 1997, The University of Texas at Austin.

Branlant, C., A. Krol, J. Sriwidada and R. Brimacombe, *RNA sequences associated with proteins L1, L9, and L5, L18, L25, in ribonucleoprotein fragments isolated from the 50-S subunit of Escherichia coli ribosomes.* Eur. J. Biochem., 1976. **70**(2): p. 483-92.

Breci, L.A., D.L. Tabb, J.R.I. Yates and V.H. Wysocki, *Cleavage N-Terminal to Proline: Analysis of a Database of Peptide Tandem Mass Spectra.* Anal. Chem., 2003. **75**(9): p. 1963-71.

Breuker, K., H. Oh, D.M. Horn, B.A. Cerda and F.W. McLafferty, *Detailed unfolding and folding of gaseous ubiquitin ions characterized by electron capture dissociation.* J. Am. Soc. Mass Spectrom., 2002. **124**(22): p. 6407-20.

Brooks, B.R., R.E. Bruccoleri, B.D. Olafson, D.J. States, S. Swaminathan, and M. Karplus, *CHARMM: A program for macromolecular energy, minimization, and dynamics calculations.* J. Comput. Chem., 1983. **4**: p. 187-217.

Bruccoleri, R.E., *Conformational Search and Protein Folding*, in *The Protein Folding Problem and Tertiary Structure Prediction*, K. Merz, Jr. and S. Le Grand, Editors. 1994, Birkhauser: Boston. p. 125-40.

Busman, M., A.L. Rockwood and R.D. Smith, *Activation energies for gas-phase dissociations of multiply charged ions from electrospray ionization mass spectrometry.* J. Phys. Chem., 1992. **96**(6): p. 2397-400.

Butcher, D.J., K.G. Asano, D.E. Goeringer and S.A. McLuckey, *Thermal dissociation of gaseous bradykinin ions.* J. Phys. Chem. A, 1999. **103**(43): p. 8664-71.

Carr, S.A., M.J. Huddleston and M.F. Bean, *Selective identification and differentiation of N- and O-linked oligosaccharides in glycoproteins by liquid chromatography-mass spectrometry.* Protein Sci., 1993. **2**(2): p. 183-96.

Cassady, C.J., J. Wronka, G.H. Kruppa and F.H. Laukien, *Deprotonation reactions of multiply protonated ubiquitin ions.* Rapid Commun. Mass

Spectrom., 1994. **8**: p. 394-400.

Chen, R., et al., *Trapping, Detection, and Mass Determination of Coliphage T4 DNA Ions of 10^8 Da by Electrospray Ionization Fourier Transform Ion Cyclotron Resonance Mass Spectrometry.* Anal. Chem., 1995. **67**: p. 1159-63.

Chorush, R.A., D.P. Little, S.C. Beu, T.D. Wood and F.W. McLafferty, *Surface-induced dissociation of multiply-protonated proteins.* Anal. Chem., 1995. **67**: p. 1042-6.

Chowdhury, S.K., V. Katta and B.T. Chait, *Differences in Charge States of Electrosprayed Native and Denatured Proteins.* J. Am. Chem. Soc., 1990. **112**: p. 9012.

Chowdury, S.K., V. Katta and B.T. Chait, *Probing Conformational Changes in Proteins by Mass Spectrometry.* J. Am. Chem. Soc., 1990. **112**: p. 9012-3.

Clemmer, D.E., R.R. Hudgins and M.F. Jarrold, *Naked Protein Conformations: Cytochrome c in the Gas Phase.* J. Am. Chem. Soc., 1995. **117**: p. 10141-2.

Cole, R.B., ed. *Electrospray Ionization Mass Spectrometry*. 1997, John Wiley & Sons,Inc.: New York. 1-577.

Covey, T. and D.J. Douglas, *Collision Cross Sections for Protein Ions.* J. Am.

Soc. Mass Spectrom., 1993. **4**: p. 616-23.

Covey, T.R., R.F. Bonner, B.I. Shushan and J.D. Henion, *The determination of protein, oligonucleotide and peptide molecular weights by ion-spray mass spectrometry.* Rapid Commun. Mass Spectrom., 1988. **2**(11): p. 249-56.

Cox, K.A., R.K.J. Julian, R.G. Cooks and R.E.J. Kaiser, *Conformer selection of protein ions by ion mobility in a triple quadrupole mass spectrometer.* J. Am. Soc. Mass Spectrom., 1994. **5**(3): p. 127-363.

Cox, K.A., S.J. Gaskell, M. Morris and A. Whiting, *Role of Site Protonation in the Low Energy Decompositions of Gas-Phase Peptide Ions.* J. Am. Soc. Mass Spectrom., 1996. **7**(6): p. 522-31.

de Hoffman, E., *Tandem mass spectrometry: a primer.* J. Mass Spectrom., 1996. **31**(2): p. 129-37.

Dikler, S., J.W. Kelly and D.H. Russell, *Improving mass spectrometric sequencing of arginine-containing peptides by derivatization with acetylacetone.* J. Mass Spectrom., 1997. **32**(12): p. 1337-49.

Dole, M., L.L. Mack, R.L. Hines, R.C. Mobley, L.P. Ferguson, and M.B. Alice, *Molecular beams of macroions.* J. Phys. Chem., 1968. **49**: p. 2240.

Dongre, A.R., J.L. Jones, A. Somogyi and V.H. Wysocki, *Influence of peptide*

composition, gas-phase basicity, and chemical modification on fragmentation efficiency: Evidence for the mobile proton model. J. Am. Chem. Soc., 1996. **118**(35): p. 8365-74.

Downard, K.M. and K. Beimann, *Charging behavior of highly basic peptides during electrospray ionization. A predilection for protons.* Int. J. Mass Spectrom. Ion Processes, 1995. **148**: p. 191-202.

Downard, K.M. and K. Beimann, *The effect of charge state and the localization of charge on the collision-induced dissociation of peptide ions.* J. Am. Soc. Mass Spectrom., 1994. **5**(11): p. 966-75.

Edmonds, C.G., J.A. Loo, C.J. Barinaga, H.R. Udseth and R.D. Smith, *Capillary Electrophoresis-Electrospray Ionization Mass Spectrometry.* J. Chromatogr., 1989. **474**: p. 21-37.

Electrospray Ionization Mass Spectrometry. 1 ed, ed. R.B. Cole. 1997, New York: John Wiley & Sons, Inc.

Elliott, W.H. and D.C. Elliott, *Biochemistry and Molecular Biology*. 1997, New York: Oxford University Press, Inc. 437.

Emmett, M.R. and R.M. Caprioli, *Micro-Electrospray Mass Spectrometry: Ultra-High-Sensitivity Analysis of Peptides and Proteins.* J. Am. Soc. Mass

Spectrom., 1994. **5**: p. 605-13.

Feng, R. and Y. Konishi, *Stepwise Refolding of Acid-Denatured Myoglobin: Evidence from Electrospray Mass Spectrometry.* J. Am. Soc. Mass Spectrom., 1993. **4**: p. 638-45.

Fenn, J.B., *Ion formation from charged droplets: roles of geometry, energy, and time.* J. Am. Soc. Mass Spectrom., 1993. **4**(7): p. 524-35.

Fenn, J.B., M. Mann, C.K. Meng, S.F. Wong and C.M. Whitehouse, *Electrospray Ionization for Mass Spectrometry of Large Biomolecules.* Science, 1989. **246**: p. 64-71.

Fenn, J.B., M. Mann, C.K. Meng, S.F. Wong and C.M. Whitehouse, *Electrospray Ionization- Principles and Practice.* Mass Spectrom. Rev., 1990. **9**: p. 37-70.

Fenn, J.B., M. Mann, C.K. Meng, S.F. Wong and C.M. Whitehouse, *Electrospray.* Mass Spectrom. Rev., 1990. **9**: p. 37-70.

Fenselau, C., *Beyond Gene Sequencing: Analysis of Protein Structure with Mass Spectrometry.* Ann. Rev. Biophys. Chem., 1991. **20**: p. 205-20.

Freitas, M.A., C.L. Hendrickson, M.R. Emmett and A.G. Marshall, *Gas-Phase Bovine Ubiquitin Cation Conformations Resolved by Gas-Phase*

Hydrogen/Deuterium Exchange Rate and Extent. Int. J. Mass Spectrom., 1999. **185/186/187**: p. 565-75.

Gard, E., M.K. Green, J. Bregar and C. Lebrilla, *Gas Phase Hydrogen/Deuterium Exchange as a Molecular Probe for the Interaction of Methanol and Protonated Peptides.* J. Am. Soc. Mass Spectrom., 1994. **5**: p. 623-31.

Garrett, R., H. and C. Grisham, M., *Biochemistry*. 1st ed. 1995, Orlando, FL: Saunders College Publishing. 1100.

Gauthier, J.W., T.R. Trautman and D.B. Jacobson, *Sustained Off-resonance Irradiation for CAD Involving FTMS. CAD Technique that Emulates Infrared Multiphoton Dissociation.* Anal. Chim. Acta, 1991. **246**: p. 199-210.

Gill, A.C., J.K. R., W. T. and B.M. T., *Conformations of biopolymers in the gas phase: a new mass spectrometric method.* Int. J. Mass Spectrom., 2000. **196**: p. 685.

Gorman, G.S., J.P. Speir, C.A. Turner and I.J. Amster, *The proton affinities of the twenty commom alpha-amino acids.* J. Am. Chem. Soc., 1992. **114**: p. 3986-8.

Gorshkov, M.V., L. Pasa-Tolic and R.D. Smith, *Pressure limited sustained*

off-resonance irradiation for collision-activated dissociation in Fourier transform mass spectrometry. J. Am. Soc. Mass Spectrom., 1999. **10**(1): p. 15-8.

Grandori, R., *Origin of the conformational dependence of protein charge-state distributions in electrospray ionization mass specrometry.* J. Mass Spectrom., 2003. **38**: p. 11-15.

Green, M.K., E. Gard, J. Bregar and C.B. Lebrilla, *H-D exchange kinetics of alcohols and protonated peptides: effects of structure on proton affinity.* J. Mass Spectrom., 1995. **30**: p. 1103-10.

Green, M.K.L.C.B., *Ion-molecule reactions as probes of gas-phase structures of peptides and proteins.* Mass Spectrom. Rev., 1997. **16**(2): p. 53.

Gu, C., G. Tsaprailis, L. Breci and V.H. Wysocki, *Selective Gas-Phase Cleavage at the Peptide Bond C-Terminal to Aspartic Acid in Fixed-Charge Derivative of Asp-Containing Peptides.* Anal. Chem., 2000. **72**: p. 5804-13.

Guan, S. and A.G. Marshall, *Stored waveform inverse Fourier transform (SWIFT) ion excitation in trapped-ion mass spectrometry: Theory and applications.* Int. J. Mass Spectrom. Ion Processes, 1996. **157/158**: p. 5-37.

Guan, S., *Generation of Optimal Excitation Pulses for Two Energy Level*

Systems Using an Inverse FT Method. J. Chem. Phys., 1992. **96**: p. 7959-64.

Guan, S., H.S. Kim, A.G. Marshall, M.C. Wahl, T.D. Wood, and X. Xiang, *Shrink-Wrapping an Ion Cloud for High-Performance Fourier Transform Ion Cyclotron Resonance Mass Spectrometry.* Chem. Rev., 1994. **94**(8): p. 2161-82.

Guan, Z., J.J. Drader, V.L. Campbell and D.A. Laude, *Real-Time Monitoring of the Gas Phase Reactions of Single Ion Population Using the Remeasurement Experiment in Fourier Transform Ion Cyclotron Resonance Mass Spectrometry.* Anal. Chem., 1995. **67**: p. 1453-8.

Guan, Z., S.A. Hoftstadler and D.A. Laude, Jr., *Remeasurement of Electrosprayed Proteins in the Trapped Ion Cell of a Fourier Transform ICR Mass Spectrometer.* Anal. Chem., 1993. **65**: p. 1588-93.

Guan, Z., V.L. Campbell, J.J. Drader, C.L. Hendrickson and D.A. Laude, *High performance detection of biomolecules using a high magnetic field electrospray ionization source/Fourier transform ion cyclotron resonance mass spectrometer.* Rev. Sci. Instrum., 1995. **66**(9): p. 4507-15.

Gur, E.H., L.J. De Koning and N.M.M. Nibbering, *Gas-phase hydrogen-deuterium exchange of protonated alkyldipeptides with (S)- and (R)-butan-2-*

ol. J. Mass Spectrom., 1996. **31**(3): p. 325-7.

H.M. Berman, et al., *The Protein Data Bank.* Nucleic Acids Research, 2000. **28**: p. 235-242.

Harper, C.J., T.A. Torres, E.G. Schmidt, C.R. Arkin and D.A. Laude, *On-Line HPLC Interface for a Magnetic Field Focusing ESI/FTICR.* Proc. 44th Amer. Soc. Mass Spectrom. Conf. on Mass Spectrom. & Allied Topics, 1996: p. 486.

Harrison, A.G., *The Gas-Phase Basicities and Proton Affinities of Amino Acids and Peptides.* Mass Spectrom. Rev., 1997. **16**: p. 201-17.

Havel, H.A., *Spectroscopic Methods for Determining Protein Structure in Solution*. 1994, New York: VCH Publishers, Inc. 250.

Hendrickson, C.L. and D.A. Laude, Jr., *Quadrupolar axialization for improved control of electrosprayed proteins in FTICR mass spectrometry.* Anal. Chem., 1995. **67**: p. 1717-1721.

Henry, K.D., E.R. Williams, B.-H. Wang, F.W. McLafferty, J. Shabanowitz, and D.F. Hunt, *Fourier-Transform Mass Spectrometry of Large Molecules by Electrospray Ionization.* Proc. Natl. Acad. Sci. U.S.A., 1989. **86**: p. 9075-8.

Hillenkamp, F., M. Karas, R.C. Beavis and B.T. Chait, *Matrix-Assisted Laser*

Desorption/Ionization Mass Spectrometry of Biopolymers. Anal. Chem., 1991. **63**(24): p. 1193A-1203A.

Hoffman, D.W., C.S. Cameron, C. Davies, S.W. White and V. Ramakrishnan, *Ribosomal Protein L9: A Structure Determination by the Use of X-ray Crystallography and NMR Spectroscopy.* J. Mol. Biol., 1996. **264**: p. 1058-71.

Hoffman, D.W., et al., *Crystal Structure of Prokaryotic Ribosomal Protein L9: a bi-lobed RNA-binding Protein.* EMBO J., 1994. **13**: p. 205-12.

Hofstadler, S.A. and D.A. Laude, *Ion ejection from Fourier transform mass spectrometry trapped ion cells due to non-adiabatic changes in trapping potentials.* Int. J. Mass Spectrom. Ion Processes, 1990. **101**(1): p. 65-78.

Hofstadler, S.A., E. Schmidt, Z. Guan and D.A. Laude, Jr., *Concentric tube vacuum chamber for high magnetic field, high-pressure ionization in a Fourier transform ICR mass spectrometer.* J. Am. Soc. Mass Spectrom., 1993. **4**: p. 168-76.

Hofstadler, S.A., J.H. Wahl, R. Bakhtiar, G.A. Anderson, J.E. Bruce, and R.D. Smith, *Capillary Electrophoresis Fourier Transform Ion Cyclotron Resonance Mass Spectrometry with Sustained Off-Resonance Irradiation for*

the Characterization of Protein and Peptide Mixtures. J. Am. Soc. Mass Spectrom., 1994. **5**: p. 894-9.

Holtje, H.-D. and G. Folkers, *Molecular Modeling: Basic Priniples and Applications*. Methods and Priniciples in Medicinal Chemistry, ed. R. Mannhold, H. Kubinyi and H. Timmerman. Vol. 5. 1997, New York: VCH Publishers, Inc. 194.

Horn, D.M., R.A. Zubarev and F.W. McLafferty, *Automated reduction and interpretation of high resolution electrospray mass spectra of large molecules.* J. Am. Soc. Mass Spectrom., 2000. **11**: p. 320-32.

Horn, D.M., Y. Ge and F.W. McLafferty, *Activated Ion Electron Capture Dissociation for Mass Spectral Sequencing of Larger (42 kDa) Proteins.* Anal. Chem., 2000. **70**(20): p. 4778-84.

Iribarne, J.V. and B.A. Thomson, *On the evaporation of small ions from charged droplets.* J. Chem. Phys., 1976. **64**(6): p. 2287-94.

Ishikawa, K., T. Nishimura, Y. Koga and Y. Niwa, *Role of Coulomb energy in promoting collisionally activated dissociation of multiply charged peptides formed by electrospray ionization.* Rapid Commun. Mass Spectrom., 1994. **8**(12): p. 933-8.

Jockusch, R.A., P.D. Schnier, W.D. Price, E.R. Strittmatter, P.A. Demirev, and E.R. Williams, *Effects of Charge State on Fragmentation Pathways, Dynamics, and Activation Energies of Ubiquitin Ions Measured by Blackbody Infrared Radiative Dissociation.* Anal. Chem., 1997. **69**: p. 1119-26.

Johnson, R.S., S.A. Martin, K. Biemann, J.T. Stults and J.T. Watson, *Novel Fragmentation Process of Peptides by Collision-Induced Decomposition in a Tandem Mass Spectrometer: Differentiation between Leucine and Isoleucine.* Anal. Chem., 1987. **59**: p. 2621-5.

Kaltashov, I.A. and C. Fenselau, *Proton Locations in Doubly Charged Peptides and Association with Fragmentation Pathways.* Int. J. Mass Spectrom. Ion Processes, 1997. **160**(1-3): p. 331-8.

Kaltashov, I.A. and C. Fenselau, *Thermochemistry of Multiply Charged Melittin in the Gas Phase Determined by the Modified Kinetic Method.* Rapid Commun. Mass Spectrom., 1996. **10**(7): p. 857.

Kaltashov, I.A., D. Fabris, A. Lee, Z. Szilagyi and C. Fenselau, *Thermochemistry and conformation of multiply charged peptides in a solvent-free environment.* Adv. Mass Spectrom., 1998. **14**.

Karas, M., U. Bahr, A. Ingendoh and F. Hillenkamp, Angew. Chem. Int. Ed.

Engl., 1989. **28**: p. 760-1.

Katta, V. and B.T. Chait, *Conformational changes in proteins probed by hydrogen-exchange electrospray-ionization mass spectrometry.* Rapid Commun. Mass Spectrom., 1991. **5**(4): p. 214-7.

Kebarle, P. and L. Tang, *From Ions in Solution to Ions in the Gas Phase: The Mechanism of Electrospray Mass Spectrometry.* Anal. Chem., 1993. **65**: p. 972A-986A.

Kelleher, N.L., M.W. Senko, M.M. Siegel and F.W. McLafferty, *Unit Resolution Mass Spectra of 112 kDa Molecules with 3 Da Accuracy.* J. Am. Soc. Mass Spectrom., 1997. **8**: p. 380-3.

Konermann, L. and D.J. Douglas, *Acid-induced unfolding of cytochrome c at different methanol concentrations: Electrospray ionization mass spectrometry specifically monitors changes in the tertiary structure.* Biochem., 1997. **36**(40): p. 12296-302.

Koradi, R., M. Billeter and K. Wuthrich, *MOLMOL: A Program for Display and Analysis of Macromolecular Structures.* J. Mol. Graphics, 1996. **14**: p. 51-55.

Kraulis, P.J., *MOLSCRIPT: A Program to Produce Both Detailed and*

Schematic Plots of Protein Structures. J. Appl. Crystallogr., 1991. **24**: p. 946-50.

Kuhlman, B., H.Y. Yang, J.A. Boice, R. Fairman and D.P. Raleigh, *An exceptionally stable helix from the ribosomal protein L9: implications for protein folding and stability.* J. Mol. Biol., 1997. **270**(5): p. 640-7.

Kuhlman, B., J.A. Boice, R. Fairman and D.P. Raleigh, *Structure and Stability of the N-terminal Domain of Ribosomal Protein L9: Evidence for Rapid two-state folding.* Biochem., 1998. **37**: p. 1025-32.

Laaksonen, L., *A Graphics Program for the Analysis and Display of Molecular Dynamics Trajectories*. J. Mol. Graphics, 1992. **10**: p. 33-4.

Lasater, M.A., *Studies of Sub-Micron Sized Electrospray Droplets in Mass Spectrometry*, Dissertation Thesis, Department of Chemistry and Biochemistry, 2001, The University of Texas at Austin.

Laude, D.A., E. Stevenson and J.M. Robinson, *Electrospray ionization/Fourier transform ion cyclotron resonance mass spectrometry*, in *Electrospray Ionization Mass Spectrometry*, R.B. Cole, Editor. 1997, John Wiley & Sons, Inc.: New York. p. 291-319.

Le Blanc, J.C.Y., D. Beuchemin, K.W.M. Siu, R. Guevremont and S.S. Berman, *Thermal denaturation of some proteins and its effect on their electrospray mass spectra.* Org. Mass Spectrom., 1991. **26**(10): p. 831-9.

Lillemoen, J. and D.W. Hoffman, *An investigation of the dynamics of ribosomal protein L9 using heteronuclear NMR relaxation measurements.* J. Mol. Biol., 1998. **281**(3): p. 539-51.

Lillemoen, J., C.S. Cameron and D.W. Hoffman, *The stability and dynamics of ribosomal protein L9: investigations of a molecular strut by amide proton exchange and circular dichroism.* J. Mol. Biol., 1997. **268**(2): p. 482-93.

Lillemoen, J., *Internal dynamics of biological macromolecules: investigations of ribosomal protein L9 and bacteriophage T2 gene 32 RNA pseudoknot.*, Dissertation Thesis, Department of Chemistry and Biochemistry, 1998, The University of Texas at Austin.

Limbach, P.A., P.B. Grosshans and A.G. Marshall, *Experimental Determination of the Number of Trapped Ions, Detection Limite, and Dynamic Range in Fourier Transform Ion Cyclotron Resonance Mass Spectrometry.* Anal. Chem., 1993. **65**: p. 135-140.

Lin, H. and C. Dass, *Conformational changes in b-endorphin as studied by*

electrospray ionization mass spectrometry. Rapid Commun. Mass Spectrom., 2001. **15**(23): p. 2341-6.

Little, D.P., J.P. Speir, M.W. Senko, P.B. O'Connor and F.W. McLafferty, *Infrared Multiphoton dissociation of large multiply-charged ions for biomolecule sequencing.* Anal. Chem., 1994. **66**(18): p. 2809-15.

Loo, J.A. and R.R. Ogorzalek Loo, *Electrospray Ionization Mass Spectrometry of Peptides and Proteins*, in *Electrospray Ionization Mass Spectrometry*, R.B. Cole, Editor. 1997, John Wiley & Sons, Inc.: New York. p. 385.

Loo, J.A. and R.R. Ogorzalek Loo, *Electrospray Ionization Mass Spectrometry of Peptides and Proteins*, in *Electrospray Ionization Mass Spectrometry*, R.B. Cole, Editor. 1997, John Wiley & Sons, Inc.: New York. p. 385-419.

Loo, J.A., C.G. Edmonds and R.D. Smith, *Tandem mass spectrometry of very large molecules. 2. Dissociation of multiply charged proline-containing proteins from electrospray ionization.* Anal. Chem., 1993. **65**(4): p. 425-38.

Loo, J.A., C.G. Edmonds and R.D. Smith, *Tandem mass spectrometry of very large molecules: serum albumin sequence information from multiply charged*

ions formed by electrospray ionization. Anal. Chem., 1991. **63**(21): p. 2488-99.

Loo, J.A., C.G. Edmonds, H.R. Udseth and R.D. Smith, *Effect of reducing disulfide-containing proteins on electrospray ionization mass spectra.* Anal. Chem., 1990. **62**(7): p. 693-8.

Loo, J.A., H.R. Udseth and R.D. Smith, *Collisional Effects on the Charge Distribution of Ions from Large Molecules, Formed by Electrospray-ionization Mass Spectrometry.* Rapid Commun. Mass Spectrom., 1988. **2**(10): p. 207-10.

Loo, J.A., J.P. Quinn, S.I. Ryu, K.D. Henry, M.W. Senko, and F.W. McLafferty, *High-resolution Tandem Mass Spectrometry of Large Biomolecules.* Proc. Natl. Acad. Sci. U.S.A., 1992. **89**: p. 286-9.

Loo, J.A., R.R. Ogorzalek Loo and P.C. Andrews, *Primary to quaternary protein structure determination with electrospray ionization and magnetic sector mass spectrometry.* Org. Mass Spectrom., 1993. **28**(12): p. 1640-9.

Loo, J.A., R.R. Ogorzalek Loo, H.R. Udseth, C.G. Edmonds and R.D. Smith, *Solvent-Induced Conformational Changes of Polypeptides Probed by Electrospray-Ionization Mass Spectrometry.* Rapid Commun. Mass

Spectrom., 1991. **5**(3): p. 101-5.

Luisi, D.L., B. Kuhlman, K. Sideras, P.A. Evans and D.P. Raleigh, *Effects of Varying the Local Propensity to form Secondary Structure on the Stability and Folding Kinetics of a Rapid Folding alpha/beta Protein: Characterization of a Truncation Mutant of the N-Terminal Domain of the Ribosomal Protein L9.* J. Mol. Biol., 1999. **289**: p. 167-74.

Luisi, D.L., W.-J. Wu and D.P. Raleigh, *Conformational Analysis of a Set of Peptides Corresponding to the Entire N-terminal Domain of the Ribosomal Protein L9: Evidence for a Stable Native-like Secondary Structure in the Unfolded State.* J. Mol. Biol., 1999. **287**: p. 395-407.

Manjunatha, K.R. and H. Evans, J., *Molecular Modeling of Proteins: a Strategy for Energy Minimization by Molecular Mechanics in the AMBER force field.* J. Biomol. Struct. Dynamics, 1991. **9**(3): p. 475-88.

Mao, D., K.R. Babu, Y.-L. Chen and D.J. Douglas, *Conformations of Gas-Phase Lysozyme Ions Produced from Two Different Solution Conformations.* Anal. Chem., 2003. **75**(6): p. 1325-30.

Marshall, A.G., C.L. Hendrickson and G.S. Jackson, *Fourier Transform Ion Cyclotron Resonance Mass Spectrometry: A Primer.* Mass Spectrom. Rev.,

1998. **17**(1): p. 1-35.

Marshall, A.G., T.-C.L. Wang and T.L. Ricca, *Tailored Excitation for Fourier Transform Ion Cyclotron Resonance Mass Spectrometry.* J. Am. Chem. Soc., 1985. **107**: p. 7893-7.

Marzluff, E.M. and J.L. Beauchamp. in *Proc. 42nd Amer. Soc. Mass Spectrom. Conf. on Mass Spectrom. & Allied Topics*. 1994. Chicago, IL: Amer. Soc. Mass Spectrom.

McIver, R.T., Jr., *Trajectory Calculations for Axial Injection of Ions Into a Magnetic Field: Overcoming the Magnetic Mirror Effect With an R. F. Quadrupole Lens.* Int. J. Mass Spectrom. Ion Processes, 1990. **98**(1): p. 35-50.

McLafferty, F.W., *High-Resolution Tandem FT Mass Spectrometry above 10 kDa.* Acc. Chem. Res., 1994. **27**: p. 379-86.

McLafferty, F.W., Z. Guan, U. Haupts, T.D. Wood and N.L. Kelleher, *Gaseous Conformational Structures of Cytochrome c.* J. Am. Chem. Soc., 1998. **120**(19): p. 4732-40.

Miao, S., L. Ziser, R. Aebersold and S.G. Withers, *Identification of Glutamic Acid 78 as the Active Site Nucleophile in Bacillus subtilis Xylanase Using*

Electrospray Tandem Mass Spectrometry. Biochem., 1994. **33**(23): p. 7027-32.

Mirza, U.A., S.L. Cohen and B.T. Chait, *Heat-induced conformational changes in proteins studied by electrospray ionization mass spectrometry.* Anal. Chem., 1993. **65**(1): p. 1-6.

Nair, H. and V.H. Wysocki, *Are peptides without basic residues protonated primarily at the amino terminus?* Int. J. Mass Spectrom. Ion Processes, 1998. **174**: p. 95-100.

Nakanishi, K., N. Berova and R.W. Woddy, *Circular Dichroism: Principles and Applications*. 1994, New York: VCH Publishers, Inc.

Nelson, R.W., D. Dogruel and P. Williams, *Detection of human IgM at m/z approximately 1 MDa.* Rapid Commun. Mass Spectrom., 1995. **9**(7): p. 625.

O'Connor, P.B., J.P. Speir, M.W. Senko, D.P. Little and F.W. McLafferty, *Tandem mass spectrometry of carbonic anyhdrase (29 kDa).* J. Mass Spectrom., 1995. **30**: p. 88-93.

Ogorzalek Loo, R.R., N. Dales and P.C. Andrews, *Surfactant effects on protein structure examined by electrospray ionization mass spectrometry.* Protein Sci., 1994. **3**(11): p. 1975-83.

Oh, H., K. Breuker, S.K. Sze, Y. Ge, B.K. Carpenter, and F.W. McLafferty, *Secondary and tertiary structures of gaseous protein ions characterized by electron capture dissociation mass spectrometry and photofragment spectroscopy.* Proc. Natl. Acad. Sci. USA, 2002. **99**(25): p. 15863-8.

Okur, A., B. Strockbine, V. Hornak and C. Simmerling, *Using PC Clusters to Evaluate the Transferability of Molecular Mechanics Force Fields for Proteins.* J. Comput. Chem., 2003. **24**(1): p. 21-31.

Papac, D.I., J.E.J. Oatis, R.K. Crouch and D.R. Knapp, *Mass spectrometric identification of phosphorylation sites in bleached bovine rhodopsin.* Biochem., 1993. **32**(23): p. 5930-4.

Papayannapoulos, I.A., *The interpretation of collision-induced dissociation tandem mass spectra of peptides.* Mass Spectrom. Rev., 1995. **14**(1): p. 49-73.

Pasa Tolic, L., J.E. Bruce, Q.P. Lei, G.A. Anderson and R.D. Smith, *In-Trap Cleanup of Proteins from Electrospray Ionization Using Soft Sustained Off-Resonance Irradiation with Fourier Transform Ion Cyclotron Resonance Mass Spectrometry.* Anal. Chem., 1998. **70**: p. 405-8.

Poulter, L. and L.C.E. Taylor, *A Comparison of Low and High Energy Collisionally Activated Decomposition MS-MS for Peptide Sequencing.* Int. J.

Mass Spectrom. Ion Processes, 1989. **91**: p. 183-97.

Price, W.D., P.D. Schnier and E.R. Williams, J. Phys. Chem. B, 1997. **101**: p. 664-73.

Price, W.D., P.D. Schnier and E.R. Williams, *Tandem Mass Spectrometry of Large Biomolecule Ions by Blackbody Infrared Radiative Dissociation.* Anal. Chem., 1996. **68**: p. 859-66.

Price, W.D., P.D. Schnier, R.A. Jockusch, E.F. Strittmatter and E.R. Williams, *Unimolecular Reaction Kinetics in the High-Pressure Limit without Collisions.* J. Am. Chem. Soc., 1996. **118**: p. 10640-4.

Purves, R.W., D.A. Barnett and R. Guevremont, *Separation of protein conformers using electrospray-high field asymmetric waveform ion mobility spectrometry-mass spectrometry.* Int. J. Mass Spectrom., 2000. **197**: p. 163-77.

Purves, R.W., D.A. Barnett, B. Ells and R. Guevremont, *Gas-phase conformers of the [M + 2H]2+ ion of bradykinin investigated by combining high-field asymmetric waveform ion mobility spectrometry, hydrogen/deuterium exchange, and energy-loss measurements.* Rapid Commun. Mass Spectrom., 2001. **15**(16): p. 1453-6.

Qin, J. and B.T. Chait, *Preferential Fragmentation of Protonated Gas-Phase Peptide Ions Adjacent to Acidic Amino Acid Residues.* J. Am. Chem. Soc., 1995. **117**: p. 5411-2.

Ramachandran, G.N. and V. Sasisekharan, *Conformation of polypeptides and proteins.* Adv. Protein Chemistry, 1968. **23**: p. 283-437.

Rockwood, A.L., M. Busman and R.D. Smith, *Coulombic effects in the dissociation of highly charged ions.* Int. J. Mass Spectrom. Ion Processes, 1991. **111**: p. 103-29.

Rockwood, A.L., M. Busman and R.D. Smith, *Coulombic effects in the dissociation of highly charged ions.* Int. J. Mass Spectrom. Ion Processes, 1991. **111**: p. 103-29.

Rockwood, A.L., M. Busman, H.R. Udseth and R.D. Smith, *Thermally induced dissociation of ions from electrospray mass spectrometry.* Rapid Commun. Mass Spectrom., 1991. **5**(12): p. 582-5.

Roepstorff, P., *Proposal for a common nomenclature for sequence ions in mass spectra of peptides.* Biomed. Mass Spectrom., 1984. **11**(11): p. 601.

Rossomando, A.J., et al., *Identification of Tyr-185 as the site of tyrosine autophosphorylation of recombinant mitogen-activated protein kinase*

p42mapk. Proc. Natl. Acad. Sci. U.S.A., 1992. **89**(13): p. 5779-83.

Rost, B. and r.C. Sande, *Jury returns on structure prediction.* Nature, 1992. **360**(6404): p. 540.

Sanger, F. and E.O.P. Thompson, *Amino acid sequence in the glycycl chain of insulin. II. Peptides from enzymic hydrolyzates.* Biochem. J., 1953. **53**: p. 366-74.

Sato, S. and D.P. Raleigh, *pH Dependent Stability and Folding Kinetics of a Protein with an Unusual alpha-beta Topology: The C-Terminal Domain of Ribosomal Protein L9.* J. Mol. Biol., 2002. **318**: p. 571-82.

Sato, S., B. Kuhlman, W.-J. Wu and D.P. Raleigh, *Folding of the multidomain ribosomal protein L9: The two domains fold independently with remarkably different rates.* Biochem., 1999. **38**(17): p. 5643-50.

Sato, S., D.L. Luisi and D.P. Raleigh, *pH Jump Studies of the Folding of the Multidomain Ribosomal Protein L9: The Structural Organization of the N-Terminal Domain Does Not Affect teh Anomolously Slow Folding of the C-Terminal Domain.* Biochem., 2000. **39**(16): p. 4995-62.

Schnier, P.D., D.S. Gross and E.R. Williams, *On the Maximum Charge State and Proton Transfer Reactivity of Peptide and Protein Ions Formed by*

Electrospray Ionization. J. Am. Soc. Mass Spectrom., 1995. **6**: p. 1086-97.

Schnier, P.D., W.D. Price, R.A. Jockusch and E.R. Williams, *Blackbody infrared radiative dissociation of bradykinin and its analogues: energetics, dynamics and evidence for salt-bridge structures in the gas phase.* J. Am. Chem. Soc., 1996. **118**: p. 7178-89.

Senko, M.W., C.L. Hendrickson, M.R. Emmett, S.D.-H. Shi and A.G. Marshall, *External Accumulation of Ions for Enhanced Electrospray Ionization Fourier Transform Ion Cyclotron Resonance Mass Spectrometry.* J. Am. Soc. Mass Spectrom., 1997. **8**: p. 970-6.

Senko, M.W., et al., *Electrospray Ionization FT-ICR Mass Spectrometry at 9.4 Tesla.* Rapid Commun. Mass Spectrom., 1996. **10**: p. 1824-8.

Senko, M.W., J.D. Canterbury, S. Guan and A.G. Marshall, *A High-Performance Modular Data System for FT-ICR Mass Spectrometry.* Rapid Commun. Mass Spectrom., 1996. **10**: p. 1839-44.

Senko, M.W., J.P. Speir and F.W. McLafferty, *Collisional activition of large multiply-charged ions using Fourier transform mass spectrometry.* Anal. Chem., 1994. **66**: p. 2801-8.

Senko, M.W., S.C. Beu and F.W. McLafferty, *Determination of monoisotopic*

masses and ion populations for large biomolecules from resolved isotopic distributions. J. Am. Soc. Mass Spectrom., 1995. **6**: p. 229-33.

Senko, M.W., S.C. Beu and F.W. McLafferty, *High-Resolution Tandem Mass Spectrometry of Carbonic Anhydrase.* Anal. Chem., 1994. **66**: p. 415-7.

Shirts, M.R., J.W. Pitera, W.C. Swope and V.S. Pande, *Extremely Precise Free Energy Calculations of Amino Acid Side Chain Analogs: Comparison of Common Molecular Mechanics Force Fields for Proteins.* J. Chem. Phy., 2003. **119**(11): p. 5740-61.

Siuzdak, G., *Mass Spectrometry for Biotechnology*. 1st. ed. 1996, San Diego: Academic Press, Inc. 161.

Slupsky, C.M. and B.D. Sykes, *NMR Solution Structure of Calcium-Saturated Skeletal Muscle Troponin C.* Biochem., 1995. **34**: p. 563-7.

Smith, R.D., C.J. Barinaga and H.R. Udseth, *Tandem Mass Spectrometry of Highly Charged Cytochrome c Molecular Ions Produced by Electrospray Ionization.* J. Phys. Chem., 1989. **93**: p. 5019-22.

Smith, R.D., J.A. Loo, C.G. Edmonds, C.J. Barinaga and H.R. Udseth, *New developments in biochemical mass spectrometry: electrospray ionization.* Anal. Chem., 1990. **62**: p. 882-899.

Smith, R.D., J.A. Loo, C.J. Barinaga, C.G. Edmonds and H.R. Udseth, *Capillary zone electrophoresis and isotachophoresis-mass spectrometry of polypeptides and proteins based upon an electrospray ionization interface.* J. Chromatogr., 1989. **480**: p. 211-32.

Smith, R.D., J.A. Loo, C.J. Barinaga, C.G. Edmonds and H.R. Udseth, *Collisonal activation and collison-activated dissociation of large multiply charged polypeptides and proteins produced by electrospray ionization.* J. Am. Soc. Mass Spectrom., 1990. **1**(1): p. 53-65.

Smith, R.D., J.A. Loo, R.R. Ogorzalek Loo, M. Busman and H.R. Udseth, *Electrospray MS Review.* Mass Spectrom. Rev., 1991. **10**: p. 359-451.

Smith, R.D., J.A. Loo, R.R. Ogorzalek Loo, M. Busman and H.R. Udseth, *Principles and Practice of Electrospray Ionization- Mass Spectrometry for Large Polypeptides and Proteins.* Mass Spectrom. Rev., 1991. **10**: p. 359-451.

Smith, R.D., K.J. Light-Wahl, B.E. Winger and J.A. Loo, *Preservation of non-covalent associations in electrospray ionization mass spectrometry: multiply charged polypeptide and protein dimers.* Org. Mass. Spectrom., 1992. **27**(7): p. 811-21.

Speir, J.P., G.S. Gorman, C.C. Pitsenberger, C.A. Turner, P.P. Wang, and I.J. Amster, *Remeasurement of Ions Using Quadrupolar Excitation Fourier Transform Ion Cyclotron Resonance Spectrometry.* Anal. Chem., 1993. **65**(13): p. 1746-52.

Speir, J.P., M.W. Senko, D.P. Little, J.A. Loo and F.W. McLafferty, *High-resolution Tandem Mass Spectra of 37-67 kDa Proteins.* J. Mass Spectrom., 1995. **30**(1): p. 39-42.

Stacey, C.C., et al., *Reverse-phase Liquid Chromatography/Electrospray-Ionization Fourier-Transform Mass Spectrometry in the Analysis of Peptides.* Rapid Commun. Mass Spectrom., 1994. **8**(7): p. 513-6.

Stevenson, E., *Dissociation Studies of Charge and Structure Effects on Electrosprayed Proteins*, Dissertation Thesis, Department of Chemistry and Biochemistry, 1998, The University of Texas at Austin.

Stimson, E., O. Truong, W.J. Richter, M.D. Waterfield and A.L. Burlingame, *Enhancement of charge remote fragmentation in protonated peptides by high energy CID MALDI-TOF-MS using "cold" matrixes.* Int. J. Mass Spectrom. Ion Processes, 1997. **169/170**: p. 231-40.

Suckau, D., et al., *Co-Existing Stable Conformations of Gaseous Protein Ions.*

Proc. Natl. Acad. Sci. U.S.A., 1993. **90**: p. 790-3.

Summerfield, S.G. and S.J. Gaskell, *Fragmentation efficiencies of peptide ions following low energy collisional activation.* Int. J. Mass Spectrom. Ion Processes, 1997. **165/166**: p. 509-21.

Tanaka, K., H. Waki, Y. Ido, S. Akita and S. Yoshida, Rapid Commum. Mass Spectrom., 1991. **5**: p. 117.

Tanaka, K., H. Waki, Y. Ido, S. Akita, Y. Yoshida, and T. Yoshida, *Protein and Polymer Analyses up to m/z 100000 by Laser Ionization Time-of-Flight Mass Spectrometry.* Rapid Commun. Mass Spectrom., 1988. **2**: p. 151-3.

Tang, X.J. and P.B. Thibault, R. K., *Fragmentation reactions of multiply-protonated peptides and implications for sequencing by tandem mass spectrometry with low-energy collision-induced dissociation.* Anal. Chem., 1993. **65**(20): p. 2824-34.

Tang, X.J. and P.B. Thibault, R. K., *Fragmentation reactions of multiply-protonated peptides and implications for sequencing by tandem mass spectrometry with low-energy collision-induced dissociation.* Anal. Chem., 1993. **65**(20): p. 2824-34.

Thomson, B.A. and J.V. Iribarne, *Field-induced ion evaporation from liquid*

surfaces at atmospheric pressure. J. Chem. Phys., 1979. **71**: p. 4451.

Thorne, L.R. and J.L. Beauchamp, *Gas Phase Ion Chemistry*, ed. M.T. Bowers. Vol. 3. 1984, New York: Academic.

Thulin, C.D. and K.A. Walsh, *Identification of the Amino Terminus of Human Filaggrin Using Differential LC/MS Techniques: Implications for Profilaggrin Processing.* Biochem., 1995. **34**(27): p. 8687-92.

Tsaprailis, G., A. Somogyi, E.N. Nikolaev and V.H. Wysocki, *Refining the model for selective cleavage at acidic residues in arginine-containing protonated peptides.* Int. J. Mass Spectrom., 2000. **195/196**: p. 467-79.

Tsaprailis, G., et al., *Influence of Secondary Structure on the Fragmentation of Protonated Peptides.* J. Am. Chem. Soc., 1999. **121**(22): p. 5142-54.

Tumminia, S.J., W. Hellmann, J.S. Wall and M. Boublik, *Visualization of protein-nucleic acid interactions involved in the in vitro assembly of the Escherichia coli 50 S ribosomal subunit.* J. Mol. Biol., 1994. **235**(4): p. 1239-50.

Valaskovic, G.A., N.L. Kelleher, D.P. Little, D.J. Aaserud and F.W. MdLafferty, *Attomole-Sensitivity Electrospray Source for Large-Molecule Mass Spectrometry.* Anal. Chem., 1995. **67**: p. 3802-5.

Valentine, S.J. and D.E. Clemmer, *H/D Exchange Levels of Shape Resolved Cytochrome c Conformers in the Gas Phase.* J. Am. Chem. Soc., 1997. **119**: p. 3558-66.

Valentine, S.J., *Probing gas-phase biomolecular ion conformation with ion mobility/mass spectrometry techniques*, Dissertation Thesis, 2000, Indiana University.

Valentine, S.J., *Probing gas-phase biomolecular ion conformation with ion mobility/mass spectrometry techniques*, Dissertation Thesis, 2000, Indiana University.

Vijay-Kumar, S., C.E. Bugg, K.D. Wilkinson and W.J. Cook, *Structure of ubiquitin refined at 1.8 A resolution.* J. Mol. Biol., 1987. **194**(3): p. 531-44.

Voet, D. and J.G. Voet, *Biochemistry*. 1 ed. 1990, New York: John Wiley & Sons, Inc. 1223.

von Helden, G., M.T. Hsu, P.R. Kemper and M.T. Bowers, *Structures of carbon cluster ions from 3 to 60 atoms: Linears to rings to fullerenes.* J. Chem. Phys., 1991. **95**: p. 3835-37.

Wagner, D.S. and R.J. Anderegg, *Conformation of cytochrome c studied by deuterium exchange-electrospray ionization mass spectrometry.* Anal. Chem.,

1994. **66**(5): p. 706-11.

Waltho, J.P., V.A. Feher, G. Merutka, H.J. Dyson and P.E. Wright, *Peptide Models of Protein Folding Sites. 1. Secondary Structure Formation by Peptides Corresponding to the G- and H-helicies of myoglobin.* Biochem., 1993. **32**: p. 6337-47.

Wang, F., M.A. Freitas, A.G. Marshall and B.D. Sykes, *Gas-phase memory of solution-phase protein conformation: H/D exchange and Fourier transform ion cyclotron resonance mass spectrometry of the N-terminal domain of cardiac troponin C.* Int. J. Mass Spectrom., 1999. **192**: p. 319-25.

Wang, G. and R. Cole, *Solution, Gas-Phase and Instrumental Parameter Influences on Charge-State Distributions in Electrospray Ionization Mass Spectrometery*, in *Electrospray Ionization Mass Spectrometry*, R.B. Cole, Editor. 1997, John Wiley & Sons, Inc.: New York. p. 137-74.

Wattenberg, A., A.J. Organ, K. Schneider, R. Tyldesley, R. Bordoli, and R.H. Bateman, *Sequence Dependent Fragmentation of Peptides Generated by MALDI Quadrupole Time-of_Flight (MALDI Q-TOF) Mass Spectrometry and its Implications for Protein Identification.* J. Am. Soc. Mass Spectrom., 2002. **13**: p. 772-83.

Wattenberg, A., A.J. Organ, K. Schneider, R. Tyldesley, R. Bordoli, and R.H. Bateman, *Sequence Dependent Fragmentation of Peptides Generated by MALDI Quadrupole Time-of_Flight (MALDI Q-TOF) Mass Spectrometry and its Implications for Protein Identification.* J. Am. Soc. Mass Spectrom., 2002. **13**: p. 772-83.

Wells, J.M., J.L. Stephenson and S.A. McLuckey, *Charge dependance of protonated insulin decompositions.* Int. J. Mass Spectrom., 2000. **203**(1-3): p. A1-A9.

Williams, E., *Proton Transfer Reactivity of Large Multiply Charged Ions.* J. Mass Spectrom., 1996. **31**: p. 831-42.

Williams, E.R., *Tandem FTMS of Large Biomolecules.* Anal. Chem., 1998. **70**(5): p. 179A-185A.

Wood, T.D., R.A. Chorush, F.M.I. Wampler, D.P. Little, P.B. O'Connor, and F.W. McLafferty, *Gas phase folding and unfolding of cytochrome c cations.* Proc. Natl. Acad. Sci. U.S.A., 1995. **92**: p. 2451-4.

Wu, D. and F.E. Regnier, *Native protein separations and enzyme microassays by capillary zone and gel electrophoresis.* Anal. Chem., 1993. **65**(1): p. 2029-35.

Wu, D. and F.E. Regnier, *Native protein separations and enzyme microassays by capillary zone and gel electrophoresis.* Anal. Chem., 1993. **65**(15): p. 2029-35.

Wu, Q., S. Van Orden, X. Cheng, R. Bakhtiar and R.D. Smith, *Characterization of Cytochrome c Variants with High-resolution FTICR Mass Spectrometry: Correlation of Fragmentation and Structure.* Anal. Chem., 1995. **67**: p. 2498-509.

Wu, Q., S. Van Orden, X. Cheng, R. Bakhtiar and R.D. Smith, *Characterization of Cytochrome c Variants with High-resolution FTICR Mass Spectrometry: Correlation of Fragmentation and Structure.* Anal. Chem., 1995. **67**: p. 2498-509.

Wu, Q., X. Cheng, S.A. Hofstadler and R.D. Smith, *Specific metal-oligonucleotide binding studied by high resolution tandem mass spectrometry.* J. Mass Spectrom., 1996. **31**(6): p. 669-75.

Wu, Z. and C. Fenselau, *Gas-phase basicities and proton affinities of lysine and histidine measured from the dissociation of proton-bound dimers.* Rapid Commum. Mass Spectrom., 1994. **8**(9): p. 777-80.

Wu, Z. and C. Fenselau, *Proton affinity of arginine measured by the kinetic*

approach. Rapid Commum. Mass Spectrom., 1992. **6**(6): p. 403-5.

Wu, Z. and C. Fenselau, *Structural determinants of gas phase basicities of peptides.* Tetrahedron, 1993. **49**(41): p. 9197-206.

Wysocki, V.H., G. Tsaprailis, L.L. Smith and L.A. Breci, *Mobile and localized protons: a framework for understanding peptide dissociation.* J. Mass Spectrom., 2000. **35**: p. 1399-406.

Wyttenbach, T. and B.M. T., *Gas phase conformations of biological molecules: The hydrogen/deuterium exchange mechanism.* J. Am. Soc. Mass Spectrom., 1999. **10**(1): p. 9.

Yamashita, M. and J.B. Fenn, *Electrospray Ion Source. Another Variation on the Free-Jet Theme.* J. Phys. Chem., 1984. **88**: p. 4451-4459.

Yi, Q. and D. Baker, *Direct evidence for a two-state protein unfolding transition from hydrogen-deuterium exchange, mass spectrometry, and NMR.* Protein Science, 1996. **6**(5): p. 1060-1066.

Yu, W., J.E. Vath, M.C. Huberty and S.A. Martin, *Identification of the Facile Gas-Phase Cleavage of the Asp-Pro and Asp-Xxx Peptide Bonds in Matrix-Assisted Laser Desorption Time-of-Flight Mass Spectrometry.* Anal. Chem., 1993. **65**(21): p. 3015-23.

Zeleny, J., J. Phys. Rev., 1917. **10**: p. 1.

Zubarev, R.A., et al., *Electron capture dissociation for structural characterization of multiply charged protein cations.* Anal. Chem., 2000. **72**(3): p. 563-73.

Zubarev, R.A., N.L. Kelleher and F.W. McLafferty, *Electron Capture Dissociation of Multiply Charged Protein Cations. A Nonergodic Process.* J. Am. Chem. Soc., 1998. **120**(13): p. 3265-6.

Zubay, G.L., *Biochemistry*. 4th ed. 1998, New York, NY: Wm. C. Brown Publishers. 990.

Vita

Carla Allison Patrice Armorgan was born on August 17, 1976 in Port-of-Spain, Trinidad to Angela and Carlisle Armorgan. After completing high school at St. Augustine Girls' High School, Trinidad in 1994, she attended Barry University, Miami Shores, FL. In May, 1998 she graduated *cum laude* with a Bachelor's of Science degree in Chemistry (Environmental), and a minor in Biology. She entered The University of Texas at Austin in June, 1998 and attained her Ph.D. in Analytical Chemistry in November, 2003 under the supervision of Professor David A. Laude.

Permanent address: 11160 Jollyville Road, #434 Austin, TX 78759.

This dissertation was typed by the author.